Czech Technical University in Prague
Faculty of Mechanical Engineering, Department of Mechanics, Laboratory of Biomechanics of Man

Dissertation

Mathematical simulation of the hip joint loading

RNDr. Matej Daniel

Study Branch: Biomechanics

Advisor Doc. Ing. Miroslav Sochor, CSc.
Co-advisor Prof. Dr. Veronika Kralj-Iglič

2004 Prague

Type of publication	PhD. Dissertation
Title	Mathematical simulation of the hip joint loading
Author	RNDr. Matej Daniel
Advisor	Doc. Ing. Miroslav Sochor, CSc. Department of Mechanics, Faculty of Mechanical Engineering, Czech Technical University in Prague, Czech Republic
Co-advisor	Prof. Dr. Veronika Kralj-Iglič Institute of Biophysics, Medical Faculty, University of Ljubljana and Department of Orthopaedic Surgery, University Medical Centre, Ljubljana, Slovenia
University	Czech Technical University in Prague
Faculty	Faculty of Mechanical Engineering
Department	Department of Mechanics, Laboratory of Biomechanics of Man
Address	Technická 4, Prague 6, 166 07, Czech Republic
Study Branch	Biomechanics
Number of pages	161
Number of supplements	1
Number of figures	46
Number of tables	11

ANNOTATION

This work deals with the biomechanical variables acting in the human hip joint with emphasis on application of the results in the practice. The hip joint reaction force and the hip contact stress distribution were studied, using mathematical models. These mathematical models were further improved to assess the contact stress distribution in normal and the dysplastic hips during routine activities and to assses the stress distribution in hips subjected to avascular necrosis of the femoral head. Methods were proposed and verified that enable biomechanical analysis to be applied in clinical practice, and these methods have been used in clinical studies. The results of the research have been applied in the new design of an artificial acetabular cup for total hip replacement that optimises the contact stress distribution.

ANOTACE

Tato práce se zabývá zatížením kyčelního kloubu s ohledem na praktickou aplikaci výsledků matematické simulace v praxi. Výslední sílu působící v kyčelním kloubu a rozložení kontaktního tlaku v normálním kyčelním kloubu jsme zkoumali pomocí matematických modelů. Tyto matematické modely jsme následně přizpůsobili tak, abychom mohli modelovat rozložení kontaktního tlaku u normálních a dysplastických kyčelních kloubů v průběhu různé aktivity a rozložení kontaktního tlaku u kloubů postižených aseptickou nekrózou hlavice femuru. Navrhli a ověřili jsme způsob, pomocí kterého lze uplatnit biomechanickou analýzu v každodenní klinické praxi. Na základě výsledků matematické simulace jsme navrhli nový typ acetabulární komponenty pro totální artroplastiku, který optimalizuje rozložení kontaktních tlaků.

Herewith I declare that the thesis comprises only my original work except where indicated and due acknowledgement has been made in the text to all other material used.

. . . . . .

Matej Daniel
in Prague, 11.2.2004

ACKNOWLEDGEMENTS

This work was made in the Laboratory of Biomechanics of Man, Department of Mechanics, Czech Technical University in Prague in collaboration with Department of Orthopaedic Surgery, Clinical Centre, Ljubljana, Slovenia and Group of Applied Physics, Faculty of Electrical Engineering, Ljubljana, Slovenia. Research in this work was supported by the Slovenian Ministry of Education within student exchange program CEEPUS, No. A-0103, Czech Ministry of Education Project MSN 21000012 and Czech Technical University Grant CTU 031083035.

First I would like to give thanks to my advisor doc. Miroslav Sochor from the Czech Technical University in Prague and to my co-advisor prof. Veronika Kralj-Iglič from the University of Ljubljana who gave me a lot of important guidance for my thesis and work.

I would like to thank prof. Aleš Iglič from the University of Ljubljana for his invaluable advices and prof. Svatava Konvičková from the Czech Technical University for constant support during this research. I thank the Chair of the Department of Orthopaedic Surgery Medical Faculty in Ljubljana, prof. Srečko Herman for his support and for the access to the data from the archives. I am also thankful to prof. Georg Bergmann from the Free University of Berlin who provided measurements of the hip contact force used in the part of this study and helped me to analyse them.

I thank prof. Stanislav Holý from the Czech Technical University, prof. Franjo Pernuš from the University of Ljubljana and doc. Vane Antolič from the Department of Orthopaedic Surgery in Ljubljana, prof. Jozef Vojtaššák from the Second Orthopaedic Clinic in Bratislava for all their help.

I am thankful to all staff members of the Department of Mechanics at the Czech Technical University in Prague for their professional advices and encouragement during the course of the study. Particularly I am grateful for collaboration with Tomáš Mareš, Karel Doubrava, Zdeněk Horák, Tomáš Goldmann, Jaroslav Vtípil, Miloslav Vilímek, Radek Sedláček, Pavel Růžicka, Jana Rosenkrancová, Lukáš Horný, Karel Vítek, Miroslav Španiel and Jiřina Heráčková. I am also appreciatory for the help to my colleagues from the Department of Orthopaedic Surgery and Group of Applied Physics, Ljubljana: to dr. Drago Dolinar, dr. Rok Vengust, Miha Foršnarič, dr. Blaž Mavčič, dr. Klemen Bohinc, dr. Oskar Zupanc, dr. Borut Pompe, dr. Boštjan Kersnič, dr. Matej Drobnič and dr. Anton Jaklič.

LIST OF SYMBOLS

A	weight-bearing area
$\mathcal{A}$	constraints coefficient matrix
C	pelvic width
$\mathbf{F}$	muscle force
$\mathbf{F}_{max}$	maximum isometrical muscle force
$\mathbf{F}_{\text{eff}}$	effective muscle force
H	pelvic height
G	optimisation function
G_p	stress gradient index
$\mathbf{M}$	muscle moment
$\mathbf{M}_{max}$	muscle moment at isometrical contraction
$\mathbf{M}_I$	intersegmental moment
N	number of muscles
N_{GTO}	number of Golgi tendon organs
$PCSA$	physiological cross-sectional area
$\mathbf{R}$	hip joint resultant force
S	synergism index of the muscle activity
$\mathcal{T}$	coordinate system transformation matrix
$\mathbf{T}$	ligament force
V_0	resting muscle volume
W	muscle work
$\mathbf{W}_B$	body weight force
$\mathbf{W}_L$	leg weight force
$\mathbf{a}$	moment arm of force $\mathbf{W}_B - \mathbf{W}_L$
b	coordinate of the arm of force $\mathbf{W}_L$
$\mathbf{b}$	vector of constraints
c	coordinate of the arm of the ground reaction force
$\mathbf{c}$	weight coefficients vector
$\mathbf{e}$	unit vector of the muscle direction
l	interhip distance
l_0	resting muscle length
m	muscle mass
$\mathbf{n}$	unit vector
$\mathbf{l}_x$	vector of lower bounds of internal forces
p	contact stress
p_0	contact stress at the stress pole
p_{max}	peak contact stress
r	radius of the femoral head
$\mathbf{r}$	radius vector of the muscle proximal attachment point
$\mathbf{r}'$	radius vector of the muscle distal attachment point
$\mathbf{r}_P$	radius vector to the stress pole
$\mathbf{u}_x$	vector of upper bounds of internal forces
v	muscle contraction velocity
w	relative weights
x	trochanter position coordinate
$\mathbf{x}$	vector of internal forces
x_0	length of the femur
z	trochanter position

	coordinate
x, y, z	coordinates of the global coordinate system
x_a, y_a, z_a	coordinates of the local acetabular coordinate system
x_p, y_p, z_p	coordinates of the local pelvic coordinate system
x', y', z'	coordinates of the rotated coordinate system
r, φ, ϑ	spherical coordinates
$\mathbf{e}_r, \mathbf{e}_\vartheta, \mathbf{e}_\varphi$	orthogonal spherical unit vectors
Φ	spherical coordinate of the stress pole
Θ	spherical coordinate of the stress pole
α	muscle endurance time
β	angle describing position of the acetabular cup
γ	angle describing position of the acetabular cup
δ	segmental displacement
φ	angle of the rotation of the pelvis in the frontal plane
φ_N	spherical coordinate of the femoral head necrosis
φ_R	spherical coordinate of the resultant hip force
ϑ	angle of the rotation of the femur in the frontal plane
ϑ_0	size of the femoral head necrosis
ϑ_{AC}	acetbular angle
ϑ_{CE}	center-edge angle of Wiberg
ϑ_F	functional angle
ϑ_R	spherical coordinate of the resultant hip force
ϑ_L	angle of the lateral border of the weight-bearing area
ϑ_M	angle of medial border of the weight-bearing area
ϑ_N	spherical coordinate of the femoral head necrosis
ϑ_{US}	inclination angle of the acetabulum
ν	angle between point on the articular surface and the stress pole
ρ	muscle density
ρ_{spindle}	density of the muscle spindles
σ	muscle stress
σ_{max}	maximum allowable tensile stress

TABLE OF CONTENTS

Chapter 1

INTRODUCTION

The hip joint is a common site of orthopaedic trauma and disease [14]. Since the disease of the hip joint yields to immobility of the patient a considerable research has been directed toward understanding its development [118, 148, 188]. It is acknowledged that the status of the hip can be estimated by the centre-edge angle of Wiberg ϑ_{CE} [118, 189] and also by some other geometrical parameters of the pelvis and proximal femur e.g., the inclination angle of the acetabulum ϑ_{US}, ACM angle, acetabular angle ϑ_{AC} or a combination of these parameters – the hip index, Severin's index [10]. These parameters were introduced to represent mechanical quantities such as forces and stresses in the hip joint and the size of the weight bearing area. The main biomechanical parameters which have been used to determine biomechanical status of the hip are the hip joint reaction force $\mathbf{R}$ [9, 22, 23, 44] and the contact stress distribution p in the hip joint articular surface [24, 63, 162].

Various techniques have been developed to study biomechanical parameters acting in the hip joint (Tabs. 3.2, 3.3). However, the majority of these techniques are too complex to be applied in the everyday clinical practice. For example, the measurements of $\mathbf{R}$ using implanted instrumented endoprostheses, that may provide the most accurate results, are technically very complex [19, 37, 66] and may be applied in operated patients only [18, 80]. The hip joint reaction force can be estimated also using mathematical models. The forward dynamical analysis is a useful method, but this method is computationally very demanding and therefore unsuitable for acquiring informations about load in individual cases. Moreover, it was shown that the internal forces obtained using the simpler method of inverse dynamics are equivalent to the forces obtained by the forward dynamics approach [8]. The dynamical inverse dynamics models require sophisticated opto-electronical devices to measure the external forces and the motion of the body [44, 143]. Although a significant progress has been obtained in utilising the motion analysis system in clinical analysis [180], this method is not available in common. Therefore in most clinical studies the simple static analysis is performed [127]. In these analyses the load on the hip is usually computed by the reduction method [63, 70, 134, 135]. Since the standard examination of the patient in the clinical practice presents an anteroposterior radiograph [188], models for calculation of the hip joint reaction

force have been introduced recently that may be adapted for individual patient according to their anteroposterior radiograph [63, 94].

The stress distribution in the hip joint can be assessed by instrumented hemiarthroplasty but due to technical complexity and the method unusefulness in non-operated hips, various mathematical models for calculation of the contact stress distribution in the hip joint were used [24, 29]. In these mathematical models the complex nature of the hydrodynamic system of the cartilage in the hip joint is usually not taken into account. Also the specific molecular structure of the glycoprotein bilayer, where two layers are adsorbed on the two contact surfaces [144], the role of the intermediate fluid film [79] and the molecular structure of the cartilage giving rise to the electrostatic forces [35] are neglected. These mechanisms can be realistically described only on the molecular level, by the methods of polymer and molecular physics. Therefore the calculated stress distribution in the hip joint within different macroscopic continuum mechanics approaches can be considered as a rough estimation.

The finite element method (FEM) is widely used for calculating the stress distribution in the hip joint [12, 61, 162]. The FEM may give accurate results for the stress distribution if the strain/stress relationships and the loads of the biological structures are known on the microscopic level. Unfortunately, it is hard to fulfill these requirements in a complex biological structure like the hip joint and it takes much time and effort to make and analyse a three-dimensional FEM model, so this method is not suitable for acquiring information on the stress distribution in the individual clinical cases [64]. Hence, simpler mathematical models can also be used for a roughly estimation of the contact stress distribution in the human hip joint [28, 76, 78, 98].

The hips with a small lateral coverage of the femoral head, i.e., dysplastic hips [63, 188], and hips with decreased articular area due to the collapse of the part of the femoral head, i.e., hips subjected to the aseptic necrosis of the femoral head [62, 173, 182]) are known to be at higher risk for the coxarthrosis development [21, 57]. In both the above mentioned diseases the contact area of the hip is decreased indicating an increased contact stress. Therefore the dysplastic hips and the hips subjected to avascular necrosis of the femoral head will be considered further in this work.

Chapter 2

AIM OF THE WORK

The purpose of this study is to develop and analyse analytical mathematical models that are suitable for estimation of the biomechanical status of the dysplastic hips and hips subjected to the aseptic necrosis of the femoral head, to transform the algorithms of the mathematical models into a form that allows them in the clinical practice, to test the relevance of the mathematical models in the clinical studies and to show applications of the basic research in the prosthesis design.

The study specific aims are to define a complex three-dimensional model of the human hip musculature and to use this model for evaluating of the hip joint resultant force after various optimisation criteria, to propose a method for visualisation of the musculoskeletal system, to derive and analyse model for calculating the contact stress distribution in the normal hips, dysplastic hips and hips subjected to the avascular necrosis of the femoral head, to define new biomechanical parameters that reflect the stress distribution over the weight-bearing area, to create methods that allow to estimate the biomechanical parameters for an individual patient and test them in the clinical study, to define a new design of the total hip replacement that optimise the stress distribution between the femoral and acetabular components. Results of this work should contribute to understanding the biomechanical conditions in the normal and disordered hips and therefore help in optimal decision for the treatment of diseased hips. The methods proposed in this work should improve the application of biomechanical analysis in everyday clinical practice.

Chapter 3

REVIEW OF LITERATURE

3.1 Hip joint reaction force

One of the main problem in the biomechanics of the musculoskeletal system is to determine forces acting in various anatomical structures [143]. Measuring the forces applied to the joint and estimating how these forces are distributed to the muscles, ligaments and articular surface is fundamental for understanding the joint function, injury and disease [123]. In case of the hip joint, we are interested in the load on the hip joint, i.e., in the forces transmitted from the acetabulum to the head of the femur [118]. Sum of the forces transmitted across the hip joint is denoted as the hip joint reaction or resultant force **R** [16,18]. In the following text we will describe methods which are used for evaluation of the hip joint resultant force in biomechanics. Summary of the methods used to determine the hip joint resultant force and values of **R** in the representative position of the one-legged stance are given in Tab. 3.2.

3.1.1 Measurement of the hip joint resultant force by implanted instrumented endoprosthesis

To measure the hip joint reaction force in the hip under vital conditions special endoprostheses of the hip were designed and implanted into human subject [15, 16, 26]. These prosthetic devices were provided with strain gauges by means of which magnitudes and direction of the resultant hip force acting on the hip could be determined [19, 167]. Due to technical complexity of such measurements only few implanted instrumented endoprostheses for measurements of the force **R** have been developed up to now [26, 66, 167].

3.1.2 Mathematical modelling of the hip joint load

Direct measurements can be performed in the patients with the implanted endoprosthesis only [26]. Moreover, these measurements do not explain how the other structures of the hip (e.g. muscles and ligaments) contribute to the hip joint resultant force [41, 131]. Therefore several mathematical models were introduced to estimate the load of the hip and the forces in other anatomical structures of

the hip [8, 94, 163, 181].

In the mathematical modelling of the musculoskeletal system human body is usually modelled as a system of absolutely stiff segments connected by joints and motion of the segments is realized by the muscles spanning the joints [143, 170]. From this point of view, the human body is perceived as a multibody mechanical system controlled by the equations of dynamic equilibrium [163]. The simulation of the mechanical system can be performed by so-called inverse or by forward dynamics. In the following we will briefly describe basic principles of these two approaches. Detailed description of the inverse and of the forward dynamics can be found elsewhere [143, 170, 191, 197].

3.1.2.1 Inverse dynamics

When performing inverse dynamics, motion of the segments of the body and external forces acting on the body are assumed to be known (Fig. 3.1). Using the equilibrium equations the magnitudes of the internal forces of the mechanism, i.e., the muscle, ligament and joint forces [41, 163], could be in principle determined. However, in most cases the number of muscles and ligaments crossing a joint in the human body considerably exceeds the number of the associated equations of motion [181, 191], which is often referred as "muscle redundancy" [197]. This comes from the fact that there are more muscles available than necessary to drive a given motion [163] and the problem becomes mathematically indeterminate. The degree of redundancy equals the difference between the number of unknowns internal forces and the number of associated equations and constraints [181].

There exist two basic approaches to solve the problem of multiple muscles. The first one is based on reducing the degree of redundancy until the mathematically determinate problem is obtained (*reduction method*) while in the second approach the existence of several solutions is accepted and the optimum solution is searched (*optimisation method*).

The reduction method is certainly the oldest and the most utilised in the text-books (e.g. Hall, 1995, Adams, 2002, Brinckmann, 2002). Muscles with the same effect are lumped into groups and considered as a single muscle [25, 197]. It can be shown that the problem is mathematically determinate if the number of the muscles crossing the joint is equal to the degree of the freedom of the joint [163]. In the hip biomechanics, this approach was introduced by Inman, 1947 [147]. He reduced the problem into two dimensions and assumed only one force representing the effect of abductors. The model is simple and provides a rough estimation of the hip joint resultant force. This model was used by many authors with small or withouth any improvements [22, 63, 70, 111, 118, 135, 148].

Expanding the problem into three dimensions allows to include three unknown muscle forces [20]. This approach was utilised by Williams & Svensson [190]. In their model, all the muscles of the hip were represented by three muscle groups.

Alternatively, the mathematically determinate problem can be obtained if the number of associated equations is increased by introducing new constraints to the system [41]. For example, in our work we have adapted a three dimensional model of the hip joint load in one-legged stance [94, 95, 96]. This model takes into account nine effective muscles. The muscles are not lumped into groups but they are divided into three parts: anterior, medius and posterior and within each part the same muscle stress is assumed. This model will be described in detail in the section 4.2.

Models created by the reduction method are usually limited to the static equilibrium [197] or to slow dynamic motions [127, 147, 179]. Although the reduction methods can easily be applied, reduction in the number of the independent muscle forces, spanning a joint results in the loss of information about the function of individual muscles [181]. Therefore the models based on reduction method may not be suitable to predict internal forces in the complicated multi-muscle systems during dynamic motion [25, 197].

The second approach to solve the indeterminate problem of the muscle forces is called the optimisation method. The optimisation method follows in vivo processes where indeterminateness is solved by the central neural system (CNS) [44, 43]. For a given position CNS determine which muscles should be active to maintain equilibrium [46, 130, 157, 184]. The basic assumption of the optimisation method is that a pattern of the activation of the muscles is optimised to perform given activity [170, 184]. Unfortunately, we do not know the optimisation criterion used by the CNS. The optimisation criterion is only estimated by a scalar optimisation function G [133] (called also the cost function [176] or performance function [197]). The most appropriate solution of the muscle redundancy problem is defined as a solution with maximum or minimum value of G (Fig. 3.1) [41, 163, 181]. Furthermore, because of the restrictions of the human body, owning to its complex structure, different constraints can be imposed [181]. Generally, an optimisation task is formulated as a constrained optimisation [143, 159]. Overview of the optimisation criteria used in the inverse dynamics is given in Tab. 3.1.

In a simple case, the minimum or maximum of the cost function and the corresponding internal forces can be found analytically [143, 158, 161]. In more complex muscle systems the equations of the dynamics equilibrium are iteratively solved until a solution is found that results in the optimum value for the cost criteria [26].

According to Zajac and Winters, 1990, the general form of the optimisation

function could be expressed as :

$$G = \sum_i w_{Fi} (F_i)^m + \sum_i w_{\sigma i} (\sigma_i)^n + \sum_j w_{Tj} (T_j)^p + \sum_k w_{Rk} (R_k)^q + \sum_l w_{\delta l} (\delta_l)^r \quad (3.1)$$

where w_{Fi} are relative weights of the individual muscle forces F_i and i runs over all muscles, $w_{\sigma i}$ are relative weights of the individual muscle stresses σ_i, w_{Tj} are relative weights of the individual forces of ligaments T_j and j runs over all ligaments, w_{Rk} are relative weights of individual joint forces R_k and k runs over all joints, $w_{\delta l}$ are relative weights of the individual segmental displacements and the rotations δ and l run over all the segments. The general form of the cost function (Eq. 3.1) can be, from the mathematical point of view, denoted as a polynomial cost function [161, 163]. The muscle stress in the i-th muscle is usually taken to be the ratio of the muscle force in the i-th muscle (F_i) and its physiological cross-sectional area $PCSA$ [27, 94, 130, 143]:

$$\sigma_i = \frac{F_i}{PCSA_i} \quad (3.2)$$

The physiological cross-sectional area of the i-th muscle can be estimated by the following relation [130]:

$$PCSA_i = \frac{V_{0i}}{l_{0i}} \quad (3.3)$$

where V_0 and l_0 are the resting volume and resting length of the i-th muscle, respectively.

In the performance function (3.1) only the sum of one variable is usually taken, i.e., sum of the muscle forces [43, 108] or sum of the muscle stresses [197, 155, 181]. Combination of the several variables in the cost function occurs rarely and such a function is called the multi-criteria cost function [176].

As suggested in Lebar, 1993 and Tsirakos et al., 1997, optimisation functions could be divided according to their historical development and mathematical complexity into linear and nonlinear. The linear functions, which are older and simpler to solve [181], are expressed as a combination of linear variables, i.e., all the coefficients determining the roots of variables in Eq. (3.1) are equal to one ($m = n = p = q = r = 1$) [181, 197]. It is worth noticing that the linear optimisation requires, in addition to a linear cost function, also a linear model of system dynamics. The optimisation problems, based on the linear optimisation function, can be easily solved using the simplex method as discussed later (section 4.2.3.1). For the first time, the linear optimisation was applied to the muscle force prediction by Seireg & Aarvikar [171], where the minimum of the muscle forces was used as an optimisation criterion. The disadvantage of the linear optimisation is that only

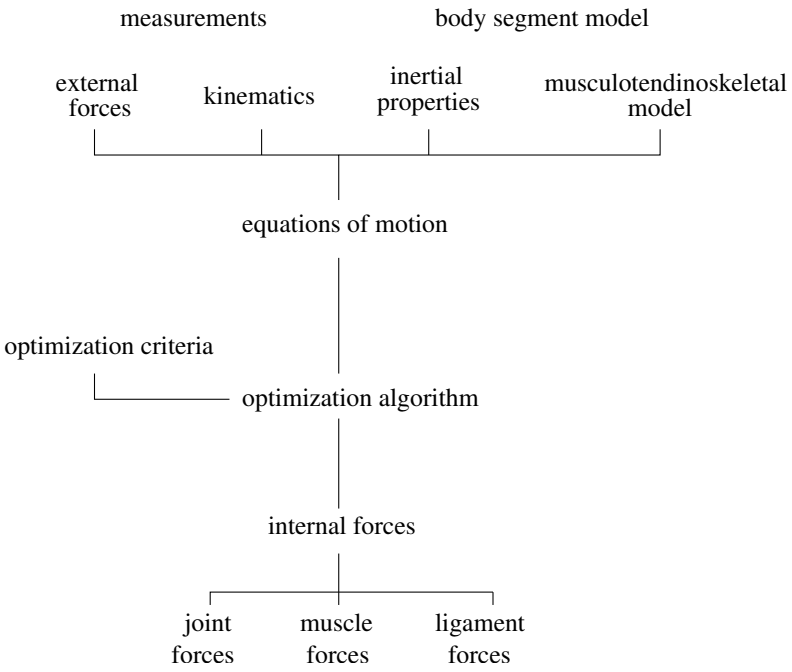

Figure 3.1: Schematic diagram of the inverse dynamic method. After Brand, 1994

few muscles, which are the most appropriate for given motion (the muscles with the largest moment arms), are selected [181]. The forces generated by these muscles are very high while the forces generated by other muscles are almost zero [38]. To avert this situation and maintain advantages of the simple linear programming, an alternative procedure has been suggested that involves formulating and solving two linear programming models sequentially [38, 163, 172]. First, the solution minimising the maximum muscle stress is chosen and then, within this solution, the sum of the muscle and joint forces is minimised [172, 181]. This approach is called the double linear programming [172] or the sequential linear programming [181].

Another possibility how to avoid high forces in the muscles is to redefine optimisation criterion in such way, that the muscles with high forces or stresses will considerably increase the value of the cost function [143, 181]. As the optimum muscle activation pattern should have minimal value of the cost function, large forces in the muscles would be unfavourable since they would increase the value of the cost function significantly [41, 155]. High values of the variables in Eq. (3.1) can be penalised if these variables are squared, cubed or even powered to higher degree [8, 43, 74, 155, 158, 181]. Such performance functions are denoted as nonlinear [131]. Nonlinear optimisation was introduced into biomechanics of walking by Crownishield et al., 1981. They defined optimisation criterion as a minimisation of the sum of the muscle stresses cubed. The proposed nonlinear criterion was based

on the experimentally determined fact that the muscle force is nonlinearly related to the endurance time [43] and the idea that we walk in a way that minimises the energy expenditure or maximises the endurance time [7, 25, 184].

Neither linear nor nonlinear functions ensure that the value of the force or stress in the particular muscle exceeds its physiological upper bound [74, 155, 163]. Furthermore, the mathematical solution of the optimisation problem can give negative values of the forces or stresses in the muscle [181]. Therefore the above mentioned criteria (Eq. 3.1) are only physiologically meaningful if they are equipped with additional constraints that prevent individual muscles from exceeding their physiological maximum and restrict the forces and stresses to positive values (Tab. 3.1) [41, 44, 59, 74].

In the following, other types of the cost function which can not be described by Eq. (3.1), will be discussed briefly. The need for the additional constraints to avoid overloaded muscles is eliminated in maximisation of the soft saturation cost function [163, 181]:

$$G = \sum_i \sqrt{1 - \left(\frac{F_i}{F_{max}}\right)^2} \tag{3.4}$$

where F_{max} is the maximum muscle force and i runs over all the muscles. The criterion (3.4) ensures that no muscle reaches its maximum force if another, less-loaded muscle can contribute to carrying the external load [163].

It is widely accepted that an individual selects a walking speed that minimises the metabolic energy expended per unit distance travelled [7, 184]. Therefore several polynomial criteria, based on the muscle forces or stresses, were suggested that are expected to minimise the energy expenditure during the motion (Tab. 3.1 remarks) [43, 153]. In an other approach, the mechanical work performed by muscles is minimised directly:

$$G = \sum_i \Delta W_i \tag{3.5}$$

where ΔW_i is the work done by the i-th muscle between two following time frames [41].

Optimisation criterion	Constraints	Model / References	Remark
$\min \sum_i F_i$	$F_i \geq 0 \wedge F_i \leq F_{max}$	lower limb - walking [41]	
	$F_i \geq 0$	knee joint [108]	
	$F_i \geq 0$	lower limb - cycling [155]	
$\min \sum_i w_i F_i^2$	$F_i \geq 0 \wedge F_i \leq F_{max}$	lower limb - walking [41]	
	$F_i \geq 0$	upper limb - flexion [159]	
	$F_i \geq 0$	lower limb - cycling [155]	
$\min \sum_i F_i^3$	$F_i \geq 0$	lumbar spine - lifting [38]	
	$F_i \geq 0$	lower limb - cycling [155]	
$\min \sum_i F_i^4$	$F_i \geq 0$	lower limb - cycling [155]	
$\min \sum_i F_i^6$	$F_i \geq 0$	lower limb - cycling [155]	
$\min \sum_i F_i^\infty$	$F_i \geq 0$	lower limb - cycling [155]	
$\min \sum_i \frac{F_i}{F_{i\max}}$	-	[181]	
$\min \sum_i \sigma_i$	$\sigma_i \geq 0 \wedge \sigma_i \leq \sigma_{max}$	lower limb - walking [41, 44]	
	$F_i \geq 0$	lower limb - cycling [155]	
$\min \sum_i \sigma_i^2$	$\sigma_i \geq 0 \wedge \sigma_i \leq \sigma_{max}$	upper limb [153]	(1)
	$\sigma_i \geq 0 \wedge \sigma_i \leq \sigma_{max}$	lower limb - walking [41]	
	$\sigma_i \geq 0$	lower limb - cycling [155]	
	$\sigma_i \geq 0 \wedge \sigma_i \leq \sigma_{max}$	elbow - flexion [163]	

Table. 3.1 continued on next page

Optimisation criterion	Constraints	Model / References	Remark
	$\sigma_i \geq 0$	lumbar spine and hip [50]	
$\min \sum_i \sigma_i^3$	$\sigma_i \geq 0 \wedge \sigma_i \leq \sigma_{max}$	lower limb - walking [8, 26]	
		[43, 74, 150]	(2)
	$\sigma_i \geq 0$	lumbar spine - lifting [38]	
	$\sigma_i \geq 0$	lower limb - cycling [155]	
	$\sigma_i \geq 0 \wedge \sigma_i \leq \sigma_{max}$	elbow - flexion [163]	
$\min \sum_i \sigma_i^4$	$\sigma_i \geq 0$	lower limb - cycling [155]	
$\min \sum_i \sigma_i^5$	$\sigma_i \geq 0 \wedge \sigma_{max}$	elbow - flexion [163]	
$\min \sum_i \sigma_i^6$	$\sigma_i \geq 0$	lower limb - cycling [155]	
$\min \sum_i \sigma_i^{10}$	$\sigma_i \geq 0 \wedge \sigma_i \leq \sigma_{max}$	elbow - flexion [163]	
$\min \sum_i \sigma_i^{100}$	$\sigma_i \geq 0 \wedge \sigma_i \leq \sigma_{max}$	elbow - flexion [163]	
$\min \sum_i \sigma_i^{\infty}$	$\sigma_i \geq 0$	lower limb - cycling [155]	
$\min \sigma_{max}$	$\sigma_i \geq 0$	lumbar spine - lifting [38]	(3)
	$\sigma_i \geq 0$	lumbar spine and hip [50]	
	$\sigma_i \geq 0$	elbow - flexion [163]	
$\min \sum_i \sigma_i$ and then $\min \sum_i F_i$	-	[181]	(4)
$\min \sum_i \left(\frac{F_i}{M_i}\right)^p$	-	[181]	
$\min \sum_i v_i \left(\frac{F_i}{F_{i\max}}\right)^p$	-	[181]	
$\min \sum_i w_i \left(c_1\sigma_i + c_2 \left(\frac{F_i}{F_{max}}\right)^2\right)$	$\sigma_i \geq 0 \wedge \sigma_i \leq \sigma_{max}$	upper limb [153]	(5)

Table. 3.1 continued on next page

Optimisation criterion	Constraints	Model / References	Remark
$\min \sum_j w_j T_j$	$T_j \geq 0 \wedge F_i \geq 0$	lower limb - cycling [155]	(6)
$\min \sum_i R_i$	$F_i > 0$	hip - standing [133, 132]	
	$\sigma_i \geq 0 \wedge \sigma_i \leq \sigma_{max}$	lower limb - walking [41]	
$\max \sum_i \sqrt{1 - \left(\frac{F_i}{F_{max}}\right)^2}$	$F_i \geq 0$	elbow - flexion [163]	(7)
$\min \sum_i \Delta W_i$	$\sigma_i \geq 0 \wedge \sigma_i \leq \sigma_{max}$	lower limb - walking [41, 130]	(8)
$\max \frac{1}{\alpha_i}$	$F_i \geq 0$	lower limb - cycling [155]	(9)

Table 3.1: Optimisation criteria used in the inverse dynamics. F_i - muscle force of i-th muscle, σ_i - muscle stress of i-th muscle, T_i - ligament force of i-th ligament, R_i - joint contact force in i-th joint, W_i - work of i-th muscle, α_i - i-th muscle endurance time, v_i - contraction velocity of i-th muscle, i runs over all muscles, j runs over all ligaments, w_i, w_j, c_1, c_2, p - coefficients, *Remarks.* (1) economy of metabolic energy expenditure, (2) maximise endurance, (3) minimise the maximal muscle stress, (4) double linear programming, (5) minimise energy consuming, (6) minimise sum of the forces transmitted by the cruciate ligaments, (7) soft saturation criterion, (8) minimise instantaneous muscle power, (9) maximise endurance time.

Notice that there are no integral signs in the performance criteria (Eqs. 3.1–3.5, Tab. 3.1). These models therefore optimise the input according to some criterion without regarding where the segments are or how the segments will move as a consequence of the optimised current input [75, 178]. The algorithm must run repeatedly to find the internal forces in other instant [8, 25, 197]. Hence, inverse dynamic models are denoted as "quasistatic" since they are focused only on the present state of the body (Fig. 3.1) [191, 197].

Several disadvantages of the inverse dynamic approach follow from above. First, the results are heavily influenced by the accuracy of the available experimental data, particularly the measured limb motion [7]. Second, the time independent inverse dynamic optimisation makes it relatively difficult to incorporate muscle

physiology properly [8, 75]. Finally, analyses based on inverse dynamics approach may not be appropriate to describe neuromuscular regulation [8, 197]. Muscle dynamics must be calculated backward in time, since the resulting motion is the result of earlier muscle activation and this is difficult to incorporate in the inverse optimisation algorithm [129, 75]. These limitations were eliminated in the forward dynamic optimisation approach.

3.1.2.2 Forward dynamics

In a forward dynamics model, the motion is calculated as a result of neural input [75, 129, 178]. The muscle dynamics is calculated backward in time, since the resulting motion is the result of earlier muscle activation (Fig. 3.2) [191, 194, 197]. Here only basic principles of the forward dynamics approach will be described. Detailed description of the forward dynamics can be found in Zajac & Winters, 1990 or in Martin & Schovanec, 1998.

The forward dynamics approach demands not only a mathematical description of the system dynamics but also a mathematical description of the performance criterion similarly to the inverse dynamics [8, 178, 194]. In contrast to the inverse dynamics, the internal forces are treated as a time-dependent state variables [8] and the time integral performance criterion includes multiple subcriteria related to kinematics aspects [194], energy expenditure [7], duration of forces developed by muscles [197] or neuromuscular activation [178]. Then the optimisation algorithm determines a neuromuscular activation that minimises the performance criterion. Forward dynamics method determines continuous control that can be optimised over the entire time-frame of the simulation, rather than just at discrete instants [194]. The forward optimisation allows to predict not only the muscle forces but also the kinematics of the movement [7, 197].

The predictive value of the forward dynamics can be used in modelling the effects of the musculoskeletal alterations (e.g., due to surgery, physical therapy and orthotic interventions) since the movement and internal forces can be predicted before the actual alterations are performed [194]. However, the forward optimisation of multi-joint systems with many muscles is computationally very demanding. Therefore only few models of gait have been developed so far [7, 72, 178, 194]. To decrease the time of computation, new algorithms were introduced combining the advantages of the fast inverse dynamic approach and the complex forward dynamic approach (IFDO, inverse/forward dynamic optimisation) [72, 178].

In the previous part modelling of the musculoskeletal system was discussed with focus on the methods of inverse and forward dynamics. However, other computational method have been introduced recently to simulate the muscle function

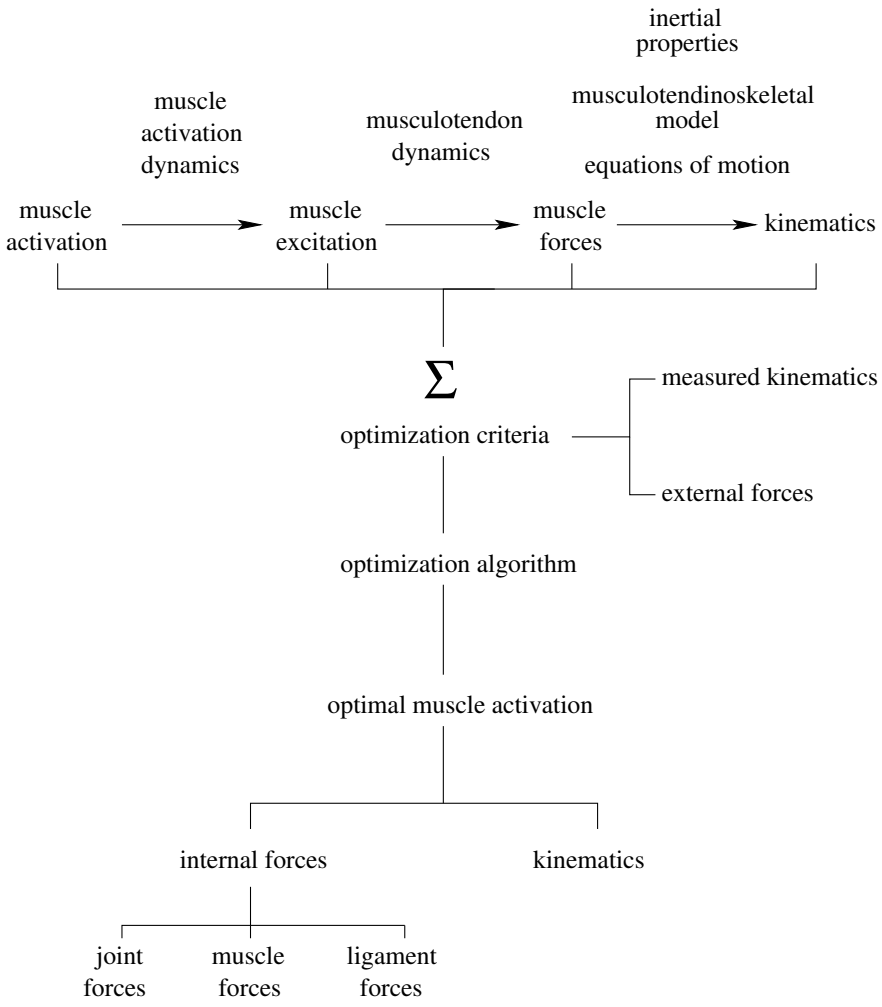

Figure 3.2: Schematic diagram of the forward dynamic method. After Winters, 2000.

in the musculoskeletal system like genetic algorithms [160] or theory of neural networks [114].

3.1.3 Direct measurement of the muscle forces

Apart from mathematical modelling, muscle activity can be determined also by measurements. Direct measurements of the muscle forces by sensors implanted into tendons [143] are invasive and could not be performed in all the muscles.

In biomechanics, recording of the electrical signals during the muscle activity (electromygraphy - EMG) is widely used. It is said that EMG is a "window" onto neuromuscular control [123]. The EMG-driven models use the measured muscle activity to estimate the muscle force (for review see [105, 180]). The main advantage of the EMG approach is that it requires no minimising principle [2]. The

EMG measurement of the muscle activity can be used to validate mathematical models mentioned above, as shown in [8, 131], or to apply an additional input into optimisation models [60].

An other noninvasive method to estimate muscle activity exists besides the EMG measurements. Indication of the energy consumption in the working muscle can be achieved by measuring the muscle oxygen consumption with Near Infrared Spectroscopy (NIRS) [153].

Tab. 3.2 shows values of the magnitude of the hip joint reaction force normalized to the body weight (R/W_B) in one-legged stance obtained by different methods as described above.

Author	**Year**	R/W_B	**Activity**	**Method**	**Reference**
Rydell	1966	2.5	gait	direct measurement	[167]
Bergmann et al.	1993	3	gait	direct measurement	[16]
Brand et al.	1994	1.8	gait	direct measurement	[26]
Bergmann	2001	2.18	static	direct measurement	[15]
Inman	1947	$2.4 - 2.6$	static	inverse dynamics reduction, 2D	in [147]
Blount	1956	3.4	static	inverse dynamics reduction, 2D	in [190]
Backmann	1957	2.92	static	inverse dynamics reduction, 2D	in [190]
Williams & Swensson	1968	6	static	inverse dynamics reduction, 3D	[190]
McLeish & Charnley	1970	2.3	static	inverse dynamics reduction, 2D	[137]
Pauwels	1976	4	static	inverse dynamics reduction, 2D	[148]
Bombelli	1983	3.7	static	inverse dynamics reduction, 2D	[22]
Maquet	1985	1.8	gait	inverse dynamics reduction, 2D	[127]
Legal	1987	3.08	static	inverse dynamics reduction, 2D	[118]
Iglič	1993	2.38	static	inverse dynamics reduction, 3D	[90]
Crownishield et al.	1978	3*	gait	inverse dynamics optimisation, 3D	[44]
Maček-Lebar	1993	2.37	static	inverse dynamics optimisation, 3D	[133]
Collins	1995	1.3	gait	inverse dynamics optimisation, 2D	[41]
Pedersen et al.	1997	2.2*	gait	inverse dynamics optimisation, 3D	[150]
Heller et al.	2001	2*	gait	inverse dynamics optimisation, 3D	[74]
Stansfield et al.	2003	1.9*	gait	inverse dynamics, optimisation, 3D	[172]
Anderson et al.	2001	2.3*	gait	inverse dynamics, optimisation 3D	[8]
		2.3*	gait	forward dynamics optimisation	
Hurwitz et al.	2003	2.3*	gait	EMG-assisted, 2D	[87]

Table 3.2: Predicted values of the magnitude of the hip joint reaction force R with respect to body weight W_B in one-legged stance in static posture or during gait (* approximated from graph).

3.2 Contact stress in the human hip joint

It was shown that stresses in the biological tissues could play an important role in remodelling the tissues [83, 148]. Also from the clinical point of view, it is well known that the clinical status of the hip is affected not only by the factors which influence the hip joint resultant force but also by the factors which change the stress distribution in the hip joint, i.e., by the radius of the femoral head or the lateral coverage of the femoral head [118, 134, 189]. Therefore, besides the hip joint resultant force we are also interested in the stress distribution in the hip joint.

The distribution of the stress on the hip joint articular surface can be determined from the direct measurements or by simple or more sophisticated mathematical models (for summary see Tab. 3.3).

3.2.1 Direct measurement of the contact stress distribution in the hip joint

A direct measurements of the intra-articular contact stress in seventeen cadaveric hips were performed by Brown, 1983. Local stresses were sensed by the arrays of 24 compliant miniature pressure transducers inset superficially in the femoral head cartilage.

Hodge et al., 1989 measured the hip contact stress distribution after hemiarthroplasty by an implanted prosthesis in one patient. With pressure transducers mounted in the prosthetic head, the contact stresses in discrete points of the articular cartilage were measured during different activities [37, 80].

However, other methods for estimation of the stress distribution were proposed. The method of the stress distribution measurement using the prescale pressure sensitive films has been developed [3, 14, 24]. Pressure sensitive film resolves the distribution of the stress over the static contact area, however film thickness may alter joint mechanics [3].

The pressure distribution can be estimated from the analysis of the relative motion between the articular surfaces using the method of stereophotogrammetry [5]. Stereophotogrammetry is noninvasive, but joint is indirectly inferred [14].

Pauwels, 1978 proposed that the elevated stress of the bone in the roof of acetabulum provokes the bony apposition. Harrison, Schajowicz and Trueta, 1953 [67] suggested that the trabecular arrangement with the femoral head defines pressure areas on the articular surface. Therefore the magnitude and distribution of the compressive stress in the human hip can be estimated indirectly from the radiographic measurements of the bone density [118, 148].

Another quantity that is related to the stress distribution in the biarticular joints is the size of the weight-bearing area. The weight-bearing area A of the hip

is an area of the articular surface where the stress differs from zero [94, 152, 186]. Dye transfer and exclusion method measure the size of the contact area [14, 67, 68, 162], but they present an invasive method. Stereophotogrammetry [5] and measurements from the magnetic resonance imaging [40] have also been used to determine the size of the weight-bearing area.

3.2.2 Mathematical models of the stress distribution in the hip joint.

A non-invasive method used to estimate the contact stress in the hip is the mathematical modelling. In the mathematical modelling the load of the hip (resultant hip force or distribution of the muscle force) is assumed to be known [63, 89, 134]. Force $\mathbf{R}$ can be determined from mathematical modelling [64, 94, 118] or from the direct measurements [100, 98]. It is also assumed that the geometry of the hip and mechanical properties of the structures of the hip are given [28, 162]. According to the method the mathematical models can be divided into two main categories: analytical and numerical models.

3.2.2.1 Analytical models

In the human hip we can discriminate between the tensile stress, the shear stress and the compressive stress [118]. In the most of the analytical models, the tensile stresses and the shear stresses that arise in the proximal femur and the shear stress in the hip joint articular surface due to friction are neglected for smooth, well lubricated femoral and acetabular articular surfaces which are spherical and congruent [28, 94, 121]. It means that the articular cartilage behaves "hydrostatically", so the forces transmitted across the articular surface are all normal. Therefore only normal (radial) stress on the articular surface is considered [64, 93, 121]. This compressive stress is denoted as contact stress p.

The main assumption of the analytical models is that the whole hip joint resultant force is distributed over the articular surface [45, 94, 118], i.e., the integration of the contact stress p over the articular surface should give the resultant hip force ($\mathbf{R}$).

$$\int_A p \, \mathrm{d}\mathbf{A} = \mathbf{R} \tag{3.6}$$

$$\mathrm{d}\mathbf{A} = \mathbf{n} \, \mathrm{d}A \tag{3.7}$$

where $\mathbf{n}$ is unit vector parallel to the normal to $\mathrm{d}A$. If the geometry of the articular surface is known, one can express $\mathrm{d}\mathbf{A}$ at any point of the weight-bearing area. Then the unknowns are the values of stress over the articular surface (p). The problem

can be solved if the stress distribution is described parametrically, i.e., if it is described by a mathematical function. Then the parameters of the mathematical function can be obtained by solving Eq. (3.6). Since Eq. (3.6) presents three equations for the components of the force **R**, the stress distribution should be described by the function with the maximum number of three parameters to have a mathematically determinate problem.

Legal, 1977 considered a homogeneous distribution of the stress on the weight bearing-area that is symmetrical with respect to the direction of the force **R**. The only parameter is the value of the stress p_{const}. The model provides rough estimation of the stress value, but the stress distribution does not correspond to the studies of radiographic bone density that indicate that the stress in the hip joint increases toward the acetabular margin [148].

Therefore Legal, 1978 developed a model of linear decrease of pressure in the plane perpendicular to **R**. Within this model the stress distribution function is defined by two parameters: values of the contact stress at the acetabular margin and the rate of the stress decrease.

Greenwald and O'Connor, 1971 [68] derived a stress distribution function which is based on the assumption that the radial stress on the articular surface of the hip is proportional to the radial strain of the cartilage layer. It was proposed that for the congruent acetabulum and the femoral head the radial strain as well as the contact stress is proportional to the cosine of the angle ν between that point and the position of the point of the maximum stress (p_0) [28, 68], $p = p_0 \cos \nu$ (for detailed description see page 52). The cosine stress distribution has been used by several authors [28, 36, 45, 93, 100, 118, 186]. The cosine distribution function can be corrected by taking into account the corresponding corrective coefficients for the incongruity between the acetabulum and femur [99].

The shape of the stress distribution can also be described by the ellipsoidal or paraboloidal function [36]. Like the cosine stress distribution function the pressure distribution can be written as the product of the peak value (p_0) and a stress shape function of the angle between a given point at the weight-bearing area and the point of peak stress (ν). The shape functions are $\sqrt{1 - 4\,\nu^2/\pi^2}$ and $1 - 4\,\nu^2/\pi^2$ for ellipsoidal and paraboloidal stress distribution, respectively.

3.2.2.2 Numerical models

The finite element method (FEM) is widely used for calculating the stress distribution within the hip joint [12, 31, 61, 162]. Originally the FEM method was introduced as a process of solving structural mechanics problems [13, 198]. The basic concept of the finite element method is that a body or structure may be

Author	**Year**	p_{max} [MPa]	**Method**	**Reference**
Rushfeld	1979	6.8	instrumented hemiarthroplasty	[3, 24]
Hodge et al.	1989	2.5–18	instrumented hemiarthroplasty	[80]
Brown	1983	2.92–8.80	in vitro pressure transducers	[30]
Adams & Swanson	1985	9.57	in vitro pressure transducers	[3]
Afoke et al.	1987	2.9–8.6	pressure-sensitive films	[3]
Bay et al.	1996	4.0–6.0	pressure-sensitive films	[14]
Hak et al.	1998	7.5–9.0	pressure-sensitive films	[24]
von Eisenhart et. al.	1999	7.7	pressure-sensitive films	[24]
Legal	1980	1.2–1.34	analytical mathematical model	[118]
Brinckmann et al.	1981	1.1–1.7	analytical mathematical model	[28]
Iglič et al.	1990	1.6	analytical mathematical model	[96]
Hadley et al	1990	0.5–4	analytical mathematical model	[70]
Ipavec et al	1999	1.6–2.7	analytical mathematical model	[98]
Mavčič et al.	2002	2.4	analytical mathematical model	[134]
Genda et al.	1995	2.0–2.45	numerical mathematical model	[64]
Hipp et al.	1999	2.1	numerical mathematical model	[78]

Table 3.3: The estimates of the values of the hip joint peak contact stress in normal hips from the various authors.

divided into smaller elements of finite dimensions called as the finite elements. The original body or structure is then considered as an assemblage of these elements connected at a finite number of nodes. The properties of the elements are formulated and combined to obtain the properties of the entire body. The equations of equilibrium for the entire structure or body are obtained by combining the equilibrium equation of each element such that the continuity is ensured at each node. The necessary boundary conditions are then imposed and the equations of equilibrium are solved to obtain the required variables such as stress and strain [198].

Various software systems exists that incorporates algorithms of FEM for solving the stress distribution [61]. Using these engineering systems a complete stress

distribution in the anatomical structures of the hip can be obtained [12, 162].

Alternative method for determination of the hip joint contact stress distribution is a discrete elements analysis (DEA) [63]. Within this method the acetabulum and the femur are modelled as smooth fine mesh elements arrays connected by an array of linear springs [64]. Stress on the articular surface is taken to be equal to the deformation of the springs after relative displacement of the femoral head toward the acetabulum [63].

Tab. 3.3 shows values of the peak contact stress in normal human hips obtained by different methods as described above.

3.3 Clinical biomechanics of the hip

3.3.1 Dysplasia of the hip

In medical terminology dysplasia means any abnormal development [34]. Dysplasia of the hip refers to mechanical deformations and deviations in the size and shape or mutual proportions between femur and acetabulum [54]. Various methods have been used to study the contact stress distribution in normal and dysplastic hips [24, 63, 134, 148]. In clinical studies it was shown that the peak contact stress is on average higher in dysplastic hips than in the normal hips [63, 134].

The dysplastic hips can be treated conservatively [188] or by a chirurgical intervention (joint preserving operations or total hip replacement) [23, 186]. The joint preserving operations changes the bony geometry of the proximal femur and acetabulum of the dysplastic hips to postpone or even stop development of the pathological changes in the hip joint [10, 188]. The effect of various osteotomies on the proximal femur on the hip joint reaction force has been studied [23, 89, 127, 148]. Also the change of the biomechanical conditions in the hip by increasing the lateral roof of the acetabulum (Chiari osteotomy) [76], rotation of the acetabulum (Bernoise tripple osteotomy) [93] or changing the geometry of the pelvis (Salter osteotomy) [186] have been studied. If the hip joint is damaged to an irreversible extent the total hip joint replacement is indicated [82, 188].

3.3.2 Avascular necrosis of the femoral head

Avascular necrosis (osteonecrosis) of the femoral head is a relatively common disorder of the human hip [86]. It is characterised by decay of the bone tissue in part of the femoral head as a result of disruption of the blood supply in the diseased region of the bone [1].

Osteonecrosis can be classified into two main forms: posttraumatic and nontraumatic. The majority of causes are secondary to trauma [11]. Some fractures and dislocations of the hip joint head affect the arterial blood supply of the femoral head and are known to cause osteonecrosis [103]. The exact etiology of nontraumatic avascular necrosis remains unclear [86]. Two major theories are intraluminal obliteration (embolus in patients with coagulopathy [103], embolic lipid clot due to alcoholism [6], nitrogen bubbles in decompression sickness [88], immune complexes [1] or sickle cell anemia [77]), and extraluminal obliteration (increased marrow pressure by Gaucher cell proliferation [1] and increased marrow fat due to corticosteroid usage [139]). However, there exist a large number of cases of nontraumatic avascular necrosis in which no main causative factor can be found [11, 86], probably due to complex multifactorial etiology of the disease [103].

Due to insufficient blood supply, a process of decay within the femoral head may lead to the collapse of a portion of the surface of the femoral head [151, 173]. In the terminal phase of the necrotic process the whole hip joint is affected and osteoarthritis is superimposed on the deformed femoral head [57, 62].

Currently two treatment practices are used: conservative treatment (range motion exercises, anti-inflammatory medicines) or surgery [151, 193]. If the osteoarthritis is developed the surgical solution is usually a total hip replacement. Since the patients affected by avascular necrosis are commonly middle-aged or younger (an average onset at 38 years of age while 25% of patients are younger than 25 [85]), and due to the limited life of joint implants, other surgical procedures are also implemented. These procedures include reducing the intraosseous pressure (core decompression [151]), providing mechanical support for the subchondral bone (cortical bone grafts), or translocation of the necrotic segment away from the load transmitted area (osteotomies [1, 12, 23, 49, 86]). Hips subject to avascular necrosis of the femoral head and the effects of various operations in these hips were previously studied using the finite element method [12, 31, 32, 33, 182].

3.3.3 Total hip replacement

With respect to the immobility and pain of the patient afflicted with arthritis of the hip, surgeons have been trying to treat this debilitating disease. Initial attempts to treat arthritic hips included arthrodesis (fusion) [20], osteotomy [168, 186], and joint debridements [56].

In 1923, one of the first artificial hip socket components was installed in a patient by Smith-Peterson [20]. In 1938, a stainless steel total hip was designed by Wiles in England [138]. This hip is considered as the first modern construction of the total hip replacement (THR) since both the acetabulum and femoral head were replaced. The next noticeable advance in hip surgery came from Sir John Charnley who replaced an arthritic hip socket with a plastic cup and replaced the femoral head with a metal prosthesis [142]. The method of allowing the metal femoral head component to slide smoothly on the plastic cup surface turned out to work rather well, leading to a standard in the total hip replacement surgery [20, 142, 138]. Advances such as bone cement used for fixation, refinements in the design of the prosthesis [82], application of bioceramics [138] and Ultra-High Molecular Weight Polyethylene (UHMWPE) [107, 142] for reducing implant wear increased the success rates of the surgery and hence the appeal and feasibility of the THR surgery. Further research has been trying to yet improve the methods of fixation. Occasionally it was found that the bone cement fixation breaks down with time [142]. Therefore implants with textured surfaces which allow bone to

grow into them have been developed [107].

However, in some patients the total hip replacements fails. The mechanisms of the failure of the total hip replacement during the time can be various such as lysis, sepsis or loosening [142]. Application of UHMWPE in artificial joints gives rise a problems that are connected to its limited resistance to wear [136]. The wear particles from the acetabular UHMWPE interacts with the organism and may cause osteolysis and loosening of the endoprosthesis. Therefore alternatives to UHMWPE such as metals and ceramics were tested but they lack shock absorbing properties [142]. The loosening of the implant may also be related to the atrophy of the bone that anchors the implant. It was suggested that the bone atrophy and remodelling is related to the high pressures at the bone prosthesis interface [83].

Chapter 4

MATHEMATICAL MODELS

4.1 QUANTITATIVE ANATOMY OF THE HUMAN HIP MUSCULATURE

In static biomechanical analyses whole muscles are usually represented as single vectors with a certain line of action and force magnitude [43, 150, 176]. The line of action of a muscle may be considered to go directly from the origin to the insertion site [130, 170].

The muscle force generation potential depends on the size, structure, and length of the muscle [46, 175]. The size of the muscle characterises its physiological cross-sectional area $PCSA$ which is related to the strength of the muscle [25]. The capability of the muscle to generate the force under static conditions can be determined by the magnitude of the maximum force at isometric contraction (F_{max}) [27].

Information about the activity of the muscles is sensed by special sensors: the muscle spindles and the Golgi tendon organs [55, 169]. To define a regulation model that takes into account signals coming from the load receptors, in addition to the mechanical properties of the muscles, neurological properties of the muscles (like type and density of the innervation) should be taken into account.

A purpose of this section is to combine data from available sources to quantify anatomy of all the muscles crossing the hip joint in a form generally suitable for static analysis of the muscle forces and the hip joint resultant force. It requires definition of the muscle attachments, size of the muscle, force generating capacity, and density of the muscle receptors. The computer system for visualisation of the musculoskeletal structures developed within this work and its practical application will be presented.

4.1.1 New computer system for visualisation of the musculoskeletal system

Up to now there exists no available free software for visualisation of the musculoskeletal system. The commercial packages that offer such possibility, do not allow arbitrary manipulation with the muscle model or the skeletal model (e.g., a parallel visualisation of the force and stress analysis) [47]. Therefore we have decided to develop our own system for visualisation of the musculoskeletal system.

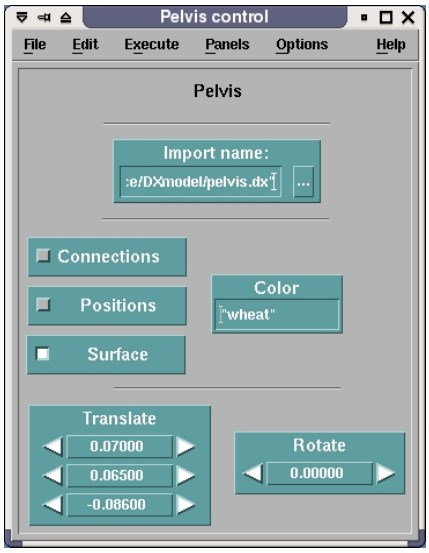

Figure 4.1: Input form of the skeletal object in the OpenDX.

The system for visualisation was programmed in the scientific visualisation environment OpenDX – also known as Data Explorer (DX)[1]. OpenDX is a programming environment for data visualisation and analysis that employs a data-flow driven client-server execution model [97]. It provides a graphical program editor that allows the user to create an interactive visualisation. In our work a graphical user interface, visual programming, and a high-level scripting language was used to build complete application.

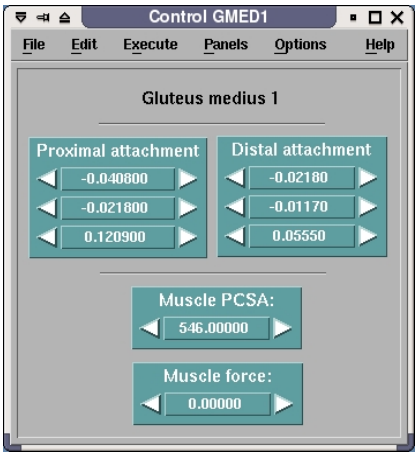

Figure 4.2: Input form of the muscle module in the OpenDX.

[1]OpenDX is freely distributable program under GNU public licence [58].

Skeletal structures in the OpenDX can be visualised as polygonal models or can be obtained directly from 3D computer tomography [97]. In our work the polygonal models of the lower extremity skeleton presented by Delph, 1990 were used (Fig. 4.5–4.9). These polygonal models were transformed into internal data structure of the OpenDX. Five objects representing the bony structure of pelvis, femur, patella, tibia, fibula, talus, and foot were defined. A simple interactive form that allows user to control the displacement, rotation, colour and opacity of the bony structures was created (Fig. 4.1).

For visualisation of the muscles we have developed a special module for the OpenDX called *muscle.net*. This module creates a three-dimensional representation of the muscle. The points of the attachments are shown as balls and tube represents the line of the muscle (Figs. 4.5–4.9). The width of the tube is proportional to the physiological cross-sectional area ($PCSA$) of the muscle (Fig. 4.3). A user-friendly interface was developed to fill in the input data of the muscle: a position of the attachment points, $PCSA$ of the muscle and force of the muscle (Fig. 4.2). The colour or opacity of the muscle tube can be changed according to the muscle force after the user-defined colormap.

Results of the visualisation are rendered in the Image window (Fig. 4.3). The visualisation program OpenDX allows to manipulate with the data representation, i.e., rotate, zoom, save image, print image, etc. The visualisation of the musculoskeletal system can be run on any platform the OpenDX has been ported on (Linux and FreeBSD platforms, several commercial Unix systems such as SGI, HP, Sun or AIX and Windows/Intel platform).

4.1.2 Complex muscle model of the hip joint

A global Cartesian coordinate system based on the work of Iglič et al., 2002 was estabilished with the origin in the center of the rotation of the hip joint, i.e., in the centre of the femoral head. x and z axis lie in the frontal plane while y axis points in the posterior direction (Fig. 4.10). All the muscle attachment points described below are defined in this coordinate system (Tabs. 4.1, 4.2).

The position of the proximal muscle attachment point is given by the radius vector $\mathbf{r} = (x, y, z)$ while the position of the distal muscle attachment point is given by the radius vector $\mathbf{r}' = (x', y', z')$. The muscles that are attached over a large area are divided into several muscular units and each of the unit is considered as an individual muscle. The radius vectors $\mathbf{r}$ and $\mathbf{r}'$ were taken from the work of Delph & Loan, 1995.

The values of the physiological cross-sectional area beeing equal to the volume divided by the muscle length (Eq. 3.3), were taken from the work of Yamaguchi,

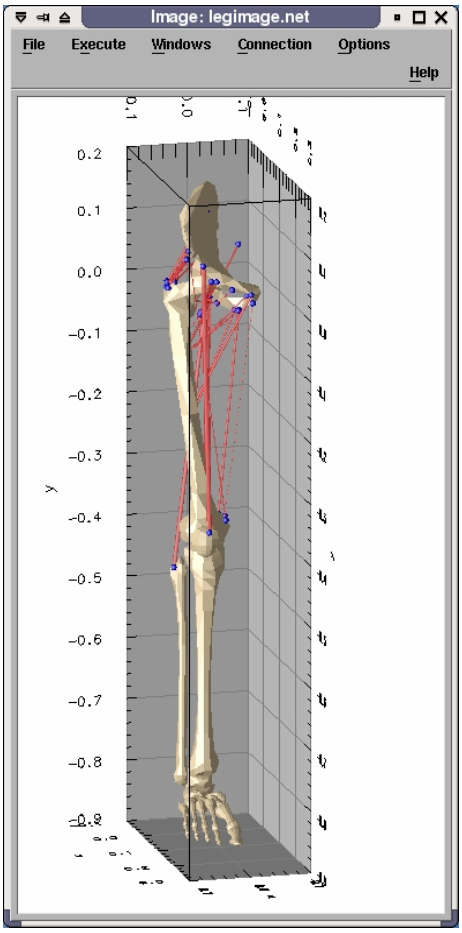

Figure 4.3: Image window with representation of the musculoskeletal model.

1995. The values of the magnitudes of the maximum forces at the isometrical contraction for the muscles of the lower extremity were measured by Brand et al., 1986. The neurophysiological properties of the muscles were defined by the density of the muscle spindles ρ_{spindle}. The density of the muscle spindles were taken from the work by Stillman, 2000.

The muscles of the hip can be divided according to the motion in the hip they produce in the hip. Bellow we describe particular muscles of the hip, their representation in the mathematical model and their functions about the hip. The properties of the muscles are shown in Tab. 4.1.

4.1.2.1 Flexion and extension

The major flexors of the hip are iliacus and psoas (Fig. 4.4). Since the musculus iliacus and musculus psoas are wrapped around the acetabulum [140] their effective origin points are taken to lie on the upper rim of the acetabulum.

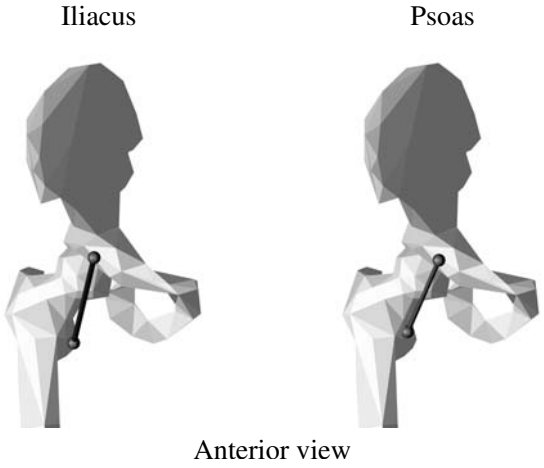

Figure 4.4: The major flexors of the hip.

Also other muscles are active in flexion [71]: rectus femoris, tensor fascia latae, sartorius and pectineus . These muscles are shown in Fig. 4.5.

The hip extensors are: gluteus maximus (Fig. 4.7), biceps femoris, semimembranosus, and semitendinosus. The muscles biceps femoris, semimembranosus and semitendinosus are called the hamstrings [71] (Fig. 4.6). The fibres of the gluteus maximus have a wide insertion on the pelvis and sacrum [197]. Therefore the gluteus maximus was decomposed into three lumped compartments: anterior (1), middle (2) and, posterior (3) (Fig. 4.7).

4.1.2.2 Abduction and adduction

The gluteus medius (Fig. 4.7) is the major abductor acting in the hip with the gluteus minimus (Fig. 4.7) assisting [71]. These muscles stabilise the pelvis during the support phase of walking and running and in the one-legged stance [4]. Like the gluteus maximus, each of them is represented by three muscular units: anterior (1), middle (2) and posterior (3) (Fig. 4.7).

The hip adductors are the muscles that cross the joint medially: adductor longus, adductor brevis, adductor magnus, and gracilis (Fig. 4.8). Adductor longus is attached over a wide area on the femur and is therefore considered as three muscles: superior (1), middle (2) and inferior (3) (Fig. 4.8). The hip adductors also contribute to the flexion and internal rotation of the hip, particularly when the femur is externally rotated [71].

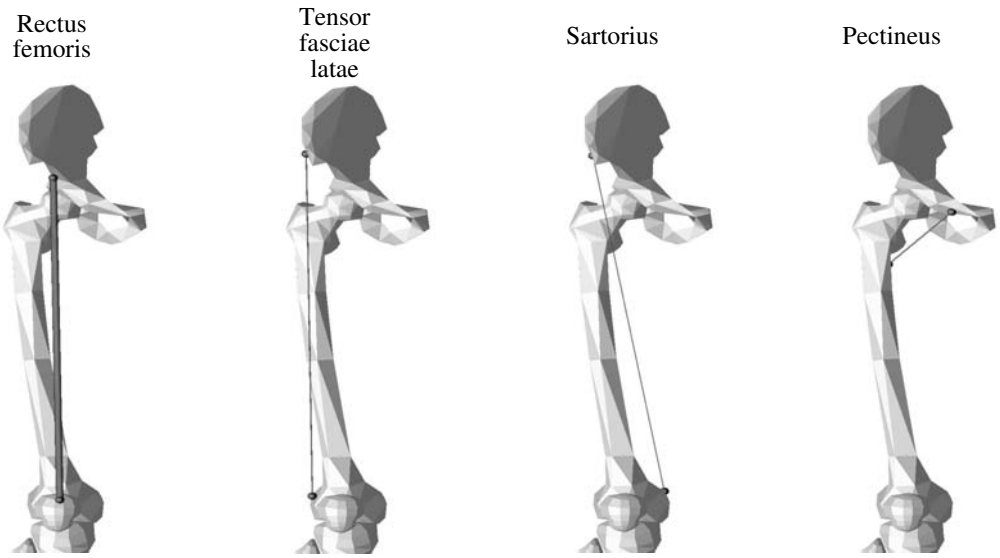

Figure 4.5: Assistant flexor muscles of the hip.

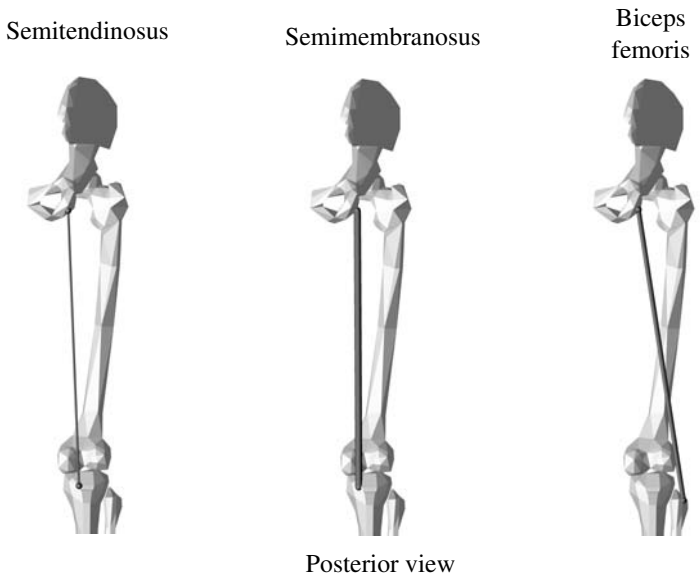

Figure 4.6: The hamstrings, posterior view.

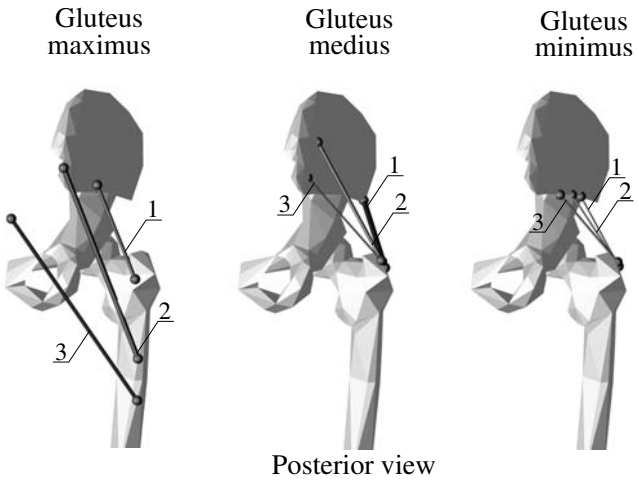

Figure 4.7: The three gluteal muscles.

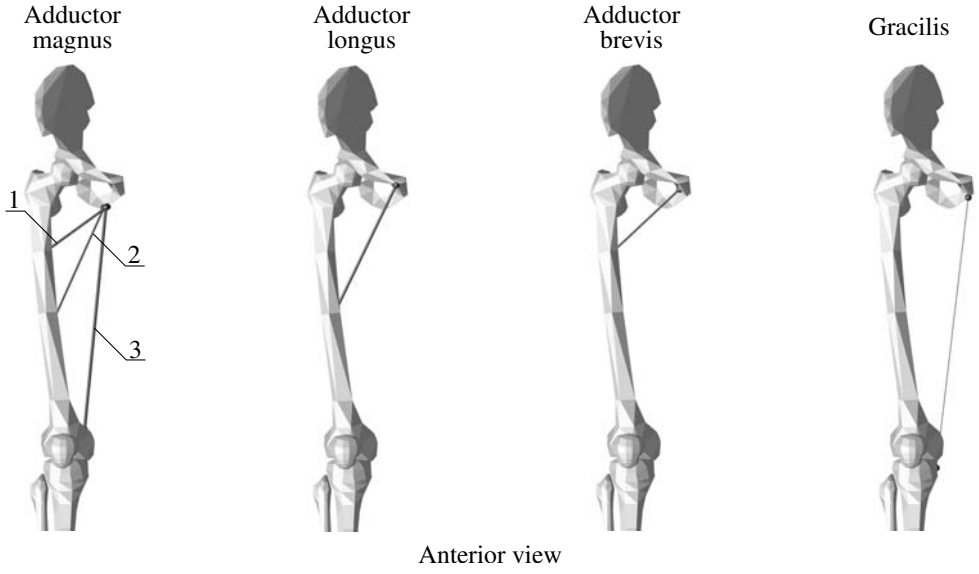

Figure 4.8: Adductor muscles of the hip.

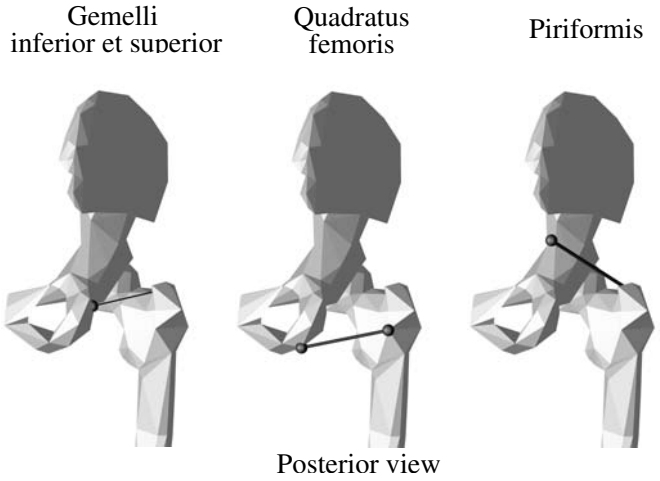

Figure 4.9: The lateral rotators muscles of the femur.

4.1.2.3 Medial and lateral rotation

Although several muscles contribute to the lateral rotation of the femur, there are six muscles acting solely as lateral rotators. These are: piriformis, gemellus superior, gemellus inferior, obturator internus, obturator externus, and quadratus femoris [4]. Musculus gemelus superior and inferior represents one muscle unit (Fig. 4.9). The muscles obturator externus, obturator internus and musculus piriformis were lumped together into one muscular unit called after the musculus piriformis (Fig. 4.9).

The major medial rotator of the femur is the gluteus minimus with the assistance of the tensor fascia latae, semitendinosus, semimembranosus, and the four adductor muscles [71] (Figs. 4.5, 4.6, 4.8).

i	Muscle	r_x [cm]	r_y [cm]	r_z [cm]	r'_x [cm]	r'_y [cm]	r'_z [cm]	$PCSA$ [cm^2]	F_{max} [N]	ρ_{spindle} [1/g]
1	adductor brevis	3.5	-1.7	5.2	12.0	-0.1	-2.9	6.4	286	1.3
2	adductor longus	2.7	-4.4	5.1	21.1	-0.5	-2.3	21.1	418	1.1
3	adductor magnus 1	6.1	-0.3	4.3	12.1	0.4	-3.4	35.2	346	0.9
4	adductor magnus 2	6.3	0.7	3.7	22.9	-0.5	-2.3	25.3	312	0.9
5	adductor magnus 3	6.2	0.1	4.1	38.4	-0.7	2.7	23.4	444	0.9
6	gemelli inferior et superior	2.5	3.7	-0.3	0.3	1.4	-4.4	10.0	109	3.7
7	gluteus maximus 1	-11.8	4.3	-0.2	5.7	2.8	-4.7	27.9	382	0.8
8	gluteus maximus 2	-7.4	5.9	1.2	10.2	1.6	-4.2	27.0	546	0.8
9	gluteus maximus 3	-2.5	7.9	6.2	14.2	0.6	-4.1	27.5	368	0.8
10	gluteus medius 1	-8.7	-3.5	-5.3	1.2	2.2	-5.5	35.5	546	1.0
11	gluteus medius 2	-10.1	0.9	-0.8	0.6	2.6	-5.3	22.5	382	1.0
12	gluteus medius 3	-6.7	4.6	0.3	0.5	3.1	-5.2	29.4	435	1.0
13	gluteus minimus 1	-4.9	-2.9	-3.8	1.0	0.7	-5.6	10.2	180	2.2
14	gluteus minimus 2	-5.0	-1.3	-3.1	1.0	1.0	-5.6	12.5	190	2.2
15	gluteus minimus 3	-5.0	0.7	-1.7	0.8	1.4	-5.5	18.4	215	2.2
16	iliacus	-9.3	-0.9	-1.7	6.2	1.9	-1.3	31.9	429	1.8
17	pectineus	2.0	-3.3	2.3	8.2	1.2	-2.5	5.9	177	1.3
18	piriformis	-5.7	6.4	4.5	0.4	1.5	-4.4	35.0	296	3.5
19	psoas	-14.5	-1.1	3.9	6.0	1.9	-1.0	29.9	371	1.8
20	quadratus femoris	5.8	3.8	1.6	3.6	3.8	-3.7	20.9	254	1.9
21	biceps femoris long	4.3	4.8	0.1	46.0	-0.8	-4.6	25.4	717	0.8
22	gracilis	4.7	-2.0	6.0	47.1	-2.2	2.0	3.1	108	1.5
23	sartorius	-5.5	-6.1	-5.6	47.1	-4.0	2.2	6.4	104	1.2
24	semimebranosus	4.5	4.3	-0.1	44.1	0.8	1.6	52.8	1030	0.6
25	semitendinosus	4.8	4.8	0.8	48.3	-1.9	1.6	12.7	328	1.5
26	tensor fascie latae	-7.8	-4.5	-5.6	43.6	-2.2	-3.3	10.6	155	1.0
27	rectus femoris	-2.6	-4.7	-2.9	41.5	-4.3	-0.2	35.1	779	0.9

Table 4.1: Muscles of the hip. The coordinate of the proximal muscle attachment (r_x, r_y, r_z) and the distal muscle attachment (r'_x, r'_y, r'_z) after Delph & Loan, 1995, physiological cross-sectional area of the muscle ($PCSA$) after Yamaguchi, 1990, maximum isometrical force F_{max} after Brand et al., 1986 and density of the muscles spindles organs (ρ_{spindle}) after Stillman, 2000.

4.2 HIP JOINT REACTION FORCE IN ONE-LEGGED STANCE

In our work the model for the calculation of the resultant hip force in the one-legged stance was used. The basis of this model has been developed by A. Iglič and coworkers at the University of Ljubljana [93, 95, 94]. They used a method of reduction for solving the problem of muscle redundancy. In our work we have upgraded the current model by increasing the number of muscles (see section 4.1). Since the large amount of muscles does not allow to use a method of reduction we have used the method of optimisation to assess unknown muscle forces. In this part we will describe assumption and derivations of the equations of the model.

The model assumes that the body is in static position of one-legg standing. Assuming static state of equilibrium simplifies the calculation since the motion of the segments of human body and inertial forces related to the motion need not to be considered (Fig. 3.1). Static position of the body could also be used to estimate load of the hip joint during swing phases of gait in which acceleration is small [45, 152].

The one-legged stance was chosen by many authors [22, 96, 111, 118, 148, 190] as the most appropriate position to assess the load of the hip joint because it represents one of the most frequent body position in everyday activities. The one-legged stance corresponds to phase 16 of the stance period of gait after Fischer [121].

The human body could be divided into two segments in the one-legged stance. The first segment is the loaded leg and the second segment is the rest of the body. In the one-legged stance the hip joint bears partial body weight ($\mathbf{W}_B - \mathbf{W}_L$), where $\mathbf{W}_B$ is the body weight and the $\mathbf{W}_L$ is the weight of the loaded leg. Since the first and the second segment of the human body defined above are assumed to behave as stiff bodies, it is obvious that rotation can occur in the hip joint only (Fig. 4.10). Therefore, the muscle force is needed to maintain balance [118, 148, 127].

In the one-legged stance pelvis and loaded leg are rotated with respect to the neutral posture [94]. The rotation of the pelvis in the frontal plane around the y-axis is described by the angle φ while the rotation of the femur around y-axis is described by the angle ϑ (Fig. 4.10). In the one-legged stance the values of the φ was taken to be 0° while the angle ϑ was computed as [95]:

$$\vartheta = \arcsin\frac{b}{x_0} \tag{4.1}$$

where $x_0 = 42.3$ cm [51] is the length of the femur and b is the z-coordinate of the moment arm of the weight of the loaded leg $\mathbf{W}_L$ (Fig. 4.10).

The muscles are modelled as spring elements connecting their proximal ($\mathbf{r}_i$) and distal attachment ($\mathbf{r}'_i$) (section 4.1.2). The unit vector in the direction of the

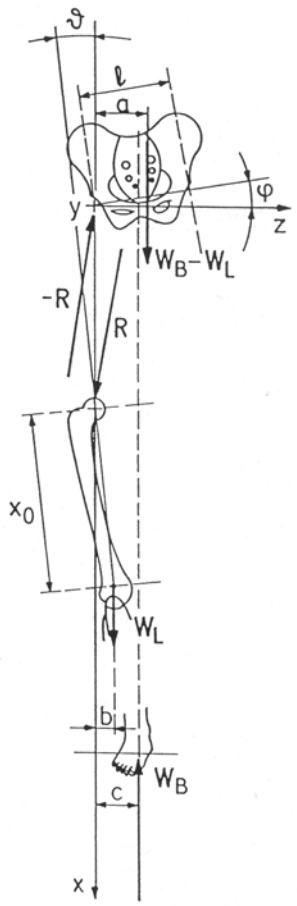

Figure 4.10: The characteristic forces, moments arms and geometrical parameters of the described model of the hip in one-legged stance body position. After Iglič et al., 2002.

force of i-th muscle is expressed: [95]:

$$\mathbf{e}_i = \frac{\mathbf{r}'_i - \mathbf{r}_i}{|\mathbf{r}'_i - \mathbf{r}_i|} \tag{4.2}$$

and the force of i-th muscle is:

$$\mathbf{F}_i = F_i\, \mathbf{e}_i \tag{4.3}$$

where F_i is the magnitude of the force $\mathbf{F}_i$.

In the static posture the force and moment equilibrium equations for the upper body (second segment) must be fulfilled [89].

$$\sum_{i=1}^{N} \mathbf{F}_i - \mathbf{R} + (\mathbf{W}_B - \mathbf{W}_L) \;=\; 0 \tag{4.4}$$

$$\sum_{i=1}^{N}(\mathbf{r}_i \times \mathbf{F}_i) + \mathbf{a} \times (\mathbf{W}_B - \mathbf{W}_L) = 0 \tag{4.5}$$

where N is the number of muscles, $\mathbf{a} = (0, 0, a)$ is the moment arm of the weight of the upper body $(\mathbf{W}_B - \mathbf{W}_L)$ and i runs over all muscles. The magnitude of the moment arm of the force $(\mathbf{W}_B - \mathbf{W}_L)$ is determined from the y-component of the moment equilibrium equations for the first and the second body segment:

$$-W_B\, c + W_L\, b - M_{I,y} = 0 \tag{4.6}$$

$$(W_B - W_L)\, a + M_{I,y} = 0 \tag{4.7}$$

where a is z-coordinate of the moment arm $\mathbf{a}$, c is z-coordinate of the moment arm of the ground reaction force $-\mathbf{W}_B$ (Fig. 4.10) and $M_{I,y}$ is y-component of intersegmental moment $\mathbf{M}_I = \sum_i(\mathbf{r}_i \times \mathbf{F}_i)$. It follows from Eqs. (4.6) and (4.7) [137]:

$$a = \frac{W_B\, c - W_L\, b}{W_B - W_L} \tag{4.8}$$

The coordinates b and c are expressed by the interhip distance l: $b = 0.24\, l$ and $c = 0.5\, l$ [137]. The weight of the leg can be approximated by the relation $W_L = 0.16\, W_B$ [94].

In this mathematical model the equilibrium of the body in the one-legged stance is described by six scalar equations given by three components of the vector equilibrium given by Eqs. (4.4) and (4.5) and $3 + N$ unknowns (three components of the force $\mathbf{R} = (R_x, R_y, R_z)$) and N unknown magnitudes of the muscle forces (Eq. 4.3). The number of unknowns exceeds number of the model equations which makes the problem mathematically indeterminate [197].

In the original model of Iglič et al., 1993 nine muscular units were included: gluteus medius part 1–3; gluteus minimus part 1–3, tensor fasciae latae, rectus femoris, and gluteus piriformis [96] (Tab. 4.2). Position of the attachment points in the neutral upright posture were taken from Dostal & Andrews, 1981. $PCSA$ of each muscle is taken from Johnston et al., 1979 (Tab. 4.2). The force of each individual muscle included in the model were written as [96]:

$$\mathbf{F}_i = \sigma_i\, A_i\, \mathbf{e}_i \tag{4.9}$$

The problem of the muscle redundancy has been solved by the reduction method [94]. The muscles were divided into three groups according to their anatomical positions: anterior (α), middle (β) and posterior (γ) (Tab. 4.2) and average tension in the particular muscle group were assumed to be equal: σ_α in the anterior group,

i	Muscle	Group	r_x [cm]	r_y [cm]	r_z [cm]	r'_x [cm]	r'_y [cm]	r'_z [cm]	$PCSA$ [cm^2]
1	glutes medius 1	α	-10.2	-2.7	-6.2	2.6	1.8	-7.3	26.6
2	gluteus minimus 1	α	-7.3	-2.9	-4.1	2.7	-0.4	-6.9	13.3
3	tensor fasciae latae	α	-7.8	-4.5	-5.6	43.6	-2.2	-3.3	12.0
4	rectus femoris	α	-3.7	-4.3	-2.6	41.5	-4.3	-0.2	40.0
5	gluteus medius 2	β	-13.2	0.2	-1.8	2.6	1.8	-7.3	26.6
6	gluteus minimus 2	β	-8.8	0.4	-2.0	2.7	-0.4	-6.9	13.3
7	gluteus medius 3	γ	-9.7	4.8	1.5	2.6	1.8	-7.3	26.6
8	gluteus minimus 3	γ	-7.1	2.6	0.0	2.7	-0.4	-6.9	13.3
9	gluteus piriformis	γ	-5.5	7.8	4.7	0.1	0.1	-5.5	10.0

Table 4.2: Muscles of the model of Iglič et al., 1993. The proximal muscle attachment point (r_x, r_y, r_z), distal muscle attachment point (r'_x, r'_y, r'_z) and physiological cross-sectional area $(PCSA)$.

σ_β in the middle group and σ_γ in the posterior group. The equilibrium equations (Eqs. 4.4 and 4.5) can than be solved and the unknowns quantities (components of the hip joint reaction force R_x, R_y, R_z and stresses in particular muscle groups $\sigma_\alpha, \sigma_\beta, \sigma_\gamma$) are obtained.

The same model of the force in the hip joint was solved using optimisation procedure [94,132,133] . The optimisation criterion of minimal possible magnitude of the hip joint reaction force, i.e., minimal possible bone loading was taken. However, only one optimisation criterion was used and only nine muscles were taken into account (Tab. 4.2). This work is intended to test how the choice of the optimisation criterion in the optimisation method influences the load of the hip joint in the model with increased number of muscles.

4.2.1 Definition of the optimisation problem

Optimisation criterion has the form of the optimisation function G, which gives the relevance of the solution [41, 155, 163]. The problem of the optimisation algorithm is to find the solution that gives minimum or maximum value of the optimisation function while the equilibrium equations are fulfilled [143, 158, 181]. By taking into account equilibrium of the forces and the moments acting on the pelvis in the one-legged stance (Eqs. 4.4 and 4.5) the optimisation problem can be

defined:

$$\begin{array}{ll} \text{maximize or minimize} & G(F_1, \ldots, F_N, R_x, R_y, R_z) \\ \text{subject to} & \sum_{i=1}^{N} \mathbf{F}_i - \mathbf{R} + (\mathbf{W}_B - \mathbf{W}_L) = 0 \\ & \sum_{i=1}^{N} (\mathbf{r}_i \times \mathbf{F}_i) + \mathbf{a} \times (\mathbf{W}_B - \mathbf{W}_L) = 0 \end{array} \tag{4.10}$$

The definition of the optimisation problem (4.10) does not ensure that all the muscle forces will be non-compressive and do not exceed their physiological limits [74,181]. Therefore additional inequality constraints were defined which restrict the range of the muscle forces F_i.

$$0 \leq F_i \leq \sigma_{max}\, PCSA_i \qquad i = 1, \ldots, N \tag{4.11}$$

where the maximum allowed muscle force of the i-th muscle is directly proportional to the physiological cross-sectional area [44] and the maximum allowed tensile stress in the muscle (σ_{max}). In our work the value of 1 MPa was taken for σ_{max} [43, 74].

4.2.2 Optimisation criteria

In Tab. 3.1 different optimisation principles for muscle selection used in the inverse dynamical analysis are shown. To evaluate the model of the hip joint load in one-legg posture (section 4.2), optimisation criteria suitable for static analysis were taken.

- *Principle of minimal muscle force*: minimise the sum of the individual muscle forces to the power of n required for static equilibrium of the hip.

$$\text{minimize} \quad G_{F^n} = \sum_{i=1}^{N} F_i^n \tag{4.12}$$

  where different values of power n: 1,2,3,4,5,6 and 7 define seven optimisation criteria G_F, G_{F^2}, G_{F^3}, G_{F^4}, G_{F^5}, G_{F^6} G_{F^7}.

- *Principle of minimal muscle stresses*: minimise the sum of the average muscle stresses to the power of n.

$$\text{minimize} \quad G_{\sigma^n} = \sum_{i=1}^{N} \sigma_i^n \tag{4.13}$$

  where different values of power n: 1,2,3,4,5,6 and 7 define seven optimisation

criteria G_{σ}, G_{σ^2}, G_{σ^3}, G_{σ^4}, G_{σ^5}, G_{σ^6}, G_{σ^7}.

- *Principle of minimal normalised muscle force*: minimise the sum of the muscle force normalised to the maximal isometrical force F_{max} to the power n.

$$\text{minimize} \quad G_{(F/Fmax)^n} = \sum_{i=1}^{N} \left(\frac{F_i}{F_{max,i}} \right)^n \tag{4.14}$$

where different values of power n: 1,2 define two optimisation criteria $G_{F/Fmax}$, $G_{(F/Fmax)^2}$. The sum of the muscle forces can be also normalised to the magnitude of the joint moments at the maximal isometrical contraction M_{max}

$$\text{minimize} \quad G_{(F/Mmax)^n} = \sum_{i=1}^{N} \left(\frac{F_i}{M_{max,i}} \right)^n \tag{4.15}$$

where different values of power n: 1,2 define two optimisation criteria $G_{F/Mmax}$, $G_{(F/Mmax)^2}$ and $M_{max,i}$ is defined as following:

$$\mathbf{M}_{max,i} = F_{max,i} \left(\mathbf{r}_i \times \mathbf{e}_i \right) \tag{4.16}$$

To include antagonistic muscles in solving the indeterminate problems the values of the weight coefficients in polynomial criteria (coefficients w in Eq. 3.1) for antagonist have to be opposite sign than the sign of their agonists [158]. In the one-legged stance the equilibrium is maintained by the abductors (section 4.1.2.2) with the antagonistic muscles adductors. Abductors and adductors cause rotation of the pelvis in the frontal plane [71]. The sign of the y-component of the joint moment at the maximum isometrical contraction of the i-th muscle (M_{max,i_y}) determine the direction of the rotation of the pelvis in the frontal plane (Fig. 4.10), i.e., the abduction or adduction. In this work we modify the criterion (4.15) following the sign of the joint moment of i-th muscle. The new definition of the criterion should improve the activation of adductors.

$$\text{minimize} \quad G_{M_y(F/Mmax)^n} = \sum_{1}^{N} \text{sign} \left(M_{max,i_y} \right) \left(\frac{F_i}{M_{max,i}} \right)^n \tag{4.17}$$

where different values of power n: 1,2 define two optimisation criteria $G_{M_y(F/Mmax)}$ and $G_{M_y(F/Mmax)^2}$.

- *Principle of minimal contact force in the hip joint*: minimise the magnitude of the hip joint reaction force $\mathbf{R}$. We present two different criteria: one for

linear (G_{Rlin}) and one for nonlinear optimisation (G_{Rnonlin}).

$$\text{minimize} \quad G_{\text{Rlin}} = |R_x| + |R_y| + |R_z| \tag{4.18}$$
$$\text{minimize} \quad G_{\text{Rnonlin}} = \sqrt{R_x^2 + R_y^2 + R_z^2} \tag{4.19}$$

- *Double linear programming*: minimise the maximum muscle stress and than minimise the sum of the total muscle forces with the value of σ_{max} from the first optimisation as an upper muscle stress constraint.

$$\text{minimize} \quad \max_i \sigma_i \quad \text{and} \quad \text{then} \quad \text{minimize} \quad G_F \tag{4.20}$$

- *Soft saturation criterion*

$$\text{maximize} \quad G_{\text{soft saturation}} = \sum_{i=1}^{N} \sqrt{1 - \sigma^2} \tag{4.21}$$

4.2.3 Optimisation algorithm

According to the mathematical complexity, the optimisation functions can be divided into two groups: linear and nonlinear functions (section 3.1.2.1). The linear optimisation function consists of linear combination of the optimised variables. Among linear function there are G_F, G_σ, $G_{F/Fmax}$, $G_{F/Mmax}$, $G_{M_y(F/Mmax)}$ and G_{Rlin}. Other functions defined above are nonlinear.

The type of the optimisation algorithm depends on the type of the optimisation function. If G is a linear function, the problem (4.10) can be solved using simplex method. For nonlinear expression of $G(x)$ more sophisticated algorithms have to be applied.

4.2.3.1 Linear optimisation - simplex method

The linear optimisation called also linear programming concerns itself with the following problem [115, 154]:

$$\begin{aligned} &\text{minimize} && \mathbf{c} \cdot \mathbf{x} \\ &\text{subject to} && \mathcal{A}\mathbf{x} \leq \mathbf{b} \\ & && \mathbf{x} \geq 0 \end{aligned} \tag{4.22}$$

where $\mathbf{x} \in R^{N+3}$ are in our case internal forces of the mechanism, $N + 3$ is equal to the number of muscle forces plus components of the joint force, $\mathbf{c} \in R^{N+3}$ is a column vector of constants corresponding to weight coefficients in Eq. (3.1), $\mathcal{A}$ is a

matrix of constraint's coefficients with $N+3$ columns and M rows, where M is the number of constraints and $\mathbf{b} \in R^M$ is a column vector. The matrix $\mathcal{A}$ is generally not square, it has usually more rows than columns, and is therefore undetermined, leaving great latitude in the choice of $\mathbf{x}$ with which to minimise $\mathbf{c} \cdot \mathbf{x}$ [154]. The function to be minimised as well as the constraints are in the linear form. The coefficients $\mathbf{A}, \mathbf{b}, \mathbf{c}$ can have either sign or be zero [154].

We have solved the linear optimisation program (4.22) by the simplex method implemented in the GNU Octave as the module lin_prog (Appendix C). The simplex method is based on fixing enough of the variables at their bounds to reduce the constraints $\mathcal{A}\mathbf{x} \leq \mathbf{b}$ to a square system, which can be solved for unique values of the remaining variables [115]. The simplex method is an iterative procedure, solving these system of linear equations in each of its steps, and stopping when the optimum is reached. Detailed description of the algorithms of the simplex method can be found in specialised literature [154].

4.2.3.2 Nonlinear optimisation

For solving nonlinear optimisation problems the SOLNP module for MATLAB was used (Appendix D). After minor adjustments of the source code, it was possible to use this module in GNU Octave as well. The SOLNP module was written by Ye, 1989 and it solves the general nonlinear optimisation programming problem in the form:

$$\begin{aligned} &\text{minimize} && f(\mathbf{x}) \\ &\text{subject to} && g(\mathbf{x}) = 0 \\ & && \mathbf{l}_h \leq h(\mathbf{x}) \leq \mathbf{u}_h \\ & && \mathbf{l}_x \leq \mathbf{x} \leq \mathbf{u}_x \end{aligned} \tag{4.23}$$

where in our case $\mathbf{x}$ are variables such as joint forces and muscle stresses with its lower and upper bounds $\mathbf{l}_x$ and $\mathbf{u}_x$ respectively, $g(\mathbf{x})$ corresponds to equilibrium equations (Eqs. 4.4, 4.5) and $f(\mathbf{x})$ is a cost function. The module SOLNP requires: $\mathbf{x} \in R^{N+3}$, $f(\mathbf{x}) : R^{N+3} \rightarrow R$, what means that function $f(\mathbf{x})$ gives a scalar which is consistent with the definition of the optimisation function G (Eq. 3.1), $g(\mathbf{x}) : R^N \rightarrow R^m$, where $m = 6$ is equal to the number of equilibrium equations (Eq. 4.10), $\mathbf{l}_x, \mathbf{u}_x \in R^{N+3}$ and $\mathbf{l}_x < \mathbf{u}_x$. Lower and upper bonds of the variable $\mathbf{x}$ ($\mathbf{l}_x$ and $\mathbf{u}_x$ respectively) correspond to the physiological constraints of the muscle force (Eq. 4.11). The additional constraint $h(\mathbf{x})$ was not used in our calculations

and the problem (4.23) was converted into:

$$\begin{array}{ll} \text{minimize} & f(\mathbf{x}) \\ \text{subject to} & g(\mathbf{x}) = 0 \\ & \mathbf{l}_x \leq \mathbf{x} \leq \mathbf{u}_x \end{array} \tag{4.24}$$

The k-th major iteration of SOLNP iteratively solves a linearly constrained optimisation problem with an augmented Lagrangian objective function using a combination of linear programming and sequential quadratic programming using Broyden-Fletcher-Goldfarb-Shanno's technique. The further description of the algorithms used in the module SOLNP is given in Ye, 1989.

4.2.4 Synergism index of the muscle activity

It has been suggested that optimal activation pattern of the muscle should be related to the muscle synergism [52, 133, 181]. Synergism of the muscle activity means that the net force for the given activity is distributed between several muscles. To describe the synergism of the muscle we define a new variable: the muscle synergism index S. The definition of the muscle synergism index is based on the assumption that the maximum synergism is obtained if the stress σ_i (Eq. 3.2) in all muscles is the same. For a given activation pattern of the muscles the muscle synergism index (S) is defined as following:

$$S = \sum_{i=1}^{N} \frac{\sigma_i}{\max\limits_j \sigma_j} - 1 \tag{4.25}$$

where $\max\limits_j \sigma_j$ is the maximum value of the muscle stress for a given muscle force pattern. If only one muscle is active, i.e. it exists no muscle synergism, the muscle synergism index is zero. The highest synergism index could be obtained if the stress in all muscles would be the same and it would have the value of $N-1$ where N is the number of the muscles.

4.2.5 New type of the optimisation criterion

The optimisation criteria mentioned above (section 4.2.2) operate with the physical quantities like the muscle forces and stresses (Tab. 3.1), but they do not take into account how these mechanical variables are sensed in the human body. If the muscle activity is controlled by the central neural system, then the inputs into this system may play a crucial role in the final regulation. In this section we will propose a new type of the optimisation function which is based on the signals from the mechanoreceptors in the human body. In further consideration

the human body will be assumed to be in the static state of equilibrium. This assumption allows us to neglect signals that refer to human motion.

The process, by which the body can vary muscle contraction in response to incoming information is defined as proprioception [169]. The proprioception refers to all sensor inputs from the musculoskeletal system, which includes inputs from the joint receptors as well as the muscle spindles and the tendon receptors [166]. The latter two were most thoroughly studied and identified as having important and specific action on the motor neuron and somatic muscle [55, 116, 169]. Muscle spindles are encapsulated adapted muscle fibres placed parallel to the force generating muscle fibres [169]. The muscle spindles provide information about the changes in the length of the muscle and are considered to be included in the processes of the preservation of the muscle tone [46, 157, 169]. Golgi tendon organs are encapsulated corpuscles consisting of an elongated fascicle of the collagen bundles attached at one end to individual tendons of a small fascicle of muscle fibres and at other end to the complete muscle tendon or aponeurosis [166]. Each receptor is thus placed "in series" with a set of the muscle fibres. The tension of the collagen bundles causes compression of the intertwined afferent axons, making these axons very sensitive to small changes of the muscle force. In conclusion, Golgi tendon organs can be regarded as receptors of the muscle force and force changes while the muscle spindles react in response to the muscle length and its changes [156, 166, 169].

Our definition of the optimisation function is intended to be used in the static model of the one-legg posture (section 4.2). Therefore the signals from the receptors which refer to changes in the muscle length (the muscle spindles) are assumed to be negligible.

A comparison of the hip joint contact force in vivo measured with those calculated hip joint contact force showed a good agreement if the minimisation of the muscle force was used as the optimisation criterion [74]. Receptors which responds to the muscle force sensation are the Golgi tendon organs [42, 192]. It seems reasonable to assume that for regulation of the muscle activity by the central neural system in static posture the signal from the Golgi tendon organ may be important [192]. Considering the reasoning mentioned above we suggest a following hypothesis of the regulation of the muscle forces:

The muscle activity is regulated to obtain a minimum signal from the Golgi tendon receptors.

To be used in the inverse dynamics this criterion should be expressed analytically by an optimisation function. In the following, two modes of this criterion are presented: linear and nonlinear.

4.2.5.1 *Linear criterion*

In the linear criterion we will assume that the signal from the Golgi tendon receptor is proportional to the muscular force what is admissible for static response of the Golgi tendon organs [42, 156]. Since the resultant force of the muscle is proportional to the number of the motor fascicle activated, the accumulated signal from the Golgi tendon organs of the whole muscle is proportional to the resultant muscle force. The density of the receptors will affect the resultant signal from the muscles as well. The higher the muscular force and the more Golgi tendon organs are present, the higher the afferent signal. Mathematically linear optimisation function G_{lin} can be expressed:

$$\text{minimize} \quad G_{\text{GTOlin}} = \sum_{i=1}^{N} w_i \, F_i \tag{4.26}$$

where w_i are relative weights F_i which corresponds to the number of the Golgi tendon organs in the i-th muscle $N_{\text{GTO}i}$.

$$w_i = N_{\text{GTO}i} \tag{4.27}$$

As there are about 80% as many tendon organs in a typical limb muscle as spindles [157], the number of the Golgi tendon organs can be estimated from the number of the muscle spindles in the i-th muscle.

$$N_{\text{GTO}i} = 0.8 \, \rho_{\text{spindle}i} \, m_i \tag{4.28}$$

where $\rho_{\text{spindle}i}$ is the density of the muscle spindles of the i-th muscle and m_i is the mass of the i-th muscle which can be expressed:

$$m_i = \rho \, l_{0i} \, PCSA_i \tag{4.29}$$

where ρ is the muscle density, $PCSA$ is the physiological cross-sectional area of the i-th muscle (Tabs. 4.1, 4.2) and l_{0i} is its resting length. It was assumed, that the muscle density of all muscles of the hip is equal to 1040 kg/m^3 [165]. Length of the muscle can be computed from the position of the attachments points of the i-th muscle (Tab. 4.1, 4.2).

$$l_{0i} = |r_i - r'_i| \tag{4.30}$$

Constant	Unit	Model 1	Model 2
a	impulses/s	40	-
b	1/N	0.3524	-
c	N	0.857	-
$F_{\text{threshold1}}$	N	0.17	-
A	impulses/s	-	60
B	N	-	4

Table 4.3: Golgi tendon organ models parameters. After Rådman, 2002 and Lin & Crago, 2002.

4.2.5.2 Nonlinear criterion

Nonlinear transfer function follows from the measurements of the response of a single Golgi tendon organ [166]:

$$r_i = a\left(b\left(F_{\text{eff1}i}\right) + \left(1 - e^{-\frac{F_{\text{eff1}i}}{c}}\right)\right) \tag{4.31}$$

where r_i is the response in impulses per second of a single Golgi tendon organ activated by the force F_{1i} and $F_{\text{eff1}i}$ is the effective force sensed by a single Golgi tendon organ, i.e., the force over its threshold level $F_{\text{threshold1}}$:

$$F_{\text{eff1}i} = \begin{cases} 0 & F_i \leq F_{\text{threshold1}} \\ F_{1i} - F_{\text{threshold1}} & F_{1i} > F_{\text{threshold1}} \end{cases} \tag{4.32}$$

where F_{1i} is the force acting on a single Golgi tendon organ in the i-th muscle. Coefficients a, b and $F_{\text{threshold1}}$ were determined experimentally [42] and their values are presented in Tab. 4.3. We will assume that the resultant muscle force of the i-th muscle is equal to the sum of the muscle forces of all muscle fascicles and that an activity of a muscle fascicle is sensed by a single Golgi tendon organ. The muscle fibres are not activated uniformly throughout the muscle and force in particular fascicles differs [46]. Up to now, the exact activation of the fibres within a muscle has not been described. Therefore, we will assume that all the muscle fibres in a given muscle are activated uniformly and the force generated by one muscle fascicle is:

$$F_{1i} = \frac{F_i}{N_{\text{GTO}i}} \tag{4.33}$$

where F_i is the force of the i-th muscle and $N_{\text{GTO}i}$ is the number of the Golgi tendon units in the i-th muscle (Eq. 4.28).

In the work of Lin & Crago, 2002 the nonlinearity of the Golgi tendon organ

as muscle force sensor was approximated as following:

$$r_i = A \ln\left(\frac{F_{1i}}{B} + 1\right) \tag{4.34}$$

where A and B are constants mentioned in Tab. 4.3.

As stated above in the new optimisation criteria the afferent signals into the central neural system will be minimised.

$$\text{minimize} \quad G_{\text{GTOnonlin}n} = \sum_{i=1}^{N} N_{\text{GTO}i}\, r_i \tag{4.35}$$

where $G_{\text{GTOnonlin1}}$ computes the response of Golgi tendon organs by Eq. (4.31) while $G_{\text{GTOnonlin2}}$ computes the response of Golgi tendon organs by Eq. (4.34).

4.3 MEASUREMENT OF THE HIP JOINT RESULTANT FORCE BY AN IMPLANTED INSTRUMENTED ENDOPROSTHESIS

The values of the hip joint resultant force $\mathbf{R}$ used in this work in activities other than one-legg standing were determined by prof. Bergmann in Germany using an implanted instrumented prosthesis [19]. The hip prostheses were instrumented with strain gauges and a telemetric device inside the hollow neck [16, 19]. From the strain gauge signals the three-dimensional vector of the resultant hip joint force $\mathbf{R}$ was determined. The described technique allows accuracy of the measurement of $\mathbf{R}$ to within 1% at a rate of approximately 200 Hz [16]. Together with the measurement of the force, a video motion analysis was performed in order to determine the kinematics of the segments of the body [18].

A detailed description of the method used for measuring of $\mathbf{R}$ and the corresponding experimental device is given in Heller et al., 2001. The measurements of $\mathbf{R}$ were performed in four (51 to 76 year-old) patients (3 men and 1 woman). Each walking cycle was performed several times by each patient. These single trials were then averaged, first for the individual patients and finally for all four patients. To average the values of $\mathbf{R}$ from the different patients, the measured values of $\mathbf{R}$ are taken relative to body weight $\mathbf{R}/W_B$. In our study we used the averaged data of all trials.

The hip joint resultant force was measured in a coordinate system which was fixed with respect to the femur [18]. Using the data of the motion of the pelvis and of the femur, the hip joint resultant force was first given within a coordinate system that is fixed with respect to the pelvis [15]. As discussed below, for calculating the stress distribution in the hip joint it is more appropriate that the coordinate system is fixed with respect to the acetabulum.

The position of the acetabular cup with respect to the pelvis coordinate system is determined as described in Bergmann, 2001. The origin of the pelvis Cartesian coordinate system and of the acetabular Cartesian coordinate system coincides with the centre of the femoral head. In the orthogonal coordinate system of the pelvis, the plane $x_p z_p$ is defined by the centres of the femoral head and by the centre of the L5-S1 body. The x_p axis passes through the centre of the femoral heads and points medially, the y_p axis points anteriorly, and the z_p axis points superiorly. The local coordinate system of the acetabulum is obtained after rotation of the pelvis coordinate system [15] for angle β around the x axis and then for angle γ around the z axis (Fig. 4.11). After the rotation the acetabular $x_a z_a$-plane is identical with the basis of the acetabular hemisphere and the $-y_a$ axis points to the top of the acetabular shell.

4.4 MATHEMATICAL MODELLING OF THE CONTACT STRESS DISTRIBUTION IN THE HIP

The basic assumptions of the mathematical model of the hip joint contact stress distribution presented in this work were described earlier [94, 98], where a mathematical model of the hip joint contact stress distribution for an arbitrary direction of force $\mathbf{R}$ was developed. However, the derivation of the model equations was rather long and intricate. Therefore we present in this work a new method for deriving of the model equations based on the special choice of the acetabular coordinate system and a new type of integration area elements. This approach considerably simplifies the derivation of the model equation and makes it more transparent.

In deriving the model equations, the following simplifications concerning the geometry of the hip and the mechanical properties of the articular cartilage were introduced: It is assumed that the femoral head has a spherical shape while the acetabulum forms a hemisphere (Fig. 4.11). The gap between these two rigid spherical surfaces is occupied by a cartilage which is considered to be an ideally elastic material, i.e., it is assumed that it obeys Hooke's law. Upon loading, the femoral head is moved toward the acetabulum and the cartilage is squeezed. Due to the assumed sphericity of the bone surfaces there is only one point where the spherical surfaces of the acetabulum and the femur are the closest. This point is called the stress pole (Fig. 4.11) [29]. Since the cartilage completely fills the gap, the deformation of the cartilage is highest at the stress pole. From the sphericity of the bone surfaces it can be derived that the strain in the cartilage layer at any point of the weight bearing area is proportional to the cosine of the angle between this point and the stress pole [28, 68]. According to Hooke's law the contact stress in the cartilage is proportional to the strain in the cartilage, i.e., to the displacement of the femoral head with respect to the acetabulum. The sphericity of the hip surfaces and the ideal cartilage elasticity described above yield the cosine stress distribution function with its maximum at stress pole p_0 [28]:

$$p = p_0 \cos \nu \tag{4.36}$$

where ν is the angle between the given point and the stress pole. The area of nonzero contact stress is called the weight bearing area A.

Integration of the contact stress over the weight bearing area A gives the resultant hip force $\mathbf{R}$:

$$\int_A p \, \mathrm{d}\mathbf{S} = \mathbf{R} \tag{4.37}$$

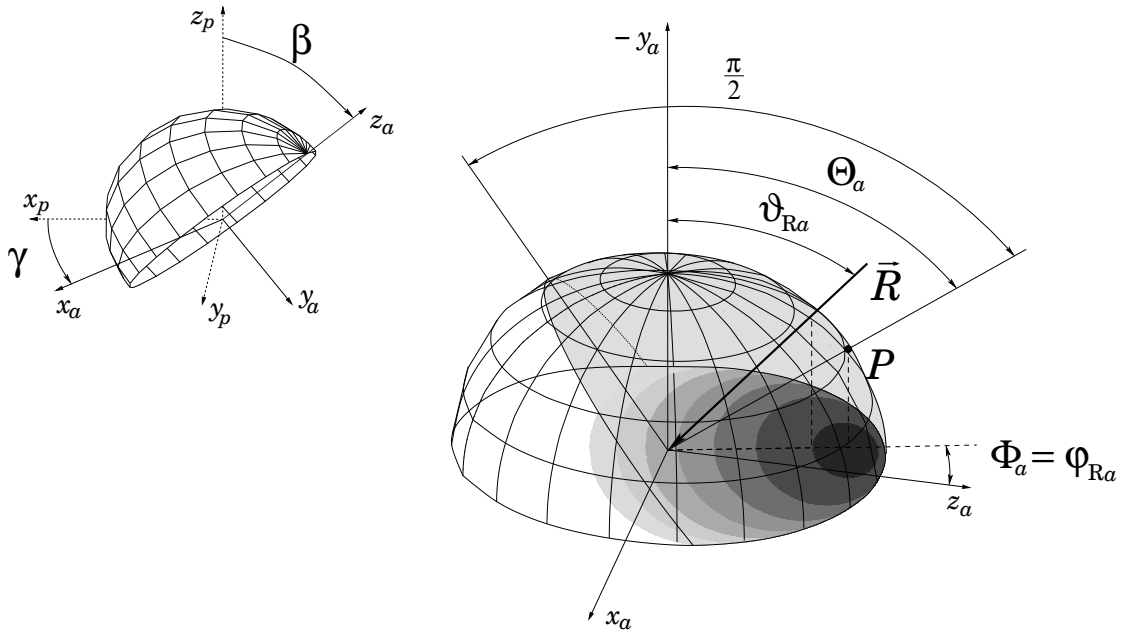

Figure 4.11: Position of the acetabular coordinate system (x, y, z) with respect to the pelvic coordinate system (x_p, y_p, z_p) [15] (left) and schematical presentation of the acetabular hemisphere and the acetabular coordinate system (right). The weight bearing area is marked by shading, symbol P denotes position of the stress pole (right). The projection of the stress distribution in the xz-plane is also shown.

As the stress distribution function is known (Eq. 4.36), we have to determine the position of the stress pole and the value of the stress at the pole (p_0) in order to describe the stress distribution uniquely.

In contrast to the previous work [98], we now use the local coordinate system, which is fixed with respect to the acetabulum instead of global coordinates. The acetabular coordinate system is defined in accordance with Bergmann, 2001. The $-y_a$-axis is the axis of the symmetry of the acetabular hemisphere, x_a-axis points anteriorly and z_a-axis points laterally (Fig. 4.11). Introducing the acetabular coordinate system takes advantage of the symmetry of the acetabular hemisphere. In the acetabular coordinate system the hip joint resultant force $\mathbf{R}$ is defined by its magnitude R and by its direction, given by the spherical coordinates $\vartheta_{Ra}, \varphi_{Ra}$ (Fig 4.11). The position of the stress pole is also determined by spherical coordinates Θ_a and Φ_a (Fig. 4.11). The polar angles ϑ_{Ra} and Θ_a describe the angular displacement from the $-y_a$-axis, while the azimuthal angles φ_{Ra} and Φ_a describe the angular displacement of the pole from the $x = 0$ plane in counterclockwise direction.

Due to the symmetry of the acetabular coordinate system, where the y_a axis

is the axis of symmetry of the acetabular shell, angle Φ_a is given by the direction of force φ_{Ra} only. As shown in Fig. 4.11, force $\mathbf{R}$ and the y-axis of the acetabular coordinates determine the symmetry plane which divides the acetabular hemisphere into two equal parts. The contact stress distribution should satisfy the condition that integration of p over the area of both halves of the acetabular hemisphere (Fig. 4.12) gives the resultant hip force (Eq. 4.37). As the stress distribution in our model is symmetrical with respect to the stress pole (Eq. 4.36), the stress pole must lie in this symmetry plane defined by R and the y-axis ($\Phi_a = \varphi_{Ra}$).

Using appropriate rotation of the coordinate system around the y_a-axis for angle φ_{Ra} we obtain a new orthogonal coordinate system x'_a, y'_a, z'_a (Fig. 4.12). In the rotated coordinate system the pole of stress P as well as force $\mathbf{R}$ lie in the $x'_a = 0$ plane (Figs 4.11, 4.12).

In order to solve Eq. (4.37) the classical spherical coordinate system (Fig. 4.11) was used in the previous papers [93,98]. Classical spherical coordinates lead to the complex expression for the boundaries of the weight-bearing area. Therefore the corresponding integrals in Eq. (4.37) are mathematically complicated [98]. If the alternative spherical coordinate system is used the calculation of the integrals in vector Eq. (4.37) becomes much more simple and transparent [76]. The alternative spherical coordinates are defined as following:

$$x'_a = r \sin\varphi \tag{4.38}$$

$$y'_a = -r \cos\varphi \cos\vartheta \tag{4.39}$$

$$z'_a = r \cos\varphi \sin\vartheta \tag{4.40}$$

where r is the radius of the articular surface. Angles ϑ and φ are depicted in Fig. 4.12. In the rotated alternative coordinate system (Fig. 4.12) force $\mathbf{R}$ and the stress pole will have the spherical coordinates $\varphi'_{Ra} = 0$, $\vartheta'_{Ra} = \vartheta_{Ra}$ and $\Phi'_a = 0$, $\Theta'_a = \Theta_a$, respectively. In the rotated spherical coordinates the angle ν between the radius vector to the stress pole $\mathbf{r}_\mathrm{P} = (0, -r\cos\Theta_a, r\sin\Theta_a)$ and the radius vector to the given point on the articular surface $\mathbf{r} = (r\sin\varphi, -r\cos\varphi\cos\vartheta, r\cos\varphi\sin\vartheta)$ can be expressed using the scalar product of $\mathbf{r}_\mathrm{P}$ and $\mathbf{r}$:

$$\cos\nu = \frac{\mathbf{r}\cdot\mathbf{r}_\mathrm{P}}{r^2} = \cos\varphi\cos\vartheta\cos\Theta_a + \cos\varphi\sin\vartheta\sin\Theta_a \tag{4.41}$$

Then the stress distribution function (Eq. 4.36) is expressed in the alternative coordinate system with the pole in the $x'_a = 0$ plane, as follows

$$p = p_0\,(\cos\varphi\cos\vartheta\cos\Theta_a + \cos\varphi\sin\vartheta\sin\Theta_a) \tag{4.42}$$

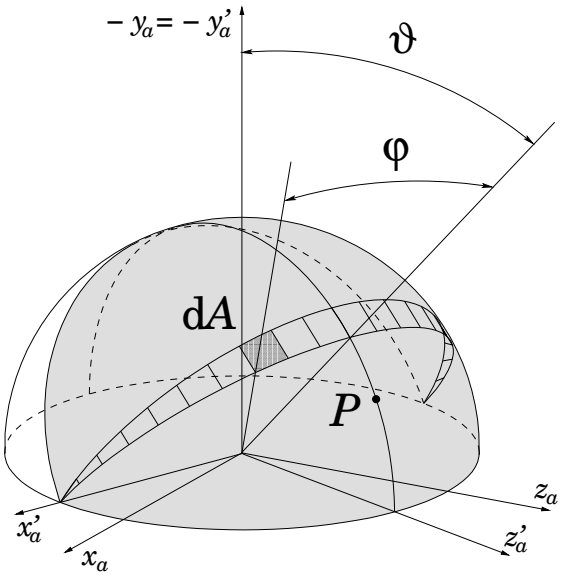

Figure 4.12: Rotated acetabular coordinate system (x'_a, y'_a, z'_a) and the alternative spherical coordinate system in the acetabular reference frame. Weight-bearing area is shaded and the elementary area dA is shown. The symbol P denotes the position of the stress pole.

The elementary infinitesimal integration area in the alternative coordinate system is:

$$\mathrm{d}\mathbf{A} = r^2 \cos\varphi\,(\sin\varphi, -\cos\varphi\,\cos\vartheta, \cos\varphi\,\sin\vartheta)\,\mathrm{d}\vartheta\,\mathrm{d}\varphi \tag{4.43}$$

In the new alternative coordinate system the integration in Eq. (4.37) can be performed over the fixed boundaries of the weight-bearing area, which considerably simplifies the derivation. The weight bearing area is limited at the lateral border by the acetabular rim ($\vartheta_L = \pi/2$, see Fig. 4.11) while the medial border is determined by the curve where the stress vanishes (Eq. 4.36), i.e., the lateral border consists of points with a constant angular distance $\pi/2$ from the stress pole ($\vartheta_M = \Theta_a - \pi/2$) (Fig. 4.11). Since the symmetry plane defined by force $\mathbf{R}$ and the y-axis splits the acetabular hemisphere into two symmetrical parts (Fig. 4.12), in the new alternative coordinate system angle φ runs from $-\pi/2$ to $\pi/2$ over the whole weight-bearing area.

It follows from Eqs. (4.42) and (4.43) that the y'_a and z'_a components of force $\mathbf{R}$ in Eq. (4.37) can be expressed in the form:

$$R\,\cos\vartheta_{Ra} = p_0\,r^2 \int_{\vartheta_M}^{\vartheta_L} \cos\vartheta\cos(\vartheta - \Theta_a)\,\mathrm{d}\vartheta \int_{-\frac{\pi}{2}}^{\frac{\pi}{2}} p\,\cos^3\varphi\,\mathrm{d}\varphi \tag{4.44}$$

$$R \sin \vartheta_{Ra} = p_0 \, r^2 \int_{\vartheta_M}^{\vartheta_L} \sin \vartheta \cos(\vartheta - \Theta_a) \, \mathrm{d}\vartheta \int_{-\frac{\pi}{2}}^{\frac{\pi}{2}} p \, \cos^3 \varphi \, \mathrm{d}\varphi \tag{4.45}$$

The integral for the x'_a component of force $\mathbf{R}$ is identically equal to zero due to the symmetry of the rotated coordinate system as discussed above (Fig. 4.12).

It follows from Eqs. (4.44) and (4.45) that the unknown spherical coordinate of the stress pole (Θ_a) can be obtained by solving the nonlinear equation:

$$\tan(\vartheta_{Ra} + \Theta_a) = \frac{\sin^2 \Theta_a}{\pi - \Theta_a + \sin \Theta_a \cos \Theta_a} \tag{4.46}$$

When the position of the stress pole (Θ_a, Φ_a) is calculated as described above, the value of the stress at the pole is then determined from the expression:

$$p_0 = \frac{3 \, R \, \cos(\vartheta_{Ra} + \Theta_a)}{2 \, r^2 \, (\pi - \Theta_a + \sin \Theta_a \cos \Theta_a)} \tag{4.47}$$

These equations are equivalent to the previously derived equations [98]. If the pole of the stress is located inside the weight-bearing area the peak contact stress p_{max} is equal to p_0. If the stress pole lies outside the weight-bearing area, the peak contact stress occurs at the point of the weight-bearing area closest to the stress pole and can be determined by using Eq. (4.36). In determining the position of the stress pole, not only the angle Θ_a, which defines the inclination of the pole from the acetabular axis of symmetry (Fig. 4.11), but also angle Φ_a should be taken into account, since it defines the meridional position of the pole with respect to the acetabular hemisphere. As was shown above, Φ_a is given by the direction of the force $\mathbf{R}$ (φ_{Ra}).

4.4.1 *Contact stress distribution in hips subjected to dysplasia of the hip*

The main radiographic parameter, that is used for assessment of the hip dysplasia, is the centre-edge angle of Wiberg ϑ_{CE} [189]. The centre-edge angle of Wiberg is an angle between the most lateral point of the acetabular roof visible on radiograph, centre of the femoral head, and sagittal plane [63, 118]. The size of ϑ_{CE} gives a numerical value of lateral coverage of the femoral head. The range from 20° to 25° is considered to be lower limit for normal hips, while the value below 20° is pathognomic for the hip dysplasia [118]. Therefore in our work the dysplastic hips were modelled as hips with a small lateral coverage of the femoral head.

As discussed above, for the calculating the stress distribution in the hip joint it is more appropriate that the coordinate system is fixed with respect to the acetabulum (Fig. 4.11). The same hip joint resultant force in global coordinates of the pelvis may attain various directions in the acetabular coordinates as the position of the acetabulum differs in normal and dysplastic hips. In our work the transformation to the acetabular coordinates depends on the method used to obtain force **R**.

If the force **R** is obtained after measurements by the implanted instrumented endoprosthesis [18, 19], the transformation from the pelvic coordinate system to the acetabular coordinate system is performed by two consequent rotations of the coordinate system around x and z axis for the angles β and γ respectively (see section 4.3). The values of the angles β and γ for a normal hip were taken from Bergmann, 2001, and are 70.3° and 49.4°, respectively. The centre-edge angle of Wiberg (ϑ_{CE}), which is the angle of the inclination of the acetabular cup against the z_p-axis (measured in the frontal plane), can be determined by angles β and γ [15]:

$$\vartheta_{CE} = \operatorname{arctg}(\tan\beta \sin\gamma) \tag{4.48}$$

If γ is equal to 90° then β is equal to the centre-edge angle. It can be seen from Fig. 4.11 that angle β also describes the lateral coverage of the acetabulum. Therefore we modelled dysplastic hips by taking angle β equal to 10° (Fig. 4.13). Angle γ is the same in normal hips and dysplastic hips.

If the mathematical model for calculation of the hip joint resultant force in one-legged stance was used, the force **R** was defined in the global coordinate system that origins in the centre of the femoral head (Fig. 4.10). The centre-edge angle of Wiberg gives the inclination of the acetabular cup in the frontal plane, which is identical to the xz plane in Fig. 4.10 [45, 118]. The force **R** in the acetabular coordinates can be obtained by rotating the coordinate system for angle

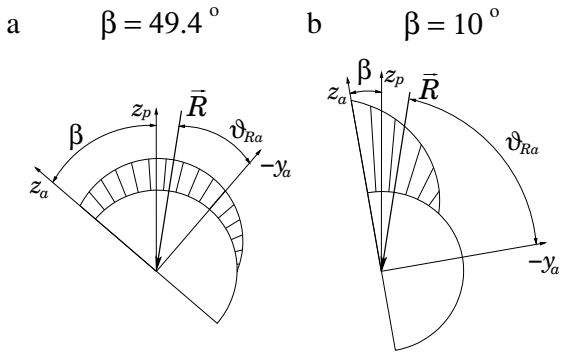

Figure 4.13: Schematical representation of the inclination of the acetabular cup and calculated stress distribution in normal (a) and dysplastic hip (b).

ϑ_{CE} around the y axis if no acetabular anteversion is assumed [64, 118]. However, the acetabular coordinate system obtained after a simple rotation for ϑ_{CE} would not agree to the acetabular coordinate system used to derive the equations of the model for contact stress distribution assessment (Fig. 4.11). The hip joint reaction force in these acetabular coordinates can be obtained by multiplying the vector $\mathbf{R}$ in the global coordinates (Fig. 4.10) by a transformation matrix $\mathcal{T}$ that represents the rotation for the angle ϑ_{CE} and axis transformation.

$$\mathcal{T} = \begin{pmatrix} 0 & -\sin\vartheta_{CE} & -\cos\vartheta_{CE} \\ 1 & 0 & 0 \\ 0 & -\cos\vartheta_{CE} & \sin\vartheta_{CE} \end{pmatrix} \tag{4.49}$$

The value of the centre-edge angle of Wiberg for a given patient can be measured from the standard antero-posterior radiograph as discussed below (section 5.2.1).

4.4.2 *Mathematical model of the stress on the hip joint articular surface in hips subjected to avascular necrosis of the femoral head*

A simple three dimensional mathematical model was developed for calculation of the distribution of the contact hip stress in the intact adult human hips [94,98]. This model is based on Hooke's law stating that the contact hip stress is proportional to strain within the cartilage between the femoral head and the acetabulum [28]. Such situation is present in intact hips where the bony femoral head and the acetabular shell squeeze the cartilage upon loading. However, if a part of the femoral head is damaged to such extent that it becomes too soft to be able to resist stress, this basic assumption of the above model [94,98] is no longer met over the whole surface of the femoral head. Therefore we have upgraded our previous model [94,98] by differentiating between the collapsed non-weight bearing necrotic segment and healthy weight bearing region the femoral head surface. The assumption of the collapsed necrotic part corresponds to stage IV according to Ficat [57] and Steinberg staging [173] and to stage 3 according to ARCO staging [62].

It is assumed that whole necrotic part lies inside the weight bearing area (Fig. 4.14). The non-weight bearing necrotic defect is taken to have the shape of spherical cap with the centre defined in global spherical coordinates by the angles ϑ_N and φ_N and the size defined by the angle ϑ_0 (Fig. 4.14). It means that all the points of the articular surface that have the angular direction from the centre smaller than ϑ_0 represents necrotic region and therefore could not bear weight. The Cartesian global coordinates system is identical to the coordinate system used in the previous work [93,98] and origins in the centre of the femoral head, $y = 0$ and $x = 0$ planes are identical to frontal and sagittal plane, respectively (Fig. 4.14).

If the necrotic part of the surface of the femoral head is collapsed, the non-weight bearing area appears above the collapsed region of the femoral head, decreasing the actual size of the weight bearing area. The actual size of the weight-bearing area should bear a hip joint resultant force Eq. (4.37). To simplify the solution the resultant hip force transmitted across the hip with necrosis could be expressed as:

$$\mathbf{R} = \int_A p \, \mathrm{d}\mathbf{S} - \int_{A_N} p \, \mathrm{d}\mathbf{S} \tag{4.50}$$

where the first integration is performed over the intact weight bearing area. In calculation of the first integral of Eq. (4.50) a mathematical model for the intact joint developed recently (section 4.4) could be used where the stress distribution is determined by the position of the stress pole in the global coordinates (Θ and Φ, Fig. 4.14) and by the value of the stress at the stress pole (p_0).

The second integration is performed over the necrotic region determined by

the angles ϑ_N, φ_N and ϑ_0 as described above (Fig. 4.14). The second integral in Eq. (4.50) is therefore equal to the force $\mathbf{R}_N$, which is not transmitted due to the presence of the non-weight bearing cap.

In calculation of the second integral in Eq. (4.50) we could utilise the symmetry of the non-weight bearing area. The coordinate system is rotated in such way, that the centre of the non-weight bearing cap coincides with the horizontal axis, i.e., the coordinate system is rotated for an angle φ_N about the z-axis and for an angle ϑ_N about the y-axis. In the rotated coordinate system (x', y', z') the necrosis will have coordinates $\vartheta'_N = 0$ and $\varphi'_N = 0$ and the pole of the stress will have coordinates Θ', Φ'. The classical coordinate system was used for calculation of the second integral in Eq. (4.50). The transformation equations of the classical spherical coordinate system are [110]:

$$x = r \cos\varphi \sin\vartheta \tag{4.51}$$

$$y = r \sin\varphi \sin\vartheta \tag{4.52}$$

$$z = r \cos\vartheta \tag{4.53}$$

The elementary area $\mathrm{d}\mathbf{A}$ can be expressed as following [110]:

$$\mathrm{d}\mathbf{A} = (\cos\varphi \sin\vartheta, \sin\varphi \sin\vartheta, \cos\vartheta)\, r^2 \sin\vartheta \,\mathrm{d}\vartheta \,\mathrm{d}\varphi \tag{4.54}$$

The stress distribution is described by a cosine function (Eq. 4.36). In the rotated coordinates the cosine of the angle between the radius vector to a given point on the non-weight bearing area ($\mathbf{r} = (r \cos\varphi \sin\vartheta, r \sin\varphi \sin\vartheta, r \cos\vartheta)$) and the radius vector to the stress pole ($\mathbf{r}_P = (r \cos\Phi' \sin\Theta', r \sin\Phi' \sin\Theta', r \cos\Theta')$) can be expressed using the scalar product of $\mathbf{r}_P$ and $\mathbf{r}$.

$$\cos\nu = \frac{\mathbf{r}\cdot\mathbf{r_P}}{r^2} = \cos\varphi \sin\vartheta \cos\Phi' \sin\Theta' + \sin\varphi \sin\vartheta \sin\Phi' \sin\Theta' + \cos\vartheta \cos\Theta' \tag{4.55}$$

Since it is assumed that the necrotic region has the shape of a spherical cap and lies inside the weight bearing area, the integration in the classical spherical coordinates can be performed over the fixed boundaries which rapidly simplifies the problem solution. After Eqs. (4.36), (4.54) and (4.55) the components of force $\mathbf{R}'_N$ in the rotated coordinate system (second integral in Eq. 4.50) can be expressed.

$$R'_{Nx} = \pi\, p_0\, r^2 \cos\Phi' \sin\Theta' \left(\frac{1}{3}\cos^3\vartheta_0 - \cos\vartheta_0 + \frac{2}{3}\right) \tag{4.56}$$

$$R'_{Ny} = \pi\, p_0\, r^2 \sin\Phi' \sin\Theta' \left(\frac{1}{3}\cos^3\vartheta_0 - \cos\vartheta_0 + \frac{2}{3}\right) \tag{4.57}$$

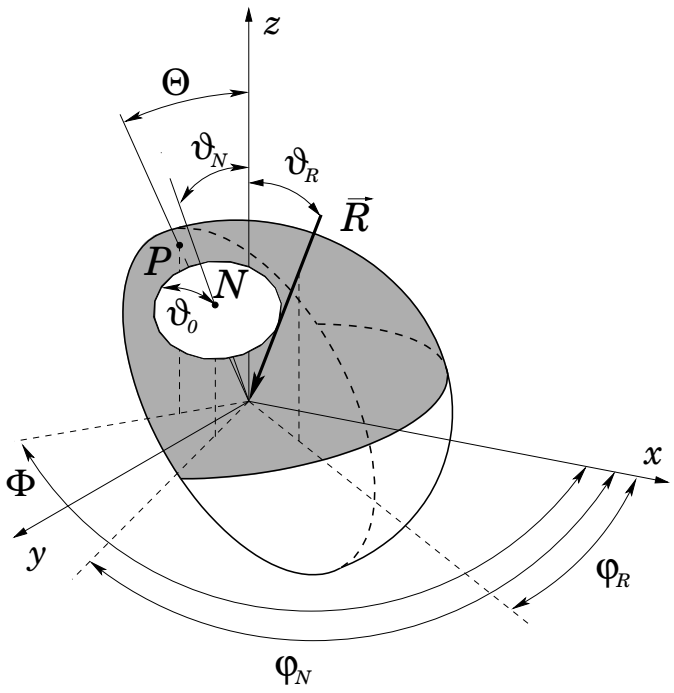

Figure 4.14: Schematical presentation of the articular surface. The weight bearing area is marked by shading, symbol P denotes the position of the stress pole and symbol N denotes the position of the centre of the necrosis.

$$R'_{Nz} = \pi\, p_0\, r^2\, \cos\Theta' \frac{2}{3}\left(1 - \cos^3\vartheta_0\right) \tag{4.58}$$

After finding the solution of the second integral in Eq. (4.50) in the rotated coordinates (Eqs. 4.56–4.58), the coordinate system is rotated to its original position, the necrotic part is returned to its original position and a proper direction of the non-transmitted force $\mathbf{R}_N$ is obtained.

Equation (4.50) is then solved numerically using the downhill-simplex method [154] and for given values of the hip joint resultant force ($\mathbf{R}$), position and size of the non-weight bearing cap ($\vartheta_N, \varphi_N, \vartheta_0$), and the geometry of the hip (r, ϑ_{CE}) the spherical coordinates of the stress pole (Θ, Φ) and the value of the stress at the stress pole (p_0) are determined. If the pole of the stress lies inside the weight bearing area than the stress pole coincides with the point of the peak contact stress (p_{max}). If the pole lies outside the weight bearing area than the point of the maximum stress is the point of the weight bearing area that is the closest to the stress pole and p_{max} in this point is calculated according to Eq. (4.36).

4.4.3 New biomechanical parameters describing status of the human hip joint

In the clinical practise it is very important to recognise a states of the hip that tends to development of the pathological processes. In these hip an appropriate therapy may postpone or even stop further disease [10, 24, 70, 186].

Diagnosis of the hip joint is usually determined after the long-term experience of the orthopaedic surgeon where clinical status of the patient and the joint's radiographic appearance (e.g. coxa valga/vara, osteophytes, trabecular trajectories in the femoral head, subchondral sclerosis in the acetabulum and the centre-edge angle) are considered [134]. However, it may be important to define a method by which the status of the hip joint can be evaluated more objectively.

Various radiographical and biomechanical parameters were suggested to evaluate the state of the hip joint [10, 118]. Usually, the centre-edge angle of Wiberg (ϑ_{CE}) (Fig. 5.12) is used as the main radiographical parameter for the assessment of the state of the hip [118, 148] since it correlates with the size of the weight bearing area and may therefore serve as an indirect measure of the hip joint contact stress [28, 93, 111, 118, 126]. However, it was suggested that besides ϑ_{CE} other geometrical parameters such as the radius of the femoral head [28, 118] or the pelvic shape [95, 91, 104] should be taken into account in assessment of the contact stress distribution. Therefore, the direct calculation of the contact stress in the hip joint has been introduced in the assessment of the biomechanical status of the hip [28, 112, 118, 186] and the peak contact stress has been established as a relevant parameter describing status of the hip joint [98, 121, 134]. However, it was suggested recently that high magnitude of gradient of contact stress could be even more important for the development of the degenerative processes in the hip joint than high value of the peak contact stress [23]. Therefore in this work we suggest two parameters that are related to the distribution of the contact stress over the hip joint articular surface. The first parameter is related to the gradient of the contact stress while the second describes the size of the weight-bearing area. These parameters can be determined using mathematical models (see sections 4.2 and 4.4). In the following definition we assume that force $\mathbf{R}$ lies in the frontal plane.

4.4.3.1 Stress gradient index

In the previous studies the peak contact stress p_{max} was used to describe biomechanical status of the hip joint which describes the stress distribution at one point of the articular sphere [64, 90, 100, 121, 134]. Therefore we tried to find some new biomechanical index which would be directly connected to the shape of the stress

distribution function. According to the recent suggestions [23,24], we have chosen the gradient of the contact stress distribution in the hip joint.

In order to calculate the stress gradient the original coordinate system is rotated so that in the rotated coordinate system the radius vector to the pole of stress distribution points in the direction of the vertical axis. In the classical spherical coordinates (Eqs. 4.51–4.53) of the rotated system (r, ϑ, φ) the stress distribution can be expressed as $p = p_0 \cos\vartheta$ (see Eq. 4.36). The gradient of contact stress (∇p) is then expressed as [110]:

$$\nabla p = \frac{\partial p}{\partial r}\,\mathbf{e}_r + \frac{1}{r}\,\frac{\partial p}{\partial \vartheta}\,\mathbf{e}_\vartheta + \frac{1}{r\,\sin\vartheta}\,\frac{\partial p}{\partial \varphi}\,\mathbf{e}_\varphi \tag{4.59}$$

where $\mathbf{e}_r$, $\mathbf{e}_\vartheta$ and $\mathbf{e}_\varphi$ are the orthogonal spherical unit vectors. Considering $p = p_0 \cos\vartheta$ (Eq. 4.36) and Eq. (4.59) we obtain :

$$\nabla p = -\frac{p_0}{r}\,\sin\vartheta\,\mathbf{e}_\vartheta \tag{4.60}$$

It follows from Eq. (4.60) that the gradient of contact stress in the hip joint is tangent to meridian of the articular sphere. In the following, our analysis is limited to the frontal plane where the angle ϑ in Eq. (4.60) is taken to be positive in the lateral direction from the radius vector to the stress pole and negative in the medial direction from the radius vector to the stress pole.

It was observed that the degenerative changes in the hip joint usually occur at the lateral acetabular rim [148]. To test the hypothesis that an increased magnitude of stress gradient at the lateral acetabular rim is biomechanically unfavourable we calculate the meridional component of stress gradient at the lateral acetabular rim :

$$G_p = -\frac{p_0}{r}\,\sin(\vartheta_{CE} - \Theta) \tag{4.61}$$

which is equal to the scalar product $\nabla p \cdot \mathbf{e}_\vartheta$ (Eq. 4.60) at the lateral rim of the acetabulum where $\vartheta = \vartheta_{CE} - \Theta$. The absolute value of G_p is equal to the magnitude of stress gradient ∇p at the lateral rim of acetabulum. We define the parameter G_p as the index of the stress gradient in the hip joint. If the pole of stress distribution lies outside the weight bearing area (i.e., if $\Theta > \vartheta_{CE}$) then $G_p > 0$. If the pole of stress distribution lies inside the weight bearing area (i.e., if $\Theta < \vartheta_{CE}$) then $G_p < 0$.

4.4.3.2 Functional angle of the weight-bearing area

The peak contact stress (p_{max}) gives a value of a physical quantity at a given point and it do not directly describe the size of the articular surface that actu-

ally bears a weight. Therefore we define another biomechanical parameter which describes the size of the weight bearing area – the functional angle ϑ_F:

$$\vartheta_F = \frac{\pi}{2} + \vartheta_{CE} - \Theta \tag{4.62}$$

The functional angle is equal to the size of the weight bearing area divided by $2\,r^2$ (Fig. 4.11). Combination of Eqs. (4.61) and (4.62) yields :

$$G_p = \frac{p_0}{r}\,\cos\vartheta_F \tag{4.63}$$

We can see that the stress gradient index G_p is in a simple way connected to the size of the weight bearing area which is proportional to the functional angle of the weight bearing area ϑ_F.

Chapter 5

ANALYSIS AND APPLICATIONS OF THE MATHEMATICAL MODELS

5.1 BIOMECHANICAL ANALYSIS

5.1.1 *Sensitivity of the hip joint reaction force on the optimisation function in the inverse dynamics*

Two different muscle models were selected to test how the choice of the optimisation criterion influence the hip joint reaction force. The original model of the load of the hip joint was taken from the literature [90,96] and it includes nine effective muscular units ($N = 9$) (Tab. 4.2). In our work we have upgraded this model by taking into account a more complex muscle model with twenty-seven effective muscular units ($N = 27$) (section 4.1). The optimisation criteria suitable for static analysis were adapted and also new neurophysiologically based criteria were defined (section 4.2.5).

In Tab. 5.1 the values of the components of the hip joint resultant force normalised to the body weight (R_x/W_B, R_y/W_B, R_z/W_B), magnitudes of the hip joint resultant force (R) and the muscle synergism indexes (S) for different optimisation criteria are shown. Optimisation criteria which are mostly used in the literature (see Tab. 3.1) and newly defined optimisation criteria (Eqs. 4.17, 4.26, 4.35) were selected to present computed muscle forces in Fig. 5.1.

The highest magnitude of the hip joint resultant force for the nine muscle model ($R = 2.43$) was obtained for G_σ, $G_{F/Mmax}$ and $G_{M_y(F/Mmax)}$. For the twenty-seven muscle model the highest load of the hip ($R/W_B = 22.19$ and 13.13) was obtained for $G_{M_y(F/Mmax)^2}$ and $G_{M_y(F/Mmax)^2}$, respectively. High resultant hip force is related to the high muscle forces (Fig. 5.1h). The lowest magnitude of $\mathbf{R}$ in both muscle models gives nonlinear criterion of the minimal muscle load (Eq. 4.19) and has value of 2.20 and 2.49 for the model with nine and twenty-seven muscles, respectively.

The values of R/W_B computed by using the model with nine muscles are in general lower than the values of R/W_B computed by using the model with twenty-seven muscles (Tab. 5.1). This may be caused by the different geometry of the muscle models. The attachment points of the muscles in the nine muscle model were taken from the work of Dostal & Andrews, 1981 (Tab. 4.2) while the attach-

	$N = 9$					$N = 27$				
Optimisation function	R_x/W_B	R_y/W_B	R_z/W_B	R/W_B	S	R_x/W_B	R_y/W_B	R_z/W_B	R/W_B	S
G_F	2.24	0.12	-0.27	2.26	0.77	2.49	0.24	-0.28	2.51	0.89
G_{F^2}	2.26	0.05	-0.43	2.31	4.46	2.72	0.24	-0.40	2.76	3.43
G_{F^3}	2.26	0.04	-0.43	2.30	4.29	2.82	0.23	-0.38	2.85	3.44
G_{F^4}	2.26	0.05	-0.43	2.30	4.27	2.85	0.24	-0.37	2.88	3.48
G_{F^5}	2.26	0.05	-0.42	2.30	4.28	2.85	0.24	-0.36	2.88	3.50
G_{F^6}	2.27	0.05	-0.42	2.30	4.28	2.87	0.24	-0.36	2.90	3.47
G_{F^7}	2.27	0.05	-0.42	2.31	4.28	2.87	0.24	-0.35	2.91	3.48
G_{σ}	2.40	0.12	-0.29	2.43	0.27	2.71	0.30	-0.30	2.75	1.72
G_{σ^2}	2.35	0.09	-0.34	2.38	3.71	2.81	0.26	-0.37	2.85	4.47
G_{σ^3}	2.33	0.08	-0.36	2.36	4.38	2.87	0.26	-0.37	2.90	6.07
G_{σ^4}	2.33	0.08	-0.37	2.36	4.73	2.90	0.27	-0.37	2.93	7.02
G_{σ^5}	2.33	0.08	-0.37	2.36	4.95	2.91	0.27	-0.36	2.94	7.60
G_{σ^6}	2.32	0.08	-0.36	2.35	5.11	2.92	0.28	-0.36	2.95	7.92
G_{σ^7}	2.32	0.08	-0.37	2.35	5.23	2.92	0.28	-0.35	2.95	8.09
$G_{F/Fmax}$	2.40	0.12	-0.29	2.42	1.15	2.71	0.30	-0.30	2.75	1.72
$G_{(F/Fmax)^2}$	2.27	0.05	-0.43	2.31	4.46	2.99	0.23	-0.30	3.01	3.88
$G_{F/Mmax}$	2.40	0.12	-0.29	2.43	0.27	2.71	0.30	-0.30	2.75	1.72
$G_{(F/Mmax)^2}$	2.34	0.10	-0.33	2.36	3.68	2.74	0.26	-0.35	2.78	4.33
$G_{M_y(F/Mmax)}$	2.40	0.12	-0.29	2.43	0.27	21.94	1.97	-2.66	22.19	10.31
$G_{M_y(F/Mmax)^2}$	2.34	0.10	-0.33	2.36	3.68	12.98	1.25	-1.54	13.13	7.07
G_{Rlin}	2.24	0.12	-0.27	2.26	0.77	2.49	0.24	-0.28	2.51	0.89
G_{Rnonlin}	2.15	-0.04	-0.45	2.20	0.83	2.46	0.25	-0.27	2.49	0.74
Double linear programming	2.30	0.09	-0.35	2.33	5.17	2.62	0.26	-0.44	2.67	7.97
$G_{\text{soft saturation}}$	2.27	0.05	-0.43	2.31	4.46	2.55	0.25	-0.40	2.59	3.63
G_{GTOlin}	2.26	-0.02	-0.48	2.31	0.09	2.51	0.28	-0.56	2.59	0.69
$G_{\text{GTOnonlin1}}$	2.32	0.08	-0.35	2.34	3.18	2.6	0.23	-0.47	2.66	2.57
$G_{\text{GTOnonlin2}}$	2.25	0.07	-0.36	2.28	3.12	2.49	0.26	-0.38	2.54	2.92

Table 5.1: The component of the hip joint reaction force normalised to the body weight ($R_x/W_B, R_y/W_B, R_z/W_B$), the magnitude of the hip joint reaction force normalised to the body weight (R/W_B) and the muscle synergism index S computed using two muscle models with different number of muscles N.

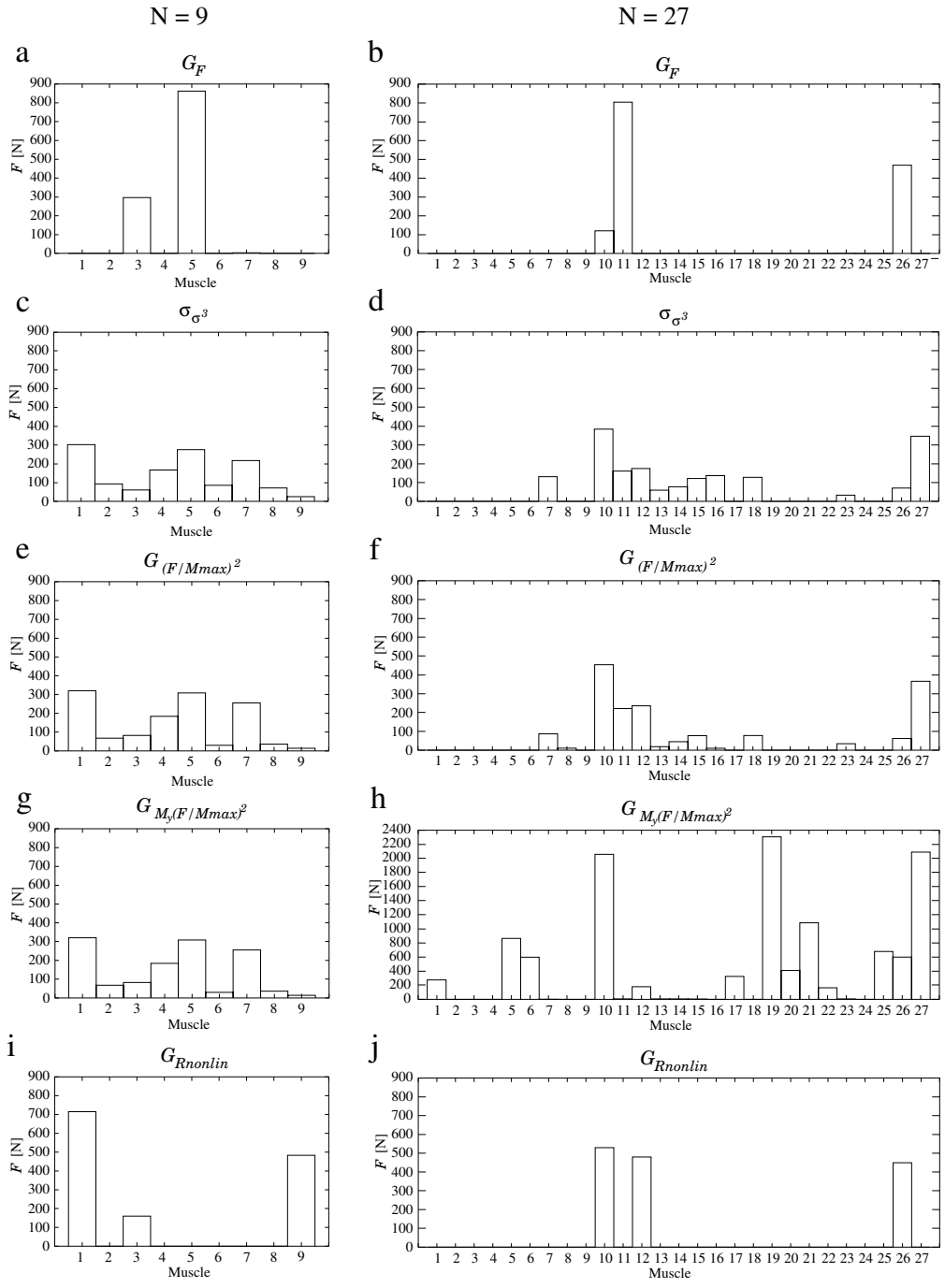

Figure 5.1: (*continued on next page*) Distribution of the muscle force in the one-legged stance computed using the muscle model of the human hip musculature with nine (a,c,e,g,i) and twenty-seven muscles (b,d,f,h,j) using various optimisation criteria.

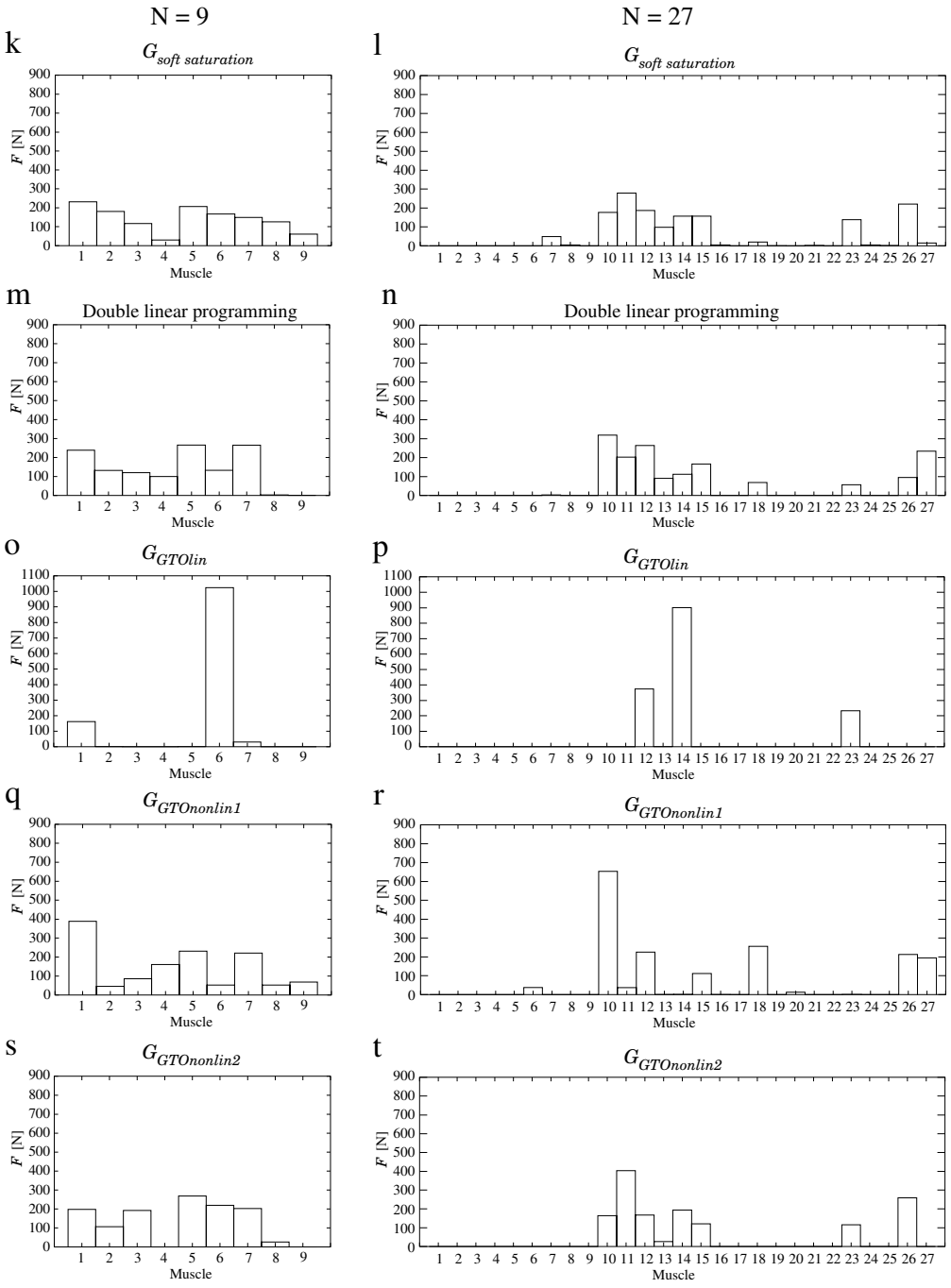

Figure 5.1: (*continued from previous page*) Distribution of the muscle force in the one-legged stance computed using the muscle model of the human hip musculature with nine (k,m,o,q,s) and twenty-seven muscles (l,n,p,q,r) using various optimisation criteria.

ments of the twenty-seven muscle model were taken from Delph, 1995 (Tab. 4.1). To test the influence of the positions of the attachments points of the muscles on the hip joint resultant force, the force **R** was computed by using a model with nine muscles (Tab. 4.2) which attachments were taken from the twenty-seven muscle model (Tab. 4.1). Using the optimisation criterion G_{σ^3}, which is the most common criterion used in the literature (Tab. 3.1), the R/W_B was found to be 2.77 with the components $R_x/W_B = 2.71$, $R_y/W_B = 0.26$ and $R_z/W_B = -0.45$. These values are close to the values computed by the twenty-seven muscle model. Therefore we can conclude that the nine-muscle model gives approximately the same values of **R** as the twenty-seven muscle model if the muscle geometry model is used.

Except of $G_{M_y(F/Mmax)}$ and $G_{M_y(F/Mmax)^2}$ in twenty-seven muscle model the values of R obtained using various optimisation criteria in both models are relatively constant. The direction of the force **R** is given mainly by its x-component (Tab. 5.1). The z-component of **R** is in the range from 11% to 22% of the magnitude of **R** for both muscle models and is negative. It means that the hip joint reaction force points medially what is in accordance with the results from literature (Fig. 4.10) [22, 111, 118, 148]. The relative size of the y-component of **R** depends on the type of the muscle model. In the nine-muscle model the y-component is less than 5% of R for all optimisation criteria (Tab. 5.1) while in the twenty-seven muscle model the size of the y-component of **R** is comparable with the size of the z-component of **R**. If the load of the hip is computed by the model with nine muscles, the hip joint reaction force lies almost in the frontal plane. If the load is computed by the model with twenty-seven muscles, the inclination of **R** from the frontal plane is also small as the R_y component is small in comparison to R_z component. The position of **R** in the frontal plane in the one-legg standing is in accordance with the previous works [93, 94, 148].

It can be concluded that for a given muscle model the force **R** is almost constant in the magnitude and direction independently on the type of the optimisation criterion by which the muscle forces are computed (except of $G_{M_y(F/Mmax)}$ and $G_{M_y(F/Mmax)^2}$).

This conclusion is not valid for the distribution of the muscle force over the muscles. The distribution of the forces (Fig. 5.1) as well as the muscle synergism index (Tab. 5.1) differ for different optimisation criteria. To describe the distribution of the muscle force in the multiple muscles we have defined a new variable – the muscle synergism index (S). The more muscles are involved, the higher S should be. The highest muscular forces were found when the linear criteria were used (Tab. 5.1). Linear optimisation functions activate only few muscles (Fig. 5.1a,b,o,p) which gives small values of the muscle synergism index (Tab. 5.1).

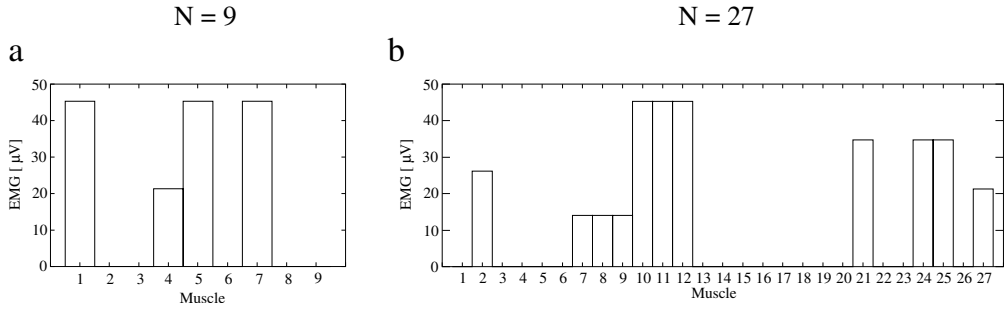

Figure 5.2: Pattern of the EMG activation of the muscles of the hip in one-legged position during walking for the muscle model with nine (a) and twenty-seven muscles (b).

Similar situation occurs also in the nonlinear criterion $G_{R\text{nonlin}}$. On the other hand, high value of the muscle synergism index and low values of the muscular forces is related to the distribution of the muscle force between multiple muscles as observed in the optimisation criteria designed to maintain muscle synergism like the double linear programming (Eq. 4.20 and Fig. 5.1m,n) or the soft saturation criterion (Eq. 4.21 and Fig. 5.1k,l).

The exponent in the polynomial cost function also influences the muscle synergism and the magnitude of the hip joint reaction force. Two types of the polynomial optimisation functions were tested: sum of the muscle forces raised to power n and sum of the muscle stresses raised to power n (Eqs. 4.12, 4.13 respectively). As mentioned above the lowest values of S were obtained for the linear functions G_F and G_σ. If the exponent n increases, the values of the muscle synergism index (S) increases as well (Tab. 5.1). The increase in S is more significant if the sum of the muscle stresses is considered (Eq. 4.13) since the definition of the muscle synergism index (Eq. 4.25) is based on the muscle stresses.

Although the forces in the muscles predicted after different optimisation criteria differ, the resemblance between the activation of the muscle groups can be observed. In both types of the muscle models the gluteus medius is the muscle which is almost always active. The force in this muscle is the highest except of G_{GTOlin} (Fig. 5.1o,p) which predicts the highest activation in the gluteus minimus. In almost all criteria the gluteus maximus is inactive. The other muscles that are mostly activated are the tensor fasciae latae (except of G_{GTOlin}, Fig. 5.1o,p) the rectus femoris (Fig. 5.1d,f,h,l,n,r) and the sartorius (Fig. 5.1d,f,l,n,p,t).

The pattern of the activation of the muscles can be also estimated from the EMG measurements of the muscle activity [60]. From the International Society of Biomechanics web data repository (`www.isbweb.org`) were obtained EMG, force

plate and kinematics data of a man during walking [185]. Using the force plate data and kinematics of the right leg the one-legg position was identified. During the motion the electromyografic activity was recorded for adductor longus, gluteus maximus, gluteus medius, rectus femoris and hamstrings. The pattern of the electromyografic activation of the muscles is shown in Fig 5.2. The highest activation was found in the gluteus medius which is in accordance with our mathematical models (Fig. 5.1). Also the activation of the rectus femoris is in accordance with the results predicted by the optimisation criteria. The relative high activation was found in the group of hamstrings (biceps femoris, semitendinosus and semimembranosus) and adductor longus which are predicted as inactive in almost all optimisation criteria. The only criterion that predicts activation of hamstrings and adductors is $G_{M_y(F/Mmax)^2}$ (Fig. 5.1h).

The hip joint reaction force has been evaluated by many authors using different methods. In Tab. 3.2 the values of the magnitude of $\mathbf{R}$ normalised to the body weight determined by several authors and using various methods are shown. The values of the hip joint reaction force determined by our model (Tab. 5.1) are in good accordance with the values obtained previously.

5.1.2 *Influence of hip joint reaction force on contact stress distribution in human hip during routine activities*

In our work we have used the measurements of the hip joint load by an implanted instrumented endoprosthesis (section 4.3) and recently developed mathematical model (section 4.4) to evaluate the stress distribution during various activities. The loading conditions in normal and dysplastic hips were assumed to be the same. Dysplastic hips were modelled as hips with small lateral coverage of the femoral head by the acetabulum (section 4.4.1). The radius of the articular surface (r) was taken 2.7 cm.

In Tab. 5.2 we present values of the maximum hip joint resultant force normalised to the body weight (R/W_B) and the maximum peak contact stress normalised to the body weight (p_{max}/W_B) during routine activities in normal and dysplastic hips. The values of normalised contact stress for dysplastic hips are significantly higher than for normal hips. This is in accordance with other works [98, 118, 134]. The highest values of p_{max}/W_B were observed in both normal and dysplastic hips during walking downstairs, and are 2006 and 8448 m^{-2}, respectively. The highest hip joint resultant force as well as the highest peak contact stress were observed when walking downstairs.

It has been reported that large differences in size and direction of $\mathbf{R}$ with respect to the situation during normal walking occur in staircase walking [17]. Since staircase walking is one of the most frequent daily activities [141], the following study is intended to determine how the variations in magnitude and direction of the force influence the contact stress distribution in the staircase and normal walking in normal and dysplastic hips. Such analysis can be done for any of the activities mentioned in Tab. 5.2.

Figs. 5.3a, 5.3b, 5.3c show the time course of the normalised hip joint resultant force (R/W_B) and the time course of the normalised peak contact stress (p_{max}/W_B) for normal and dysplastic hips during normal walking, walking upstairs and walking downstairs.

All R and p_{max} curves exhibit a typical double-peak shape. The first peak of the hip joint resultant force (R) is higher than the second peak for all types of walking cycles (Fig 5.3a). This is valid for p_{max} during normal and upstairs walking in normal hips (Fig 5.3b) and for walking upstairs in the case of dysplastic hips (Fig 5.3c). During walking downstairs in the case of normal hips (Fig 5.3b) and during normal and downstairs walking in the case of dysplastic hips (Fig 5.3c) the second peak becomes higher than the first.

To present the differences between the corresponding time curves of R/W_B, p_{max}/W_B and p_{max}/R, the positions of the first and the second maximum of R/W_B

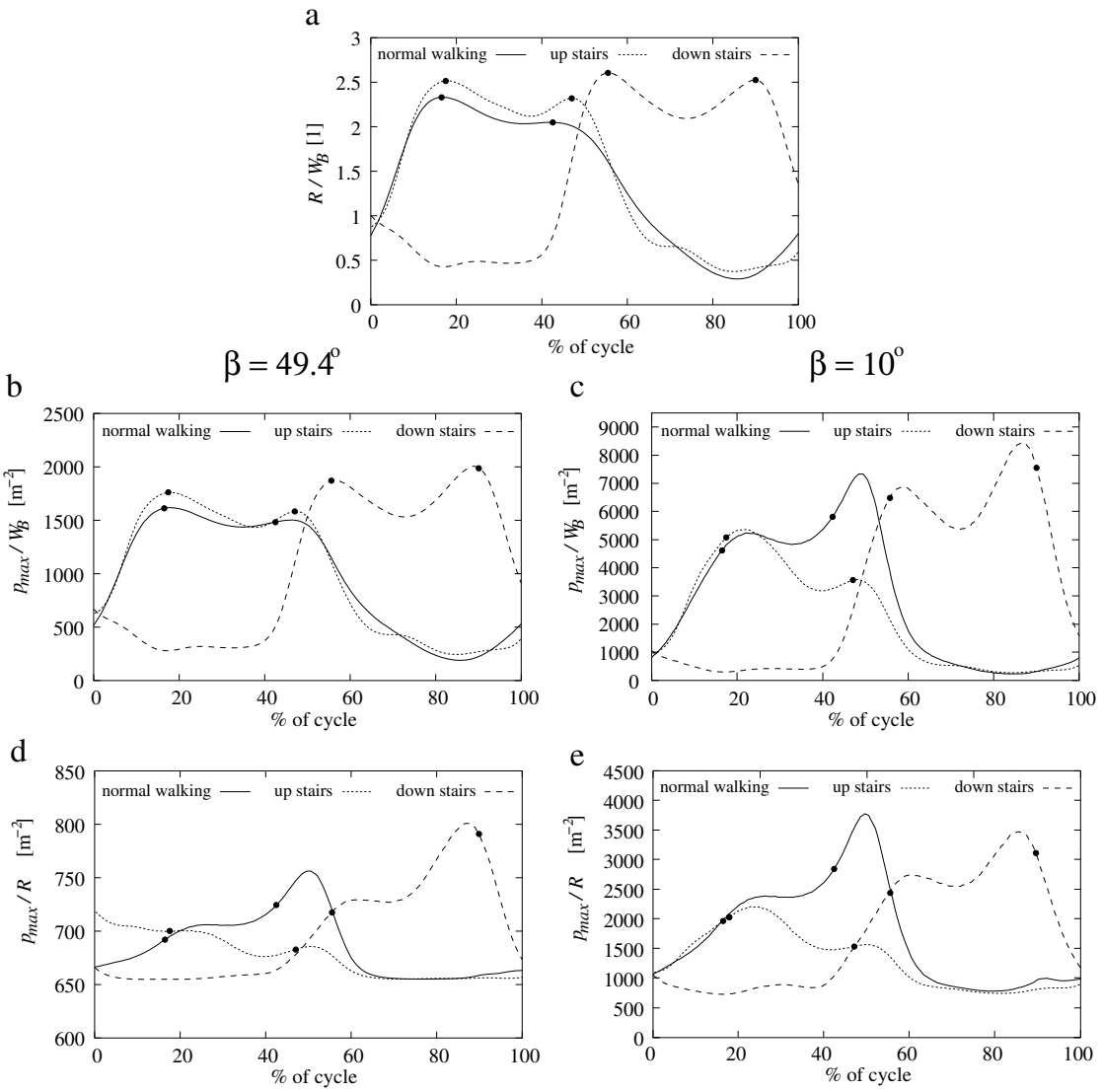

Figure 5.3: The time dependencies of the normalised hip joint resultant force R/W_B (a), normalised peak contact stress p_{max}/W_B in normal hips (b) and dysplastic hips (c) and ratio of p_{max}/R in normal hips (d) and dysplastic hips (e) during normal walking, walking upstairs and walking downstairs. Position of the force maxima are denoted by black spots at all curves. The radius of the articular hemisphere was taken to be $r = 2.7$ cm.

		Normal	Dysplastic	
Activity	R/W_B [1]	p_{max}/W_B [m^{-2}]	p_{max}/W_B [m^{-2}]	Description
Normal walking	2.33	1619	7336	average speed of all patients v = 3.9 km/h
Slow walking	2.43	1734	7695	average speed of all patients v = 3.5 km/h
Fast walking	2.51	1723	5709	average speed of all patients v = 5.3 km/h
Walking upstairs	2.52	1760	5358	stair height 17 cm, no support
Walking downstairs	2.61	2006	8448	stair height 17 cm, no support
Standing up	1.90	1364	1399	chair height 50 cm, arms hold at chest
Sitting down	1.56	1108	1150	chair height 50 cm, arms hold at chest
One-legged stance	2.32	1644	5663	arms hold at chest

Table 5.2: Normalised maximum hip joint reaction force R/W_B and normalised maximum peak contact stress p_{max}/W_B during routine activities in normal and dysplastic hips. Description of activities was taken from Bergmann et. al., 2001.

are marked in Figs. 5.3a–e. For normal hips, the positions of the peak contact stress maxima approximately correspond to the positions of the first and the second force maximum. Moreover, for normal hips the time course of p_{max} (Fig. 5.3b) during the described walking cycles differs only slightly from the corresponding curves representing the time course of R (Fig. 5.3a), leading to the conclusion that for normal hips the magnitude of the hip joint resultant force (R) is the main factor influencing the value of the peak contact stress during the walking cycle.

Fig. 5.3c shows that this conclusion is not valid for dysplastic hips. The time course of p_{max} for dysplastic hips is different for different types of walking cycle. In the time dependence of p_{max}/W_B for dysplastic hips during normal walking, the first maximum disappeared and the second maximum became more pronounced. The maxima are also more distinct in the time dependence of p_{max}/W_B in walking downstairs. In climbing stairs, p_{max}/W_B is considerably smaller than in the other two walking cycles. The differences are not only in the shapes of the p_{max} and R curves for dysplastic hips (Figs. 5.3a,c). Also the positions of the maxima of the peak contact stress do not correlate with the positions of the maxima of the hip joint resultant force.

To determine the relation between the value of the peak contact stress p_{max} and the magnitude of force $\mathbf{R}$ we present the dependence of the ratio p_{max}/R

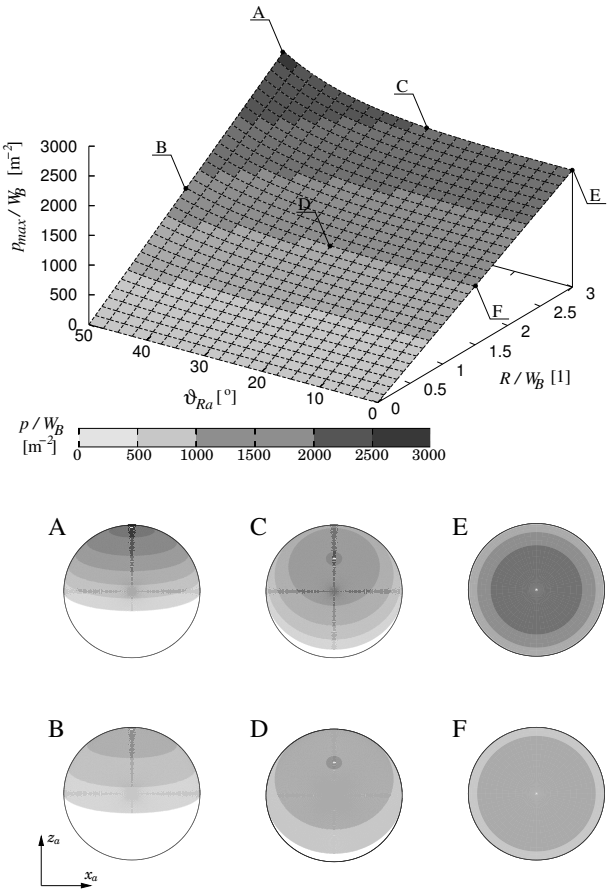

Figure 5.4: The dependence of the normalised peak contact stress p_{max}/W_B on the magnitude R/W_B and inclination of the resultant hip force ϑ_R. Patterns of the stress distribution are shown for denoted values of R, ϑ_R and $\varphi_R = 0$ as a projection of the stress distribution to xz-plane. Radius of the articular hemisphere was taken $r = 2.7$ cm. The results are presented in the acetabular coordinate system (Fig. 4.11).

during the walking cycle for normal and dysplastic hips (Fig. 5.3c,d). As expected, according to Figs. 5.3a–c the value of p_{max}/R is much higher for dysplastic hips. The value of the ratio p_{max}/R during the walking cycles varies from 650 to 800 m^{-2} approximately for normal hips, and from 720 to 3770 m^{-2} for dysplastic hips. For normal hips the highest values of the ratio p_{max}/R was observed when walking downstairs (801 m^{-2}), while for dysplastic hips the highest value was observed in normal walking (3767 m^{-2}). The minimum values of p_{max}/R for all types of walking for normal and dysplastic hips correspond to the unloaded hip (small R/W_B in Fig. 5.3a).

The differences in the time dependencies of p_{max}/R during the studied walking cycles indicates that also the direction of the force ($\mathbf{R}$) has an important influence

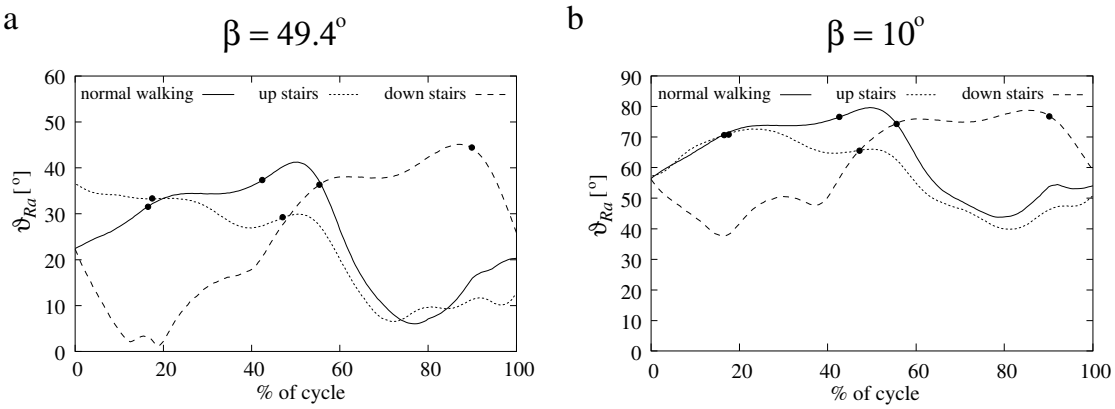

Figure 5.5: The time dependence of the inclination of the hip joint resultant force ϑ_{Ra} for normal hips (a) and dysplastic hips (b) during normal walking, walking upstairs and walking downstairs. Positions of the force maxima are denoted by black spots. The results are presented in the acetabular coordinate system (Fig. 4.11).

on the contact stress distribution. Therefore in the following the influence of the direction and magnitude of the force ($\mathbf{R}$) on the hip contact stress distribution will be studied.

In the mathematical model of the contact stress distribution the peak contact stress is proportional to the magnitude of the hip joint resultant force R while its dependence on the position of stress pole Θ_a in the coordinate system of acetabulum is nonlinear (Eq. 4.47). The value of Θ_a (Eq. 4.46) depends on the angle of the inclination of force R in the coordinate system of the acetabulum (ϑ_{Ra}). Therefore the peak contact stress depends on both the magnitude (R) and the inclination (ϑ_{Ra}) of the hip joint resultant force $\mathbf{R}$. The values of p_{max}/W_B for different values of R/W_B and different inclinations ϑ_{Ra} are shown in Fig. 5.4. As expected, for higher magnitudes of force $\mathbf{R}$ the peak stress is higher. The same holds ϑ_{Ra}, the increase in the value of p_{max} is higher for high ϑ_{Ra}.

It has recently been suggested that the patterns of the stress distribution could be even more important for cartilage longevity than the value of the peak stress [26, 152]. Figs. 5.4 A–F illustrate the influence of the magnitude of force $\mathbf{R}$ and its inclination (ϑ_{Ra}) on the stress distribution pattern. The pattern of the stress distribution does not depend on the magnitude of $\mathbf{R}$, as might have been excepted on the basis of Eq. (4.47) (Figs. 5.4 A–B, C–D and E–F). On the other hand, the pattern of hip joint contact stress at the same magnitude of $\mathbf{R}$ strongly depends on the value of the inclination of the force $\mathbf{R}$ (ϑ_{Ra}), which can be seen from a comparison of Figs. 5.4 A–C–E and Figs. 5.4 B–D–F. An increase in ϑ_{Ra} shifts the stress pole towards the acetabular rim, therefore the weight-bearing area is

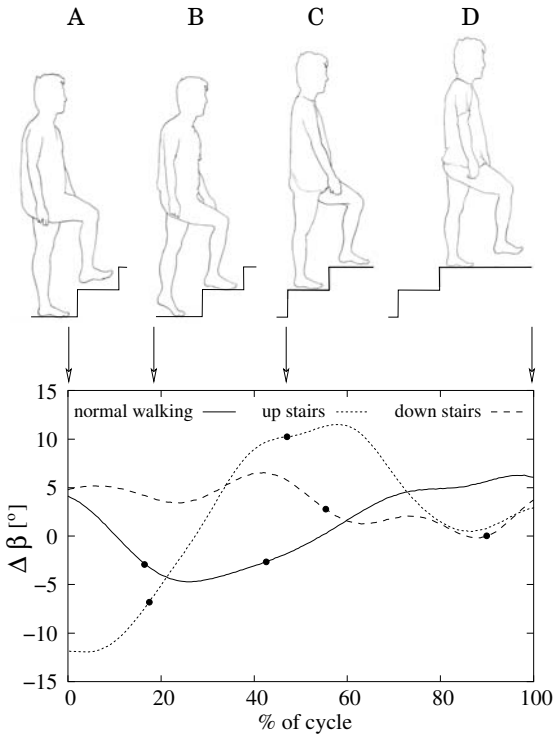

Figure 5.6: Position of the patient when walking upstairs (A-D). Time dependency of the inclination change of the acetabulum $\Delta\beta$ with respect to its position in upright posture during normal walking, walking upstairs and walking downstairs. Position of the force maxima are denoted by black spots.

decreased and the contact stress is increased (Figs.5.4 E→C→A). High values of ϑ_{Ra} lead to a stress distribution that changes considerably over the weight-bearing area (Figs. 5.4 A and B). Based on the results presented in this work it can be concluded that the inclination of force (ϑ_{Ra}) determines the pattern of stress distribution, while the magnitude of force $\mathbf{R}$ influences the values of the contact stress distribution.

According to Fig. 5.4, differences between the time courses of R and of the peak stress p_{max} during the walking cycles for normal and dysplastic hips (Fig. 5.3a–d) are caused by the variation in the inclination of the force $\mathbf{R}$ (ϑ_{Ra}). This statement is confirmed by the results presented in Fig. 5.5, where the time course of ϑ_{Ra} for normal and dysplastic hips during different types of walking cycles is shown. For dysplastic hips ϑ_{Ra} is in general higher than for normal hips, which yields a higher ratio of p_{max}/R for dysplastic hips. For both normal and dysplastic hips, during walking upstairs and normal walking, the larger inclination of force (ϑ_{Ra}) in the second maximum of R yields a higher ratio p_{max}/R in the position of the second maximum of R (Fig. 5.3 d,e). In climbing stairs ϑ_{Ra} is on an average lower than

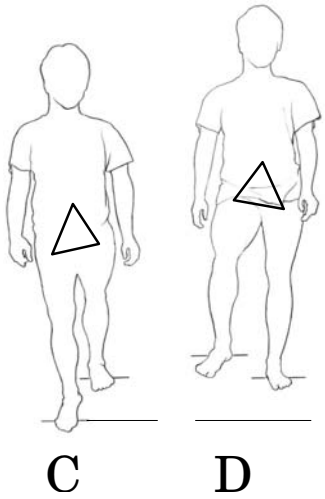

Figure 5.7: Frontal view of the position of the patient in the first (C) and in the second maximum of the peak contact stress (D) when climbing stairs. The pelvis is denoted by triangle.

its value in the other two types of walking. In general, it can be concluded that the shapes of the time dependencies of ϑ_{Ra} during the studied types of walking for normal and dysplastic hips are similar to the corresponding shape of the time course of p_{max}/W_B.

To simplify the derivation of the model equations (Eqs. 4.46, 4.47), inclination of the force ϑ_{Ra} was defined in the coordinate system of the acetabulum. Therefore the direction of the force $\mathbf{R}$ in the acetabular coordinates varies due to the alterations of the global direction of the force $\mathbf{R}$ (force in laboratory coordinate system [15]) and due to the changes in the orientation of the acetabulum. Forces in the hip muscles which contributes to the force $\mathbf{R}$ and regulation of the muscle forces have not been exactly clarified yet [181, 197]. However, we could estimate how the pelvis motion is projected into ϑ_{Ra} and p_{max}. If the global force $\mathbf{R}$ were constant in its value and direction, higher inclination of the acetabulum (higher β in Fig. 4.11) would decrease the angle ϑ_{Ra} (Fig. 4.13) and therefore decrease the peak stress (Fig. 5.4). We have expressed the inclination of the acetabulum during the walking cycle as a deviation from its position in the neutral upright two-leg posture. Values of the changes in the acetabular inclination $\Delta\beta$ during described activities with respect to its position in neutral posture are shown in Fig. 5.6. The widest range of $\Delta\beta$ was found in walking upstairs (from -10 to 10 degrees) unlike walking downstairs when β varies only a little. It is worth noticing that angle β in both force maxima in normal walking is nearly the same (Fig. 5.6). The largest differences in $\Delta\beta$ were observed in climbing stairs, while the differences in the

time course of ϑ_{Ra} and p_{max}/W_B are relatively small in comparison to the other two walking cycles. Therefore we describe motion of the body in the climbing stairs in details. The positions of the patient when walking upstairs are shown in Fig. 5.6A-D. The first maximum value of the hip joint reaction force was reached when the unloaded leg was lifted from the stair below (Fig. 5.6B) [17]. The second maximum of R was reached when the thigh was flexed before hitting the next stair (Fig. 5.6C). Position of the pelvis in the first and in the second force maximum are shown in Fig 5.7. During climbing stairs, the acetabulum is opened much more laterally (negative $\Delta\beta$ and medial inclination of the pelvis in Fig. 5.7C) in the first force maximum than in the second maximum (positive $\Delta\beta$ and lateral inclination of the pelvis in Fig. 5.7D). Inclination of the force ϑ_{Ra} should therefore be higher in the first maximum than in the second one. In fact, ϑ_{Ra} is higher in the first maximum (Fig. 5.5) but its increase is not so high as the change in the position of the acetabulum ($\Delta\beta$) (Fig. 5.6).

5.1.3 *Biomechanical analysis of the avascular necrosis of the femoral head*

We analysed the effects of the size and position of a hypothetical non-weight bearing area on the hip stress distribution corresponding to the necrotic region of the femoral head. All results were calculated for the same magnitude and direction of the resultant hip force ($R = 2.7, \vartheta_R = 5°, \varphi_R = 0°$) and the same radius of the articular surface ($r = 2.7$ cm).

Fig. 5.8 shows the effect of the size of the non-weight bearing area (represented by angle ϑ_0 (Fig. 4.14)) on the stress distribution for hips with different lateral coverages of the femoral head by the acetabulum (ϑ_{CE}). The center of the non-weight bearing area is at the top of the articular sphere. Fig. 5.8a shows the dependence of p_{max}/W_B on angle ϑ_0, while Fig. 5.8b shows the dependence of the position of pole Θ on angle ϑ_0. For illustration, schematic representations of the stress distributions for ϑ_{CE} equal to 30° and different sizes of the necrosis ϑ_0 are shown in Fig. 5.11A-D. The points at which the stress distributions are shown are marked in Fig. 5.8. Point A ($\vartheta_0 = 0°$) corresponds to a normal hip, i.e., a hip without avascular necrosis, and can therefore serve as a reference point to which changes in the stress distribution can be compared. It can be seen that the range of validity of the mathematical model of contact stress distribution has an upper bound of ϑ_0 determined by the situation where the lateral edge of the non-weight bearing area coincides with the respective center-edge angle, i.e., the non-weight bearing area reaches the lateral rim of the acetabulum ($\vartheta_N + \vartheta_0 = \vartheta_{CE}$) (Fig. 5.11D). The peak stress increases with increasing size of the non-weight bearing area (Fig. 5.8a), while the pole is shifted laterally (Fig. 5.8b). A small non-weight bearing area does not considerably influence the stress distribution (Figs. 5.11A,B). However, if the necrotic part of the femoral head is large, even a small increase in the size of the necrotic region causes a large increase in p_{max} (Figs. 5.11C, D). The effect of the increase in p_{max}/W_B is stronger if the hip has poor lateral coverage (represented by the center-edge angle (ϑ_{CE})), (Fig. 5.8).

Fig. 5.9 shows the effect of the medio-lateral position of the non-weight bearing area (represented by the angle ϑ_N) on the stress distribution and on the size of the weight bearing area A for different sizes of non-weight bearing area (ϑ_0). For the size of the necrosis $\vartheta_0 = 30°$, the stress distributions in the denoted points are shown in Fig. 5.11D–H. The center of the non-weight bearing area is confined to the frontal plane through the center of the femoral head. For the sake of simplicity ϑ_N is denoted as positive if $\varphi_N = 180°$, i.e., if the center of the necrotic region is located laterally from the sagittal plane passing through the center of the femoral head, and ϑ_N is negative if $\varphi_N = 0°$, i.e., if the center of the necrotic region is located medially (Fig. 5.11D–H). Fig. 5.9a shows the dependence of p_{max} on angle

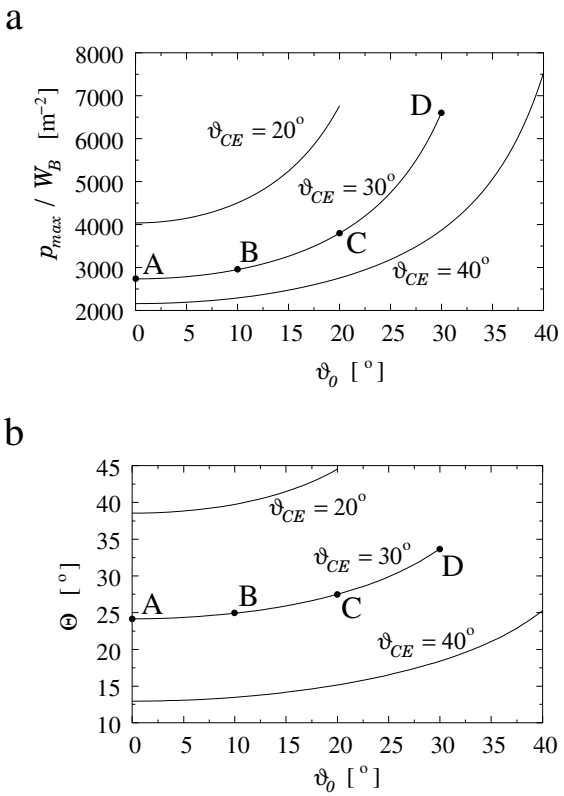

Figure 5.8: Effect of the size of the necrotic region (determined by the angle ϑ_0) on the relative peak contact stress p_{max}/W_B (a) and the position of the stress pole Θ (b) for different lateral coverage of the acetabulum (ϑ_{CE}). The centre of the necrotic region is located at the top of the articular hemisphere ($\vartheta_N = 0°$), the force $\mathbf{R}$ lies in the frontal plane ($R = 2.7, \vartheta_R = 5°, \varphi_R = 0°$) and $r = 2.7$ cm.

ϑ_N, while Fig. 5.9b shows the dependence of the position of pole Θ on angle ϑ_N. The lateral shift of the necrosis is limited by the situation when its medial border reaches the medial border of the weight bearing area (Fig. 5.11H). The peak stress decreases when the center of the non-weight bearing area is positioned medially (Fig. 5.9a). Interestingly, for medially located non-weight bearing areas the value of the peak stress falls below the corresponding value obtained for an intact hip. This was observed for all evaluated sizes of the necrotic part (ϑ_0)(Fig. 5.9a - inset). With medial shifting of the non-weight bearing area, the pole is first moved medially below the level that is observed in normal hips to reach the most medial value, and then it is shifted laterally (Fig. 5.9b). The position of the pole Θ reaches its value observed in normal hips when the center of the necrotic part (ϑ_N) approximately corresponds to the direction of the hip joint resultant force (ϑ_R=5° laterally), independently of the size of the necrosis (Fig. 5.9b). The medial shift of the pole is higher in hips where necrosis is larger in size. The point

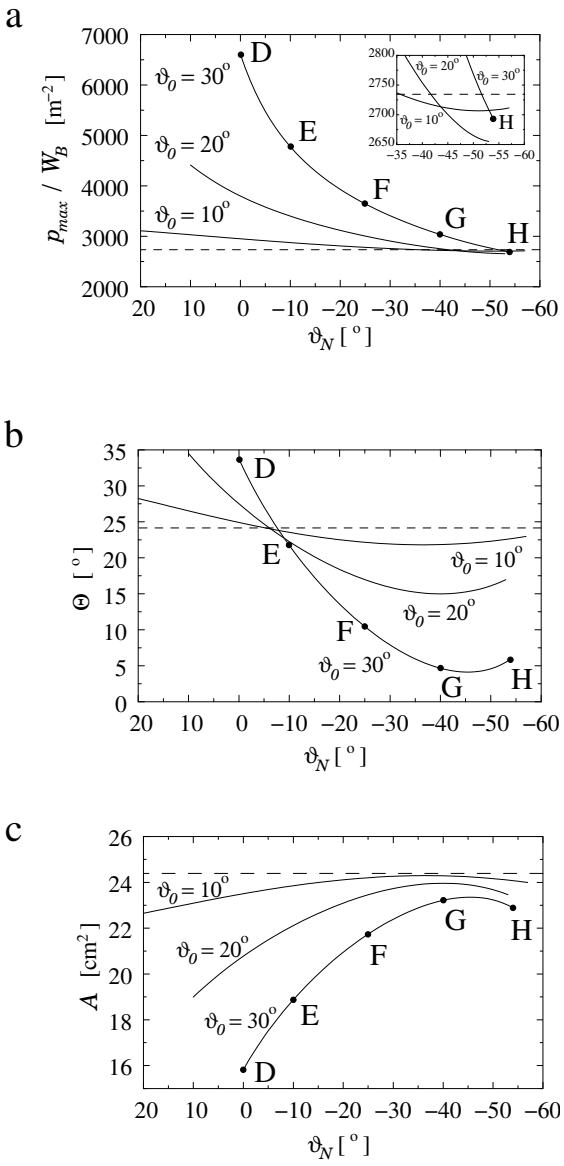

Figure 5.9: Effect of the position of the necrotic region (determined by the angle ϑ_N) on the relative peak contact stress p_{max}/W_B (a), position of the stress pole Θ (b) and on the size of the weight bearing area A (c) for different sizes of the necrotic region (ϑ_0). Dashed line shows the value of p_{max}/W_B, Θ and A in intact hip. The necrosis is located close to the frontal plane while $\varphi_N = 180°$ for positive ϑ_N and $\varphi_N = 0°$ for negative ϑ_N, the force $\mathbf{R}$ lies in the frontal plane ($R = 2.7, \vartheta_R = 5°, \varphi_R = 0°$) and $r = 2.7$ cm.

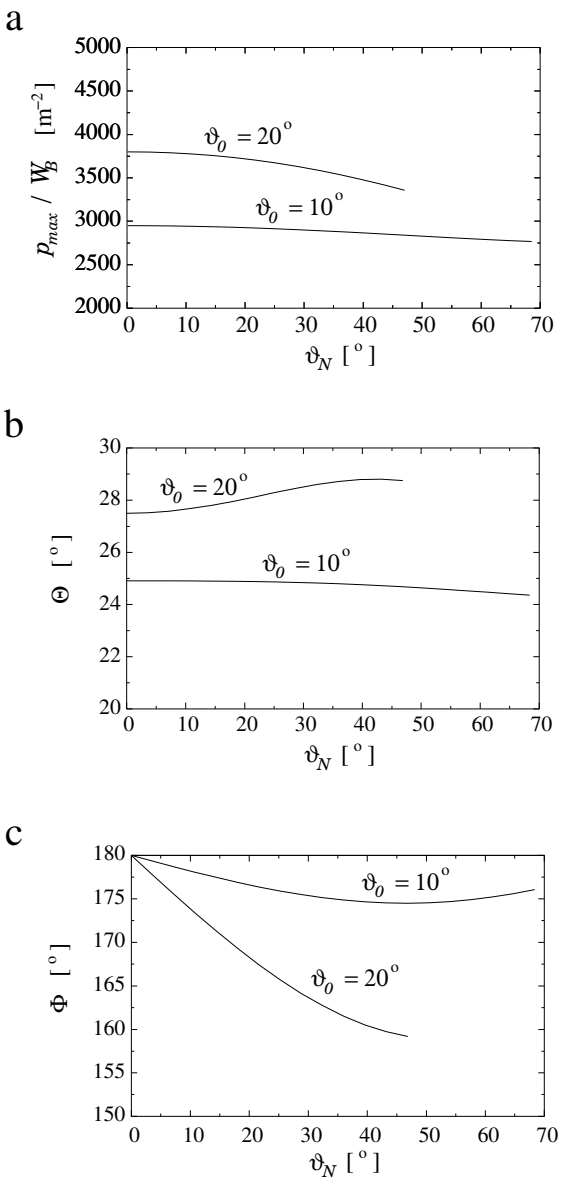

Figure 5.10: Effect of the position of the necrotic region ϑ_N on the relative peak contact stress p_{max}/W_B (a) and the position of the stress pole Θ (b) and Φ (c) for different sizes of necrotic region (ϑ_0). The centre of the necrotic part is located in the sagital plane ($\varphi_N = 90°$), the force $\mathbf{R}$ lies in the frontal plane ($R = 2.7, \vartheta_R = 5°, \varphi_R = 0°$) and $r = 2.7$ cm.

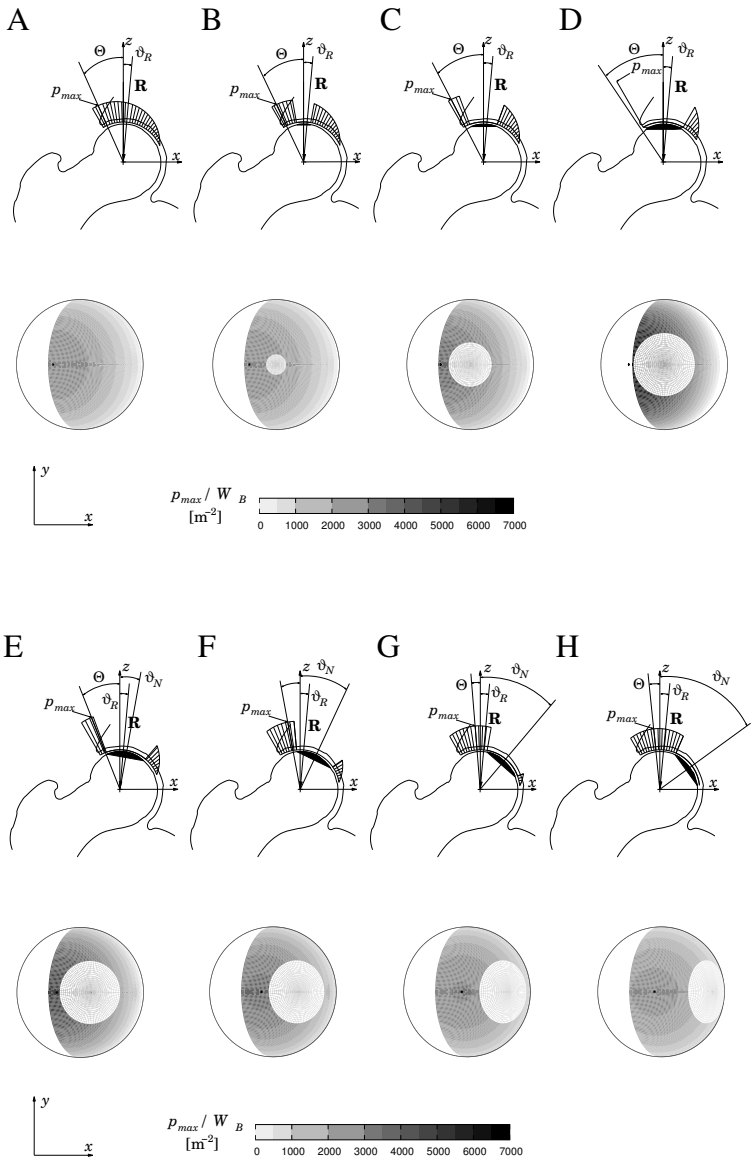

Figure 5.11: Schematical representation of the contact stress distribution for different sizes of the necrotic region ϑ_0 and $\vartheta_{CE} = 30°$ (A–D) and for different positions of the necrosis ϑ_N (D–E). Points at which stress distributions are shown are marked in Figs. 5.8 and 5.9. In the upper figures, stress distribution in the frontal plane, position of the maximum contact stress p_{max}, position of the stress pole Θ and the direction of the force $\mathbf{R}$ are shown. In the lower figures, the corresponding projection of the stress distribution in the xz-plane is shown.

of minimum Θ does not correspond to the point of minimum p_{max}. It can be seen from Figs. 5.11G,H that the medial shift of the pole contributes to redistribution of the stress, i.e., to more uniformly distributed contact stress in the hip.

Comparing Figs. 5.11D and G, it can be seen that the medial border of the weight bearing area is not fixed. As described above, the coordinate Θ of the pole determines the position of the medial border of the weight bearing area, as this border is defined to lie $\pi/2$ away from the pole. The changes in the size of the weight bearing area (Fig. 5.9c) are therefore similar to the changes in the position of the pole. However, the size of the weight bearing area with a non-weight bearing part is smaller than the size of the weight bearing area in a normal hip for any position of the necrosis.

Fig. 5.10 shows the effect of the anterior shift of the non-weight bearing area on the contact stress distribution. The center of the non-weight bearing area is shifted in the sagittal plane through the center of the femoral head. This is ensured by taking φ_N equal to 90° (Fig. 4.14). Fig. 5.10a shows the dependence of p_{max}/W_B on the angle ϑ_N, Fig. 5.10b shows the dependence of the coordinate of pole Θ on angle ϑ_N, while Fig. 5.10c shows the dependence of the coordinate of pole Φ on angle ϑ_N. The peak stress decreases slightly with the shift of the center of the non-weight bearing area over angle ϑ_N (Fig. 5.10a), while the coordinate of pole Φ follows the shift of the center of the non-weight bearing area (Fig. 5.10c). The coordinate of pole Θ decreases if the necrosis is small ($\vartheta_{CE} = 10°$), while it increases if the necrosis is larger ($\vartheta_{CE} = 20°$), (Fig. 5.10b).

5.2 Biomechanics of the hip - towards the clinical practice

5.2.1 Determination of the contact stress distribution from anteroposterior radiograph

The geometry of the pelvis, proximal femur and hip joint is individual for every patient [113]. Since the hip joint reaction force is a result of the muscle activity (Eq. 4.4), the variations in the positions of the muscle attachments related to different bony geometry influence the muscle forces and the hip joint reaction force as well. Also the position of the acetabulum varies between the patients (section 4.4.1) changing the direction of the force $\mathbf{R}$ in the acetabular coordinates (Fig. 4.11). The hip joint reaction force individual for every patient together with the individual geometry of the hip (i.e., radius of the articular surface, position of the acetabulum) yields characteristic contact stress distribution for every patient [91, 95]. To study the stress distribution in a group of patients it seems to be necessary to have the method for evaluation the stress distribution that can be adjusted for individual patient.

The most accurate three dimensional shape of the bones of the hip joint and the positions of the muscle attachments could be obtained by the radiographic methods that provide three-dimensional reconstruction of the human body, like computer tomography (CT) or nuclear magnetic imaging (NMR) [40,109,179,188]. These examinations of the patients are not widely applied and the processing of the three-dimensional data is complicated [106]. In order to determine the stress distribution in the everyday clinical practice the standard radiographs may be more appropriate.

The mathematical model of the hip joint reaction force as well as the mathematical model of the stress distribution described above (sections 4.2 and 4.4) were designed so that they can be easily adjusted for individual patient [94]. Iglič & Kralj-Iglič, 1999 showed how could the calculation the contact stress distributions be adjusted for an individual patients if certain geometrical parameters of the pelvis and proximal femur determined from radiograph are known.

The one-legged stance as representative body position for calculation the hip joint reaction force was chosen because it is most frequently attained in everyday activities [45, 94, 96]. It was shown above (page 69) that increasing the number of muscles in the model of the muscle musculature does not markedly change the magnitude and the direction of the hip joint resultant force. Moreover, it was shown that the hip joint reaction force calculated by the method of reduction proposed by Iglič, 1990 is almost the same as when the optimisation procedure is applied [131, 133]. Therefore in the further analysis model with nine effective

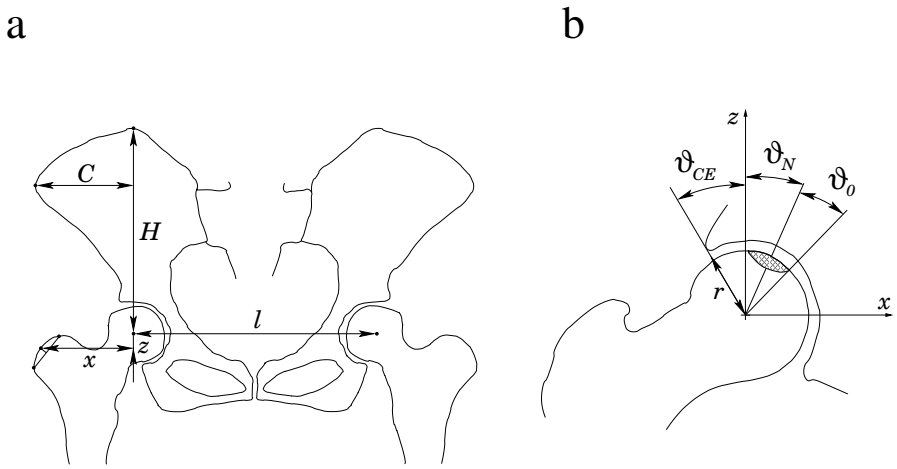

Figure 5.12: Characteristic parameters of the pelvis and proximal femur used to adjust model for calculation of the hip joint reaction force (a) and parameters describing geometry of the hip and geometry the avascular necrosis of the femoral head needed to determine contact stress distribution (b).

muscles included is used (Tab. 4.2) and the problem of the muscles forces required in order to maintain balance is solved by using reduction method proposed by Iglič et al., 2002 (see section 4.2). The coordinates of the muscle attachments are adjusted to each patient according to the geometry of the pelvis and proximal femur determined from the standard antero-posterior radiograph (Fig. 5.12a). The input parameters are the width of the pelvis C, the height of the pelvis H, horizontal and vertical position of the greater trochanter z and x, respectively and the interhip distance l. Denotation of the hip geometrical parameters is shown in Fig. 5.12a. These parameters are determined in relative frame, where line connecting centres of the femurs define horizontal direction and line perpendicular to it defines vertical direction. After adjustment of the direction of the muscle forces and by taking into account equilibrium equations [93, 94] the hip joint reaction force can be determined for each patient individually [45].

To determine the stress distribution in the normal hip joint we need besides the hip joint resultant force also other geometrical parameters describing intrinsic geometry of the hip joint (Fig. 5.12b). These parameters are the radius of the articular surface r which is taken to be the mean radius of the acetabulum and the femoral head and lateral coverage of the acetabulum determined by the center-edge angle of Wiberg (ϑ_{CE}). The center-edge angle is an angle between the the most lateral point at the acetabular roof, center of the femoral head and the sagital plane [189].

In the hips subjected to the avascular necrosis the size and the location of

the necrotic region should be known in advance. Three-dimensional CT or NMR examinations give the most accurate position and shape of the avascular necrotic region [109]. If the CT slides are not available, we can estimate the position of the centre of the necrotic region ϑ_N also from the anteroposterior radiographs as an arithmetic average of the angles determining the most lateral and the most medial point of the necrotic collapsed part (Fig. 5.12b). The size of the necrosis (ϑ_0) is an angular distance between the centre and the most lateral or the most medial point of the necrotic collapsed part (Fig. 5.12b). However, from antero-posterior radiograph φ_N could not be evaluated. Therefore if φ_N is not known, we will assume that the centre of the necrotic region lies in the frontal plane, i.e., $\varphi_N = 0°$ or $\varphi_N = 180°$.

The geometrical parameters of the pelvis and proximal femur can be obtained from the radiographs directly by using a ruler (for the distances) and Mose's rings (for the radius of the hip joint articular surface) [45]. If the required tools are available, the image can also be represented by the profiles which are then transformed into a digital form and processed by the computer [63, 101].

5.2.2 The HIPSTRESS computer system

The mathematical models that have been proposed above to evaluate the stress distribution in the hip joint are too complicated to be directly used by a clinician in everyday practise. It would be useful to have a method that offers a possibility to a clinician to easily determine the stress distribution for an individual patient. Therefore we have developed the HIPSTRESS computer program that offers a user-friendly graphical environment for determination the contact stress distribution

The HIPSTRESS computer program integrates the algorithms of the mathematical models for determining the hip joint reaction force (section 4.2) as well as the algorithms of the mathematical model for determining the contact stress distributions (section 4.4) in the hip. The HIPSTRESS computer system allows determination of the contact stress distribution in the hip joint for known pelvic and hip geometrical parameters. These parameters can be determined directly from the anteroposterior radiograph (section 5.2.1).

The original version of the HIPSTRESS was written in TURBO PASCAL© [92]. It consists of two programs. The advantage of this version is that it does not have requirement to operation system and runs on any computer with installed TURBO PASCAL©.

Because of the necessity of the user-friendly system for clinical praxis the new version in the Microsoft Visual Basic© was developed within this work. New version offers a user-friendly graphical interface and the graphical representation of the results. It also allows the input of the personal data of the patient and manipulation with the data – i.e., printing the results, saving the results and importing the data from the archives. The data are saved in text form, so they can be imported to other programs. Using of the program is described in more details in the help file that is distributed together with the program. This version of the HIPSTRESS requires operating system Microsoft Windows 95© or higher version of this operating system. It was also tested on Microsoft Windows 98©, Microsoft Windows 2000© and Microsoft Windows XP©.

The main executable file is called `HIPSTRESS.exe`. After running it a main window appears (Fig. 5.13). Control of the program is provided by the pop-up menu or by the command buttons in the upper part of the form. After click on the button New (Fig. 5.13) an input form appears (Fig. 5.14). The input form is divided into three parts. In the first part the personal data of the patient can be filled, the filling of this part is optional. The filling of the second part, where the characteristic parameters of the hip joint are, is required as these parameters are used for calculation the stress distribution. Notation of the characteristic

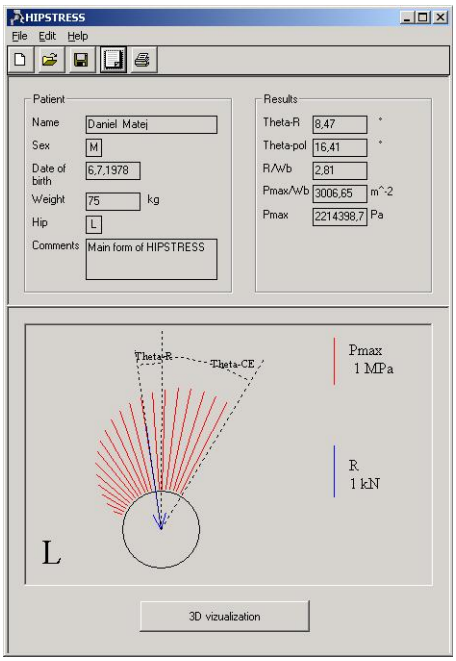

Figure 5.13: The main form of the HIPSTRESS program.

parameters of the hip in the input form is consisted with Fig. 5.12. The third part of the input form is hidden by default and can be shown after click on the button in the lower right edge of the data (button Input data, Fig. 5.14). Than the image of the input parameters appears. The image is interactive and highlights the geometrical parameters that are currently filled in. To run the computation of the contact stress click on the button OK (Fig. 5.14) and you will be returned to the main window. If the computation was finished successfully the results (magnitude of the force $\mathbf{R}$, inclination of the force $\mathbf{R}$ from the vertical axis in the frontal plane (ϑ_R) and position of the stress pole (Θ)) appears in the right part of the

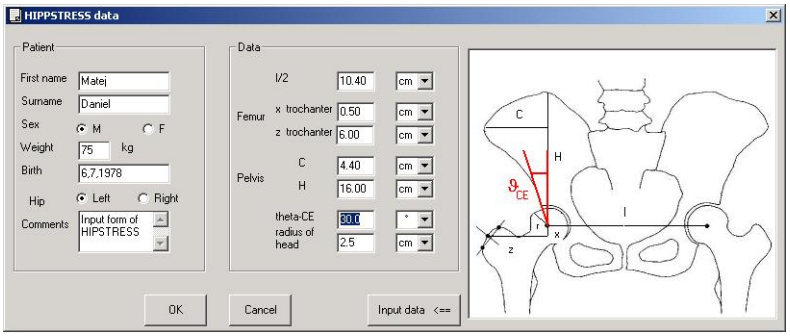

Figure 5.14: The input form of the HIPSTRESS program.

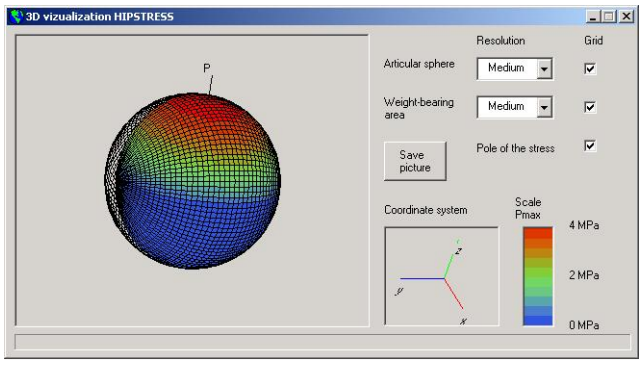

Figure 5.15: The three-dimensional representation of the contact stress distribution in the HIPSTRESS computer program.

main window. The left part of the main form features personal data of patient. In the lower part of the main window a schematical distribution of the contact stress in the frontal plane, hip joint reaction force and position of the stress pole are showed (Fig. 5.13). These results can be saved by click on the button Save, printed by click on the button Print or the input data can be changed by click on the button Change (Fig. 5.13).

The HIPSTRESS computer program offers also three-dimensional representation of the contact stress distribution in the hip joint. After click on the button 3D in the lower part of the main form (Fig. 5.13) a three dimensional representation of the articular sphere appears (Fig. 5.15). The legend in the right side of the form shows the colours corresponding to the values of the stress. The 3D representation of the stress distribution is interactive, it can be rotated by click on it by pointer and drag. The change of coordinate system of the pelvis according to the rotation of the articular sphere is also showed (Fig. 5.15). Resolution of the mesh in which the stress distribution is shown and appearance of the label pointing to the position of the stress pole can be adjusted by interactors in the right part of the form. Resulting image of the stress distribution can be saved in the bitmap format after click on the button Save image (Fig. 5.15).

For extensive clinical studies the algorithms of the program were included as a macro in the Microsoft Excel© yielding the possibility of easy examination of large groups of patients and postprocessing of the results using this table editor (e.g. creating graphs, statistical calculations, manipulation with the data). For developmental purposes the algorithms of the mathematical models for calculation the contact stress distribution are available as script m-files for GNU Octave or Matlab©.

The HIPSTRESS computer system is available from the authors free of charge

only to be used for scientific purposes and according to ethical principles as described in README file that is distributed together with the program.

5.2.3 *Determination of the contact hip stress from nomograms based on a mathematical model*

In the section 5.2.2 the computer program for calculation of the stress distribution over the weight-bearing area was described. From the studies of the stress distribution over the articular surface during gait it has been established that the biomechanical status of the hip can be represented by the maximal value of stress attained on the weight bearing area p_{max} [98, 100]. In this part we present a method for estimation of the maximal hip stress p_{max} without the direct use of the computer. This may sometimes be of advantage since no additional tools and skills are required. If the problem under consideration involves analysis of an individual case or a small number of cases, this method may also be faster.

The nomograms were calculated by using the HIPSTRESS program [92] that is based on the two mathematical models described above (section 4.2 and 4.4). These mathematical models can be adjusted according to the characteristic geometry of the pelvis and proximal femur (section 5.2.1)

The nomograms are presented in the Supplement to Disertation, Appendix J. Below we present only a sample of the nomograms and describe how the peak stress on the weight bearing area can be determined by using the standard anteroposterior radiographs and the presented nomograms. The notation of the input parameters of the hip used for the evaluation of p_{max} by nomograms (Fig. 5.12) is identical to the notation used in the section 5.2.1.

Figs. J.2 to J.6 present the dependencies of the inclination of the resultant hip force ϑ_R in the frontal plane (Fig. 4.14) on the half of the interhip distance ($l/2$). The figures are characterised by the values of the pelvic width (C). Different curves on each graph represent different values of the horizontal distance between the centre of the femoral head and the effective muscle attachment point on the greater trochanter (z) while different values of the pelvis height (H) are taken into account by presenting three different graphs in each figure. For example, Fig.5.16 presents the nomograms for determination of the inclination of the resultant hip force with respect to the vertical ϑ_R if $C = 3$ cm.

Fig. 5.17 presents the dependence of the magnitude of the resultant hip force normalised by the body weight W_B on the half of the interhip distance $l/2$. Different curves on the graph represent different values of the horizontal distance between the centre of the femoral head and the effective muscle attachment point on the greater trochanter z.

Figs. J.7–J.9 present the dependence of the maximal stress on the weight bearing area divided by the body weight and multiplied by the square of the femoral head radius $p_{max}\, r^2/W_B$ on the sum of the angles ϑ_R and ϑ_{CE}. Fig. J.9 is presented

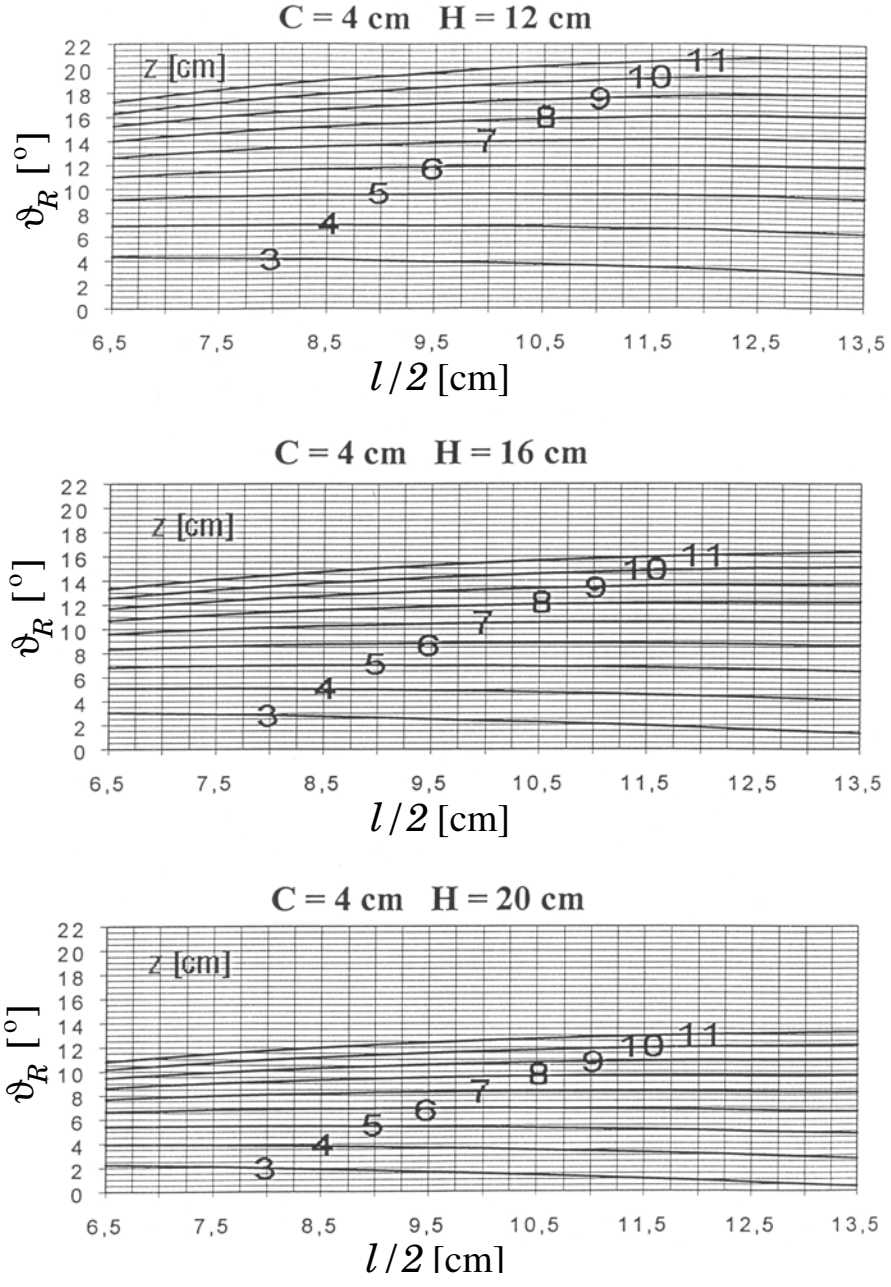

Figure 5.16: The nomograms for determination of the inclination of the resultant hip force with respect to the vertical ϑ_R ($C = 4$ cm)

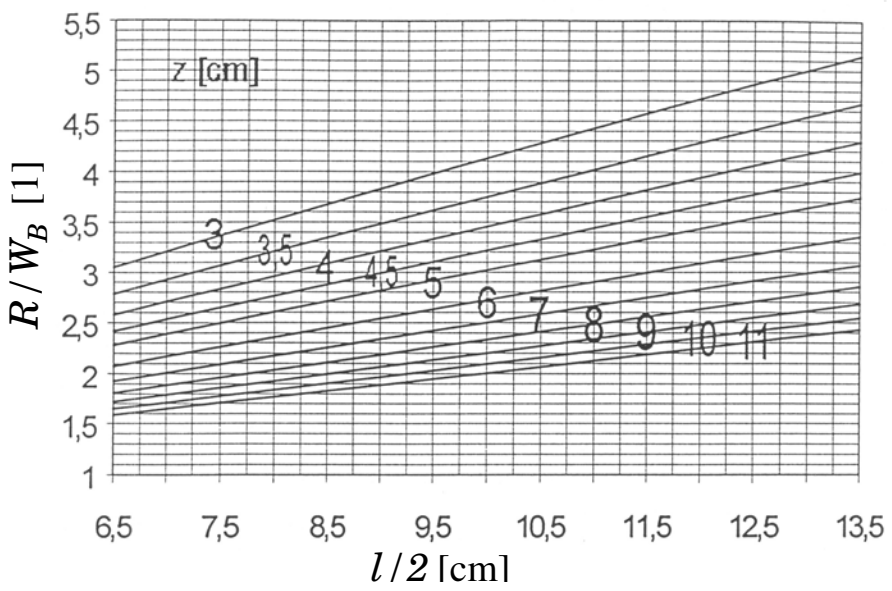

Figure 5.17: The nomogram for determination of the magnitude of the resultant hip force normalised by the body weight R/W_B

here as Fig 5.18 The figures are characterised by the range of $\vartheta_R + \vartheta_{CE}$: Fig. J.7 accounts for the interval of $\vartheta_R + \vartheta_{CE}$ between 10 and 20 degrees, Fig. J.8 accounts for the interval of $\vartheta_R + \vartheta_{CE}$ between 20 and 30 degrees while Fig. J.9 accounts for the interval of $\vartheta_R + \vartheta_{CE}$ between 30 and 60 degrees. Different curves on the graph represent different values of R/W_B.

5.2.3.1 Determination of the peak contact stress using nomograms – step-by-step instructions

As there are many parameters that influence the maximal value of stress in the hip joint articular surface p_{max}, it is necessary to perform the determination of the maximal stress stepwise as described below.

1. In the first step we determine the geometrical parameters $C, H, z, x, l/2, \vartheta_{CE}$ and r (Fig. 5.12). A standard anteroposterior radiograph can be used. We determine the body weight W_B.

2. In the second step we determine the inclination of the resultant hip force ϑ_R from Figs. J.2–J.6. We chose the figure corresponding to the pelvic width C that is the closest to the measured value of C and the graph in this figure that corresponds to the pelvic height H that is the closest to the measured value of H. We chose the curve on the graph that corresponds to the horizontal

coordinate of the effective muscle attachment point on the greater trochanter z that is the closest to the measured value of z. We take into account the value of the interhip distance $l/2$ on the abscissa of the graph and determine the angle ϑ_R on the ordinate.

3. In the third step we determine the magnitude of the resultant hip force normalised with respect to the body weight R/W_B from Fig. J.1. In contrast to the corresponding inclination of the resultant hip force, only one graph is sufficient to represent the magnitude of the resultant hip force to yield the same precision of p_{max}. We chose the curve on Fig. J.1 that corresponds to the horizontal coordinate of the effective muscle attachment point on the greater trochanter z that is the closest to the measured value of z. We take into account the value of the interhip distance $l/2$ on the abscissa of the graph and determine the relative magnitude of the force R/W_B on the ordinate.

4. In the fourth step we determine the maximal stress on the weight bearing area divided by the body weight and multiplied by the square of the femoral head radius, $p_{max}\, r^2/W_B$ from Figs. J.7– J.9. We add the angle ϑ_R obtained in step 2 to the centre-edge angle ϑ_{CE} and chose the figure corresponding to the range that encloses the obtained sum $\vartheta_R + \vartheta_{CE}$. On the graph we choose the curve corresponding to the normalised resultant hip force obtained R/W_B in step 3. We take into account the value of the sum $\vartheta_R + \vartheta_{CE}$ on the abscissa of the graph and determine the relative maximal stress $p_{max}\, r^2/W_B$ on the ordinate.

5. In the fifth step we determine the maximal hip joint stress p_{max}. We multiply the normalised value obtained in step 4 by the body weight W_B and divide it by the square of the femoral head radius (r^2).

The resultant hip force can be obtained directly from direct measurements using implanted instrumented endoprosthesis [18,26,167] or from the external laboratory measurements in combination with mathematical models [8, 43, 74, 150, 171, 172, 178]. In such case, the peak stress can be determined from Figs. J.7–J.9 using only steps 4 and 5.

Sometimes, especially in the studies of the data from the archives, the information about the body weight is not available. In such case the normalised quantity p_{max}/W_B is also useful in evaluation of the biomechanical status of the hip.

For example, we would like to determine the maximal stress for a hip with l=17 cm, C=4.5 cm, H=13 cm, z=4 cm, $\vartheta_{CE} = 25°$, r=2.5 cm and W_B=750 N.

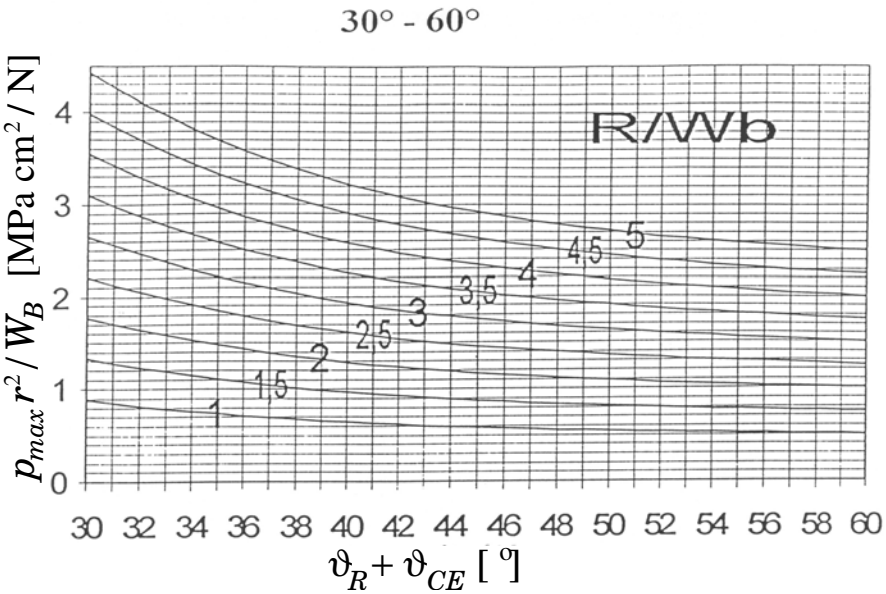

Figure 5.18: The nomogram for determination of the maximal stress on the weight bearing area divided by the body weight and multiplied by the square of the femoral head radius $p_{max}\,r^2/W_B$ ($\vartheta_R + \vartheta_{CE}$ between 30 and 60 degrees).

We choose Fig. 5.16, the first graph on the top of the figure. It can be seen from the curve labelled by the number 4 that the inclination ϑ_R corresponding to the value of $l/2$=8.5 cm is 7°. Then we consider Fig. 5.17, choose the curve labelled by the number 4 and obtain the value of the normalised force R/W_B to be 3.1. The sum $\vartheta_R + \vartheta_{CE}$ is apparently $7° + 25° = 32°$, therefore we choose Fig. 5.18 to determine the normalised maximal stress. In Fig. 5.18 we choose the curve labelled by the number 3. The value of $p_{max}\,r^2/W_B$ that corresponds to the sum $\vartheta_R + \vartheta_{CE} = 32°$ is 2.5. To obtain the maximal stress p_{max} we multiply the result by the body weight W_B and divide it by the square of the femoral head radius r^2, 2.5 750 N/6.25 cm^2 = 3.0 MPa.

The value of p_{max} obtained directly by the HIPSTRESS program [92,94] for the above data is 3.2 MPa, therefore the error made by using the nomograms instead of the program is in this particular case about 7%. For illustration Fig. 5.19 shows the distribution of the difference between the value of p_{max} determined by the computer and using nomograms for thirty-eight patients. The average difference between the value of p_{max} determined by the HIPSTRESS computer program and manually using the nomograms was 4.6%. It can therefore be concluded that within this precision there was no need for presenting additional nomograms to account for different values of the vertical coordinate of the effective muscle

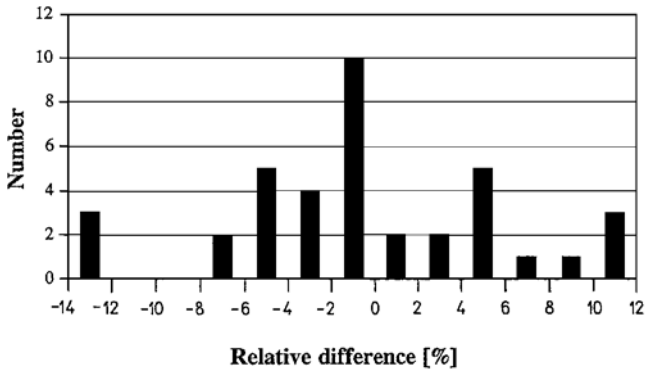

Figure 5.19: Histogram of the relative differences between the values of p_{max} determined by the HIPSTRESS computer system and p_{max} determined manually using nomograms given in Figs. J.2–J.9. The analysis was performed for 38 patients.

attachment point on the greater trochanter $x \in (-1 \text{ cm}, 1 \text{ cm})$.

5.3 CLINICAL STUDIES

5.3.1 Contact stress in the normal and the dysplastic human hips

The group of dysplastic hips and the group of normal hips were examined with respect to the peak contact stress p_{max} and above defined new biomechanical parameters: the stress gradient index G_p (Eq. 4.61) and the functional angle of the weight-bearing area ϑ_F (Eq. 4.62). The correlation between the index p_{max}, G_p, ϑ_F and the centre-edge angle ϑ_{CE} is studied.

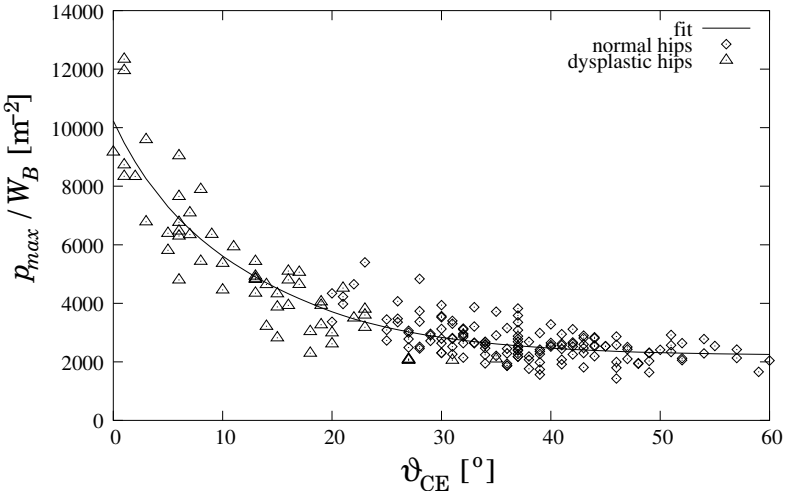

Figure 5.20: The correlation between the index of the peak contact stress (p_{max}) normalised with respect to the body weight (W_B) and the centre-edge angle ϑ_{CE}. The values for the normal hips are denoted by the symbol $\diamond$ and the values for the dysplastic hips are denoted by $\triangle$.

The standard anteroposterior radiographs of the hips were taken from the medical records of the Department of Traumatology and Department of Orthopaedic Surgery, Medical Centre, Ljubljana, Slovenia. In total we have 56 dysplastic hips of 20 subjects with unilateral dysplasia and 18 subjects with bilateral dysplasia. In the group of dysplastic hips 9 hips belonged to male persons and 47 belonged to female persons, 32 hips were right and 24 were left. The normal hips belonged to 146 persons who were subject to the X-ray examination of the pelvic region for reasons other than degenerative diseases of the hip joints. These radiographs showed no signs of the hip pathology. In the group of normal hips only one hip was taken into account from each subject.

The body weight of the patients in the each group was not known. The contours of the bony structures in each anteroposterior radiograph were put into digital form and the measurements of the geometrical parameters were performed by a

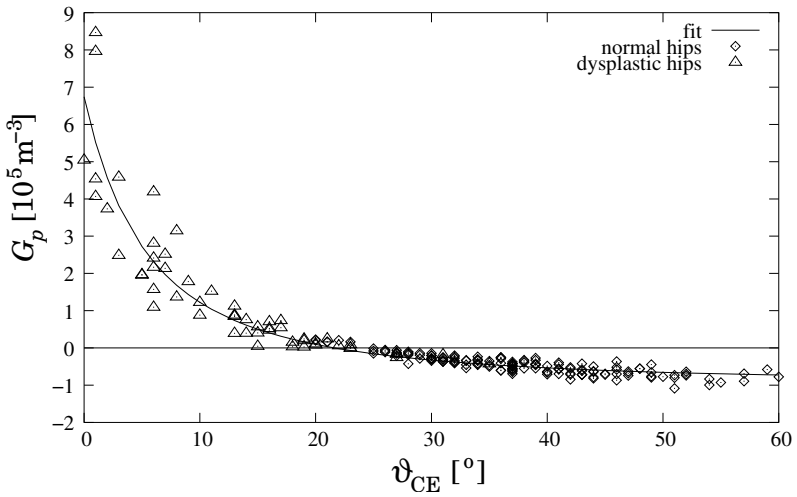

Figure 5.21: The correlation between the index of the stress gradient (G_p) normalised with respect to the body weight (W_B) and the centre-edge angle ϑ_{CE}. The values for the normal hips are denoted by the symbol $\diamond$ and the values for the dysplastic hips are denoted by $\triangle$.

Correlation	$\mathbf{R^2}$	**P**
$p_{max}/W_B - \vartheta_{CE}$	0.850	< 0.001
$G_p - \vartheta_{CE}$	0.897	< 0.001
$\vartheta_F - \vartheta_{CE}$	0.983	< 0.001

Table 5.3: Correlation coefficients between the normalised peak contact stress (p_{max}/W_B), the normalised stress gradient index (G_p/W_B), the functional angle of the weight-bearing area ϑ_F and the centre-edge angle ϑ_{CE} and their statistical significance (P).

computer program HIJOMO [91, 101, 199]. The program HIJOMO was also used to determine the centre-edge angle ϑ_{CE} and the femoral head radius r that are needed for calculation of the contact stress distribution (see section 5.2.1).

The interdependence between the centre-edge angle ϑ_{CE} and the normalised peak contact stress p_{max}/W_B, normalised stress gradient index G_p/W_B and functional angle of the weight-bearing area are shown in Figs. 5.20, 5.21 and 5.22, respectively. The shape of the numerically obtained fitting curve is consistent with the above described mathematical model [134]. The values of p_{max}/W_B are large for lower ϑ_{CE}, while for higher center-edge angles the values of p_{max}/W_B are negative (Fig. 5.20). For lower ϑ_{CE} the values of G_p/W_B are large and positive, while for higher ϑ_{CE} the values of G_p/W_B become small and negative (Fig. 5.21). The normalised stress gradient index G_p/W_B changes its sign at $\vartheta_{CE} \approx 20°$. The functional angle of the weight-bearing area is small for lower ϑ_{CE} while for higher

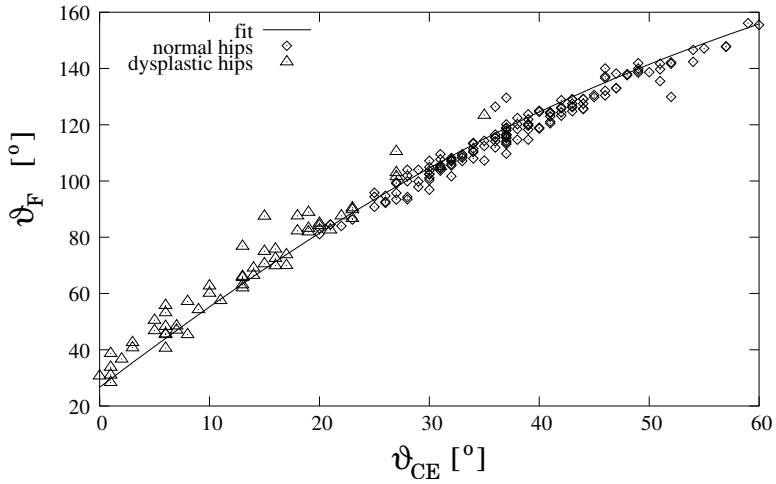

Figure 5.22: The correlation between the functional angle of the weight-bearing area (ϑ_F) and the centre-edge angle ϑ_{CE}. The values for the normal hips are denoted by the symbol $\diamond$ and the values for the dysplastic hips are denoted by $\triangle$.

	Normal	Dysplastic	Difference (P)
p_{max}/W_B [m^{-2}]	2691.6	5274.1	< 0.001
G_p/W_B [10^5 m^{-3}]	- 0.445	+ 1.481	< 0.001
ϑ_F [°]	117.0	66.8	< 0.001

Table 5.4: The average values of the normalised peak contact stress (p_{max}/W_B), the normalised stress gradient index (G_p/W_B) and functional angle of the weight-bearing area (ϑ_F) in normal and dysplastic hips.

ϑ_{CE} it is higher.

The scattering of p_{max}/W_B, G_p/W_B and ϑ_F as the function of ϑ_{CE} shows that in determining of p_{max}/W_B, G_p/W_B and ϑ_F the geometrical parameters of the hip other than ϑ_{CE} (like for example the interhip distance [95,94]) are also important. The scattering is higher for lower ϑ_{CE} (i.e., for $\vartheta_{CE} < 20°$).

To characterise the role of the particular biomechanical parameter in the assessment of the hip dysplasia the statistical significance of the difference in the average value of p_{max}/W_B, G_p/W_B and ϑ_F between the group of the normal hips and the group of the dysplastic hips was calculated by the two-tailed pooled t-test (Tab. 5.3). The null hypothesis [53] assuming the equal average values is rejected at the level lower than 0.001 for all parameters. It can be therefore concluded that all the defined biomechanical parameters (p_{max}/W_B, G_p/W_B and ϑ_F) are appropriate parameters for the assessment of the hip dysplasia.

Since the hip joint is usually considered as dysplastic for $\vartheta_{CE} < 20°$ [118] and we observed that G_p/W_B changes its sign at approximately 20° we suggest a new

definition of the hip dysplasia. It is based on the sign of the stress gradient index G_p. Hips with positive normalised stress gradient index $G_p/W_B > 0$ are taken to be dysplastic and hips with negative normalised stress gradient $G_p/W_B < 0$ index are taken to be normal.

5.3.2 *Relationship between biomechanical parameters for evaluation of the hip dysplasia and clinical status of the hip*

Besides the biomechanical and the radiographical parameters for evaluating dysplasia of the hip, the functional scores are also used in clinical practice. The Harris hip score is worldwide distributed method for clinical evaluation of the status of the hip that includes patient's opinion on pain, the functional activities and the range of motion [73]. Therefore it is of interest to compare the Harris score that is based on the subjectively determined patient's feeling to the objectively computed biomechanical parameters G_p and p_{max}.

For testing the relationship between the gradient index and the clinical score, we considered patients which were not included into the above study of normal and dysplastic hips (section 5.3.1). The new group consists of 27 patients. In total we have 45 hips. The Harris hip score was evaluated for these patients by clinician at the Department of Orthopaedic Surgery, Medical Centre, Ljubljana, Slovenia. It was obtained that the average Harris hip score was 88.4 (standard deviation 18.40).

The long-term damage threshold level of the contact stress for the acetabular cartilage was estimated in study of hips subjected to the developmental dysplasia of the hip to be 2 MPa [70]. For a normal man with a weight seventy kilogrammes the normalised peak contact stress that the cartilage can tolerate without pathological changes is 2912.5 m^{-2}. According to this value the hips were divided into two groups: normal and dysplastic. The hips with higher value p_{max}/W_B were denoted as dysplastic while the hips with lower value p_{max}/W_B were denoted as normal. The group of normal hips consists of 9 hips and the group dysplastic hips consists of 36 hips.

In our work new definition of the hip dysplasia was introduced. According to our suggestion of estimating the hip dysplasia based on the sign of the normalised stress gradient index, the same group of hips were divided into two groups: the group of dysplastic hips with positive stress gradient index ($G_p/W_B > 0$) which consists of 16 hips and the group of normal hips with negative normalised stress gradient index ($G_p/W_B < 0$) which consists of 29 hips.

For comparison, the method for estimating hip dysplasia based on the centre-edge angle was used. In clinical practice, hips with centre-edge angle ϑ_{CE} lower than 20° are considered to be dysplastic [118]. According to this classification, the control hips were divided into two groups: group of dysplastic hips with $\vartheta_{CE} < 20°$ which consists of 10 hips and group of normal hips with $\vartheta_{CE} > 20°$ which consists of 35 hips.

The difference in Harris hip score between the corresponding groups of normal

and dysplastic hips was estimated by a non-parametrical statistical test (Kolmogorov-Smirnov test). If the hips were grouped according to the value of p_{max}/W_B and G_p/W_B, then the null hypothesis assuming equal average values of Harris hip scores in both groups [53] was rejected at the level lower than 0.05 ($P = 0.023$ and $P = 0.031$, respectively), i.e., statistically significant difference in Harris hip score exists between normal and dysplastic hips. If the hips were grouped according to the value of ϑ_{CE}, no statistically significant difference between the groups of normal and dysplastic hips was observed ($P = 0.233$).

5.3.3 *Aseptic necrosis of the femoral head – biomechanical case study*

To illustrate the importance of the position and size of the weight bearing area and also of the intrinsic geometry of the hip, we calculated the stress distribution for two hips subject to avascular necrosis of the femoral head. The standard anteroposterior radiograms of two female patients with diagnosed aseptic necrosis of the femoral head were taken from the Department of Orthopaedic Surgery, Clinical Center in Ljubljana, Slovenia (Fig. 5.23). To determine the contact stress distribution, an adjustment of the mathematical model according to the anteroposterior radiograms was used as described above. We calculated the stress that the same subjects would have if no necrotic defect were present, and the stress taking into consideration the necrotic defect (Fig. 5.24). The measured geometrical parameters of the hip and the results are presented in Tab. 5.5, while the stress distribution for the two patients as visualised from the top is given in Fig. 5.24. In hip A, a higher resultant hip force and an intrinsically higher peak stress will be found if no necrosis is present than in hip B (Fig. 5.24A). In hip A the necrotic defect was positioned on the lateral edge of the acetabulum, so that the necrotic

		Hip	
		A	B
Position of the trochanter	z / [mm]	60.6	72.0
	x / [mm]	17.4	7.6
Geometry of the pelvis	l /[mm]	199.1	187.7
	C /[mm]	60.9	69.6
	H / [mm]	143.1	145.6
Geometry of the hip	r / [mm]	22.5	24.3
	ϑ_{CE} / [°]	32.0	37.0
Geometry of the aseptic necrosis	ϑ_N / [°]	4	19
	φ_N / [°]	180	0
	ϑ_0 / [°]	28	20
Resultant hip force	R/W_B/[1]	2.78	2.34
	ϑ_R / [°]	7.29	9.06
	φ_R / [°]	0	0
Stress distribution without necrosis	p_{max}/W_B/[m^{-2}]	3595	2271
	Θ / [°]	16.62	7.89
	Φ / [°]	180.0	180.0
Stress distribution with necrosis	p_{max}/W_B / [m^{-2}]	7814	2704
	Θ / [°]	29.97	4.73
	Φ / [°]	180.0	180.0

Table 5.5: The geometric parameters of the hip and the calculated biomechanical parameters in the two clinical cases (hips A and B). The biomechanical parameters are calculated for a situation with and without avascular necrosis of the femoral head.

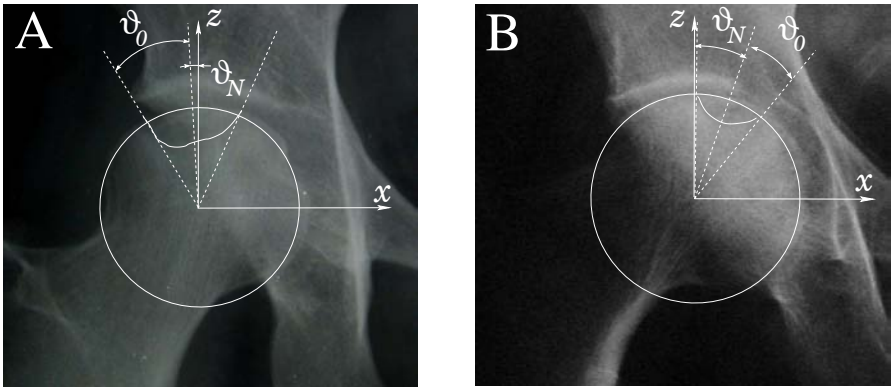

Figure 5.23: Anteroposterior radiograms of two patients subjected to avascular necrosis of the femoral head. The position and size of the necrotic region are shown. The values of the geometric parameters of the hip, the calculated resultant hip force and the calculated peak contact stress are given in Tab. 5.5.

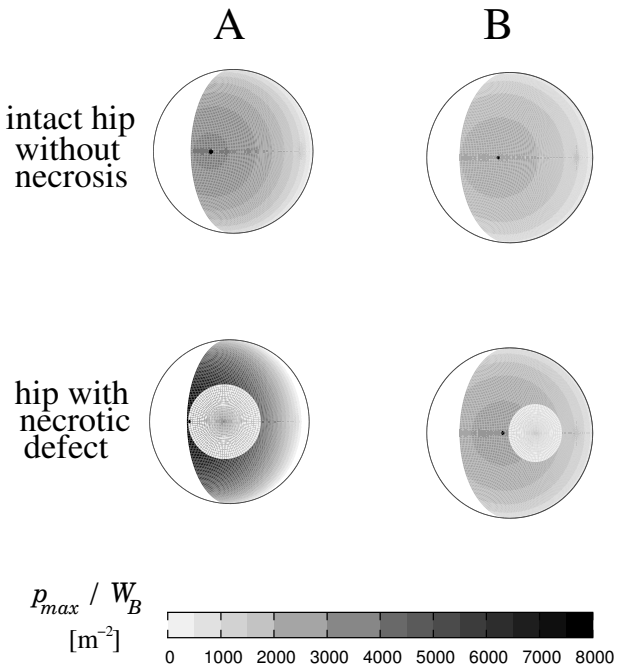

Figure 5.24: The calculated projection of the stress distribution into xy plane in hips A and B, considering intact healthy hips and hips subjected to avascular necrosis of the femoral head.

defect nearly doubled the peak stress in comparison with the hypothetical situation without necrosis (Tab. 5.5A, Fig. 5.24). Hip B is loaded by a lower hip joint reaction force, and the peak stress without necrosis would be lower than in hip A without necrosis (Fig. 5.24B). Moreover, the necrotic defect was positioned more medially and the increase in the peak stress due to the necrotic defect was rather small (Tab. 5.5, Fig. 5.24B).

5.4 Practical application of the basic research - acetabular component of total hip replacement

Common complications of the total hip replacement (THR) are the hip loosening and a wear of the UHMWPE particles [142]. Therefore numerous improvements in the design [82], materials [136] and fixation of the prosthesis [107, 142] have been proposed. Although various types of THR were designed, the articular surfaces of the artificial femoral head and the corresponding acetabular cup have, with most of them, spherical shapes [136]. It was shown (section 5.1.3) that in the normal hip the alterations in the shape of the articular surface influence the contact stress distribution in the hip. Although the artificial joint structure differs from the natural one, Sýkora, 2004, showed that the model for calculating the contact stress distribution shown in section 4.4 can be used also with the artificial joint.

According to Fig. 5.9, the medially located non-weight bearing area on the articular surface may considerably decrease the contact stress (Fig. 5.9) which is related to the contact stress redistribution (Fig. 5.11H). Lowering the contact pressure between the femoral and acetabular component of THR would decrease a wear of the acetabular component. Moreover, more uniform distribution on the wearing surface of the artificial acetabular cup would give more uniform stress distribution on the bone/cup interface, that would improve the fixation of the implant. Therefore in this part, a new type of the THR acetabular component will be presented beeing based on introducing the non-weight bearing area.

As will be discussed later, the medially situated non-weight bearing area contributes to the symmetry of the articular surface with respect to the loading force which causes the contact stress redistribution (for detailed description see section 6.2.2). Such a non-weight bearing area is observed also at the physiological

Figure 5.25: Schematic view of the physiognomic cup with skewed lateral part.

hips, where the cartilage has a horseshoe shape [4, 188]. Therefore we denote our new design as *physiognomic artificial acetabular cup*.

The vast majority of hip prostheses have spherical cobalt-chrome alloy femoral balls bearing against polyethylene acetabular cup that has a form of hemisphere [136]. In the design of new type of the acetabular component we came out from this basic type that was changed by introducing the non-weight bearing area medially. The non-weight bearing area can be obtained by cut out a piece of the original hemispherical polyethylene cup or by variation in the shape of the inner articular area. In total, three different types of the artificial acetabular cups were proposed:

Figure 5.26: Schematic view of the physiognomic cup with hole.

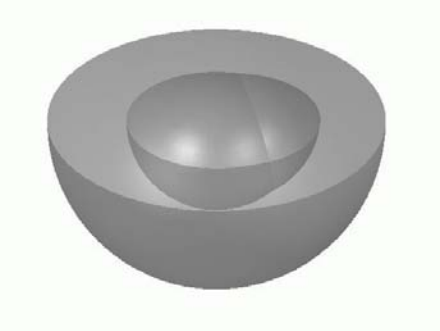

Figure 5.27: Schematic view of the physiognomic cup with medially assymetrical inner surface.

1. *Acetabular cup with skewed medial part* – the symmetry of the weight-bearing area with respect to the loading force is maintained by skew of the medial part of the acetabular cup (Fig. 5.25).

2. *Acetabular cup with a hole* – the non-weight bearing area is shaped by drilling a hole in the medial part of the acetabular cup (Fig. 5.26).

3. *Acetabular cup with medially asymmetrical inner surface* – the articular surface of the acetabular cup is medially asymmetrical by means of increase of the inner radius of the acetabular cup (Fig. 5.27).

The improvement proposal of the artificial cup described above come out from a widely used UHMWPE hemispherical cup. Its simple design allows to use this new cup in current systems for THR without any special requirements. It means that a standard femoral components and standard method of fixation may be used. This design can be applied for all types of prosthesis where the polyethylene acetabular cup is used. For example, the femoral head may be made from bioceramics or the acetabular cup may be anchored into a metallic capsule for a cementless application. Implantation of this cup type can be carried out using a standard operation technique and instruments.

A detailed description of the cup design can be found in the the utility model of the Physiognomic acetabular cup No. 2003-14728 that was registered by the Industrial Property Office of the Czech Republic. This idea of the physiognomic acetabular cup is protected by laws.

Chapter 6

DISCUSSION

6.1 Hip joint resultant force

This study was addressed to define complex three-dimensional model of the hip musculature suitable for static analysis and use this model for calculation of the hip joint resultant force in the one-legg standing. The computation of **R** was performed using inverse dynamics optimisation after various optimisation criteria. Also a new system for visualisation the musculoskeletal system was developed within this work.

A newly defined model of the hip musculature consists of twenty-seven muscle units with defined attachment points on the pelvis and lower musculature, physiological properties like physiological cross-sectional area and maximal isometrical force and density of the human spindle organs (Tab. 4.1). Since the complex muscle model was not available yet the data were obtained from various sources [27, 48, 174, 195]. The particular data were obtained from different patients using different methods and therefore the muscle model may not exactly describe a musculature of a standard patient. The distribution of the Golgi tendon organs in the muscle has not been reported and was therefore estimated on the density of the muscle spindle organs in the muscle [174]. Although the Golgi tendon organs and the muscle spindles are both involved in the proprioception, their function differs [55, 166, 169]. Hence, their density in the muscles may also differ according to various function of the muscles in the human movement.

A new visualisation system for biomechanical analysis was programmed as a part of this work (section 4.1.1). This system provides three-dimensional interactive visualisation of the bone and the muscle structures. The bone structures are visualised as polygonal objects (Fig. 4.4). The polygonal models of the bones may not be available for all bones in the human body and they may be problems with scaling of these structures to fit the individual bony geometry of the patient. Therefore the upgraded version of the visualisation system, that is under development, will proceed scans from computer tomography to reconstruct bony structures.

The complex muscle model of the hip (section 4.1.2) has been used for calculation of the hip joint reaction force by using optimisation method of inverse

dynamics. The inverse dynamics has been criticised that it is influenced by the accuracy of the measured limb motion and that is does not describes dynamics of muscle excitation as a result of earlier muscle activation [8, 75, 129, 197]. Most reservations aim against the biases of the inverse dynamics in the evaluation of the human motion. However, in our analysis static posture of one-legg standing was chosen to describe the load on the hip (**R**). It has been shown that the one-legged stance is important, not only in its own right, but also more generally due to its resemblance to the stance phase of slow gait [137]. In the static posture the neuromuscular activation is assumed to be constant in time and the position of the patient can be described more properly than during the motion. Since all the internal forces are constant as the body is in the static state of equilibrium, optimisation by the cost function integrated over the time frame as suggested in forward optimisation (Fig. 3.2) would give the same results as optimisation by the same cost function at a given instant as suggested in the inverse dynamics (Fig. 3.1). Hence, for a static position the inverse dynamics optimisation can be used instead of the forward optimisation. It should be noted that a static model is not suitable for analysis of balance maintaining where the corrective actions in the hip makes the internal forces time-dependent [164].

6.1.1 Sensitivity of the hip joint resultant force on the optimisation criterion

It is widely accepted that the muscle activity is optimised to a certain criterion [23, 41, 130, 155]. Several optimisation criteria have been proposed but none of them have been found significantly better than the others [41, 143, 181]. The aim of this study was to estimate how the choice of the optimisation criterion influences the resultant hip joint force (**R**).

The optimisation criteria that give high magnitudes of the hip joint reaction force ($G_{M_y(F/Mmax)}$ and $G_{M_y(F/Mmax)^2}$) were suggested to ensure activation of adductors (Eq. 4.17) what was really achieved (Fig. 5.1h). Activity of the abductors is certainly followed with the activity of the abductors in order to maintain equilibrium (Eq. 4.4). Fig. 5.1h shows that activation of the abductors therefore increases the overall muscle force (Fig. 5.1h) and resultant hip force (Eq. 4.5) to extremely high values which is physiologically unfavourable [181]. Therefore this function may not be suitable for the analysis of the musculoskeletal loading in one-legg standing and will be excluded from the further considerations. Increase in R for $G_{M_y(F/Mmax)}$ and $G_{M_y(F/Mmax)^2}$ was not observed in nine-muscle model, because it contains only abductors (Tab. 4.2). Therefore in the nine-muscle model the sign of the y component of $\mathbf{M}_{max}$ is the same in all muscles and the optimisation criterion (4.17) is mathematically identical to the criterion (4.15). It explains the

agreement in the results for $G_{M_y(F/Mmax)}$ and $G_{M_y(F/Mmax)^2}$ in the nine-muscle model (Tab. 5.1, Fig. 5.1e,g).

Other criteria (Eqs. 4.12–4.15, 4.18–4.21, 4.26 and 4.35) give approximately the same magnitude and direction of $\mathbf{R}/W_B$ for a given muscle model independently on the type of the optimisation criterion. Therefore it can be concluded that in evaluation of the hip joint reaction force the choice of the optimisation criterion is not crucial as the $\mathbf{R}$ obtained by various optimisation principles is the same. It would likely stand also in the forward dynamics optimisation. Anderson & Pandy, 2001 showed that the load of the hip predicted by the forward and by the inverse optimisation in walking is almost the same. The inverse optimisation is computationally less demanding in comparison to forward optimisation approach [72, 178, 191, 194] and can therefore be more appropriate for estimation of the load in individual patient.

It was shown that the nine-muscle model gives almost the same values of $\mathbf{R}$ as twenty-seven muscle model if the attachment points from the twenty-seven muscle model were taken. Therefore simple muscle models can be adequate to estimate the joint load which is related to the fact that for a given body position only few of available muscles are active to maintain equilibrium (Fig. 5.1). For example in one-legg standing the activity of abductors is required to maintain equilibrium [137] and therefore only the abductors are included in the nine-muscle model [93]. In estimation of the load in other static positions the electromyografic signals can be used as guides to choose active muscles [41, 147].

If different geometry of the attachments of the muscle models is used the values of the hip joint resultant force are changed. To improve the accuracy of the calculation of $\mathbf{R}$ the muscle model should be determined more accurately since it changes the resultant hip joint reaction force more than the choice of the optimisation criterion. Therefore a method should be developed according to which a three-dimensional muscle geometry will be determined for each patient individually using a three-dimensional imaging techniques (CT or NMR).

The type of the optimisation criterion is manifested in the force pattern of the muscles (Fig. 5.1). In this work we have introduced a new variable that describes synergism of the muscle activity - the muscle synergism index. It was shown that this new variable is suitable to describe muscle synergism. Small values of S gives mainly linear criteria and G_{Rnonlin}. If the assumption of the muscle synergism as a physiological constraint [52, 163, 181] is accepted than the criteria that gives small values of S may be unsuitable to describe physiologic activation of the muscles. Therefore the nonlinear criteria which predict better distribution of the net force between the muscles seems to be more appropriate [41, 155, 163].

The computed muscle activation pattern should agree with the muscle activation measured using electromyography [7,60,133]. All the nonlinear criteria predict high forces in the gluteus medius which is in accordance with EMG measurements (Figs. 5.1 and 5.2). On the other hand, the EMG signal shows activation of gluteus maximus and adductor longus while their activity predicted by optimisation procedure is zero. This inconsistency origins in the source of data. The EMG measurements were obtained for a walking patient while the mathematical model of the one-legged stance was derived for the static posture (section 4.2). In the static posture the inertial forces are taken to be zero, while in movement the nonzero inertial force can yield activation of other muscles. To validate the optimisation criteria the measurements of electromyografic activity of the muscles in the static state of equilibrium are required. In our study, EMG activity was available only for a few muscles. In further studies the EMG signal from more muscles in a static state of one-legg standing should be recorded.

6.1.2 Neurophysiologically based optimisation criterion

In our work we have predicted a new criterion for static optimisation which is based on the minimisation of the signal from the Golgi tendon organs (section 4.2.2). Based on the data from literature [42, 122, 156, 166] concerning the functions of the Golgi tendon organs, three types of optimisation functions were proposed: one linear and two nonlinear.

The hip joint resultant force $\mathbf{R}$ predicted by this optimisation criteria is within ranges predicted by other optimisation criteria (Tab. 5.1). Hence, the reader may come to conclusion that there is no need for definition of the new optimisation criteria as all of them give the same values of $\mathbf{R}$. However, the previous optimisation criteria did not explain regulation of the muscle activity and they are based on the optimisation of the muscle output, i.e., muscle forces, stresses or moments (Tab. 3.1). Unlike these criteria a new criterion explains the regulation of the muscle activity. In the human body the CNS activates the muscles, activity of which is sensed by the Golgi tendon organs and Golgi tendon organs sends the information about the muscle force back to the CNS (Fig. 6.1). According to our hypothesis CNS consequently regulates the output to the muscles (efferent signals) to obtain minimum of the input signals from the Golgi tendon organs (afferent signals). Such regulation presents a typical mechanism of the feedback control which is the basic regulation mechanism in the biosystems [55, 149].

The indirect evidence exists that supports this new optimisation criterion. Some of the muscles in the spine that span adjacent vertebrae are too weak to produce a net force for the spine movement [2]. However, these muscles contain

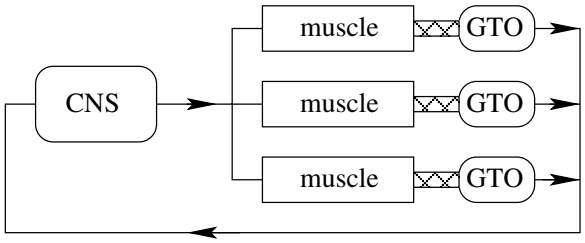

Figure 6.1: Regulation of the muscle control by Golgi tendon organs (GTO) as a feedback mechanism. Arrows indicates the path of the signal.

large number of the proprioceptional receptors [2]. In the cost function (Eq. 4.35) these muscles have higher weight coefficients and their strength considerably increases the value of the optimisation function that should be minimal. According to our hypothesis these muscles serve as the sensors of the relative movement of the vertebrae. Since the bony spine presents in addition to the load bearing structure also protection for the spinal cord [4, 71, 140] that can be injured by an extensive motion of the vertebrae, knowledge on the motion of the spine is very important for the regulation of the muscle activity of the back muscles [176].

It should be stressed that the proposed optimisation function is valid in the static posture or in the slow movement of the body only. In the fast movement the regulation is shifted from the feedback to the feedforward control [39, 166] where the pattern of the motion is generated by CNS in advance [125]. In our analysis only the signals from the Golgi tendon organs were considered. It has been suggested recently that in the regulation of the motion also other receptors like muscle spindles, joint receptors or cutaneous receptors may be involved [55, 81, 169, 174]. Also the regulation in the CNS is simplified to a simple feedback control (Fig. 6.1). The CNS is certainly the most complicated structure in the human body and in the regulation of the motion several structures may be responsible [65, 192].

6.2 Contact stress distribution on the hip joint articular surface

In this work the new derivation of the model equations for calculation of the contact stress distribution for arbitrary direction of the hip joint is presented. After introducing alternative spherical coordinate system in the acetabular frame (Fig. 4.12) the derivation became more simple and transparent.

The accuracy of the presented values and shapes of the contact stress distributions can be influenced by the assumptions of the model for calculation of the contact stress distribution. It was assumed that the stress distribution can be described by a cosine function (Eq. 4.36). The derivation of the cosine function is based on the assumption that the radial stress in the hip joint articular surface can be calculated according to Hooke's law [28, 68, 120], i.e., the radial strain in the articular surface of the hip is assumed to be proportional to the radial strain within the cartilage layer. As the cartilage was assumed to behave as ideally elastic body, stress was taken to be proportional to the strain. The experimental results imply, that the stress/strain relationship for the human articular cartilage could be approximated by a linear function, i.e., for the cartilage Hooke's law can be applied [30, 183]. The Hooke's law implies that the contact stress in the cartilage is proportional to its radial strain and thickness. A constant thickness of the cartilage layer before deformation was assumed [28,94]. In reality the articular cartilage of the acetabulum is slightly thinner at the edges [145]. The same deformation therefore causes higher stress in the thinner parts of the cartilage.

In deriving the cosine stress distribution function the underlying bones were taken to be absolutely rigid [28]. Deformations of the bone under physiological conditions could change the stress distribution as shown by Bay et al., 1995. Also deviations from the spherical shape of the bone surfaces of the femoral head and acetabulum will change the cosine stress distribution (Eq. 4.36) [3]. In the normal hips the femoral head and the acetabulum are out-of-round [98] and were found to have a shape of rotational conchoid [107]. Therefore the cosine distribution function should be further upgraded by considering special corrective coefficients that describe deviation from sphericity and by assuming different thickness of the cartilage on the weight-bearing area [99].

6.2.1 Contact stress distribution in the normal and the dysplastic hips during routine activities

The mathematical model of contact stress distribution in the human hips was used to determine the hip joint contact stress distribution for normal and dysplastic

hips during various activities: walking at different speed, staircase walking, one-legg standing, sitting down and standing up from the chair. The data of the load of the hip were determined from the measurement by special implanted instrumented endoprosthesis (section 4.3).

The highest magnitude of the hip joint resultant force normalised to the body weight (R) as well as the highest peak contact stress in the hip joint normalised to the body weight (p_{max}/W_B) were observed in walking downstairs (Tab. 5.2). Measurements by an implanted instrumented endoprosthesis showed considerable differences in the direction and magnitude of the force with respect to the normal walking [17]. It is well known that the force with a high inclination with respect to the acetabular axis of symmetry causes increase in the peak contact stress [98,134]. The high contact stress is considered to be one of the causes of osteoarthritis [64, 70,135]. The incidence of coxarthrosis is also higher in the dysplastic hips [63,134]. Therefore the factors which influence the hip joint contact stress in the normal and dysplastic hips during normal and staircase walking were studied.

The results presented in Figs. 5.3a,b may lead to the conclusion that for normal hips p_{max} as a function of the time depends on the magnitude of R only, since the corresponding shapes of R/W_B and p_{max}/W_B curves are very similar. On the other hand, for dysplastic hips the peak contact stress (p_{max}/W_B) differs from R/W_B during the walking cycle for all types of walking (Fig. 5.3c). These differences observed for dysplastic hips with further variations of the ratio p_{max}/W_B during the walking cycle for normal hips indicate that the variation of the inclination of force $\mathbf{R}$ during the walking cycle (ϑ_{Ra}) (Fig. 5.4) considerably influences the contact stress distribution. It was shown that higher inclination of force $\mathbf{R}$ from the acetabular axis of symmetry (higher ϑ_{Ra}) causes a considerable increase in the peak contact stress (Fig 5.4).

As described in section 4.3, the transformation from the pelvic to the acetabular coordinate system is based on consecutive rotations of the pelvic coordinate system for angles γ and β. Since the dysplastic hip has a smaller lateral inclination of the acetabulum (smaller β in Fig. 4.13), the same hip joint reaction force $\mathbf{R}$ in the pelvic frame has on the average a higher inclination of force $\mathbf{R}$ (ϑ_{Ra}) in the acetabular coordinate system of the dysplastic hip than for a normal hip as shown in Fig. 5.5. Due to the higher ϑ_{Ra} in a dysplastic hip, its influence on the value of peak contact stress is higher, as may be expected according to Fig. 5.4. The effect of the variation in ϑ_{Ra} on the value of p_{max} can also be observed for normal hips (Fig. 5.3d), but due to the small magnitude of ϑ_{Ra} the effect is negligible in comparison to the variation in R (Fig. 5.3a,b). The influence of ϑ_{Ra} on p_{max}/R is also manifested by the similarity in the shape of p_{max}/R and ϑ_{Ra} curves during

different types of walking (Figs 5.3d,e and 5.5a,b, respectively). The peaks of p_{max}/R during normal walking and walking upstairs are steeper than the peaks of ϑ_{Ra}. This occurs due to the nonlinear dependency of p_{max} on ϑ_{Ra} (Fig. 5.4). For higher ϑ_{Ra} even small changes yield significant changes in p_{max}/W_B by which considerable increase in the second peak of p_{max}/R for dysplastic hips during normal walking can be explained.

As discussed above the peak contact stress depends on the magnitude of force **R** and its inclination in the coordinate system of the acetabulum (ϑ_{Ra}). The shape of the stress distribution is determined by ϑ_{Ra} (Eqs. 4.36, 4.46), while the magnitude (R) determines the magnitude of the contact stress (Eq. 4.47). Larger inclination of force **R** from the acetabular axis of symmetry causes not only high peak contact stress (p_{max}) but also unfavourable stress distribution, with the point of maximum stress shifted towards the acetabular rim [29, 98] (Figs. 4.13 and 5.4 A–F).

It has been suggested that the gradient of the stress could be even more important for the development of the hip than the absolute value of the stress [3, 26, 152]. The gradient of the stress can be visualised from Figs 5.4 A–F, where the distances between the isosurfaces are inversely proportional to the gradient of the contact stress. As can be seen from Fig. 5.4 A, a high magnitude of force **R** together with a high inclination of force **R** contribute to the high gradient of the stress. If R is high and ϑ_{Ra} is low (Fig. 5.4E) or ϑ_{Ra} is high and R is low (Fig. 5.4B), the gradient of the stress is not very high. To conclude, in describing the effect of force **R** on the biomechanical status of the human hip both the magnitude of the hip joint resultant force (R) and its inclination (ϑ_{Ra}) should be taken into account.

The direction of the force **R** in the acetabular coordinates is influenced by the positioning of the pelvis during motion. It would be interesting to know, if some type of walking yields unfavourable stress distribution pattern due to a specific motion of the pelvis. Therefore, the effect of the pelvis motion on the contact stress distribution pattern was studied. The motion of the pelvis could influence the stress distribution in two ways. First, the variations of the muscle forces generated during the walking cycle change the resultant force acting in the hip joint **R** [74]. As the force acting in the hip joint **R** is an outcome of the muscle activity required to achieve the body movement, the motion of the femur and the pelvis changes directions of the muscle forces and alters the direction of **R** as well [130, 143, 176]. Second, the motion of the pelvis changes orientation of the acetabulum, i.e., the orientation of the acetabular coordinate system, therefore all the parameters that are measured in the local coordinate system of acetabulum are altered.

Activity of the muscles during the walking cycle could be estimated by a com-

plex mathematical model [26,74] while the effect of the changed coordinate system can be determined after a relatively simple motion analysis [29,180]. If the motion of the acetabular cup is known (Fig. 5.6) additional deviations in the direction of force **R** should be caused by the variations in the muscle activity. For example, in both normal walking force maxima the inclination of the acetabular cup β is approximately the same (Fig. 5.6). Therefore differences in ϑ_{Ra} between these two maxima are caused by the different muscle activation during normal walking. The similar situation occurs in walking downstairs (Fig. 5.6).

Quite different results were found in climbing stairs (Fig. 5.6). During climbing stairs relatively high changes in the position of the acetabulum $\Delta\beta$ were observed (Fig. 5.6). However, the corresponding changes in the inclination of the hip joint resultant force (ϑ_{Ra}) are smaller (Fig. 5.5). This may mean that muscle activity counteracts with the motion of the pelvis in walking upstairs. Changes in the direction of the force **R** are performed together with the movement of the acetabulum, so that ϑ_{Ra} changes only slightly unlike relatively large changes in β. It may prevent high contact stress which would be attained due to high inclination of the force in the acetabular coordinate system (ϑ_{Ra}) (Fig. 5.4).

Hodge et al., 1989 measured the contact stress distribution after hemiarthroplasty with an implanted instrumented prosthesis. They reported the pressures for a patient weighing sixty eight kilogrammes during normal walking to be as high as 5.5 MPa. For a patient of such body weight the maximum peak stress would, according to our results (Fig. 5.3b) be equal to 1.1 MPa, and for a patient with a dysplastic hip it would be 4.9 MPa (Fig. 5.3c). Both the calculated values are lower than the measured value. This inconsistency in results may be caused by the different method of measurements and the differences in the physical properties between a normal hip and a hip with an implanted femoral prosthesis. Hodge et al., 1989 reported the maximum contact stress which was measured on the weight-bearing area among all trials, while in our work the averaged load data of all trials is used. The peak contact stress determined in our study is then an average value, which is expected to be lower than the maximum value. It is reasonable to expect that in some cases the contact stress can be as high as reported by Hodge's measurements. The measurements of force **R** [17] show that in normal walking the magnitude of the peak contact stress can be more than four times the body weight. High R in combination with a high inclination of force ϑ_{Ra} can yield very high contact stresses (Fig. 5.4).

Unfortunately, no measurements of the contact stress distribution in an intact hip joint during walking cycles have been performed. Therefore we can offer only indirect evidence that supports the predictions of our model: the position of the

point of the highest stress measured by Hodge roughly corresponds to the position of the stress pole calculated by our model. The level of calculated contact stress in normal hips during all types of walking is within estimations of the maximum level of contact stress that the acetabular cartilage can tolerate [70]. Maximum computed average stress values in normal hips during the studied walking cycles do not exceed the long-term pressure damage threshold, which was estimated to be 2 MPa [70] (for a normal man weighing 80 kilogrammes when walking upstairs the maximum computed contact stress is equal to 1.7 MPa, Fig. 5.3b). The calculated values of the contact stress for dysplastic hips considerably exceed the long-term pressure damage threshold during all walking cycles (for a man weighing 80 kilogramme with dysplastic hip when walking upstairs the maximum computed contact stress is equal to 6.6 MPa, Fig. 5.3c). This confirms the hypothesis that for dysplastic hips coxarthrosis may develop due to mechanical overloading of the articular cartilage.

There is an increased evidence that climbing stairs frequently may increase risk of coxarthrosis [117, 124]. From Fig. 5.3a,d it can be concluded that for normal hips there is no significant difference neither in the load (R) nor in the peak contact stress (p_{max}) between normal walking and walking upstairs. However, the peak contact stress is increased in walking downstairs (Fig. 5.3d) due to higher R and higher ϑ_R. If we take into account hypothesis that contact stress is important for development of coxarthrosis [70,134], it can be concluded that the higher incidence of coxarthrosis is likely to be related to the walking downstairs than climbing stairs. Therefore people which are in higher risk of development of coxarthrosis should avoid walking downstairs frequently. It may be even more important in dysplastic hips in which the increase in p_{max} during walking downstairs is considerably higher.

6.2.2 Biomechanical analysis of the aseptic necrosis of the femoral head

The mathematical model of the contact stress distribution over the articular surface was upgraded to describe stress distribution in the patients subjected to aseptic necrosis of the femoral head. The conditions in the hips after the collapse of the necrotic region was assumed. The collapsed necrotic segment of the femoral head was modelled as a spherical area within the weight-bearing area, that can not bear a weight (Fig. 4.14). Then the effect of the position and shape of the non-weight bearing area on the contact stress distribution was simulated (section 5.1.3).

The theoretical results show that the peak stress and the position of the pole are considerably affected due to the presence of the necrotic non-weight bearing area. The necrotic defect causes a decrease in the available weight bearing area that may be of considerable extent. A smaller weight bearing area causes higher

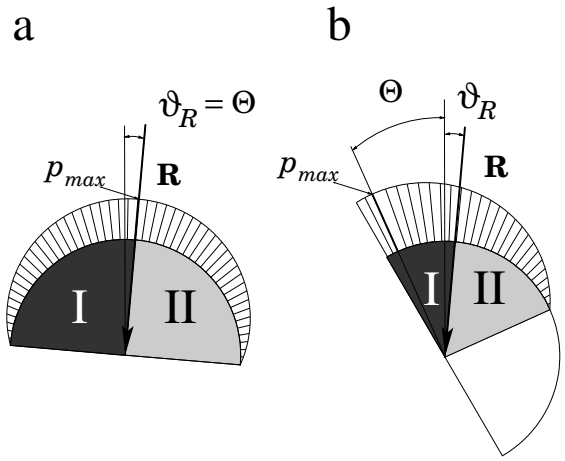

Figure 6.2: Schematic representation of the stress distribution in the frontal plane if the contact articular surface is (a) symmetric and (b) asymmetric with respect to the hip joint resultant force (**R**). It is assumed that **R** lies in the frontal plane.

contact stress. Therefore the peak contact stress (p_{max}) increases with increasing size of the necrotic region (Fig. 5.8). However, the indirect effect due to the redistribution of the stress may be even more important. In some cases the two effects may partially cancel each other, e.g. in a medial shift of the non-weight bearing area (Fig. 5.9a), where in certain positions of the necrotic non-weight bearing region the peak stress is equal to the value obtained for an intact hip of the same geometry.

To clarify the effect of the stress redistribution, the distribution of the contact stress in a normal hip (Fig. 5.11A) should be explained first. According to our model, the stress in the normal hip is nonuniformly distributed, which is in accordance with direct measurements [80, 148]. It has been suggested that the nonuniformly distributed stress is caused by the axisymmetrical loading of the hip [29](Fig. 4.14). Due to the assumed symmetry of the hip with respect to the frontal plane, the hip joint reaction force divides the acetabular surface into two parts: a medial and a lateral part (Fig. 6.2). The first part is bounded by the lateral acetabular rim and by the plane defined by the y-axis and **R**, while the second part consists of the rest of the acetabular surface (Fig. 6.2). The sum of the forces caused by the contact stress transmitted through the first and the second part of the acetabular surface should be equal to force **R** (Eq. 4.37). If both parts were equal, the stress pole would be expected to lie in the direction of force **R** (Fig. 6.2a). Since the area of the first part is smaller than the area of the second part (Fig. 6.2b), to satisfy the condition above (Eq. 4.37) the contact stress should be higher in the first part than in the second part of the acetabular surface. For

the assumption of cosine stress distribution (Eq. 4.36), this means that the pole of the stress should be located in the direction of the first part, i.e., laterally with respect to force **R**.

This analysis explains the changes in the stress distributions in the presence of the necrosis. If the necrosis is located at the top of the acetabular hemisphere it decreases mainly the area of the first part (Figs. 5.24B–D). Therefore the stress on the rest of the first part should be higher (Fig. 5.8). The increase in stress is lower if the lateral coverage of the femoral head (ϑ_{CE}) is larger, since it increases the size of the first part (Fig. 5.8a). Small lateral coverage of the hip is known to be a risk for coxarthrosis development, as in these hips the contact stress is high [70]. In hips with developed aseptic necrosis, the osteoarthritis usually develops [57,62]. According to our simulation it can be stated that the mechanism of osteoarthritis development in hips subjected to aseptic necrosis can be in some respects similar to the effect of small lateral coverage of the femoral head, as they both increase the contact stress.

The contact stress distribution depends not only on the size of the necrosis but also on its position (Figs. 5.9, 5.10). An interesting fact is that the medial location of the necrotic region decreases the peak contact stress below the level observed in normal hips (Fig. 5.9). This decrease can be explained if the above assumptions are considered. If the necrosis is located medially it decreases the size of the second part of the acetabular surface (Fig. 6.2). This makes the weight bearing area more symmetrical with respect to force **R** (Fig. 5.11H). As a result the pole of the stress is shifted medially (Fig. 5.9b). This increases the size of the weight bearing area (Fig. 5.9c) and decreases the peak contact stress (Fig. 5.9a). The decrease in the peak contact stress below the normal level can not be explained by increasing the size of the weight bearing area only, since the weight bearing area does not achieve its normal size for any position of the necrotic non-weight bearing region (Fig. 5.9c). The contact stress redistribution is essential since, due to the shift of the pole medially, the stress is distributed more uniformly and the peak stress is lower (Fig. 5.24G). This theory is supported by the fact that the value of Θ is equal to the value observed in a normal hip when the center of the necrotic region approximately coincides with the direction of the force, independently of the size of the necrotic region (Fig. 5.9b). In this case the necrosis reduces the size of the first and the second part of the acetabular surface equally (Fig. 5.11E), and the stress pattern outside the necrotic region is similar to the normal pattern (Fig. 5.11A). Of course, the absolute value of the stress is higher, as the necrosis decreases the size of the contact articular area and the remaining articular surface has to bear the same force **R**.

The effect of the position of the necrosis on the contact stress distribution can be predicted from the location of the necrotic region with respect to the pattern of the contact stress distribution in a normal hip (Fig. 5.11A). It was shown that the location of the necrosis in the acetabular region where the contact stress in normal hips is higher (e.g. close to the lateral acetabular margin) considerably increases the peak contact stress (Fig. 5.11D). However, if the necrosis lies in a region that in the normal hip does not bear so much weight (e.g. close to the medial border of the weight bearing area), it has a smaller influence on the contact stress distribution (Fig. 5.11H). This explains the calculated decrease in the peak contact stress if the center of the necrotic region is shifted anteriorly (Fig. 5.10a), because in normal hips the region of the highest stress is close to the frontal plane through the centers of the femoral heads (Fig. 5.11A). Although the peak contact stress decreases during an anterior shift of the necrotic region of size $\vartheta_0 = 20°$, the pole is shifted laterally (Fig. 5.10b). This can be explained by the fact that during the anterior shift the necrosis approaches the lateral acetabular rim similarly to Fig. 5.11D and contributes to the asymmetry of the articular surface with respect to force $\mathbf{R}$ (Fig. 6.2). However, if the necrotic area is small ($\vartheta_0 = 10°$), it reaches the lateral acetabular margin more distantly from the frontal plane, i.e. in regions that do not bear weight in normal hips. Therefore, the influence on the stress distribution is small (Fig. 5.9b).

Unlike the medial shift of the necrotic region, where its center lies in the frontal plane (Fig. 5.9), an anteriorly located non-weight bearing necrotic region makes the available articular surface asymmetrical with respect to the frontal plane. The anterior part of the articular surface with respect to the frontal plane is therefore smaller than the posterior part of the articular surface. However, as the resultant hip joint force ($\mathbf{R}$) lies in the frontal plane, the contributions of the anterior and posterior part of the articular surface to $\mathbf{R}$ should be equal. To compensate the smaller size of the anterior part of the articular surface, the contact stress should be higher on it, i.e., the stress pole should be located in the anterior part of the articular surface, as shown in Fig. 5.10c. This problem of the stress distribution for an asymmetrical articular surface is similar to the problem discussed above (Fig. 6.2). Larger necrosis ($\vartheta_0 = 20°$) causes larger asymmetry of the weight bearing area and therefore the anterior shift of the pole is higher than in the smaller necrosis ($\vartheta_0 = 10°$) (Fig. 5.10c).

Based on the results presented in this work we propose that two possible effects of necrosis on contact stress distribution should be considered. The first effect (called the direct effect) occurs when necrosis as a non-weight bearing defect in the articular surface decreases the available weight bearing area and therefore increases

the contact stress. The location of the necrosis strongly influences the stress distribution if the necrotic region is located in parts of the contact hemisphere where the contact stress would be high in intact, healthy hips (e.g. in regions close to the lateral border of the weight bearing area and also in regions closer to the frontal plane through the center of the femoral head). The second effect of necrosis on the contact stress distribution (called the indirect effect) is related to the axisymmetrical loading of the hip with respect to the acetabular shell. The medial position of the necrotic part can contribute to the symmetry of the weight bearing area with respect to the direction of the hip joint reaction force ($\mathbf{R}$). If the weight bearing area is more symmetrical with respect to $\mathbf{R}$ the contact stress is distributed more uniformly.

6.3 Methods for estimation the contact stress distribution in the hip joint for an individual patient

The mathematical models have been developed recently that allow calculation of the hip joint reaction force in one-legged stance and the contact stress distribution [93,98]. These models can be easily adjusted for an individual geometry of the patient [92,94]. However the direct use of the mathematical models for estimating the state of the hip may be complicated and unsuitable for the clinical practice. In this work the algorithms of the mathematical models were incorporated into the HIPSTRESS computer program that enables determination of the hip stress if certain geometrical parameters of the hip and the pelvis are known. Also the nomograms were presented that allows determination of the peak stress on the weight bearing area without direct use of the computer.

The attachment points of the muscles were corrected for an individual subject according to the geometry of the pelvis and proximal femur determined from the standard anteroposterior radiograph (Fig. 5.12). We outlined this method because there is a large number of data in the form of the standard anteroposterior radiographs available from the archives. However, any other method that gives the required geometrical parameters can be used. The most accurate three-dimensional position of the attachment points of the muscles would be obtained from tomographic scans (CT or NMR). However the computerised tomography is not widely distributed for this purpose because of its technical complexity and higher costs compared to the standard radiograph [106]. Also the radiation dose received by the patient in CT examination is higher than in standard radiographic examination [106]. The method that use standard anteroposterior radiographs enables to use the data from archives and requires no additional examination of the patient.

Two methods were proposed to determine the contact stress distribution in the clinical practice: computer program and nomograms. The computer program provides the complete stress distribution (i.e., maximum peak stress, value of the contact stress at the stress pole and position of the stress pole) while the nomograms provides value of the peak contact stress only. The advantage of the nomograms is in their clarity. By using nomograms the effect of various geometrical parameters on the stress distributions can be estimated. For example, it is obvious from Fig. J.7 that the small value of the sum of the centre-edge angle (ϑ_{CE}) and angle of the inclination of the force (ϑ_R) increases the peak contact stress. Small centre-edge angle is observed for example in dysplastic hips [118, 134], in which

high stress induces development of coxarthrosis [70]. Low values of ϑ_R are related to broad pelvis ($C = 7$, Fig. J.6). The width of the pelvis in women is known to be higher than in men [113] and therefore the peak contact stress should be higher in women than in men (Figs. J.6 and J.7–J.9). Since women have higher incidence of arthrosis these results favour the hypothesis that elevated stress in the hip joint could be one of the reasons for the development of arthrosis.

6.4 Clinical studies

6.4.1 New parameter for the hip dysplasia assessment

In this work we introduce a new parameter for the assessment of hip dysplasia from the anteroposterior radiographs, i.e., the stress gradient at the lateral rim of the acetabulum (Eq. 4.61). In the population study it was indicated that the normalised stress gradient index G_p/W_B changes its sign around $\vartheta_{CE} \cong 20°$. Accordingly a new definition for the hip dysplasia according to the size and sign of the normalised stress gradient index G_p/W_B was suggested. The hips with positive G_p/W_B are considered to be dysplastic while the hips with negative G_p/W_B are considered to be normal.

The proposed criterion to differentiate dysplastic hips on the basis of the normalised stress gradient index was tested on the hips with evaluated Harris hip score. Statistically significant difference in Harris hip score between the group of normal and dysplastic hips determined by the normalised stress index gradient G_p/W_B was found. The statistically significant difference in the Harris Hip Score between the group of normal and dysplastic hips was also found if the hips were divided by the normalised peak contact stress p_{max}/W_B. It confirms a previous hypothesis that a peak contact stress is important factor affecting the development of the hip [70, 118, 134]. However, there exists no decisive border between the normal and dysplastic hips in p_{max}/W_B (Fig. 5.20) and the long-term damage threshold level of peak contact stress which was used in our study was estimated only approximately in the clinical studies [70,135]. Therefore the G_p/W_B may be a better biomechanical parameter for the dysplasia assessment than p_{max}/W_B since there is an unambiguous level that discriminates between normal and dysplastic hips, the sign of the hip gradient index (Fig. 5.21). For further clarification of this statement additional clinical studies should be carried out.

The better outcome of the relation between biomechanical and clinical parameters was obtained if the body weight of the patients would be known since the obesity of the patients is a known factor related to the development of coxarthrosis [146, 128, 117, 187].

6.4.2 Aseptic necrosis of the femoral head – a case study

The two presented cases (Fig. 5.23) were chosen to show the effect of the individual geometry of the hip on the contact stress distribution. In hip A there were several factors increasing the stress in the hip joint. First, the load $\mathbf{R}$ of hip A was higher, which was mainly caused by the larger interhip distance l [95] (Fig. 5.12a). Moreover, due to the the smaller radius of the femoral head (r) and

the smaller lateral acetabular coverage in hip A (ϑ_{CE}) the weight bearing area was small and the contact stress was high before the necrosis had occurred, in comparison to the situation in hip B (Tab. 5.5A). In case A the necrosis developed in the lateral part of the femoral head (Fig. 5.23A), which is also unfavourable. As shown above, such a situation yields high contact stress (Fig. 5.9a). On the other hand, hip B has a larger radius of the femoral head (r) and larger lateral coverage (ϑ_{CE}) than hip A, which together with the lower load $\mathbf{R}$ gives a more favourable stress distribution already in the intact hip (Tab. 5.5B). In addition, the necrosis in hip B was developed on the medial side of the femoral head (Fig. 5.23B), so its effect on the value of the peak stress was relatively small due to the favourable redistribution of the stress.

Knowledge about the mechanical state of a hip subjected to avascular necrosis may offer help to the clinician in the two possible ways: first, it can clarify the etiology retrospectively, and secondly, it can help in suggesting an appropriate therapy. A biomechanical analysis can be helpful in finding the cause of the avascular necrosis of the femoral head. After comparing with the situation in hip A, with and without necrosis, it can be seen (Figs. 5.24A) that the necrosis developed in the region having the higher stress. This coincidence suggests, in addition to many other biological factors, that mechanical overloading may also contribute to the development of avascular necrosis of the femoral head. In hip B, mechanical overloading as a causative factor of the avascular necrosis of the femoral head can be rejected, since the contact stress in a hip without necrosis would be normal (Tab. 5.5 and Fig. 5.24). Also the location of the necrotic region does not coincide with the region of high contact stress in the situation without necrosis (Fig. 5.24B). Hence, in the case of hip B, other etiological factors than mechanical seem to be more important (e.g. trauma, intraluminal or extraluminal obliteration).

Knowledge of the preoperative and postoperative biomechanical state of the hip could also enhance the surgeon's decision on further therapy of the hip. For example, one could assume that in hip A (Fig. 5.24) osteoarthritis will probably develop, because the high contact stress in it will probably damage the articular cartilage [70, 134], which may lead to immobility of the patient. In hip A, therefore, a surgical procedure that improves the biomechanical state of the hip (e.g. osteotomy [12, 86]) is indicated. On the other hand, in hip B the necrosis did not considerably change (i.e., make worse) the biomechanical state of the hip. Therefore, no essential improvement of the contact stress distribution is expected through surgery and conservative treatment seems to be be more appropriate.

To conclude, the proposed method for estimating the mechanical state of the

hip can be utilised in clinical practice in order to clarify the cause of the disease and for suggesting an appropriate therapy. It is suggested that in some cases the unfavourable contact stress distribution in the hip could be important in the development of aseptic necrosis of the femoral head. To confirm this hypothesis, further studies of the contact stress distribution in a group of patients subjected to avascular necrosis are necessary.

6.5 Physiognomic acetabular component for total hip replacement

Based on the results of the mathematical analysis of the contact stress distribution in normal hips and hips subjected to avascular necrosis of the femoral head a new type of the acetabular component for the total hip replacement called the physiognomic artificial acetabular cup was designed. The contact area in the artificial cup was adjusted by adding a non-weight bearing area. Considering the discussion above, the non-weight bearing area, making the contact area symmetrical with respect to the hip joint reaction force **R**, should provide a uniform stress distribution on the contact surfaces of cup and femoral head. Three different cup modes were proposed: the skewed cup, the cup with hole and the cup with asymmetrical inner surface.

The assumptions of the positive effect of stress redistribution is valid as long as the non-weight bearing area makes the contact area symmetrical to the force **R**. However, the direction of the force **R** with respect to the acetabular cup differs during different activities [15,98] while the position of the non-weight bearing area is fixed. Therefore, the cup is to be designed in such way that any force **R** in the presence of non-weight bearing area will not significantly impair the distribution of the contact stress in the artificial hip joint. For the cup with a hole (Fig. 5.26), a force **R** direction may exists causing the movement of the femoral head towards the hole, i.e., the femoral head will sink into the hole. Consequently, there will be a concentration of the stress at the edge of the hole which can damage the cup. The similar situation may occur with the skewed cup (Fig. 5.25) where the force **R**, beeing extremely medially oriented, may cause a dislocation. To prevent such situations, the two cup types, mentioned above, should be further improved. From this point of view the most suitable cup design seems to be that of the asymmetrically shaped inner surface (Fig. 5.27).

Further studies should be addressed to the stress distribution in the new acetabular cup during the various routine activities. The load of the hip can be obtained from the measurements using implanted instrumented prosthesis [15, 18]. The calculation of the stress distribution can be carried out using the finite element engineering analysis that allows to study a complete stress distributions in the components of THR and the adjacent bone for any configuration of THR [61,82]. Also the hypothesis of the stress redistribution caused by the non-weight bearing area should be proved experimentally, e.g., the cup contact pressure measuring by applying pressure sensitive films [3,14].

The study of the fysiognomic cup for THR presents only a first small step to-

wards the application of basic research in the hip joint replacement surgery. There is still a long way, including further necessary calculations, mechanical testing and measurements, till the fysiognomic cup is to be implanted to a patient.

6.6 Hypothesis of the regulation of the protheosyntetic activity of the cartilage by mechanical loading

Articular cartilage is a complex structure, which consists of cells (chondrocytes) and intercellular matrix (fluid and structural macromolecules). Although progress has been made in understanding and predicting development of the hip by biomechanical parameters, there is no decisive answer regarding the effect of the load yet. To understand the effect of the load on the human cartilage, regulation mechanisms acting on the cellular and molecular levels should be clarified. It is the aim of this section to suggest such a theory.

It was shown in the section 5.3.1 that in dysplastic hips the peak stress on the weight bearing area is considerably and statistically significantly higher than in normal hips. According to the Hooke's law higher stress in the dysplastic hip is proportional to larger deformation of the cartilage. It was found that the deformation of the cartilage causes the deformation of the chondrocytes [69]. The changes in structure of the cartilage were found in dysplastic hips with respect to normal hips [84], (e.g., changes of the content and type of structural macromolecules - collagen and proteoglycans that are produced by the chondrocytes). indicating that the proteosynthetic activity of the chondrocytes is altered in dysplastic hips.

According to the above we suggest a hypothesis of the regulation of the proteosynthetic activity of the chondrocytes by the change of the shape of the chondrocytes induced by the load upon the cartilage.

In normal hips, the contact stress is on the average relatively low and also the peak stress is relatively low (Fig. 5.20) so that under normal conditions the cartilage is not extensively deformed. The chondrocytes are only slightly deformed from the spherical shape (Fig. 6.3b). Hypothetically such loaded chondrocytes product structural molecules that serve as a barrier against compression – proteglycans.

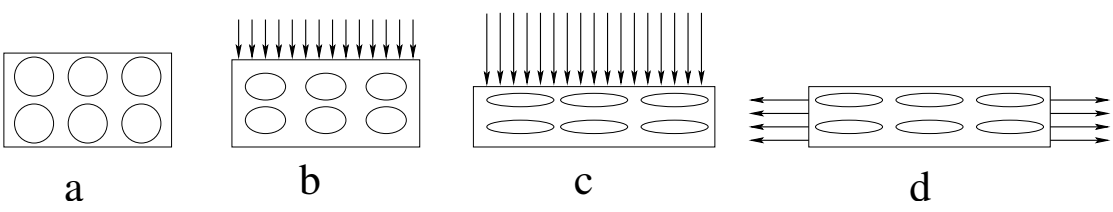

Figure 6.3: Schematic representation of the deformation of the cartilage and chondrocytes when unloaded (a), in small compressive loading (b), in large compressive loading (c) and in stretching (d)

In dysplastic hips the compressive stress is on the average higher and the peak stress is higher (Fig. 5.20). The cartilage therefore deforms to a greater extent and the deformation of the cartilage is transduced to chondrocytes (Fig. 6.3c). The change of the shape of the chondrocyte under high compression is similar to the change of the shape of the chondrocyte when stretched, i.e., the chondrocytes are elongated [69] (Fig. 6.3d). Hypothetically such deformed chondrocytes behave like mesenchymal cells subject to stretching (fibroblasts) and produce structural molecules which serve as a barrier against stretching – collagens. As the collagen cannot resist compressive stress [143], the cartilage is deformed more and more and the vicious circle starts.

Evidence exists that supports our hypothesis. The hypothesis explains the structure of the cartilage. The superficial layer of the cartilage, which undergoes highest stretching [143], contains mostly collagen [144]. Deeper layers that are subject mostly to compressive load contain more proteoglycans [143].

Further, in dysplastic hips the collagen type I was found [84] which is characteristic for tendons and is normally not present in the cartilage.

It should be noted that the dysplastic hips exhibit higher gradient of stress on the lateral edge of the acetabulum [152]. Although articular cartilage is a porous viscoelastic material, and the flow of an interstitial fluid is different than the flow of an ideal liquid [183, 107], it can be assumed in the first approximation that the velocity of the efflux of the interstitial fluid is proportional to the gradient of contact stress in the pores of the cartilage. Efflux of the interstitial fluid changes mechanical properties of the cartilage and allows higher deformations of the cartilage [183]. This would imply that the gradient of stress is important too as was suggested on the basis of clinical investigations [3, 26, 152].

To describe the effect of the load on the cartilage regulation more exactly, further studies based on the cellular level are needed. Also other mechanisms should be considered such as: reduction of the fluid film lubrication between the articular surfaces, loosening of the collagen network, disruption of the collagen fibers and loss of the proteoglycans.

Chapter 7

CONCLUSION

In this work, mathematical models serving for estimation of the hip joint reaction force and the contact stress distribution over the hip joint articular surface were created and evaluated. A special emphasis was devoted to methods that can be applied in the clinical practice to evaluate both the normal and impaired hips and to application of the biomechanical studies in the practice.

In this work, anatomy of the muscles crossing the hip was described in a standardised form to provide data generally suitable for the static biomechanical analysis of muscular forces and the hip joint contact force. Quantitative data from several sources were employed and a complex model containing twenty-seven muscle units was defined.

For presentation of the musculoskeletal system a computer program was developed in the scientific visualisation programming environment OpenDX. This program offers three-dimensional interactive visualisation of the bones of the lower extremity and muscles of the hip.

Using the new muscle model, the hip joint reaction force ($\mathbf{R}$) at the one-legged stance was computed using optimisation approach. Several optimisation criteria were tested and it was shown that the magnitude and direction of the hip joint reaction force do not depend on the choice of a optimisation criterion. It was found that at the one-legged stance the force R lies almost in the frontal plane. The alteration in the geometry of the muscle model is a factor changing the force Rsignificantly. The choice of the optimisation criterion is manifested in the distribution of the muscle forces. A muscle synergism index was defined and verified as a suitable parameter to quantify synergism of the muscle activity. To maintain a static body position, only few muscles are predicted to be active and therefore more simple muscle models also enable to estimate the load of the hip in static positions.

New optimisation criterion for static optimisation was suggested according to which the optimal muscle activity is determined by minimising the signals from Golgi tendon organs. This criterion reflects the sensation of the muscle force by the central neural system and explains regulation of the muscle activity as a feedback control.

This work contains a new simpler derivation of the model equations to calcu-

late the contact stress distribution in the normal and dysplastic human hip joints for an arbitrary direction of the force **R** based on a special choice of the spherical coordinate system. The values of the resultant hip force **R**, obtained from the measurements by a specially instrumented endoprosthesis [15], were used to calculate the stress distribution in the adult human hip joint in various daily activities in both the normal and dysplastic hips. The highest peak contact stress p_{max} was observed in the both types of the hips when walking downstairs and therefore the influence of the force **R** on the contact stress distribution during normal and staircase walking was studied. It was shown that a high inclination of **R** in the local coordinate system of the acetabular cup increases the peak contact stress and makes the stress distribution nonuniform. The contribution of the force inclination to a change in the values of the peak contact stress is more pronounced for dysplastic hips with a poor lateral coverage of the femoral head in which considerably higher values of the peak contact pressures were found for all the walking cycles studied.

The nomograms and HIPSTRESS computer program are presented enabling the hip stress assessment if certain geometrical parameters of the hip and pelvis and the body weight are known. The nomograms and HIPSTRESS program were created using previously developed mathematical models [96, 93, 94]. This simple and noninvasive method gives an insight into the biomechanical status of the hip without using any additional tools. This method can therefore be used in everyday clinical practice in planning of surgical interventions, as well as in the population studies where a great number of data in the form of the standard anteroposterior radiographs are available from the archives.

Determination of the biomechanical parameters by the above method was used in the clinical study of 202 both the normal and dysplastic human hips. The stress gradient index (G_p) and functional angle of the weight-bearing area (ϑ_F) were introduced for the assessment of dysplasia in the human hip joint. The absolute value of G_p beeing equal to the magnitude of the gradient of the contact stress at the lateral acetabular rim, while ϑ_F describes the size of the weight-bearing area. It was found that the difference in ϑ_F, G_p/W_B and p_{max}/W_B between the normal and dysplastic hips is statistically significant, where W_B is the body weight force. According to the clinical study a new definition for the hip dysplasia with respect to the size and sign of the normalised stress gradient index G_p/W_B was suggested. The hips with positive G_p/W_B are considered to be dysplastic while the hips with negative G_p/W_B are considered to be normal. The statistically significant correlation between the value of the Harris hip score, used in the clinical assessment of the hip dysplasia, and the normalised stress gradient index was found in the

clinical study of 45 hips.

To study a stress distribution in the hip subjected to avascular necrosis of the femoral head we have adapted a three dimensional mathematical model for calculation the contact stress distribution by introducing a non-weight bearing necrotic segment. It was shown that contact hip stress is considerably affected due to the presence of non-weight bearing area. The peak stress increases with increasing size of the non-weight bearing area, the effect being more pronounced in hips with a poor lateral coverage of the femoral head by the acetabulum, i.e., in the dysplastic hips. Medial position of the non-weight bearing area considerably decreases the peak stress so that it can reach the values that are even lower than the value in the intact hip. Since the hip joint reaction force is acting closer to the lateral acetabular rim the medially located non-weight bearing area contributes to the symmetry of the contact surface with respect to the loading force $\mathbf{R}$ what causes a uniform stress distribution. Also proximal and distal positions of the non-weight bearing area decrease the peak stress with respect to the central position of the non-weight bearing area. A practical method for determination of stress distribution in hips subject to avascular necrosis of the femoral head based on a standard anteroposterior radiograph is proposed. Application of this method in the clinical practice is presented in two cases.

The attempt to utilise the contact stress lowering in the prosthetic design, if medially located non-weight bearing area occurs, is a project of a new acetabular component for total hip replacement. Three different geometrical constructions of the new types of the new design of the acetabular cup were proposed.

Based on the results of the clinical studies mentioned above a hypothesis how to control a protheosynthetic activity of the chondrocytes was suggested. The cartilage deformation, caused by the contact hip joint stress, and consequent deformation of the chondrocytes are considered to be main factors that could influence the metabolism of the cartilage.

As stated above, the all objectives of dissertation listed in the section 2 were fulfilled. Individuals involved in the hip joint research at different levels: from the solutions of the basic problems in the hip biomechanics up to their practical applications may be interested in the results and findings of this study. This work also points out some new problems which should be studied further. For example, the relationship between biomechanics of the cartilage and its prostheosyntetic activity (section 6.6), which is a question of a new interdisciplinary course of study - mechanobiology, can be important for the coxarthrosis development. The hypothesis proposed of the regulation of the cartilage by its mechanical loading should be studied further using experiments and computational models. Also the

new design of the acetabular cup for total hip replacement may present a progress in the hip arthroplasty. A future development of the new type of the acetabular cup will be carried out in the Laboratory of Biomechanics of Man, Czech Technical University in Prague.

Chapter 8

LIST OF PUBLICATIONS

Journal Publications

- R. Vengust, M. Drobnič, M. Daniel, V. Antolič, F. Pernuš, A. Iglič and V. Kralj-Iglič. Role of magnification of standard anterior-posterior radiographs in determination of contact hip joint stress. *Biomedical Engineering – Applications Basis & Communication*, 12:242-244, 2000.

- M. Daniel, V. Antolič, A. Iglič and V. Kralj Iglič. Determination of contact hip stress from nomograms based on mathematical model. *Medical Engineering & Physics*, 23:347-357, 2001.

- A. Iglič, M. Daniel, V. Kralj-Iglič, V. Antolič and A. Jaklič, Peak hip-joint contact stress in male and female populations. *Journal of Musculoskeletal Research*, 5:17-21, 2001.

- R. Vengust, M. Daniel, V. Antolič, O. Zupanc, A. Iglič and V. Kralj-Iglič. Biomechanical evaluation of hip joint after Salter innominate osteotomy: a long-term follow-up study. *Archives of Orthopaedic and Trauma Surgery*, 121:511-516, 2001.

- A. Iglič, V. Kralj-Iglič, M. Daniel and A. Maček-Lebar. Computer determination of contact stress distribution and size of weight bearing area in human hip joint. *Computer Methods in Biomedical Engineering*, 5:185-192, 2002.

- B. Mavčič, B. Pompe, V. Antolič, M. Daniel, A. Iglič and V. Kralj-Iglič. Mathematical estimation of stress distribution in normal and dysplastic human hips. *Journal of Orthopaedic Research*, 20:1025-1030, 2002.

- M. Daniel, M. Sochor, A. Iglič, S. Herman and V. Kralj-Iglič. Gradient of contact stress in normal and dyplastic human hips. *Acta of Bioengineering and Biomechanics*, Suppl. 1, 4:280-281, 2002.

- M. Daniel, M. Sochor, A. Iglič and V. Kralj-Iglič. Computer system for determination of contact hip stress based on mathematical model. *Acta of Bioengineering and Biomechanics*, Suppl. 1, 4:296–297, 2002.

- D. Dolinar, S. Herman, M. Daniel, V. Pavlovič, A. Iglič and V. Kralj-Iglič. Distribution of the contact hip joint stress in avascular necrosis of femoral head. *Acta of Bioengineering and Biomechanics*, Suppl. 1, 4:302–303, 2002

- M. Daniel, V. Kralj-Iglič, A. Iglič, M. Sochor. Hypothesis of the regulation of the cartilage activity by mechanical loading. *Medical Hypotheses*, 60:936-937, 2003.

- B. Pompe, M. Daniel, M. Sochor, R. Vengust, V. Kralj-Iglič and A. Iglič. Gradient of contact stress in normal and dysplastic of the human hip. *Medical Engineering & Physics*, 25:379-385, 2003.

Papers in Conference Proceedings

- M. Daniel, S. Holý and M. Sochor. Mechano-bio-senzory založené na biologickej membráne. *Proceeding of the Summer Workshop of Applied Mechanics*. pages 1–2, Praha, 2002.

- B. Mavčič, K. Bohinc, M. Daniel, F. Ševšek, V. Kralj-Iglič and A. Iglič. Computation of shear stress in the femoral neck. *Proceeding of the Summer Workshop of Applied Mechanics*. pages 120–128, Praha, 2002.

- M. Daniel, S. Holý, M. Sochor. Mechanobiosensors. *Proceeding of the 19th Danubia-Adria Symposium on Experimental Methods in Solid Mechanics*. pages 13–14, Polanica-Zdroj, 2002.

- M. Daniel and M. Sochor. Contact stress in the human hip - mathematical model compared to direct measurement. *Proceeding of the International Conference Experimental Stress Analysis*, pages 41–42, Praha, 2002.

- M. Daniel, M. Sochor, V. Kralj-Iglič and A. Iglič. Hypothesis of the regulation of the cartilage activity by mechanical loading. *Proceedings of Biomechanics of Man 2002*. pages 22–23, Čejkovice, 2002.

- M. Daniel and M. Sochor. Biomechanical explanation of the relationship between observed the lumbar spinal curvature and resulting low back pain. *Proceedings of Biomechanics of Man 2002*. pages 72–73, Čejkovice, 2002.

- M. Daniel, S. Holý and M. Sochor. Detection of mechanical signals by biological principles. *Proceeding of the 2nd Youth Symposium on Experimental Solid Mechanics*. pages 19–20, Milano Marittima (Ravena), 2003.

- M. Daniel and M. Sochor, M. New type of optimalisation function for muscle activity. *Proceeding of the Summer Workshop of Applied Mechanics*. pages 22–77, Prague, 2003.

- M. Daniel, V. Kralj-Iglič, A. Iglič and M. Sochor. Avascular necrosis of the femoral head – mathematical model of the contact stress distribution. *Proceeding of the Summer Workshop of Applied Mechanics*. pages 28–56, Prague, 2003.

- M. Daniel, V. Kralj-Iglič, A. Iglič and M. Sochor. Comparison of the contact stress distribution in the human hip for rectangular and spherical matematical model of the avascular necrosis of the femoral head. *Proceeding of the Summer Workshop of Applied Mechanics*. pages 57–66, Prague, 2003.

- M. Daniel, V. Kralj-Iglič, A. Iglič and M. Sochor. Influence of the position of the aseptic necrosis on the contact stress distribution in the human hip joint. *Proceeding of the Summer Workshop of Applied Mechanics*. pages 67–80, Prague, 2003.

- M. Daniel, V. Kralj-Iglič, A. Iglič and M. Sochor. Evaluation of the contact stress distribution in avascular necrosis of the femoral head in the clinical practice. *Proceeding of the Summer Workshop of Applied Mechanics*. pages 81–88, Prague, 2003.

- M. Daniel, V. Kralj-Iglič, A. Iglič and M. Sochor. Aseptic necrosis of the femoral head – case study. *Proceeding of the Summer Workshop of Applied Mechanics*. pages 89–96, Prague, 2003.

- J. Kratochvílová, M. Sochor, S. Konvičková, T. Goldmann and M. Daniel. Biomechanical and clinical parameters describing status of human hip – methodology. *Proceeding of the Summer Workshop of Applied Mechanics*. pages 192–195, Prague, 2003.

- J. Sýkora, M. Sochor, S. Konvičková, T. Goldmann, and M. Daniel. Mathematical modelling of the contact stress distribution in the human hip joint. *Proceeding of the Summer Workshop of Applied Mechanics*. pages 378–380, Prague, 2003.

- M. Daniel, M. Sochor, A. Iglič and V. Kralj-Iglič. How to explain shape of the articular cartilage in the human hip joint. *Proceeding of the First International Meeting of Applied Physics*. page 430, Badajoz, 2003.

- M. Daniel, M. Sochor, A. Iglič and V. Kralj-Iglič. Mathematical modelling of stress in the hip during routine activities. *Proceeding of the First International Meeting of Applied Physics*. page 431, Badajoz, 2003.

- K. Bohinc., A. Iglič, S. Slivnik, M. Daniel and V. Kralj-Iglič. Elektrostatski potencial ravne električne dvojne plasti z okroglo odprtino. *Proceeding of ERK*. Vol. A, pages 179–182, Portorož, 2003.

Conference proceeding editorial

- S. Konvičková, D. Leitermann and M. Daniel (editors). *Proceedings of the Summer Workshop of Applied Mechanics*. Faculty of Mechanical Engineering, CTU in Prague, 2002.

- S. Konvičková, J. Zavřel and M. Daniel (editors). *Proceedings of the Summer Workshop of Applied Mechanics*. Faculty of Mechanical Engineering, CTU in Prague, 2003.

Scientific reports

- M. Daniel and M. Sochor. Mathematical modelling of the lumbar spinal load part I, *CTU Scientific Report No. 2051/02/18*. 2002.

- M. Daniel and M. Sochor. Biomechanical analysis of the aseptic necrosis of the femoral head. *CTU Scientific Report No. 2051/03/11*. 2003.

- M. Daniel, M. Sochor and S. Holý. Experimental methods in biomechanics. *CTU Scientific Report No. 2051/03/14*, 2003.

- M. Daniel and M. Sochor. Mathematical modelling of the lumbar spinal load part II. *CTU Scientific Report No. 2051/03/15*, 2003.

- M. Daniel and M. Sochor. Optimisation of the muscle forces. *CTU Scientific Report No. 2051/04/03*, 2003.

Utility models and patents

- S. Konvičková, T. Goldmann, F. Denk and M. Daniel. Acetabular component of total hip replacement. *Utility model No. PUV 2003-14728/13962.* MPT A 61 F 2/34 2/32, 26.1.2004, Industrial Property Office of the Czech Republic, 2004.

BIBLIOGRAPHY

[1] M. Abu-Shakra, D. Buskila, and Y. Shoenfeld. Osteonecrosis in patients with SLE. *Clinical Reviews in Allergy and Immunology*, 25(1):13–24, 2003.

[2] M. Adams, N. Bogduk, K. Burton, and P. Dolan, editors. *The Biomechanics of Back Pain*. Churchill Livingstone, Edinburgh, 2002.

[3] N.Y.P. Afoke, P.D. Byers, and W.C. Hutton. Contact pressures in the human hip joint. *Journal of Bone and Joint Surgery*, 69B(4):536–541, 1987.

[4] A.M.R. Agur, editor. *Grant's Atlas of Anatomy*. Wiliams & Wilkins, Baltimore, 1991.

[5] C.S. Ahmad, Z.A. Cohen, W.N. Levine, G.A. Ateshian, and V.C. Mow. Biomechanical and topographic considerations for autologous osteochondral grafting in the knee. *The American Journal of Sports Medicine*, 29(2):201–206, 2001.

[6] G.T. Allison, M.P. Bostrom, and M.J. Glesby. Osteonecrosis in HIV disease: epidemiology, etiologies, and clinical management. *AIDS*, 17(1):1–9, 2003.

[7] F.C. Anderson and M.G. Pandy. Dynamic optimization of human walking. *Journal of Biomedical Engineering*, 123:381–390, 2001.

[8] F.C. Anderson and M.G. Pandy. Static and dynamic optimization solutions for gait are practically equivalent. *Journal of Biomechanics*, 34:153–161, 2001.

[9] V. Antolič, A. Iglič, F. Srakar, and S. Herman. Clinical use of the mathematical model of the hip. *Medicinske Razgledy*, 30:527–535, 1991.

[10] V. Antolič, V. Kralj-Iglič, A. Iglič, and B. Pompe. Hip biomechanics in orthopaedic clinical practice. *Cellular & Molecular Biology Letters*, 7(2):311–315, 2002.

[11] Y. Assouline-Dayan, C. Chang, A. Greenspan, Y. Shoenfeld, and M.E. Gershwin. Pathogenesis and natural history of osteonecrosis. *Seminars on Arthritis and Rheumatism*, 32:94–124, 2002.

[12] K.J. Baker, T.D. Brown, and R.A. Brand. A finite element analysis of the effect o the intertrochanteric osteotomy on stress in femoral head osteonecrosis. *Clinical orthopaedics and related research*, 249:183–198, 1989.

[13] M. Bartoš and Z. Kestřánek. Numerical solution of the contact problem. application to a simple model of human hip joint. *Journal of Computational and Applied Mathematics*, 63:439–447, 1995.

[14] B.K. Bay, A.J. Hamel, S.A. Olson, and N.A. Shark. Statically equivalent load and support conditions produce different hip joint contact pressures and periacetabular strains. *Journal of Biomechanics*, 30(2):193–196, 1995.

[15] G. Bergmann. *Hip98, Loading of the hip joint.* Freie Universität, Berlin, 2001.

[16] G. Bergmann, F. Graichen, and A. Rohlmann. Hip joint forces during walking and running, measured in two patients. *Journal of Biomechanics*, 26:969–990, 1993.

[17] G. Bergmann, F. Graichen, and A. Rohlmann. Is staircase a risk for the fixation of hip implants. *Journal of Biomechanics*, pages 535–553, 1995.

[18] G. Bergmann, F. Graichen, and A. Rohlmann. Hip contact force and gait patterns from routine activities. *Journal of Biomechanics*, 26:859–871, 2001.

[19] G. Bergmann, F. Graichen, J. Siraky, H. Jendrzynski, and A. Rohlmann. Multichannel strain gauge telemetry for orthopaedic implants. *Journal of Biomechanics*, 21:169–176, 1988.

[20] S. Beznoska, O. Čech, and K. Lobl. *Umělé náhrady lidských kloubů.* SNTL, Praha, 1987.

[21] F. Birrell, A. Silman, P. Croft, C. Cooper, G. Hosie, and G. Macfarlane. Syndrome of symptomatic adult acetabular dysplasia (SAAD syndrome). *Annals of the Rheumatic Diseases*, 62:356–358, 2003.

[22] A. Bombelli. *Osteoarthritis of the hip.* Springer-Verlag, Berlin, 1983.

[23] R.A. Brand. Hip osteotomies: a biomechanical consideration. *Journal of American Academy of Orthopaedic Surgeons*, 5:282–291, 1997.

[24] R.A. Brand, A. Iglič, and V. Kralj-Iglič. Contact stress in the human hip: implication for disease and treatment. *Hip International*, 11:117–126, 2001.

[25] R.A. Brand and D.R. Pedersen. Computer modelling of surgery and a consideration of the mechanical effects of proximal femur osteotomies. In *The hip society award papers*, pages 193–210, USA, 1984.

[26] R.A. Brand, D.R. Pedersen, D.T. Davy, K.M. Kotzar, K.G. Heiple, and V.M. Goldberg. Comparison of the hip joint reaction force and measurements in the same patient. *Journal of Arthroplasty*, 9(1):45–51, 1994.

[27] R.A. Brand, D.R. Pedersen, and J.A. Friederich. The sensitivity of muscle force predictions to changes in physiologic cross-sectional area. *Journal of Biomechanics*, 19:589–596, 1986.

[28] P. Brinckmann, W. Frobin, and E. Hierholzer. Stress on the articular surface of the hip joint in healthy adults and persons with idiopathic osteoarthrosis of the hip joint. *Journal of Biomechanics*, 14(3):149–153, 1981.

[29] P. Brinckmann, W. Frobin, and G. Leivseth. *Musculoskeletal biomechanics*. Georg Thieme Verlag, Stuttgart, 2002.

[30] T.D. Brown. In vitro contact stress distributions in the natural human hip. *Journal of Biomechanics*, 16(6):373–384, 1983.

[31] T.D. Brown, T.A. Mutschler, and A.B. Ferguson. A non-linear finite element analysis of some early collapse processes in femoral head osteonecrosis. *Journal of Biomechanics*, 15:707–715, 1982.

[32] T.D. Brown, D.R. Pedersen, K.J. Baker, and R.A. Brand. Mechanical consequences of core drilling and bone grafting on osteonecrosis of the femoral head. *Journal of Bone and Joint Surgery*, 75A:1358–1367, 1993.

[33] T.D. Brown, M.E. Way, and A.B. Ferguson. Stress transmission anomalies in femoral heads altered by aseptic necrosis. *Journal of Biomechanics*, 13:687–699, 1980.

[34] E.E. Brueschke, editor. *The World Book/Rush-Presbyterian-St. Luke's Medical Center Medical Encyclopedia*. Word Book, Chicago, 1991.

[35] M.D. Buschmann and A.J. Godzinsky. A molecular model of proteoglycan associated forces in cartilage mechanics. *Journal of Biomedical Engineering*, 117:179–192, 1995.

[36] O. Calonius and V. Saikko. Analysis of relative motion between femoral head and acetabular cup and advances in computations of the wear factor of the prosthetic hip joint. *Acta Polytechnica*, 43(4):43–54, 2003.

[37] C.E. Carlson, R.W. Mann, and W.H. Harris. A radio telemetry device for monitoring cartilage surface pressures in the human hip. ieee transactions on biomedical engineering. *IEEE Transactions on Biomedical Engineering*, BME-21:257–264, 1981.

[38] M.K. Chung, Y.W. Song., Y. Hong, and K.I. Choi. A novel optimization model for prediciting trunk muscles forces during assymetric lifting tasks. *International Journal of Industrial Ergonomics*, 23:41–50, 1999.

[39] P. Cisek, S. Grossberg, and D. Bullock. A cortico-spinal model of reaching and proprioception under multiple task constraints. *Journal of Cognitive Neurosciences*, 10(4):425–444, 1998.

[40] Z.A. Cohen, D.M. McCarthy, S.D. Kwak, P. Legrand, F. Fogarasi, E.J. Ciaccio, and G. Ateshian. Knee cartilage topography, thickness, and contact areas from mri: in-vitro calibration and in-vivo measurements. *Osteoarthritis and Cartilage*, 7:95–109, 1999.

[41] J.J. Collins. The redundant nature of locomotor optimization laws. *Journal of Biomechanics*, 28(3):251–267, 1995.

[42] P.E. Crago and J.C. Houk. Sampling total muscle force by tendon organ. *Journal of Neurophysiology*, 47(6):1069–1083, 1982.

[43] R.D. Crownishield and R.A. Brand. A physiologically based criterion for muscle force prediction and locomotion. *Journal of Biomechanics*, 14:793–801, 1981.

[44] R.D. Crownishield, R.C. Johnston, J.G. Andrews, and R.A. Brand. A biomechanical investigation of the human hip. *Journal of Biomechanics*, 11:75–85, 1978.

[45] M. Daniel, V. Antolič, A. Iglič, and V. Kralj-Iglič. Determination of contact hip stress from nomograms based on mathematical model. *Medical Engineering & Physics*, 23:347–357, 2001.

[46] A. Davies, A.S.H. Blakely, and C. Kidd. *Human Physiology*, chapter Muscle. Churchill Livingstone, New York, 2001.

[47] S.L. Delp and J.P Loan. A software system to develop and analyze models of musculoskeletal structures. *Computers in Biology and Medicine*, 25(21–34), 1995.

[48] S.L. Delp, J.P. Loan, M.G. Hoy, F.E. Zajac, E.L. Topp, and J.M. Rosen. An interactive graphics-based model of the lower extremity to study orthopaedic surgical procedures. *IEEE Transactions on Biomedical Engineering*, 37:757–767, 1990.

[49] M. Dienst and D. Kohn. Osteonecrosis of the hip joint in adults. Implication of different osteotomies. *Orthopäde*, 29:430–441, 2000.

[50] G.A.H. Dijke, van, C.J. Snijders, R. Stoeckart, and H.J. Stam. A biomechanical model on muscle forces in the transfer of spinal load to the pelvis and legs. *Journal of Biomechanics*, 32:927–933, 1999.

[51] W.F. Dostal and J.G. Andrews. A three dimensional biomechanical model of the hip musculature. *Journal of Biomechanics*, 14:803–812, 1981.

[52] J. Dull, M.A. Towsend, R. Shiavi, and G.E. Johnson. Muscular synergism – on criteria for load sharing between synergistic muscles. *Journal of Biomechanics*, 14:663–673, 1984.

[53] R.B. Duncan, R.B. Knapp, and M.C. Miller. *Introductory biostatistics for the health sciences*. John Wiley & Sons, New York, 1977.

[54] C.W. Durnim, R. Ganz, and K. Klause. The acetabular rim syndrome - a clinical presentation of dysplasia of the hip. *Journal of Bone and Joint Surgery [Br]*, 73B:423–429, 1991.

[55] J. Duysens, F. Clarac, and H. Cruse. Load-regulating mechanisms in gait and posture: Comparative aspects. *Physiological Reviews*, 80(1):83–133, January 2000.

[56] D.T. Felson and J. Buckwalter. Débridement and lavage for osteoarthritis of knee. *The New England Journal of Medicine*, 347(2):132–133, 2002.

[57] R.P. Ficat. Idiopathic bone necrosis of the femoral head. early diagnosis and treatment. *Journal of Bone and Joint Surgery Br.*, 67B:3–9, 1985.

[58] Free Software Foundation. *GNU Public Licence*. Free Software Foundation, Boston, 2003. available online www.gnu.org/copyleft/gpl.html.

[59] J. Freund and E.-P. Takala. A dynamic model of the forearm including fatigue. *Journal of Biomechanics*, 34:597–605, 2001.

[60] D. Gagnon, C. Larivière, and P. Lisel. Comparative ability of EMG, optimization, and hybrid modelling approaches to predict trunk muscle forces and lumbar spine loading during dynamic sagittal plane lifting. *Clinical Biomechanics*, 16(5):359–372, 2001.

[61] R.H. Gallagher, B.R. Simon, P.C. Johnson, and J.F. Gross, editors. *Finite elements in biomechanics*. John Wiley & Sons, Chichester, 1982.

[62] J.W.M. Gardniers. ARCO committee on terminology and staging (report on the committee meeting at Santiago de Compostela). *ARCO Newsletter*, 5:79–82, 1993.

[63] E. Genda, N. Iwasaki, G. Li, B.A. MacWiliams, P.J. Barrance, and E.Y.S. Chao. Normal hip joint contact pressure distribution in single-leg standing – effect of gender and anatomic parameters. *Journal of Biomechanics*, 34:895–905, 2001.

[64] E. Genda, N. Konishi, Y. Hasegawa, and T. Miura. A computer simulation study of normal and abnormal hip joint contact pressure. *Archives of Orthopaedic and Trauma Surgery*, 114:202–206, 1995.

[65] S. Gilman. Joint position sense and vibration sense: anatomical organisation and asessment. *Journal of Neurology, Neurosurgery and Psychiatry*, 73(5):473–477, 2002.

[66] F. Graichen, G. Bergmann, and A. Rohlmann. Hip endoprosthesis for in vivo measurement of joint force and temperature. *Journal of Biomechanics*, 32:1113–1117, 1999.

[67] A.S. Greenwald and D.W. Haynes. Weight-bearing areas in the human hip joint. *Journal of Bone and Joint Surgery*, 54B(1):157–163, 1972.

[68] A.S. Greenwald and J.J. O'Connor. The transmission of load through human hip joint. *Journal of Biomechanics*, 4:507–528, 1971.

[69] F. Guilak. Compression-induced changes in the shape and volume of the chondrocytes nucleus. *Journal of Biomechanics*, 28(12):1529–1541, 1995.

[70] N.A. Hadley, T.D. Brown, and S.L. Weinstein. The effects of contact stress pressure elevations and aseptic necrosis in the long-term outcome of congenital hip dislocation. *Journal of Orthopaedic Research*, 8:504–513, 1990.

[71] S.J. Hall. *Basic Biomechanics*. WCB/McGraw-Hill, Boston, 1995.

[72] R. Hapee and F.C.T. van der Helm. The control shoulder muscles during goal-directed movements, and inverse dynamic analysis. *Journal of Biomechanics*, 28(10):1179–1191, 1995.

[73] W.H. Harris. Traumatic arthritis of the hip after dislocation and acetabular fractures: treatment by mold arthroplasty. *Journal of Bone and Joint Surgery*, 51–A:737–755, 1969.

[74] M.O. Heller, G. Bergmann, G. Deuretzbacher, L. Dürselen, M. Pohl, L. Claes, N.P. Haas, and G.N. Duda. Musculo-skeletal loading conditions at hip during walking and stair climbing. *Journal of Biomechanics*, 34:883–893, 2001.

[75] van der F.C.T. Helm and E.K.J. Chadwick. A forward-dynamic shoulder and elbow model. In *Proceeding of the 4th Meeting of the International Shoulder Group*, 2002.

[76] S. Herman, A. Jaklič, S. Herman, A. Iglič, and V. Kralj-Iglič. Hip stress reduction after chiari osteotomy. *Medical and Biological Engineering and Computing*, 40:369–375, 2002.

[77] P. Herningou, D. Bachir, and D. Galacteros. The natural history of symptomatic osteonecrosis in adults with sickle-cell disease. *Journal of Bone and Joint Surgery Am.*, 85A:500–504, 2003.

[78] J.A. Hipp, N. Sugano, M.B. Millis, and S.B. Murphy. Planning acetabular redirection osteotomies based on joint contact pressures. *Clinical Orthopaedics and Related Research*, 364:134–143, 1999.

[79] M. Hlaváček. Squeeze-film lubrication of the human ankle joint with synovial fluid filtrated by articular cartilage with the superficial zone worn out. *Journal of Biomechanics*, 33:1415–1422, 2000.

[80] W.A. Hodge, K.L. Carlson, R.S. Fijan, R.G. Burgess, P.O. Riley, W.H. Harris, and R.W. Mann. Contact pressures from an instrumented hip endoprostheses. *Journal of Bone and Joint Surgery*, 71A:1378–1386, 1989.

[81] T. Hogervorst and R.A. Brand. Mechanoreceptors in joint function. *Journal of Bone and Joint Surgery*, 80A(9):1365–1377, 1998.

[82] R. Huiskes and R. Boeklagen. Mathematical shape optimization of hip prosthesis design. *Journal of Biomechanics*, 22:793–804, 1989.

[83] R. Huiskes, R. Ruimerman, G.H. van Lenthe, and J.D. Janssen. Effects of mechanical forces on maintenance and adaptation of form in trabecular bone. *Nature*, 404:704–706, 2000.

[84] I. Hulín, editor. *Patofyziológia*. Slovak Academy Press, Bratislava, 1998.

[85] D. Hungerford. Treatment of avascular necrosis in young patients. *Orthopaedics*, 18:822–833, 1995.

[86] M. Hungerford, E. Shirley, P. Khanuja, and D. Hungerford. Osteotomies as treatment for osteonecrosis. *Current Opinion in Orthopaedics*, 14:17–23, 2003.

[87] D.E. Hurwitz, K.C. Foucher, and T.P. Andriacchi. A new parametric approach for modelling hip forces during gait. *Journal of Biomechanics*, 36:113–119, 2003.

[88] C.D.D. Hutter. Dysbaric osteonecrosis: a reassessment and hypothesis. *Medical Hypotheses*, 54:585–590, 1998.

[89] A. Iglič, V. Antolič, V. Kralj-Iglič, and F. Srakar. Congenital coxa vara: a biomechanical analysis. *Medicinske Razgledy*, 32:625–633, 1993.

[90] A. Iglič, V. Antolič, and F. Srakar. Biomechanical analysis of various hip joint rotation center shift. *Archives of Orthopaedic and Trauma Surgery*, 112:124–126, 1993.

[91] A. Iglič, M. Daniel, V. Kralj-Iglič, V. Antolič, and A. Jaklič. Peak joint contact stress in male and female population. *Journal of Musculoskeletal Research*, 5(1):17–21, 2000.

[92] A. Iglič and V. Kralj-Iglič. Computer system for determination of hip joint contact stress distribution from antero-posterior radiograph. *Radiol Oncol*, 33(4):263–266, 1999.

[93] A. Iglič, V. Kralj-Iglič, V. Antolič, F. Srakar, and U. Stanič. Effect of the periacetabular osteotomy on the stress on the human hip joint articular surface. *IEEE Transaction on rehabilitation*, 1(4):207–212, 1993.

[94] A. Iglič, V. Kralj-Iglič, M. Daniel, and A. Maček-Lebar. Computer determination of contact stress distribution and the size of the weight-bearing area in the human hip joint. *Computer Methods in Biomechanics and Biomedical Engineering*, 5:185–192, 2002.

[95] A. Iglič, F. Srakar, and A. Antolič. Influence of the pelvic shape on the biomechanical status of the hip. *Clinical Biomechanics*, 8:233–234, 1993.

[96] A. Iglič, F. Srakar, V. Antolič, V. Kralj-Iglič, and V. Batagelj. Mathematical analysis of chiari osteotomy. *Acta Orthopedica Iugoslavica*, 20:35–39, 1990.

[97] International Business Machines Corporation, New York, USA. *IBM Visualization Data Explorer User's Guide*, version 3 release 1 modification 4 edition.

[98] M. Ipavec, R.A. Brand, D.R. Pedersen, B. Mavčič, V. Kralj-Iglič, and A. Iglič. Mathematical modelling of stress in the hip during gait. *Journal of Biomechanics*, 32:1229–1235, 1999.

[99] M. Ipavec, A. Iglič, V. Kralj-Iglič, and V. Antolič. Influence of the non-spherical shape of the femoral head on the compressive stress in the hip

joint articular layer. In *Proceedings of the 6th Conference of Slovenian IEEE Section*, pages 351–354, Ljubljana, 1997.

[100] M. Ipavec, V. Kralj-Iglič, and A. Iglič. Stress in the hip joint articular surface during gait. *Engineering Modelling*, 8:7–14, 1995.

[101] A. Jaklič and F. Pernuš. Morfometrična analiza ap rentgenogramov medenice in kolka. In *Proceedings of the third electrotechnical and computer science conference ERK 94*, volume B, pages 352–355, Portorož, 1995.

[102] R.C. Johnston and R.A. Brand. Reconstruction of the hip. *Journal of Bone and Joint Surgery*, 61A:639–652, 1979.

[103] J.P. Jones. Epidemiological risk factors for non-traumatic osteonecrosis. *Orthopäde*, 29:370–379, 2000.

[104] B. Kersnič, A. Iglič, V. Kralj-Iglič, F. Srakar, and V. Antolič. Increased incidence of arthrosis in women could be related to femoral and pelvic shape. *Archives of Orthopaedic and Trauma Surgery*, 116:345–347, 1997.

[105] R.F.M. Kleissen, J.H. Buurke, J. Harlaar, and G. Zilvold. Electromyography in the biomechnical analysis of human movement and its clinical application. *Gait and Posture*, 8:143–158, 1998.

[106] N. Konishi and T. Mieno. Determination of acetabular coverage of the femoral head with use of a single anteroposterior radiograph. *Journal of Bone and Joint Surgery*, 75–A:1318–1333, 1993.

[107] S. Konvičková and J. Valenta. *Biomechanika kloubů člověka a jejich náhrady.* VIENALA a ŠTROFFEK, Praha, 2000.

[108] A. Kralj. Optimum coordination and selection of muscles for functional electrical simulation. In *Proceeding of the 8th ICMBE*, page 7, Chicago, 1969.

[109] J. Kramer, M. Breitenseher, M. Imhof, M. Urban, H. Plenk, and S. Hofmann. Imaging modalities in avascular necrosis of the hip. *Orthopäde*, 29:380–388, 2000.

[110] E. Kreyszig. *Advanced engineering mathematics.* John Willey & Sons, New York, 1993.

[111] B. Kummer. Biomechanishe grundlagen der statik des hüftgelenkes. *Zeitschrift für Orthopädie und ihre Grenzgebiete*, 129:179–187, 1986.

[112] B. Kummer. Die klinische relevanz biomechanischer analysen der hüftregion. *Zeitschrift für Orthopädie und ihre Grenzgebiete*, 129:285–294, 1991.

[113] V. Kuželka. Osteometrie. In M. Stloukal, editor, *Antropologie*. Národní muzeum, Praha, 1999.

[114] Wang L. and T.S. Buchanan. Prediction of joint moments using a neural network model of muscle activations from EMG signals. *IEEE Transactions on Neural Systems and Rehabilitation Engineering*, 10(1):30–37, 2002.

[115] A. Larson and B. Edwards. *Elementary linear algebra*, chapter Linear programming. Houghton Mifflin Company, Pennsylvania, 2000.

[116] P.J. Lattanzio and R.J. Pertrella. Knee proprioception: A review of mechanisms, measurements and implications of muscular fatique. *Orthopaedics*, 21(4):463–470, 1998.

[117] E.C. Lau, C. Cooper, D. Lam, V.N.H. Chan, K.K. Tsang, and A. Sham. Factors associated with osteoarthritis of the hip and knee in Hong Kong Chinese: Obesity, joint injury, and occupational activities. *American Journal of Epidemiology*, 152:855–862, 2000.

[118] H. Legal. Introduction to the biomechanics of the hip. In D. Tönis, editor, *Congenital dysplasia and dyslocation of the hip*. Springer-Verlag, Berlin, 1987.

[119] H. Legal and M. Reinecke. Zur biostatischen analyse des hüftgelenkes II. *Zeitschrift für Orthopädie und ihre Grenzgebiete*, 116:889–896, 1978.

[120] H. Legal and M. Reinicke. Zur biostatischen analyse des hüftgelenkes III. *Zeitschrift für Orthopädie und ihre Grenzgebiete*, 118:804–815, 1980.

[121] H. Legal and H. Ruder. Zur biostatischen analyse des hüftgelenkes. *Zeitschrift für Orthopädie und ihre Grenzgebiete*, 115:215–234, 1977.

[122] C.C.K. Lin and P. Crago. Neural and mechanical contributions to the stretch reflex: A model synthesis. *Annals of Biomedical Engineering*, 30:54–67, 2002.

[123] D. Lloyd and F.T. Besier. An EMG-driven musculoskeletal model to estimate muscle forces and knee joint movements in vivo. *Journal of Biomechanics*, 36:765–776, 2003.

[124] N. Luepongsak, S. Amin, D.E. Krebs, C.A. McGibbon, and D. Felson. The contribution of type of daily activity to loading across the hip and knee joint in the elderly. *Osteoarthritis and Cartilage*, 10:353–359, 2002.

[125] M. MacKay-Lyons. Central pattern generation: A review of the evidence. *Physical Theraphy*, 82(1):69–81, 2002.

[126] T.A. Malvitz and S.L. Weinstein. Closed reduction of congenital dysplasia of the hip. *Journal of Bone and Joint Surgery*, 76A:1777–1791, 1994.

[127] P.G.J. Maquet. *Biomechanics of the hip*. Springer-Verlang, Berlin, 1985.

[128] R. Marks and J.P. Allegrante. Body mass indices in patients with disabling hip osteoarthritis. *Arthritis Research*, 4:112–116, 2001.

[129] F.C. Martin and L. Schovanec. Muscle mechanics and dynamics of ocular motion. *Journal of Mathematical Systems, Estimation and Control*, 8(2):1–15, 1998.

[130] W. Maurel. *3D Modeling of the Human Upper Limb including the Biomechanics of Joints, Muscles and Soft Tissues*. PhD thesis, Ecole Polytechnique Federale de Lausanne, Lausanne, Switzerland, 1998.

[131] A. Maček-Lebar. Analiza obremenitev umetnega kolčnega sklepa. Master's thesis, Faculty of Electrical Engineering, University of Ljubljana, 1995.

[132] A. Maček-Lebar, A. Iglič, and F. Antolič, V.and Srakar. Distribution of the hip abductor muscle forces in one-legged stance. *Zdravniški Vestnik*, 62:231–234, 1993.

[133] A. Maček-Lebar, A. Iglič, V. Antolič, and F. Srakar. An optimization approach to muscular load sharing in the hip joint. *Acta Pharmaceutica*, 42:329–332, 1993.

[134] B. Mavčič, B. Pompe, M. Daniel, A. Iglič, and V. Kralj-Iglič. Mathematical estimation of stress distribution in normal and dysplastic human hip. *Journal of Orthopaedic Research*, 20:1025–1030, 2002.

[135] T.A. Maxian, T.D. Brown, and S.L. Weinstein. Chronic stress tolerance level for human articular cartilage: two nonuniform contact model applied to long term follow up of cdh. *Journal of Biomechanics*, 28:159–166, 1995.

[136] H.A. McKellop. Bearing surfaces in total hip replacements: State of the art and future developments. *Instructional Course Lecture*, 50:165–179, 2001.

[137] R.D. Mcleish and J. Charnley. Abduction forces in one-legged stance. *Journal of Biomechanics*, 3:191–209, 1970.

[138] T. McTighe, L.W. Trick, and J.B. Koeneman. Design considreations for cementless total hip arthroplasty. In D.L. Wise, D.J. Trantolo, D.E. Altobelii, M.J. Yaszernski, J.D. Gresser, and E.R. Schwarts, editors, *Encyclopedic handbook of biomaterials and bioengineering*. Marcel Dekker, New York, 1995.

[139] K. Miyanishi, T. Yamamoto, T. Irisa, A. Yamashita, S. Jingushi, Y. Noguchi, and Y. Iwamoto. Bone marrow fat cell enlargement and rise in intraosseous pressure in steroid-treated rabbits with osteonecrosis. *Bone*, 30:185–190, 2002.

[140] K.L. Moore and A.T. Dalley. *Clinically oriented anatomy*. Lippincot Wiliams & Wilkins, Baltimore, 1999.

[141] M. Morlock, E. Schneider, A. Bluhm, M. Vollmer, G. Bergmann, V. Müller, and M. Honl. Duration and frequency of every day activities in total hip patients. *Journal of Biomechanics*, 34:873–888, 2001.

[142] B.F. Morrey, editor. *Biological, material and mechanical considerations of joint replacement*. Raven Press, New York, 1993.

[143] B.M. Nigg and W. Herzog. *Biomechanics of the musculo-skeletal system*. John Willey & Sons, Chichester, 1995.

[144] M. Nordin and V.H Frankel, editors. *Basic biomechanics of the musculoskeletal system*. Lea & Fibiger, Philadelphia, 1989.

[145] W. Oberländer. On biomechanics of joints. the influence of functional cartilage swelling on the congruity of regularly curved joints. *Journal of Biomechanics*, 11:151–153, 1978.

[146] S.A. Oliveria, D.T. Felson, Cirillo P.A., J.I. Reed, and A.M. Walker. Body weight, body mass index, and incident symptomatic osteoarthritis of the hand, hip, and knee. *Epidemiology*, 10(2):161–166, 1999.

[147] J.P. Paul. Strenght requirment for internal and external prostheses. *Journal of Biomechanics*, 32:381–393, 1999.

[148] F. Pauwels. *Biomechanics of the normal and diseased hips*. Springer-Verlang, Berlin, 1976.

[149] J. Pazourek. *Simulace biologických systémů*. Grada, Praha, 1992.

[150] D.R. Pedersen, R.A. Brand, and D.T. Davy. Pelvic muscle and acetabular forces during gait. *Journal of Biomechanics*, 30:959–965, 1997.

[151] H. Plenk, S. Hofman, M. Breitenseher, and M. Urban. Pathomorphological aspects and repair mechanicsms of femoral head osteonecrosis. *Orthopäde*, 29:389–402, 2002.

[152] B. Pompe, M. Daniel, M. Sochor, R. Vengust, V. Kralj-Iglič, and A. Iglič. Gradient of contact stress in normal and dysplastic human hip. *Medical Engineering & Physics*, 25:379–385, 2003.

[153] M. Praagman, H.E.J. Veeger, F.C.T. van der Helm, and E.K.J. Chadwick. Relationship between mechanical cost function and muscle oxygen consumption. In *Proceeding of the 4th Meeting of the International Shoulder Group*, Cleveland, June 2002.

[154] W.H. Press, S.A. Teukolsky, W.T. Vetterling, and B.P. Flannery, editors. *Numerical Recipes in C. The Art of Scientific Computing*, chapter Minimization or Maximization of Functions. Cambridge University Press, Cambridge, 2nd edition edition, 1992.

[155] B.I. Prilutsky and R.J. Gregor. Analysis of muscle cordination strategies in cycling. *IEEE Transactions on Rehabilitation Engineering*, 8(3):362–370, 2000.

[156] A. Prochazka. Quantifying proprioception. In M.D. Binder, editor, *Progress in Brain Research: Peripheral and Spinal Mechanisms in the Neural Control of Movement*, volume 123. Elsevier, Amsterdam, 1999.

[157] A. Prochazka and S. Yakovenko. Locomotor control: From spring-like reactions of muscles to neural prediction. In R. Nelson, editor, *The somatosensory system: Deciphering the Brain's own body image*. CRC Press, Cleveland, 2001.

[158] R.T. Raikova. About weight factors in the non-linear objective functions used for solving indeterminate problems in biomechanics. *Journal of Biomechanics*, 32:689–694, 1999.

[159] R.T. Raikova. Investigation of the pecularities of two-joint muscles using a 3 DOF model of the human upper limb in the sagittal plane: an optimization approach. *Computer Methods in Biomechanics and Biomedical Engineering*, 4:463–490, 2001.

[160] R.T. Raikova and H.Ts. Aladjov. Hierarchical genetic algorithm versus static optimisation - investigation of elbow flexion and extension movements. *Journal of Biomechanics*, 35:1123–1135, 2002.

[161] R.T. Raikova and B.I. Prilutsky. Sensitivity of predicted muscle forces to parameters of the optimization-based human leg model revealed by analytical and numerical analyses. *Journal of Biomechanics*, 34:1243–1255, 2001.

[162] D.J. Rapperport, D.R. Carter, and D.J. Schurman. Contact finite stress analysis of the hip joint. *Journal of Orthopaedic Research*, 3:435–446, 1985.

[163] J. Rasmussen, M. Damsgaard, and M. Voigt. Muscle recruitment by the min/max criterion - a comparative numerical study. *Journal of Biomechanics*, 34:409–415, 2001.

[164] B.L. Riemann, J.B. Myers, and S.M. Lephart. Comparison of the ankle, knee, hip and trunk corrective action shown during single-leg stance on firm, foam and multiaxial surface. *Archives of Physical Medicine and Rehabilitation*, 84:90–95, 2003.

[165] G. Rådegran and B. Saltin. Human femoral artery diameter in relation to knee extensor muscle mass, peak blood flow, and oxygen uptake. *American Journal of Physiology - Heart and Circulatory Physiology*, 278:162–167, 2000.

[166] L. Rådman. Simulation of responses in proprioceptive afferents during human manipulation. Master's thesis, Umeå University, Sweden, 2002.

[167] N.W. Rydell. Forces acting on the femoral head-prosthesis. *Acta Orthopaedica Scandinavica*, 37(Suppl. 88):1–132, 1966.

[168] R.B. Salter. Innominate osteotomy in treatment of congenital dyslocation of the hip. *Journal of Bone and Joint Surgery*, 8:89–102, 1975.

[169] D. Sargart. Proprioception: how does it work? A simplified overwiev of anatomical structures and neurophysiological actions involved in joint stability. *Australian Journal of Podiatric Medicine*, 34(3):86–92, 2000.

[170] D.J. Schneck. *Engineering principles of physiologic function*. New York University Press, New York, 1990.

[171] A. Seireg and R.J. Arvikar. The prediction of the muscular load sharing joint forces in the lower extremities during walking. *Journal of Biomechanics*, 8:89–102, 1975.

[172] B.W. Stansfield, A.C. Nicol, J.P. Paul, I.G. Kelly, F. Graichen, and G. Bergmann. Direct comparison of calculated hip joint contact forces with those measured using instrumented implants. an evaluation of the three-dimensional model of the lower limb. *Journal of Biomechanics*, 26:929–936, 2003.

[173] M.E. Steinberg, G.D. Hayken, and D.R. Steinberg. A quantitative system for staging avascular necrosis. *Journal of Bone and Joint Surgery Br.*, 77:34–41, 1995.

[174] B.C. Stillmann. *An investigation of the clinical assessment of joint position sense*. PhD thesis, School of Physiotheraphy, Faculty of Medicine, Dentistry and Health Sciences, The University of Melbourne, Victoria, Australia, 2000.

[175] I.A.F. Stokes and M. Gardner-Morse. Quantitative anatomy of the lumbar musculature. *Journal of Biomechanics*, 32:311–316, 1999.

[176] I.A.F. Stokes and M. Gardner-Morse. Lumbar spinal muscle activation synergies predicted by multi-criteria cost function. *Journal of Biomechanics*, 34:733–740, 2001.

[177] J. Sýkora. Matematické modelování kontaktních tlaků v kyčelním kloubu. Master's thesis, Faculty of Mechanical Engineering, Czech Technical University in Prague, 2004.

[178] D.G. Thelen, F.C. Anderson, and S.L. Delp. Generating dynamic simulations of movement using computed muscle control. *Journal of Biomechanics*, 36:321–328, 2003.

[179] S.K.S. Thorpe, Y. Li, R.H. Crompton, and R.M. Alexander. Stress in human leg muscles in running and jumping determined by force plate analysis and from published magnetic resonance images. *The Journal of Experimental Biology*, 201:63–70, 1998.

[180] M. Trew and T. Everett. *Human Movement. An introductory text*, chapter Measuring and evaluating human movement. Churchill Livingstone, New York, 2001.

[181] D. Tsirakos, V. Baltzopoulos, and R. Bralett. Inverse optimization: functional and physiological considerations related to the force sharing problem. *Critical Reviews in Biomedical Engineering*, 25(4&5):371–407, 1997.

[182] T. Ueo, S. Tsutsumi, T. Yamamuro, H. Okumura, A. Shimizu, and T. Nakamura. Biomechanical aspects of the development of aseptic necrosis of the femoral head. *Archives of Orthopaedic and Trauma Surgery*, 104:145–149, 1985.

[183] J. Valenta, editor. *Biomechanics*. Elsevier, Amsterdam, 1993.

[184] C.L. Vaughan. Theories of bipedal walking: an odyssey. *Journal of Biomechanics*, 36:513–523, 2002.

[185] C.L. Vaughan, B.L Davis, and J.C. O'Connor, editors. *Dynamics of Human Gait*, chapter attached CDROM. Human kinetics publishers, Champaign, 1992. available online http://www.isbweb.org/data/.

[186] R. Vengust, M. Daniel, V. Antolič, O. Zupanc, A. Iglič, and V. Kralj-Iglič. Biomechanical evaluation of the hip after innominate osteotomy: a long-term follow-up study. *Archives of Orthopaedic and Trauma Surgery*, 121:511–516, 2001.

[187] E. Vingård. Overweight predisposes to coxarthrosis. *Acta Orthopaedica Scandinavica*, 62(2):106–109, 1991.

[188] J. Vojtaššák. *Ortopédia*. Slovak Academy Press, Bratislava, 1998.

[189] G. Wiberg. Studies on dysplastic acetabula and congenital subluxation of the hip joint with special reference to the complications of osteoarthritis. *Acta Scandinavica Chirurgica*, 58:1–83, 1939.

[190] J.F. Williams and N.L. Svensson. A force analysis of the hip joint. *Biomedical Engineering*, 3:366–370, 1968.

[191] J.M. Winters. Terminology and foundations of movement science. In J.M. Winters and P.E. Crago, editors, *Biomechanics and Neural Control of Posture and Movement*. Springer-Verlang, New York, 2000.

[192] S.P. Wise and R. Shadmehr. Motor control. In V. S. Ramachandran, editor, *Encyclopedia of Human Brain*, volume 3. Academic Press, San Diego, 2002.

[193] J.C. Wolfe and K.L. Taylor-Butler. Avascular necrosis. A case history and literature review. *Archives of Family Medicine*, 9:291–294, 2000.

[194] G.T. Yamaguchi. Performing whole-body simulation of gait with 3-D, dynamic muskuloskeletal model. In J.M. Winters and S. L-Y. Woo, editors, *Multiple Muscle Systems - Biomechanics and Movement Organization*. Spinger-Verlang, New-York, 1990.

[195] G.T. Yamaguchi. A survey of human musculotendon actuator parameters. In J.M. Winters and S. L-Y. Woo, editors, *Multiple Muscle Systems - Biomechanics and Movement Organization*. Spinger-Verlang, New-York, 1990.

[196] Y. Ye. *SOLNP user's guide: A nonlinear optimization in MATLAB*. Department of Management Sciences, College of Bussoness Administration, University of Iowa, 1989.

[197] E.F. Zajac and J.M. Winters. Modelling muskuloskeletal movement systems: Joint and body segmental dynamics, muskuloskeletal and neuromuskular system. In J.M. Winters and S. L-Y. Woo, editors, *Multiple Muscle Systems - Biomechanics and Movement Organization*. Spinger-Verlang, New-York, 1990.

[198] O. C. Zienkiewicz. *The finite element method in engineering science*. McGraw-Hill Book Company, Inc., London, New York, 1971.

[199] O. Zupanc, V. Antolič, A. Iglič, A. Jaklič, V. Kralj-Iglič, J. Stare, and R. Vengust. Assessment of the contact stress in the hip joint after operative treatment of severe slipped capital femoral epiphysis. *International Orthopaedics (SICOT)*, 25:9–21, 2001.

Czech Technical University in Prague
Faculty of Mechanical Engineering, Department of Mechanics, Laboratory of Biomechanics of Man

Supplement to Dissertation

Mathematical simulation of the hip joint loading

RNDr. Matej Daniel

Study Branch: Biomechanics

Advisor Doc. Ing. Miroslav Sochor, CSc.
Co-advisor Prof. Dr. Veronika Kralj-Iglič

2004 Prague

PREFACE

Supplement to disertation entitled: *Mathematical simulation of the hip joint loading* by Matej Daniel contains additional results and data that were not included in the thesis. It contains also previews of the animations that are available on attached CDROM. For detailed description of the mathematical models see the dissertation thesis.

Appendix A

QUANTITATIVE DESCRIPTION OF THE HUMAN HIP MUSCULATURE

The following text contains m-scripts for GNU Octave that describe two muscle models of the hip with nine and twenty-seven muscles, respectively. The former was taken from literature (Tab. 4.2) while the latter was described within this work (section 4.1).

Software requirements	:	GNU Octave, version 2.1.50
List of files	:	`musclemodelold.m` - muscle model with 9 muscle
		`musclemodelnew.m` - musclemodel with 27 muscle
Required files	:	`RotateY.m` - rotation of vector around y axis (see section K)

musclemodelold.m

```
1;
global Muscle

Lref = 2*8.45;
Cref = 5.85;
Href = 13.52;
Xref = 7.1;
Zref = 2.65;
zasuk = 0;

lizm = Lref;
cizm = Cref;
hizm = Href;
xizm = Xref;
zizm = Zref;
Wb = 800;

Troch = [xizm, 1, zizm];
Pelv  = [hizm, 1, cizm];
TrochRef = [Xref, 1, Zref];
PelvRef  = [Href, 1, Cref];

NormTroch = Troch ./ TrochRef;
NormPelv  = Pelv ./ PelvRef;

c = 0.505 * lizm;
b = 0.24 * lizm;
```

```
Wl = 0.16 * Wb;
a = (Wb*c - Wl*b) / (Wb - Wl);

Muscle.Name = ["glutes medius anterior"
               "gluteus minimus anterior"
               "tensor fasciae latae"
               "rectus femoris"
               "gluteus medius medius"
               "gluteus minimus medius"
               "gluteus medius posterior"
               "gluteus minimus posterior"
               "gluteus piriformis"];
Muscle.Group = ["a"
                "a"
                "a"
                "a"
                "m"
                "m"
                "p"
                "p"
                "p"];
Muscle.Pelvis = [-10.2, -2.7, -6.2
                 -7.3, -2.9, -4.1
                 -7.8, -4.5, -5.6
                 -3.7, -4.3, -2.6
                 -13.2, 0.2, -1.8
                 -8.8, 0.4, -2.0
                 -9.7, 4.8, 1.5
                 -7.1, 2.6, 0.0
                 -5.5, 7.8, 4.7];
Muscle.Femur = [2.6, 1.8, -7.3
                2.7, -0.4, -6.9
                43.6, -2.2, -3.3
                41.5, -4.3, -0.2
                2.6, 1.8, -7.3
                2.7, -0.4, -6.9
                2.6, 1.8, -7.3
                2.7, -0.4, -6.9
                0.1, 0.1, -5.5];

Muscle.A = [0.266
            0.133
            0.120
            0.400
            0.266
            0.133
            0.266
            0.133
```

```
           0.100];
Muscle.A = Muscle.A * 100;
Muscle.TendonPCSA = [13
                19
                5
                24
                13
                19
                13
                19
                15];
Muscle.Fmax = [546
               180
               155
               779
               382
               190
               435
               215
               296];
Muscle.TendonLength = [0.0780
                0.0168
                0.4250
                0.3460
                0.0530
                0.0260
                0.0530
                0.0510
               0.01150];
Muscle.Spindle = [1
                 2.2
                 1
                 0.9
                 1
                 2.2
                 1
                 2.2
                 3.5];
x0 = 42.3;
theta = asin(b/x0);
ni = -0.5 * pi / 180;
for i=1:9
  Muscle.Femur(i,:) = Muscle.Femur(i,:) .* NormTroch;
  Muscle.Femur(i,:) = RotateY(Muscle.Femur(i,:), -theta);

  Muscle.Pelvis(i,:) = Muscle.Pelvis(i,:) .* NormPelv;
  Muscle.Pelvis(i,:) =  RotateY(Muscle.Pelvis(i,:), ni);
endfor
```

musclemodelnew.m

```
1;
global Muscle

Lref = 2*8.45;
Cref = 5.85;
Href = 13.52;
Xref = 7.1;
Zref = 2.65;
zasuk = 0;

lizm = Lref;
cizm = Cref;
hizm = Href;
xizm = Xref;
zizm = Zref;
Wb = 800;

Troch = [xizm, 1, zizm];
Pelv  = [hizm, 1, cizm];
TrochRef = [Xref, 1, Zref];
PelvRef  = [Href, 1, Cref];

NormTroch = Troch ./ TrochRef;
NormPelv  = Pelv ./ PelvRef;

c = 0.505 * lizm;
b = 0.24 * lizm;

Wl = 0.16 * Wb;
a = (Wb*c - Wl*b) / (Wb - Wl);

i = 0;
Muscle.Name = ["adductor brevis"
               "adductor longus"
               "adductor magnus 1"
               "adductor magnus 2"
               "adductor magnus 3"
               "gemelli inferior et superior"
               "gluteus maximus 1"
               "gluteus maximus 2"
               "gluteus maximus 3"
               "gluteus medius 1"
               "gluteus medius 2"
               "gluteus medius 3"
               "gluteus minimus 1"
               "gluteus minimus 2"
```

```
              "gluteus minimus 3"
              "iliacus"
              "pectineus"
              "piriformis"
              "psoas"
              "quadratus femoris"
              "biceps femoris long"
              "gracilis"
              "sartorius"
              "semimebranosus"
              "semitendinosus"
              "tensor fascie latae"
              "rectus femoris"];
i = i+1;
#Muscle.Name(:) = "adductor brevis";
Muscle.Pelvis(i,:) = [-0.0587 -0.0915 0.0164];
Muscle.Femur(i,:) = [0.0009 -0.1196 0.0294];
Muscle.A(i) = 6.39;
Muscle.Fmax(i) = 286;
Muscle.TendonLength(i) = 0.0200;
Muscle.Spindle(i) = 1.3;
i = i+1;
#Muscle.Name(i) = "adductor longus";
Muscle.Pelvis(i,:) = [-0.0316 -0.0836 0.0169];
Muscle.Femur(i,:) = [0.0050 -0.2111 0.0234];
Muscle.A(i) = 21.08;
Muscle.Fmax(i) = 418;
Muscle.TendonLength(i) = 0.1100;
Muscle.Spindle(i) = 1.1;
i = i+1;
#Muscle.Name(i) = "adductor magnus 1";
Muscle.Pelvis(i,:) = [-0.0732 -0.1174 0.0255];
Muscle.Femur(i,:) = [-0.0045 -0.1211 0.0339];
Muscle.A(i) = 35.17;
Muscle.Fmax(i) = 346;
Muscle.TendonLength(i) = 0.0600;
Muscle.Spindle(i) = 0.9;
i = i+1;
#Muscle.Name(i) = "adductor magnus 2";
Muscle.Pelvis(i,:) = [-0.0831 -0.1192 0.0308];
Muscle.Femur(i,:) = [0.0054 -0.2285 0.0227];
Muscle.A(i) = 25.28;
Muscle.Fmax(i) = 312;
Muscle.TendonLength(i) = 0.1300;
Muscle.Spindle(i) = 0.9;
i = i+1;
#Muscle.Name(i) = "adductor magnus 3";
Muscle.Pelvis(i,:) = [-0.0771 -0.1181 0.0276];
Muscle.Femur(i,:) = [0.0070 -0.3837 -0.0266];
```

```
Muscle.A(i) = 23.36;
Muscle.Fmax(i) = 444;
Muscle.TendonLength(i) = 0.2600;
Muscle.Spindle(i) = 0.9;
i = i+1;
#Muscle.Name(i) = "gemelli inferior et superior";
Muscle.Pelvis(i,:) = [-0.1133 -0.0820 0.0714];
Muscle.Femur(i,:) = [-0.0142 -0.0033 0.0443];
Muscle.A(i) = 10;
Muscle.Fmax(i) = 109;
Muscle.TendonLength(i) = 0.0390;
Muscle.Spindle(i) = 3.7;
i = i+1;
#Muscle.Name(i) = "gluteus maximus 1";
Muscle.Pelvis(i,:) = [-0.1195 0.0612 0.0700];
Muscle.Femur(i,:) = [-0.0277 -0.0566 0.0470];
Muscle.A(i) = 27.95;
Muscle.Fmax(i) = 382;
Muscle.TendonLength(i) = 0.1250;
Muscle.Spindle(i) = 0.8;
i = i+1;
#Muscle.Name(i) = "gluteus maximus 2";
Muscle.Pelvis(i,:) = [-0.1349 0.0176 0.0563];
Muscle.Femur(i,:) = [-0.0156 -0.1016 0.0419];
Muscle.A(i) = 27.00;
Muscle.Fmax(i) = 546;
Muscle.TendonLength(i) = 0.1270;
Muscle.Spindle(i) = 0.8;
i = i+1;
#Muscle.Name(i) = "gluteus maximus 3";
Muscle.Pelvis(i,:) = [-0.1556 -0.0314 0.0058];
Muscle.Femur(i,:) = [-0.0060 -0.1419 0.0411];
Muscle.A(i) = 27.5;
Muscle.Fmax(i) = 368;
Muscle.TendonLength(i) = 0.1450;
Muscle.Spindle(i) = 0.8;
i = i+1;
#Muscle.Name(i) = "gluteus medius 1";
Muscle.Pelvis(i,:) = [-0.0408 0.0304 0.1209];
Muscle.Femur(i,:) = [-0.0218 -0.0117 0.0555];
Muscle.A(i) = 35.51;
Muscle.Fmax(i) = 546;
Muscle.TendonLength(i) = 0.0780;
Muscle.Spindle(i) = 1.0;
i = i+1;
#Muscle.Name(i) = "gluteus medius 2";
Muscle.Pelvis(i,:) = [-0.0855 0.0445 0.0766];
Muscle.Femur(i,:) = [-0.0258 -0.0058 0.0527];
Muscle.A(i) = 22.48;
```

```
Muscle.Fmax(i) = 382;
Muscle.TendonLength(i) = 0.0530;
Muscle.Spindle(i) = 1.0;
i = i+1;
#Muscle.Name(i) = "gluteus medius 3";
Muscle.Pelvis(i,:) = [-0.1223 0.0105 0.0648];
Muscle.Femur(i,:) = [-0.0309 -0.0047 0.0518];
Muscle.A(i) = 29.41;
Muscle.Fmax(i) = 435;
Muscle.TendonLength(i) = 0.0530;
Muscle.Spindle(i) = 1.0;
i = i+1;
#Muscle.Name(i) = "gluteus minimus 1";
Muscle.Pelvis(i,:) = [-0.0467 -0.0080 0.1056];
Muscle.Femur(i,:) = [-0.0072 -0.0104 0.0560];
Muscle.A(i) = 10.2;
Muscle.Fmax(i) = 180;
Muscle.TendonLength(i) = 0.0160;
Muscle.Spindle(i) = 2.2;
i = i+1;
#Muscle.Name(i) = "gluteus minimus 2";
Muscle.Pelvis(i,:) = [-0.0633 -0.0065 0.0991];
Muscle.Femur(i,:) = [-0.0096 -0.0104 0.0560];
Muscle.A(i) = 12.5;
Muscle.Fmax(i) = 190;
Muscle.TendonLength(i) = 0.0260;
Muscle.Spindle(i) = 2.2;
i = i+1;
#Muscle.Name(i) = "gluteus minimus 3";
Muscle.Pelvis(i,:) = [-0.0834 -0.0063 0.0856];
Muscle.Femur(i,:) = [-0.0135 -0.0083 0.0555];
Muscle.A(i) = 18.42;
Muscle.Fmax(i) = 215;
Muscle.TendonLength(i) = 0.0510;
Muscle.Spindle(i) = 2.2;
i = i+1;
#Muscle.Name(i) = "iliacus";
Muscle.Pelvis(i,:) = [-0.0674 0.0365 0.0854];
Muscle.Femur(i,:) = [-0.0193 -0.0621 0.0129];
Muscle.A(i) = 31.9;
Muscle.Fmax(i) = 429;
Muscle.TendonLength(i) = 0.0900;
Muscle.Spindle(i) = 1.8;
i = i+1;
#Muscle.Name(i) = "pectineus";
Muscle.Pelvis(i,:) = [-0.0431 -0.0768 0.0451];
Muscle.Femur(i,:) = [-0.0122 -0.0822 0.0253];
Muscle.A(i) = 5.86;
Muscle.Fmax(i) = 177;
```

```
Muscle.TendonLength(i) = 0.0010;
Muscle.Spindle(i) = 1.3;
i = i+1;
#Muscle.Name(i) = "piriformis";
Muscle.Pelvis(i,:) = [-0.1396 0.0003 0.0235];
Muscle.Femur(i,:) = [-0.0148 -0.0036 0.0437];
Muscle.A(i) = 35;
Muscle.Fmax(i) = 296;
Muscle.TendonLength(i) = 0.1150;
Muscle.Spindle(i) = 3.5;
i = i+1;
#Muscle.Name(i) = "psoas";
Muscle.Pelvis(i,:) = [-0.0647 0.0887 0.0289];
Muscle.Femur(i,:) = [-0.0188 -0.0597 0.0104];
Muscle.A(i) = 29.90;
Muscle.Fmax(i) = 371;
Muscle.TendonLength(i) = 0.1300;
Muscle.Spindle(i) = 1.8;
i = i+1;
#Muscle.Name(i) = "quadratus femoris";
Muscle.Pelvis(i,:) = [-0.1143 -0.1151 0.0520];
Muscle.Femur(i,:) = [-0.0381 -0.0359 0.0366];
Muscle.A(i) = 20.92;
Muscle.Fmax(i) = 254;
Muscle.TendonLength(i) = 0.0240;
Muscle.Spindle(i) = 1.9;
i = i+1;
#Muscle.Name(i) = "biceps femoris long";
Muscle.Pelvis(i,:) = [-0.1244 -0.1001 0.0666];
Muscle.Femur(i,:) = [-0.0081 -0.0729 0.0423];
Muscle.A(i) = 25.41;
Muscle.Fmax(i) = 717;
Muscle.TendonLength(i) = 0.3410;
Muscle.Spindle(i) = 0.8;
i = i+1;
#Muscle.Name(i) = "gracilis";
Muscle.Pelvis(i,:) = [-0.0563 -0.1038 0.0079];
Muscle.Femur(i,:) = [0.0060 -0.0836 -0.0228];
Muscle.A(i) = 3.07;
Muscle.Fmax(i) = 108;
Muscle.TendonLength(i) = 0.1400;
Muscle.Spindle(i) = 1.5;
i = i+1;
#Muscle.Name(i) = "sartorius";
Muscle.Pelvis(i,:) = [-0.0153 -0.0013 0.1242];
Muscle.Femur(i,:) = [0.0243 -0.0840 -0.0252];
Muscle.A(i) = 6.36;
Muscle.Fmax(i) = 104;
Muscle.TendonLength(i) = 0.0400;
```

```
Muscle.Spindle(i) = 1.2;
i = i+1;
#Muscle.Name(i) = "semimebranosus";
Muscle.Pelvis(i,:) = [-0.1192 -0.1015 0.0695];
Muscle.Femur(i,:) = [-0.0243 -0.0536 -0.0194];
Muscle.A(i) = 52.75;
Muscle.Fmax(i) = 1030;
Muscle.TendonLength(i) = 0.03590;
Muscle.Spindle(i) = 0.6;
i = i+1;
#Muscle.Name(i) = "semitendinosus";
Muscle.Pelvis(i,:) = [-0.1237 -0.1043 0.0603];
Muscle.Femur(i,:) = [0.0027 -0.0956 -0.0193];
Muscle.A(i) = 12.7;
Muscle.Fmax(i) = 328;
Muscle.TendonLength(i) = 0.2620;
Muscle.Spindle(i) = 1.5;
i = i+1;
#Muscle.Name(i) = "tensor fascie latae";
Muscle.Pelvis(i,:) = [-0.0311 0.0214 0.1241];
Muscle.Femur(i,:) = [0.0060 -0.0487 0.0297];
Muscle.A(i) = 10.63;
Muscle.Fmax(i) = 155;
Muscle.TendonLength(i) = 0.4250;
Muscle.Spindle(i) = 1;
i = i+1;
#Muscle.Name(i) = "rectus femoris";
Muscle.Pelvis(i,:) = [-0.0295 -0.0311 0.0968];
Muscle.Femur(i,:) = [0.0121 0.0437 -0.0010]; #patella
Muscle.A(i) = 35.14;
Muscle.Fmax(i) = 779;
Muscle.TendonLength(i) = 0.3460;
Muscle.Spindle(i) = 0.9;

Muscle.Pelvis = 100 * [-Muscle.Pelvis(:,2),-Muscle.Pelvis(:,1),-Muscle.Pelvis(:,3)];
Muscle.Femur = 100 * [-Muscle.Femur(:,2),-Muscle.Femur(:,1),-Muscle.Femur(:,3)];
Pref = [-7.8, -4.5, -5.6];
Preal = [-2.14  3.11  -12.41];
Tref = [43.6, -2.2, -3.3];
Treal = [4.87  -0.60   -2.97];
Patref =[41.5, -4.3, -0.2];
Patreal = [-4.37  -1.21   0.10];
#Fref = [0.1, 0.1, -5.5];
#Freal = [ ]
PCorrection = Preal - Pref;
TCorrection = Treal - Tref;
PatCorrection = Patreal - Patref;
for i=1:rows(Muscle.Pelvis)
  Muscle.Pelvis(i,:) = Muscle.Pelvis(i,:) - PCorrection;
```

```
endfor
for i=21:(rows(Muscle.Pelvis)-1)
  Muscle.Femur(i,:) = Muscle.Femur(i,:) - TCorrection;
endfor
Muscle.Femur(rows(Muscle.Pelvis),:) = Muscle.Femur(rows(Muscle.Pelvis),:) - PatCorrection;
x0 = 42.3;
theta = asin(b/x0);
ni = -0.5 * pi / 180;
for i=1:rows(Muscle.Femur)
  Muscle.Femur(i,:) = Muscle.Femur(i,:) .* NormTroch;
  Muscle.Femur(i,:) = RotateY(Muscle.Femur(i,:), -theta);
  Muscle.Pelvis(i,:) = Muscle.Pelvis(i,:) .* NormPelv;
  Muscle.Pelvis(i,:) =  RotateY(Muscle.Pelvis(i,:), ni);
endfor
```

Appendix B

VISUALISATION OF THE HIP

Computer system for visualisation of the musculoskeletal system was developed within this work and its application was shown in the case of the hip joint (section 4.1.1). It is not possible to provide the statement of the program and the polygonal models of the skeletal structures since they contain more than 22500 lines of code. Using a high-level scripting language for OpenDX, the animation of the musculoskeletal sctructures of the hip was created. This animation can be found on attached CDROM (section L). Here we provide some figures showing the capabilities of the visualisation program.

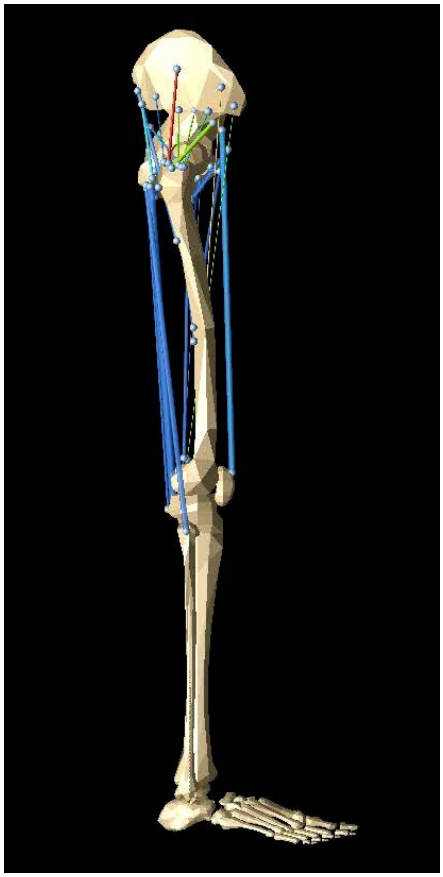

Figure B.1: View of the lower limb with the muscles of the hip showed. Colours of the muscular units corresponds to the force in the muscle.

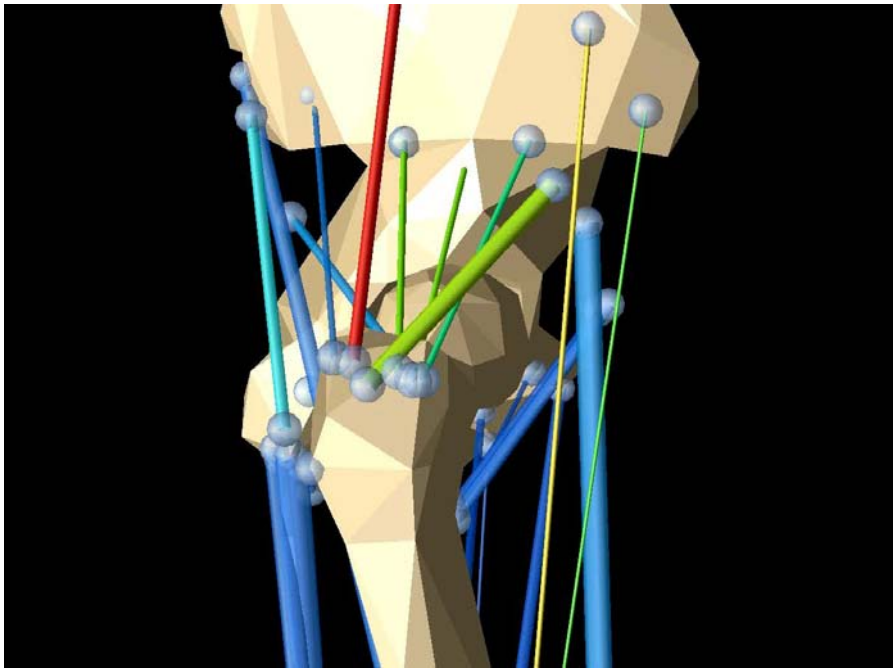

Figure B.2: Detailed view of the muscular and skeletal structures of the hip.

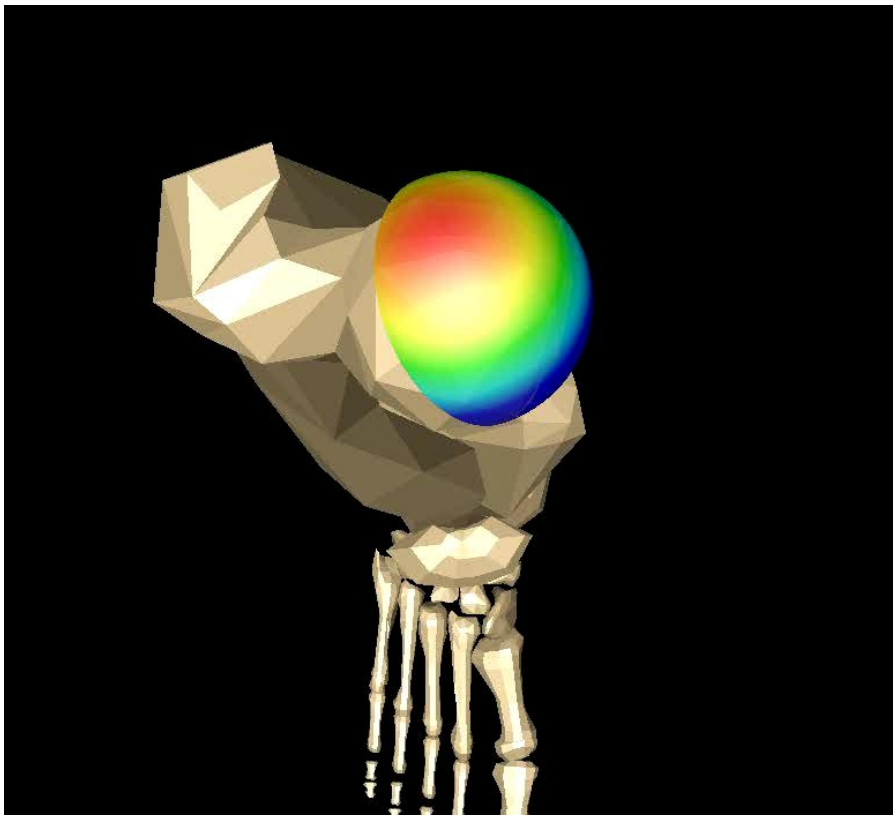

Figure B.3: Parallel visualisation of the lower leg and contact stress distribution acting on the acetabular cartilage.

Appendix C

HIP JOINT REACTION FORCE IN ONE-LEGGED STANCE – LINEAR OPTIMISATION

The following text contains m-scripts for GNU Octave after which the hip joint reaction force in one-legg standing using linear optimisation can be estimated. Main function `Head` can be called with a string parameter `'new'` or `'old'` to compute the load of the hip using the model with nine or twenty-seven muscles, respectively. Theoretical background of the linear optimisation is described in the section 4.2.3.1.

Software requirements	:	GNU Octave, version 2.1.50 with installed function `lin_prog.m`
List of files	:	`Head.m` - main function `equieq.m` - definition of the equilibrium equations `constraints.m` - definitions of the matrix of physiological constraints `eqiueqinmatrix.m` - implementation of the equilibrium equations in the matrix of constraints `costfunction.m` - definition of the weight coefficients in the optimisation function `output.m` - output of the results
Required files	:	`musclemodelold.m` - definition of the muscle model (see section A)
	:	`musclemodelnew.m` - definition of the muscle model (see section A) `VekSize.m` - size of the vector `lin_prog.m` - linear program solver

Head.m

```
function MuscleF = Head(string)

global Muscle
global B
global V
global CountMuscle
global A
global b
global c
global U
```

```
global AT
global bT
global cT
global Wb
global Wl
global ForceM

if (string == "old")
  musclemodelold;
else
  musclemodelnew;
endif

CountMuscle = rows(Muscle.A);
equieq;
constraints;
costfunction;
eqiueqinmatrix;
[x,z,info] = lin_prog(AT,bT,cT);
info
tmp = [-U(1,4:CountMuscle) * x - U(1,(CountMuscle+1))
                -U(2,4:CountMuscle) * x - U(2,(CountMuscle+1))
                -U(3,4:CountMuscle) * x - U(3,(CountMuscle+1))
                x];
Muscle.Force = [];
for i=1:CountMuscle
  Muscle.Force(i,:) =  tmp(i) * Muscle.Direction(i,:);
endfor
output;
MuscleF = ForceM;
S;
endfunction
```

equieq.m

```
1;
global Muscle
global B
global V
global Wb
global Wl

Norm = VekSize(Muscle.Femur - Muscle.Pelvis);
Muscle.Direction = (Muscle.Femur - Muscle.Pelvis) ./ ([Norm, Norm, Norm]);

Wb = [Wb, 0, 0];
Wl = [Wl, 0, 0];
V = zeros(CountMuscle,3);
for i=1:CountMuscle
```

```
  V(i,:) = cross(Muscle.Pelvis(i,:), Muscle.Direction(i,:));
endfor
B = cross(a,(Wb-Wl));
```

constraints.m

```
1;
global Muscle
global A
global b
global CountMuscle

A = zeros(2*CountMuscle, CountMuscle);
b = zeros(2*CountMuscle, 1);

for i=1:CountMuscle
  A(i,i) = 1;
  b(i) = 0;
endfor

for i=(CountMuscle+1):(2*CountMuscle)
  A(i,i-CountMuscle) = -1;
  b(i) = 100*Muscle.A(i-CountMuscle);
endfor
```

eqiueqinmatrix.m

```
1;
global Muscle
global A
global b
global CountMuscle
global c
global V
global AT
global bT
global cT
global U
V((CountMuscle+1),:) = B;
A(:,(CountMuscle+1)) = b;
T = zeros(2,(CountMuscle+1));
U = zeros(size(V'));
     T(1,:) = V'(2,:) - V'(1,:) * (V'(2,1)/V'(1,1));
     T(2,:) = V'(3,:) - V'(1,:) * (V'(3,1)/V'(1,1));
     U(3,:) = T(2,:) - T(1,:) * (T(2,2)/T(1,2));
     U(2,:) = T(1,:) - U(3,:) * (T(1,3)/U(3,3));
     U(1,:) = V'(1,:) - U(3,:) * (V'(1,3)/U(3,3)) - U(2,:) * (V'(1,2)/U(2,2));
     U(1,:) = U(1,:)/U(1,1);
     U(2,:) = U(2,:)/U(2,2);
```

```
     U(3,:) = U(3,:)/U(3,3);
for i = 1 : (2*CountMuscle)
   A(i,:) = A(i,:) - U(1,:) * (A(i,1)/U(1,1)) - U(2,:) * (A(i,2)/U(2,2)) \
       - U(3,:) * (A(i,3)/U(3,3));
endfor
for i = 1 : 3
   c = c - U(i,1:CountMuscle) * (c(i)/U(i,i));
endfor
AT = A(:,4:CountMuscle);
bT = A(:,(CountMuscle+1));
cT = c(4:CountMuscle);
```

costfunction.m

Optimisation criterion G_F.

```
1;
global Muscle
global A
global b
global CountMuscle
global c
c = ones(1,CountMuscle);
```

output.m

```
1;
global Muscle
global CountMuscle
global Wb
global Wl
global ForceM
R = sum(Muscle.Force) + (Wb-Wl);
Muscle.Sigma = VekSize(Muscle.Force)./Muscle.A;
ForceM = VekSize(Muscle.Force);
info = V(1:CountMuscle,:)' * ForceM
for i=1:rows(Muscle.Femur)
    force = ForceM(i);
    name = Muscle.Name(i,:);
    printf ("Force in %s is %d N \n", name, force);
endfor
```

Appendix D

HIP JOINT REACTION FORCE IN ONE-LEGGED STANCE – NONLINEAR OPTIMISATION

The following text contains m-scripts for GNU Octave after which the hip joint reaction force in one-legg standing using nonlinear optimisation can be estimated. Main function `Head` can be called with a string parameter `'new'` or `'old'` to compute the load of the hip using the model with nine or twenty-seven muscles, respectively. Theoretical background of the nonlinear optimisation is described in the section 4.2.3.2.

Software requirements	:	GNU Octave, version 2.1.50 with installed `SOLNP`
List of files	:	`Head.m` - main function
		`equieq.m` - definition of the equilibrium equations, listed in section C
		`constraints.m` - definitions of the matrix of physiological constraints, listed in section C
		`cost.m` - definition of the weight constraints for optimisation
		`output.m` - output of the results, listed in section C
Required files	:	`musclemodelold.m` - definition of the muscle model (see section A)
	:	`musclemodelnew.m` - definition of the muscle model (see section A)
		`VekSize.m` - size of the vector
		`solnp.m` - nonlinear program solver

Head.m

```
function MuscleF = Head(string)

global Muscle
global B
global V
global CountMuscle
global A
global b
global c
global U
global AT
global bT
```

```
global cT
global Wb
global Wl
global ForceM

if (string == "old")
  musclemodelold;
else
  musclemodelnew;
endif
CountMuscle = rows(Muscle.A);
equieq;
constraints;
eqiueqinmatrix;
xb = [A(1:rows(Muscle.A),(CountMuscle+1)), \
      A((rows(Muscle.A)+1):(2*rows(Muscle.A)),(CountMuscle+1))];
x0 = ones(rows(Muscle.A),1);
[x, oh,y] = solnp([x0 xb]);
tmp = x;
Muscle.Force = [];
for i=1:CountMuscle
  Muscle.Force(i,:) =  tmp(i) * Muscle.Direction(i,:);
endfor
output;
MuscleF = ForceM;
endfunction
```

cost.m

Optimisation criterion G_{σ^3}

```
function [f]=cost(x,par)
  global V
  global A
  global CountMuscle
  global Muscle
  tmp = [];
  f(1) = sum((x./Muscle.A).^3);
  EquiEq = x' * V(1:CountMuscle,:);
  f(2) = EquiEq(1) + V(CountMuscle+1,1);
  f(3) = EquiEq(2) + V(CountMuscle+1,2);
  f(4) = EquiEq(3) + V(CountMuscle+1,3);
endfunction
```

Appendix E

VISUALISATION OF THE HIP JOINT REACTION FORCE

Using the scientific visualisation system OpenDX, we have created the visualisation of the hip joint reaction force computed using various optimisation criteria. The femur was visualised as polygonal structure while for visualisation of the forces internal structure of the program OpenDX for the vector visualisation was used.

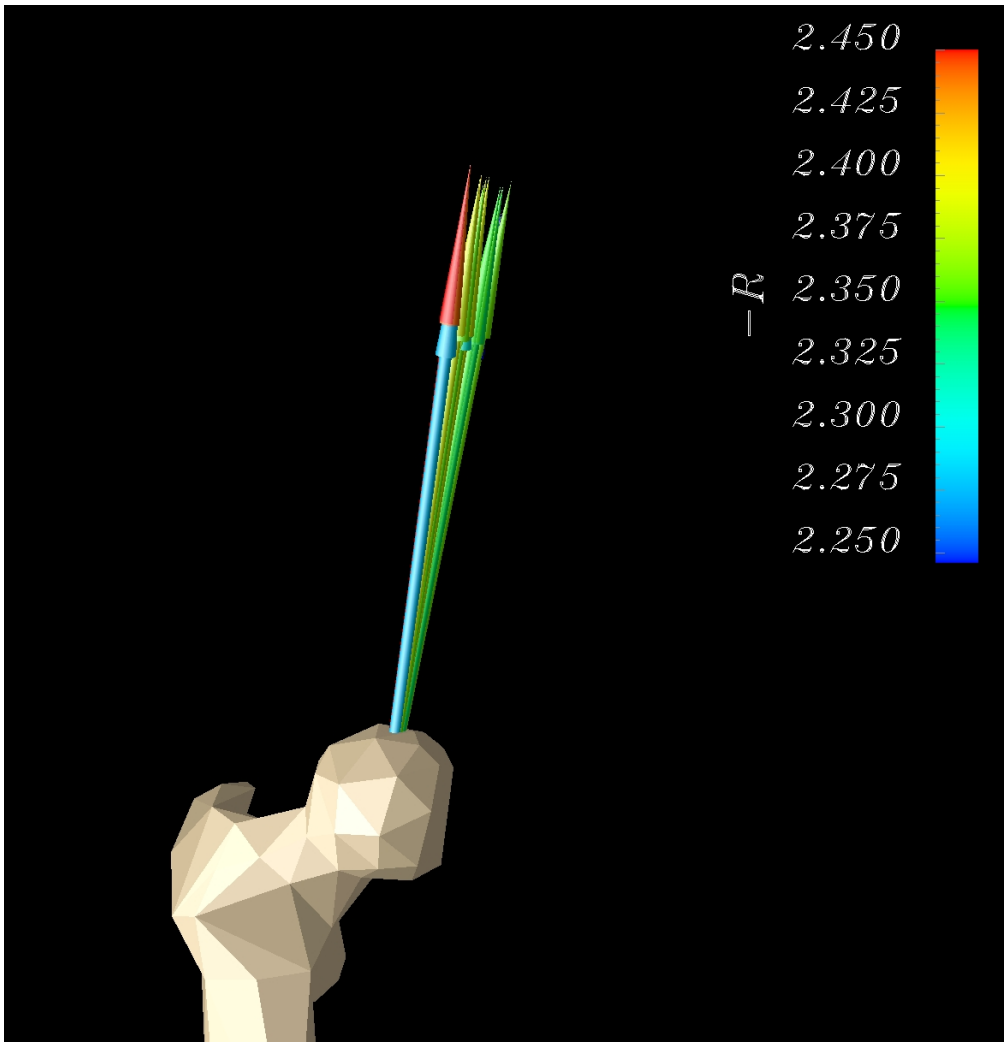

Figure E.1: Hip joint reaction force computed using various optimisation criteria.

Appendix F

CONTACT STRESS DISTRIBUTION IN THE HUMAN HIP – MATHEMATICAL MODEL

The following text contains m-scripts for GNU Octave after which the contact stress distribution in the hip can be assessed. The input parameters are the hip joint reaction force in the pelvic coordinate system (**R**), radius of the femoral head (r), position of the acetabular cup with respect to the pelvis (β and γ) (Fig. 4.11). The result is the position of the pole of the stress in the acetabular coordinates (Θ_a and Φ_a), value of the stress at the stress pole p_0, and value of the peak contact stress p_{max}.

Software requirements	:	GNU Octave, version 2.1.50
List of files	:	`Head.m` - main script file
		`CupSystem.m` - transformation of vector **R** from pelvic coordinates to acetabular coordinates
		`HIPSTRESS.m` - calculation of the stress distribution
Required files	:	`RotateX.m` - rotation of vector around the x-axis (see section K)
		`RotateY.m` - rotation of vector around the y-axis (see section K)
		`RotateZ.m` - rotation of vector around the z-axis (see section K)

Head.m

```
1;
global InitVal
r = 2.7;
InitVal = [];
RCup = zeros(rows(RPel),3);
for i=1:rows(RPel)
 RCup(i,:) = CupSystem(RPel(i,:));
endfor
RCupTrans = [-RCup(:,3), RCup(:,1),-RCup(:,2)];
Results = zeros(rows(RCupTrans),4);
for i=1:rows(RCupTrans)
 Results(i,:) = HIPSTRESS(RCupTrans(i,:), r);
endfor
```

CupSystem.m

```
function FCup = CupSystem (FPel)
Gamma = 70.3 * pi / 180;
Beta = 49.4 * pi / 180;
MatRotX =  [ 1, 0,         0
             0, cos(Beta), -sin(Beta)
             0, sin(Beta), cos(Beta)];
MatRotY =  [cos(0),  0, sin(0)
            0,       1, 0
            -sin(0), 0  cos(0)];
MatRotZ =  [cos(-Gamma), -sin(-Gamma), 0
            sin(-Gamma), cos(-Gamma),  0
            0,           0,            1];
MatRot = MatRotX * MatRotY * MatRotZ;
FCup = FPel * MatRot';
endfunction
```

HIPSTRESS.m

```
function [Result] = HIPSTRESS (R,r)
global ThetaR
global InitVal
r = r / 100;                 # [m]
ThetaR = atan(sqrt(R(1)^2+R(2)^2)/R(3));
InitVal = 50 * pi/180; #ThetaR;
  function [T] = NecroEq2(P)
    global ThetaR
    Rx = sin(ThetaR);
    Rz = cos(ThetaR);
    Rx0 = (sin(P))^2; # from the weight-bearing area
    Ry0 = 0;
    Rz0 = pi - P + (cos(P) * sin (P));
    T = abs(Rx0/Rz0 - Rx/Rz);
  endfunction

[Pole,info] = fsolve("NecroEq2",InitVal);
Rs = sqrt(R(1)^2 + R(2)^2 + R(3)^2)/100;
p0 = (3 * Rs * cos(Pole+ThetaR))/(2*r^2*(pi-Pole+sin(Pole)*cos(Pole)));
Theta = Pole * 180 / pi;
if (Theta>(pi/2))
  pmax = p0 * cos(Pole-(pi/2));
else
  pmax = p0;
endif
Result = [Rs , ThetaR*180/pi, pmax, Theta];
endfunction
```

Appendix G

VISUALISATION OF THE STRESS DISTRIBUTION IN THE HIP DURING VARIOUS ACTIVITIES

In this work we have evaluated the stress distribution in normal and dysplastic hips during routine activities (section 5.1.2). In this section we provide samples of the visualisation of the hip contact stress distribution during routine activities. Complete animations can be found on attached CDROM (section L). The visualisations were produced by the following programs: ImageMagic, GNU Gnuplot and ppmtompeg.

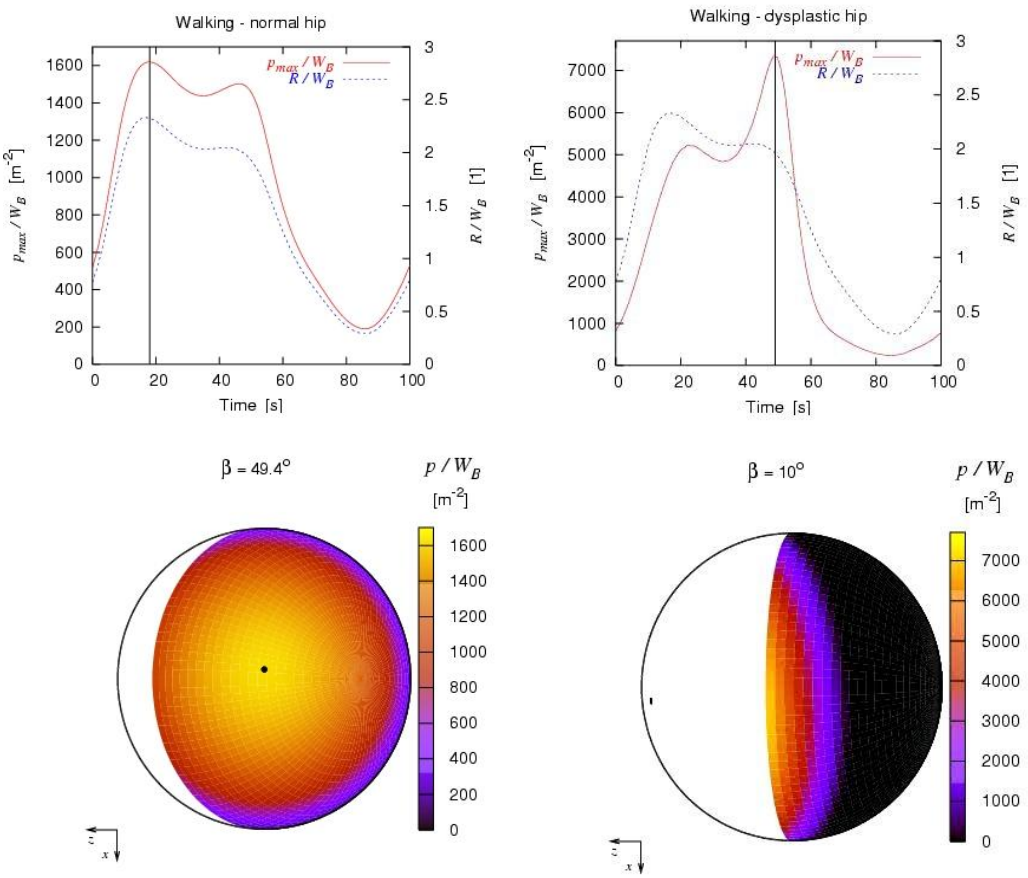

Figure G.1: The time dependencies of the normalized hip joint reaction force R/W_B and normalised peak contact stress p_{max}/W_B in normal and dysplastic hips during normal walking. The top view of the stress distribution in denoted point of the activity is shown.

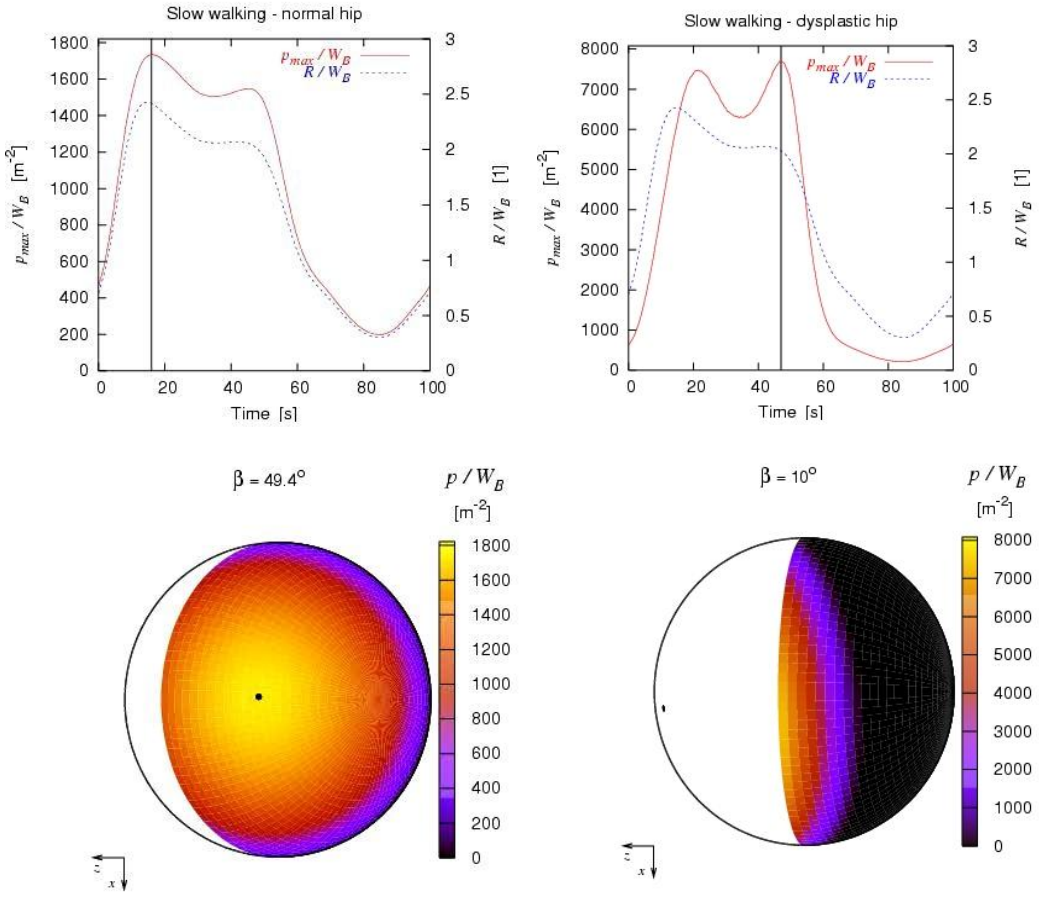

Figure G.2: The time dependendies of the normalized hip joint reaction force R/W_B and normalised peak contact stress p_{max}/W_B in normal and dysplastic hips during slow walking. The top view of the stress distribution in denoted point of the walking cycle is shown.

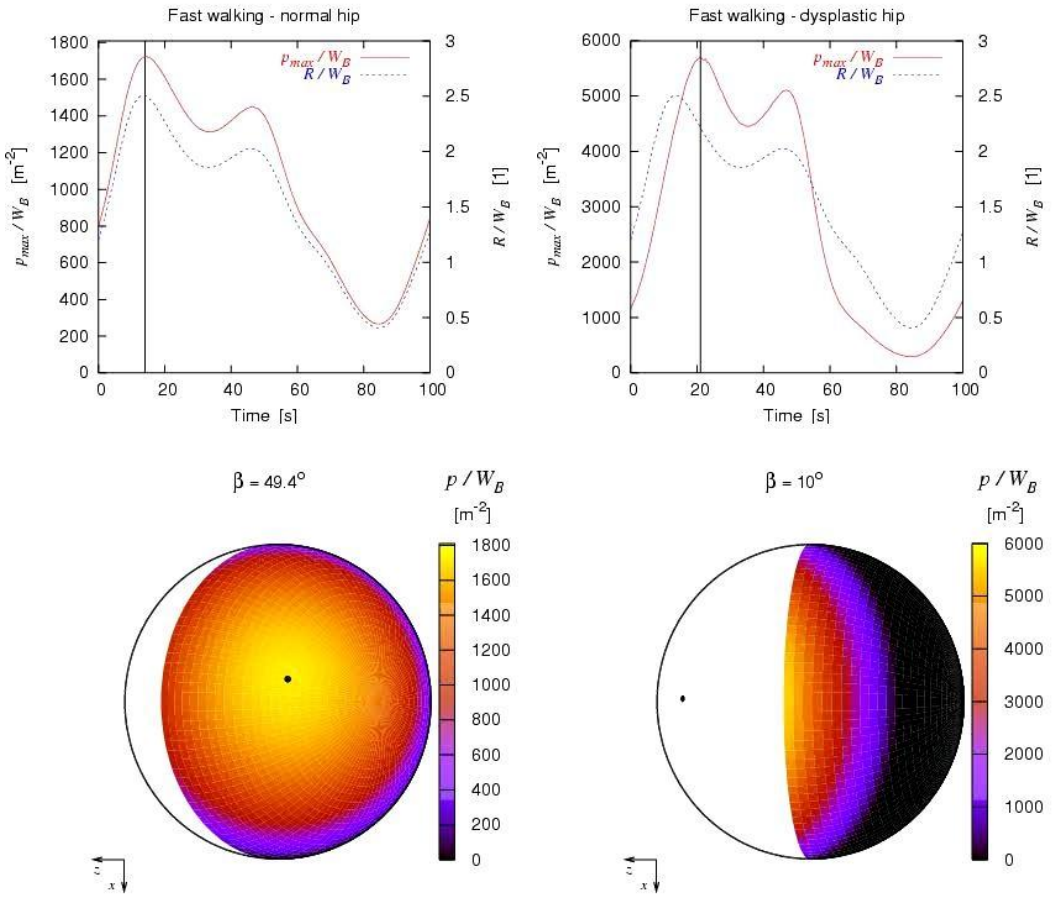

Figure G.3: The time dependendies of the normalized hip joint reaction force R/W_B and normalised peak contact stress p_{max}/W_B in normal and dysplastic hips during fast walking. The top view of the stress distribution in denoted point of the walking cycle is shown.

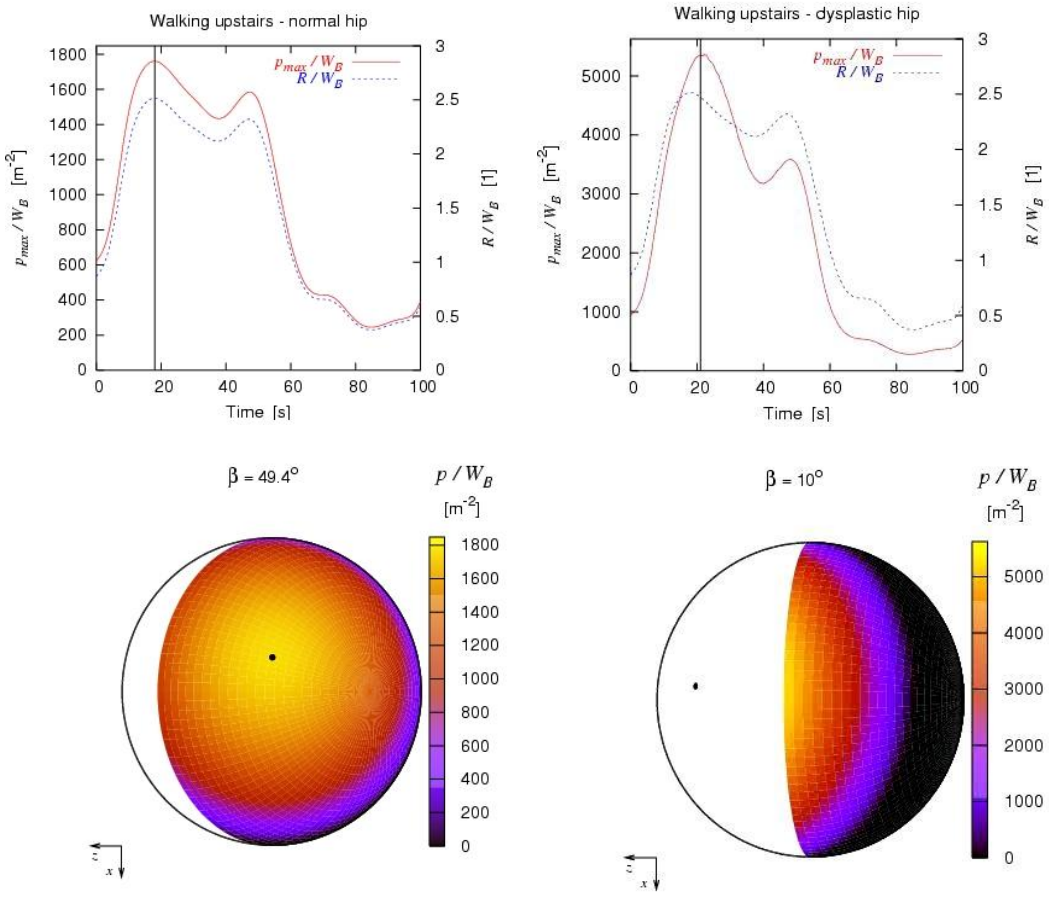

Figure G.4: The time dependencies of the normalized hip joint reaction force R/W_B and normalised peak contact stress p_{max}/W_B in normal and dysplastic hips during walking upstairs. The top view of the stress distribution in denoted point of the walking cycle is shown.

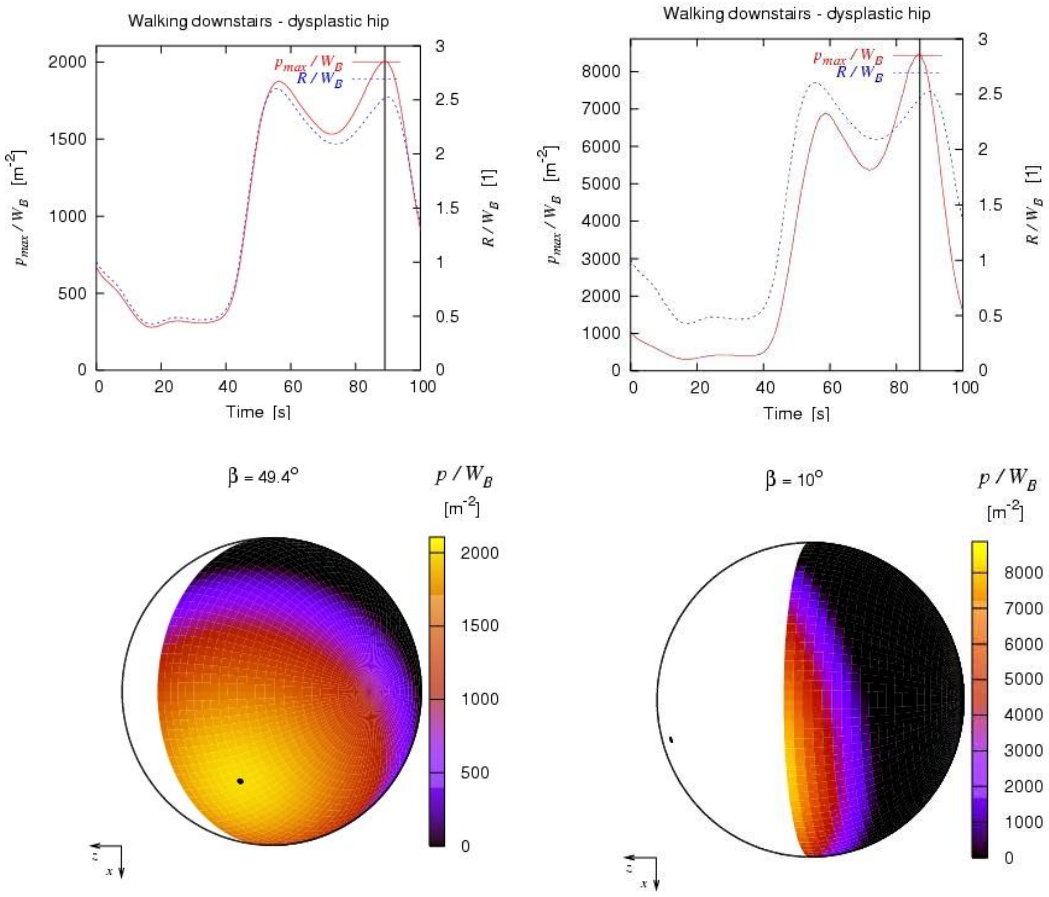

Figure G.5: The time dependencies of the normalized hip joint reaction force R/W_B and normalised peak contact stress p_{max}/W_B in normal and dysplastic hips during walking downstairs. The top view of the stress distribution in denoted point of the walking cycle is shown.

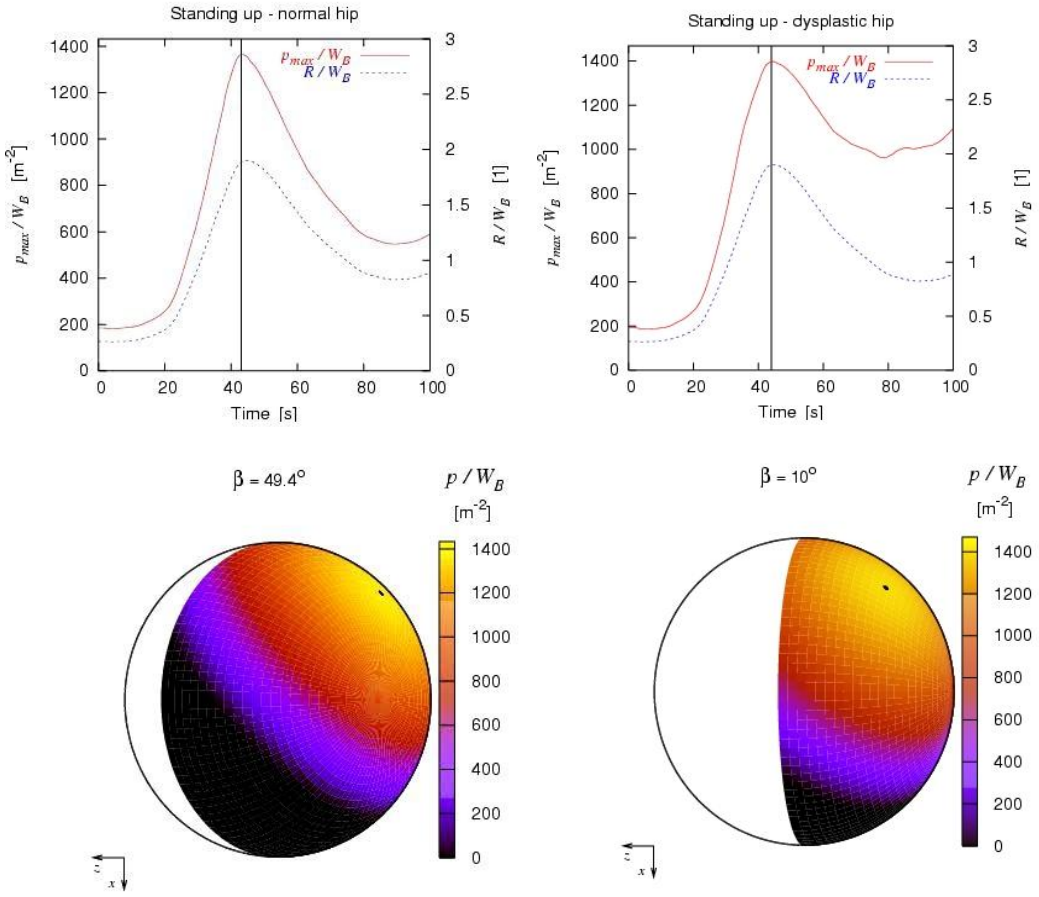

Figure G.6: The time dependencies of the normalized hip joint reaction force R/W_B and normalised peak contact stress p_{max}/W_B in normal and dysplastic hips during standing from a chair. The top view of the stress distribution in denoted point of the activity is shown.

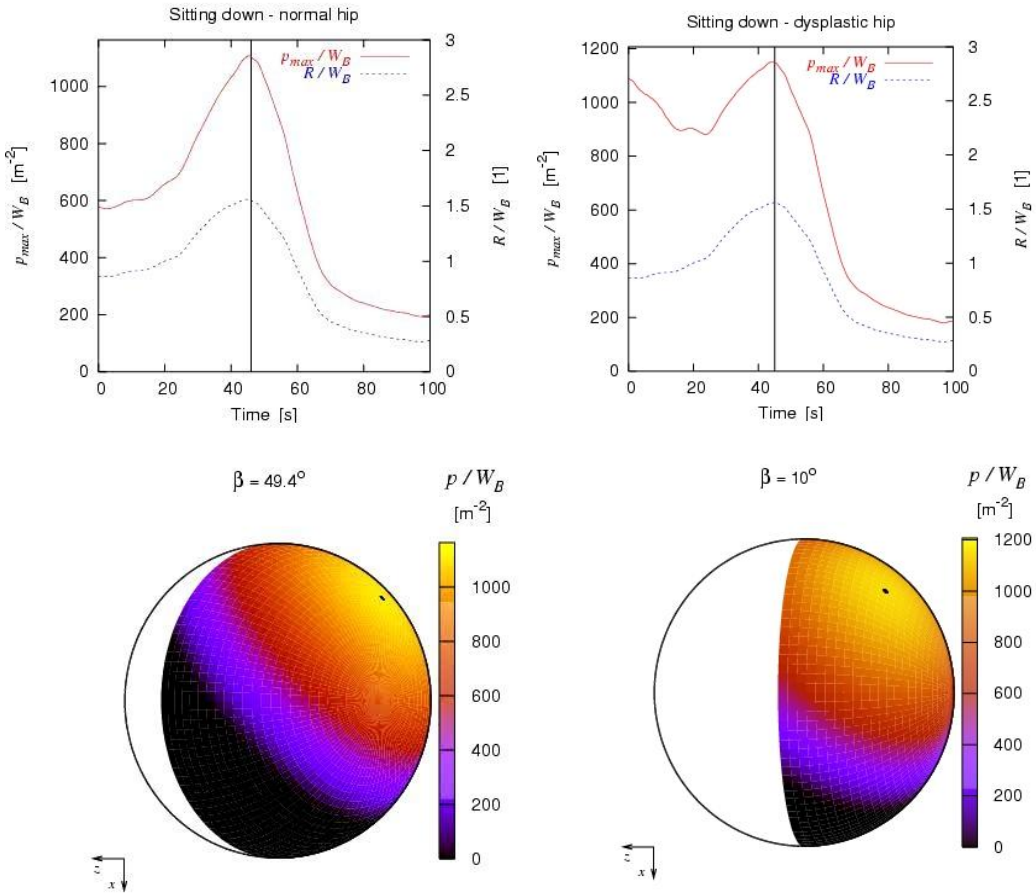

Figure G.7: The time dependencies of the normalized hip joint reaction force R/W_B and normalised peak contact stress p_{max}/W_B in normal and dysplastic hips during sitting down. The top view of the stress distribution in denoted point of the activity is shown.

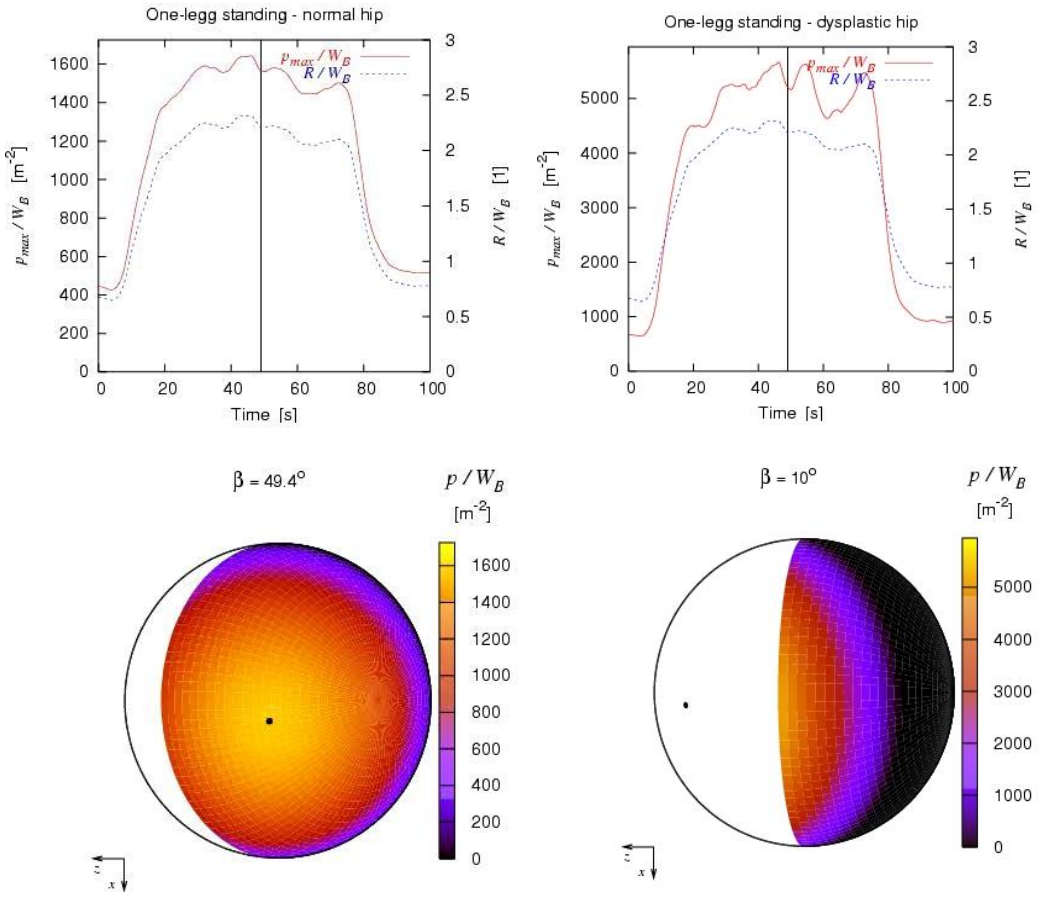

Figure G.8: The time dependendies of the normalized hip joint reaction force R/W_B and normalised peak contact stress p_{max}/W_B in normal and dysplastic hips during two-legg standing, one-legg standing and two-legg standing. The top view of the stress distribution in denoted point of the activity is shown.

Appendix H

CONTACT STRESS DISTRIBUTION IN THE HUMAN HIP SUBJECTED TO ASEPTIC NECROSIS OF THE FEMORAL HEAD – MATHEMATICAL MODEL

The following text contains m-scripts for GNU Octave after which the contact stress distribution in the hip subjected to avascular necrosis of the femoral head can be assessed. The input parameters are the hip joint reaction force in the pelvic coordinate system (**R**), radius of the femoral head (r), centre-edge angle of Wiberg ϑ_{CE}, position of the centre of the necrotic region ϑ_N, φ_N, and size of the necrotic region ϑ_0 (Fig. 4.14). The result is the position of the pole of the stress in the acetabular coordinates (Θ_a and Φ_a), value of the stress at the stress pole p_0, and value of the peak contact stress p_{max}.

Software requirements	:	GNU Octave, version 2.1.50
List of files	:	`Head.m` - input data
		`Necrosis.m` - computation of the position of the stress
		`ContactStress.m` - calculation of the peak contact stress
Required files	:	`RotateY.m` - rotation of vector around the y-axis (see section K)
		`RotateZ.m` - rotation of vector around the z-axis (see section K)
		`Cart2Sph.m` - vector transformation function from the Cartesian coordinate system to the spherical coordinate system (see section K)
		`Sph2Cart.m` - vector transformation function from the spherical coordinate system to the Cartesian coordinate system (see section K)

Head.m

```
1;
global ThetaN
global PhiN
global Theta0
global PoleDeg
global Stress
global ThetaCEa
```

```
global VKruh
global Theta0a

Theta0a = 20;
ThetaCEa = 30;
ThetaNa = [ThetaCEa-Theta0a:-1:-80];
InitVal = [];
for i=1 : length(ThetaNa)
   Theta0 = Theta0a;
   PhiN = 180;
   ThetaN = 90 - ThetaCEa + ThetaNa(i);
   Stress = [];
   PoleDeg = [];
   NecrosisKruh;
   VKruh(i,:) = [ 90 ,  Rad2Grad(ThetaN)-90+ThetaCEa,  \
             Rad2Grad(PhiN), \
            Rad2Grad(Theta0) , Stress(1),  \
             Stress(2) , \
            PoleDeg(1)-90+ThetaCEa ,  PoleDeg(2) ,  Stress(3), \
            info];
   VKruh(i,:);
endfor
```

Necrosis.m

```
1;

global R
global r
global N
global Theta0
global ThetaN
global PhiN
global PoleDeg
global Stress
global ThetaCEa

R  = 2.7;
ThetaR = 90-ThetaCEa-5;
PhiR = 180;
ThetaCE = 90;
r = 2.7;
ThetaN = 0;
PhiN = 180;
Theta0 = 0;
InitVal = [];

ThetaR = Grad2Rad(ThetaR);
PhiR = Grad2Rad(PhiR);
```

```
r = r / 100;
ThetaN = Grad2Rad(ThetaN);
PhiN = Grad2Rad(PhiN);
Theta0 = Grad2Rad(Theta0);

[R] = Sph2Cart([R,ThetaR,PhiR]);
[N] = Sph2Cart([r,ThetaN,PhiN]);

function [T] = NecroEq2(P)

  global R
  global r
  global N
  global Theta0
  global ThetaN
  global PhiN
  Theta = P(1);
  Phi = P(2);
  PolSph = [r,Theta,Phi];
  [Pol] = Sph2Cart(PolSph);
  R_A = [];
  R_Ax = 2/3 * (sin(Theta))^2;
  R_Ay = 0;
  R_Az = 2/3 * (pi - Theta + sin(Theta) \
              * cos (Theta));
  Phi_RA = Phi;
  Theta_RA = Theta - atan(R_Ax/R_Az);
  R_ASize = sqrt(R_Ax^2 + R_Az^2);
  R_ASph = [R_ASize, Theta_RA, Phi_RA];
  [R_A] = Sph2Cart(R_ASph);
  [Nrot] = RotateZ(N,PhiN);
  [Rrot] = RotateZ(R,PhiN);
  [Polrot] = RotateZ(Pol,PhiN);
  [R_Arot] = RotateZ(R_A,PhiN);
  [Nrot] = RotateY(Nrot,-ThetaN);
  [Rrot] = RotateY(Rrot,-ThetaN);
  [Polrot] = RotateY(Polrot,-ThetaN);
  [R_Arot] = RotateY(R_Arot,-ThetaN);
  [PolrotSph] = Cart2Sph(Polrot);
  Thetarot = PolrotSph(2);
  Phirot = PolrotSph(3);
  RxN =  pi * cos(Phirot) * sin(Thetarot) * \
    ((cos(Theta0))^3 / 3 - cos(Theta0) + 2/3);
  RyN =  pi * sin(Phirot) * sin(Thetarot) * \
    ((cos(Theta0))^3 / 3 - cos(Theta0) + 2/3);
  RzN =  2/3 * pi * cos(Thetarot) * (1 - \
        (cos(Theta0))^3);
  RNrot = [RxN, RyN, RzN];
  Rres = R_Arot - RNrot;
```

```
  T(1) =   Rres(1)/Rres(3) - Rrot(1)/Rrot(3);
  T(2) =   Rres(2)/Rres(3) - Rrot(2)/Rrot(3);
  printf(".");
endfunction
if (InitVal == [])
  InitVal = [ThetaR, PhiR];
endif
[Pole,info]= fsolve("NecroEq2",InitVal);
[PoleDeg] = Pole(1:2).*180/pi;
[Stress] = ContactStress(Pole);
Area = 2 * pi * r^2 * (1 - cos(Theta0));
```

ContactStress.m

```
function [Stress] = ContactStress (Pole)

global R
global r
global N
global Theta0
global ThetaN
global PhiN
global PoleDeg

Theta = Pole(1);
Phi = Pole(2);
PolSph = [r,Theta,Phi];
[Pol] = Sph2Cart(PolSph);

R_A = [];
R_Ax = 2/3 * (sin(Theta))^2;
R_Ay = 0;
R_Az = 2/3 * (pi - Theta + sin(Theta) \
             * cos (Theta));

Phi_RA = Phi;
Theta_RA = Theta - atan(R_Ax/R_Az);
R_ASize = sqrt(R_Ax^2 + R_Az^2);
R_ASph = [R_ASize, Theta_RA, Phi_RA];
[R_A] = Sph2Cart(R_ASph);
[Nrot] = RotateZ(N,-PhiN);
[Rrot] = RotateZ(R,-PhiN);
[Polrot] = RotateZ(Pol,-PhiN);
[R_Arot] = RotateZ(R_A,-PhiN);
[Nrot] = RotateY(Nrot,-ThetaN);
[Rrot] = RotateY(Rrot,-ThetaN);
[Polrot] = RotateY(Polrot,-ThetaN);
[R_Arot] = RotateY(R_Arot,-ThetaN);
[PolrotSph] = Cart2Sph(Polrot);
```

```
Thetarot = PolrotSph(2);
Phirot = PolrotSph(3);
RxN =  pi * cos(Phirot) * sin(Thetarot) * \
    ((cos(Theta0))^3 / 3 - cos(Theta0) + 2/3);
RyN =  pi * sin(Phirot) * sin(Thetarot) * \
    ((cos(Theta0))^3 / 3 - cos(Theta0) + 2/3);
RzN =  2/3 * pi * cos(Thetarot) * (1 - \
        (cos(Theta0))^3);
RNrot = [RxN, RyN, RzN];
Rres = R_Arot - RNrot;

if (ThetaN + Theta0) > pi/2
  warning ("Necrosis is out of the weight-bearing area \
      at the lateral border");
  Rrot = [0,0,0];
  PoleDeg = [-50,0];
elseif (Theta0 + Thetarot) > pi/2
  warning ("Necrosis is out of the weight-bearing area \
      at the medial border");
  Rrot = [0,0,0];
  PoleDeg = [-50,0];
endif
p_0 = Rrot(3) / (r^2 * (Rres(3)));
if (Theta > pi/2)
  gamma = Theta - pi/2;
  info = 2;
elseif (Thetarot < Theta0)
  gamma = Theta0 - Thetarot;
  info = 3;
else
  gamma = 0;
  info = 1;
endif
p_max = p_0 * cos(gamma);
Stress = [p_max, p_0, info];
endfunction
```

Appendix I

VISUALISATION OF THE STRESS DISTRIBUTION IN THE HIP SUBJECTED TO AVASCULAR NECROSIS OF THE FEMORAL HEAD

We have developed a mathematical model to study the stress distribution in hips subjected to aseptic necrosis of the femoral head (section 5.1.3). In this section we provide samples of the visualisation of the influence of the position and size of the necrotic region on the contact stress distribution in the hip. Complete animations can be found on attached CDROM (section L). The visualisations were produced by the programs ImageMagic and GNU Gnuplot.

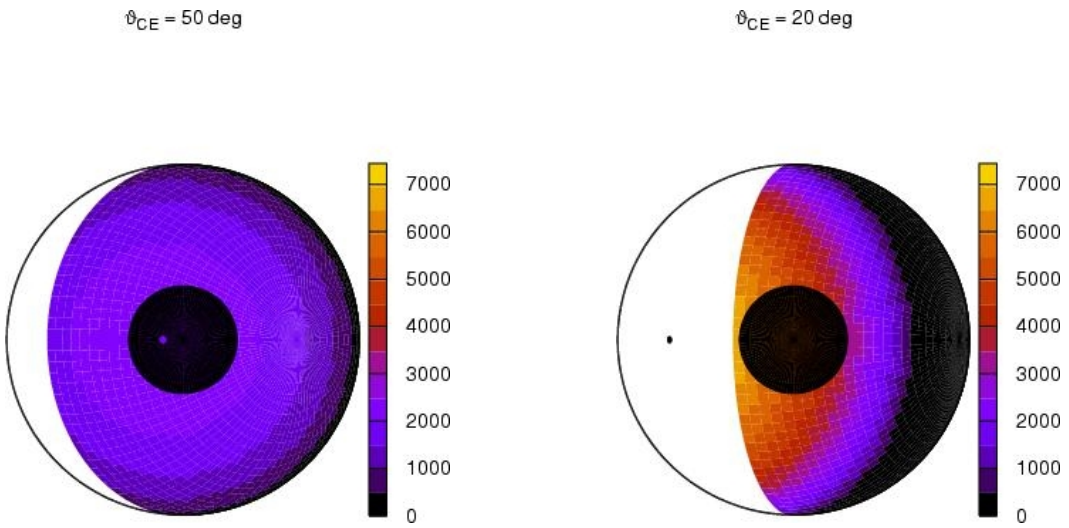

Figure I.1: Top view of the contact stress distribution in hips subjected to aseptic necrosis of the femoral head with different lateral coverage of the femoral head (ϑ_{CE}). Colorbar shows the values of p/W_B in m^{-2}.

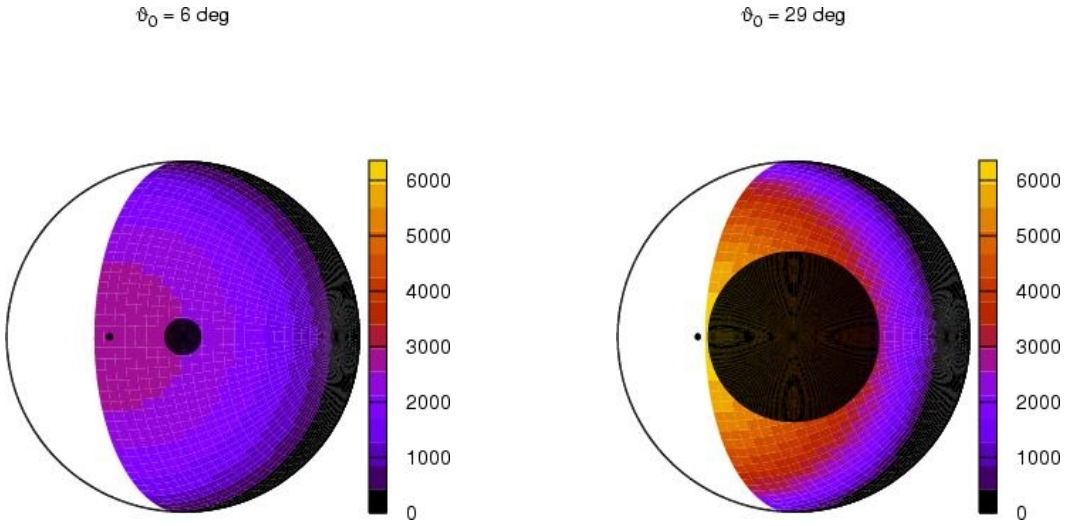

Figure I.2: Top view of the contact stress distribution in hip subjected to aseptic necrosis of the femoral head with different size of the necrosis (ϑ_0). Colorbar shows the values of p/W_B in m^{-2}.

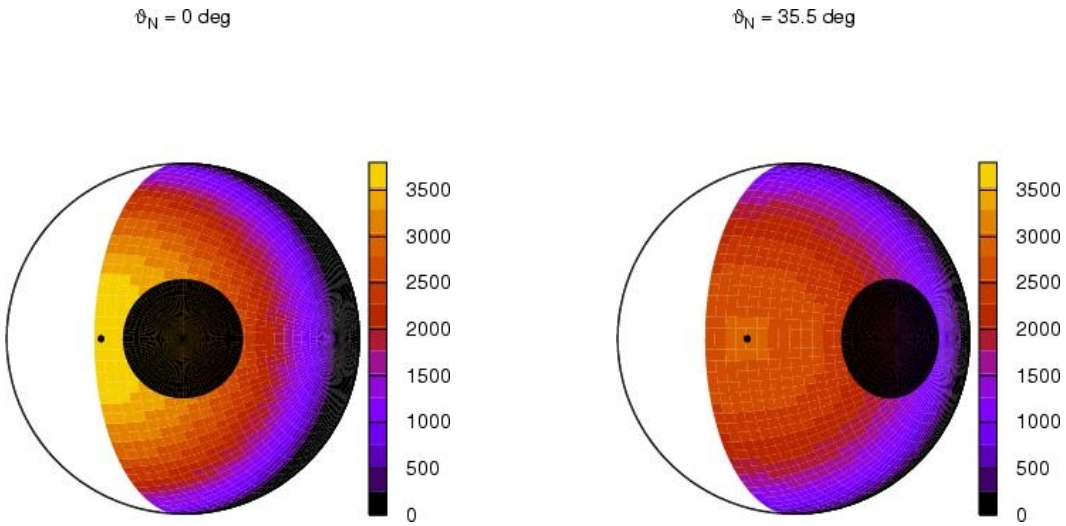

Figure I.3: Top view of the contact stress distribution in hip subjected to aseptic necrosis of the femoral head with different position of the necrosis in the frontal plane (ϑ_N). Colorbar shows the values of p/W_B in m^{-2}.

Appendix J

NOMOGRAMS FOR DETERMINATION THE CONTACT STRESS DISTRIBUTION IN THE HUMAN HIP JOINT

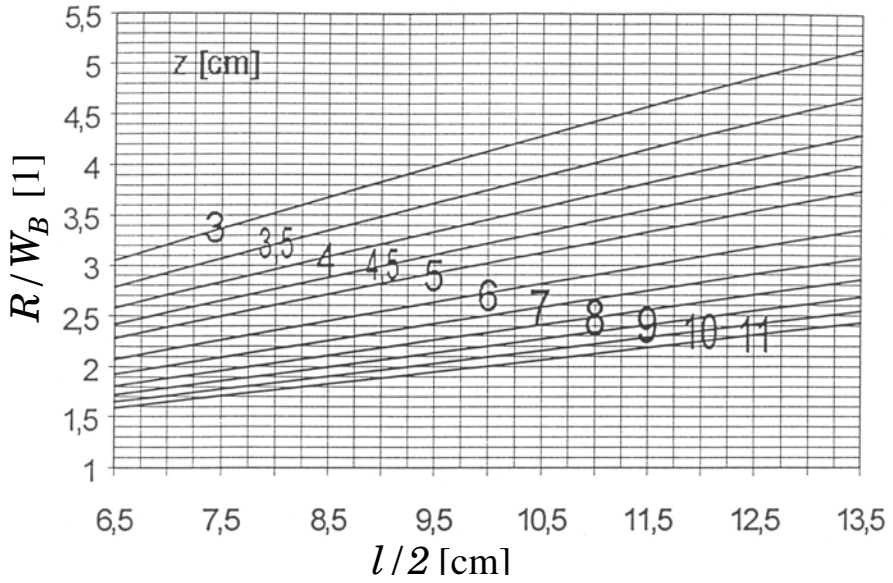

Figure J.1: The nomogram for determination of the magnitude of the resultant hip force normalised by the body weight R/W_B

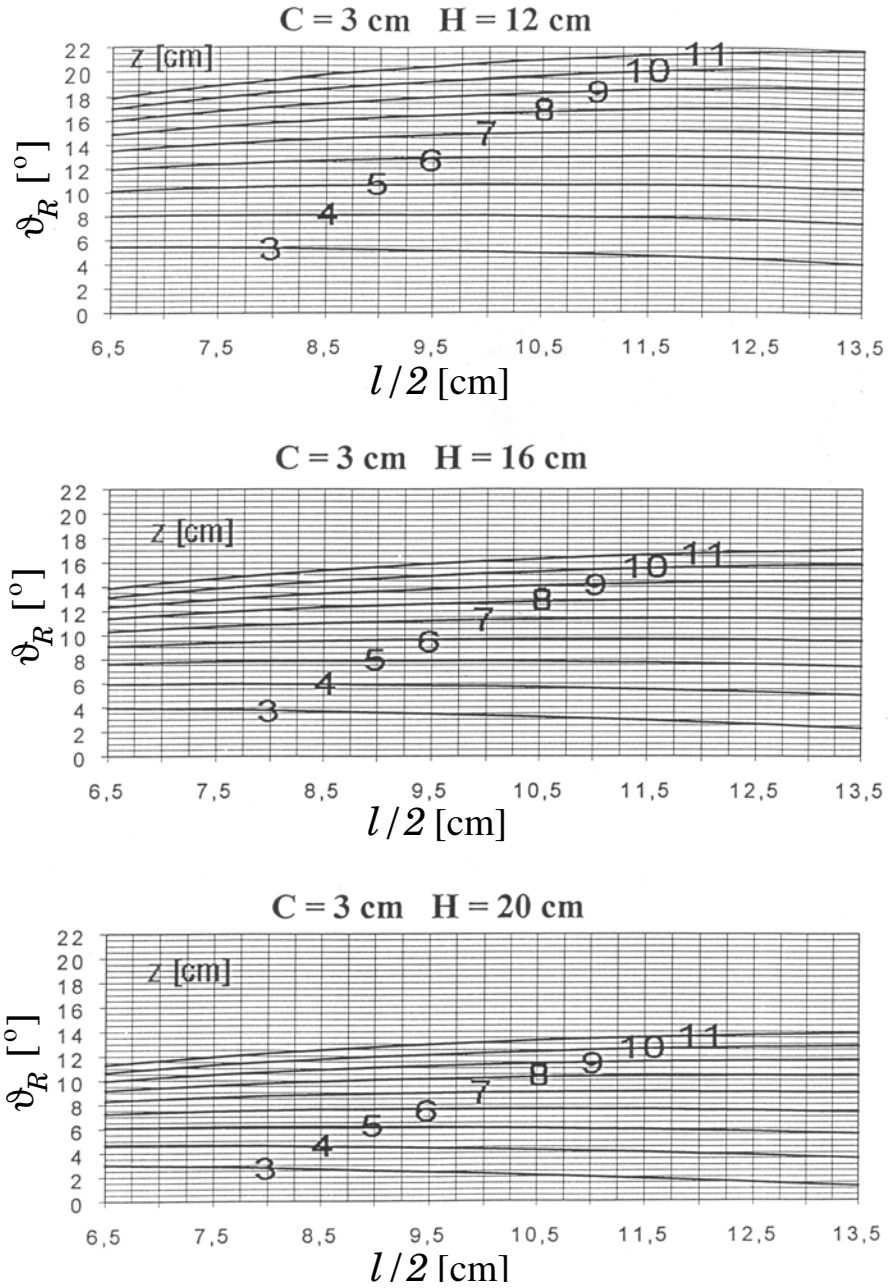

Figure J.2: The nomograms for determination of the inclination of the resultant hip force with respect to the vertical ϑ_R ($C = 3$ cm)

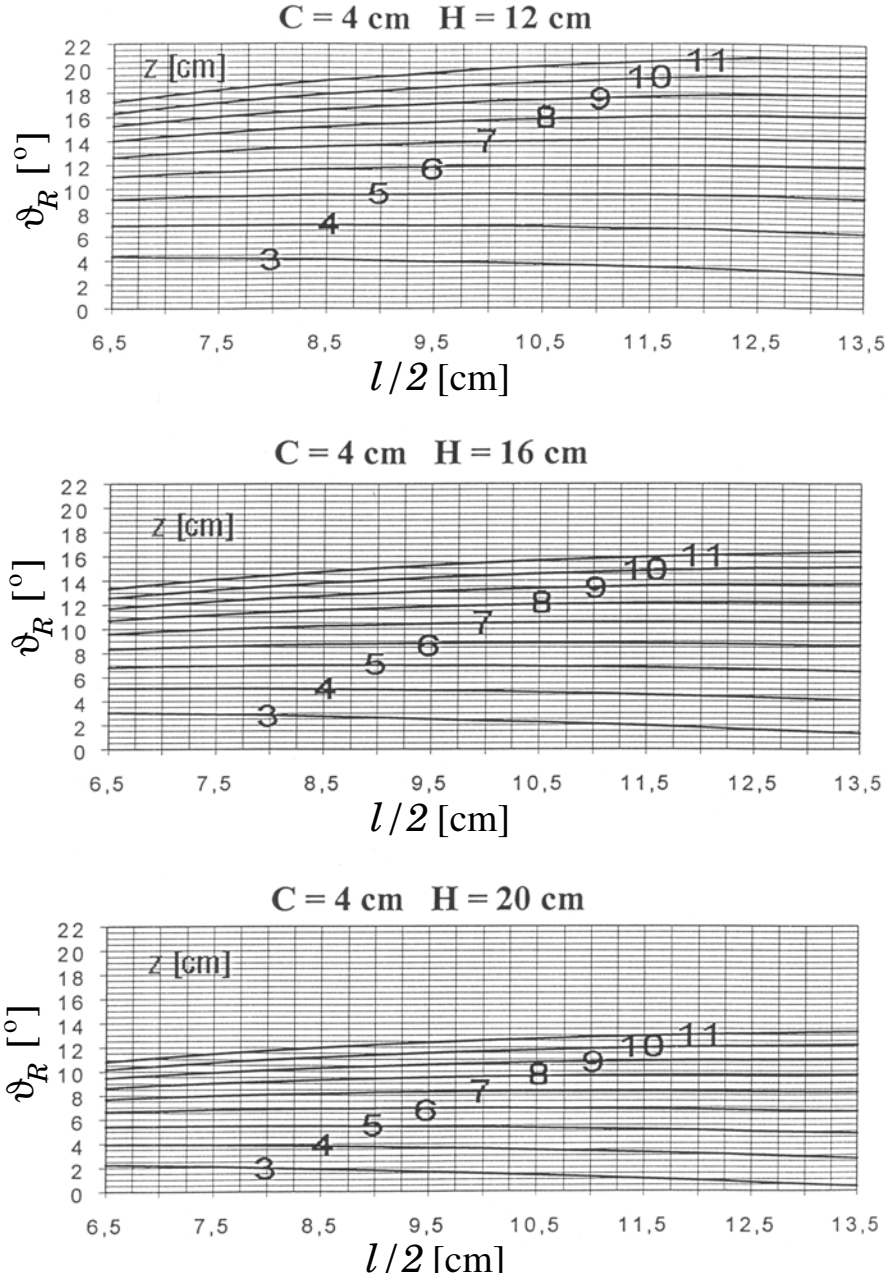

Figure J.3: The nomograms for determination of the inclination of the resultant hip force with respect to the vertical ϑ_R ($C = 4$ cm)

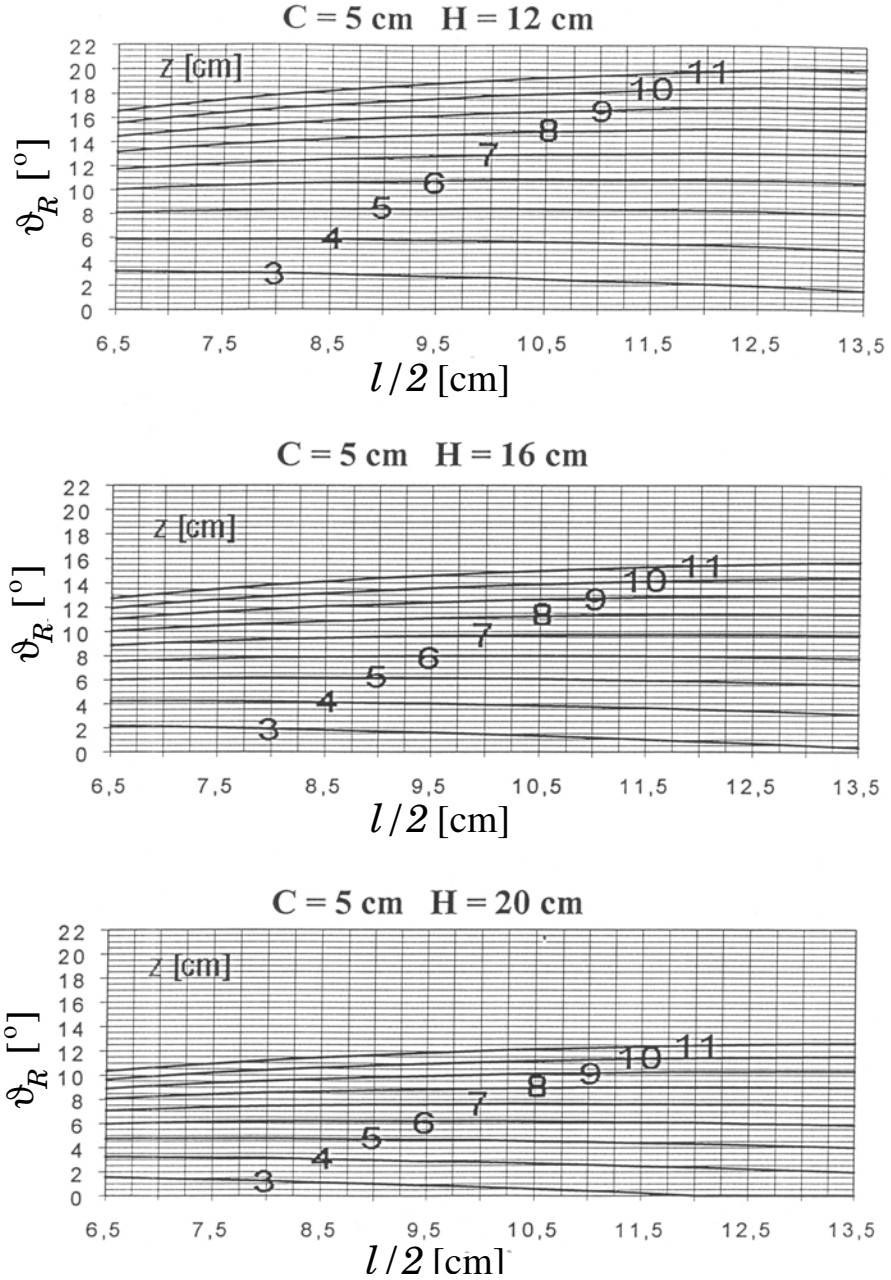

Figure J.4: The nomograms for determination of the inclination of the resultant hip force with respect to the vertical ϑ_R ($C = 5$ cm)

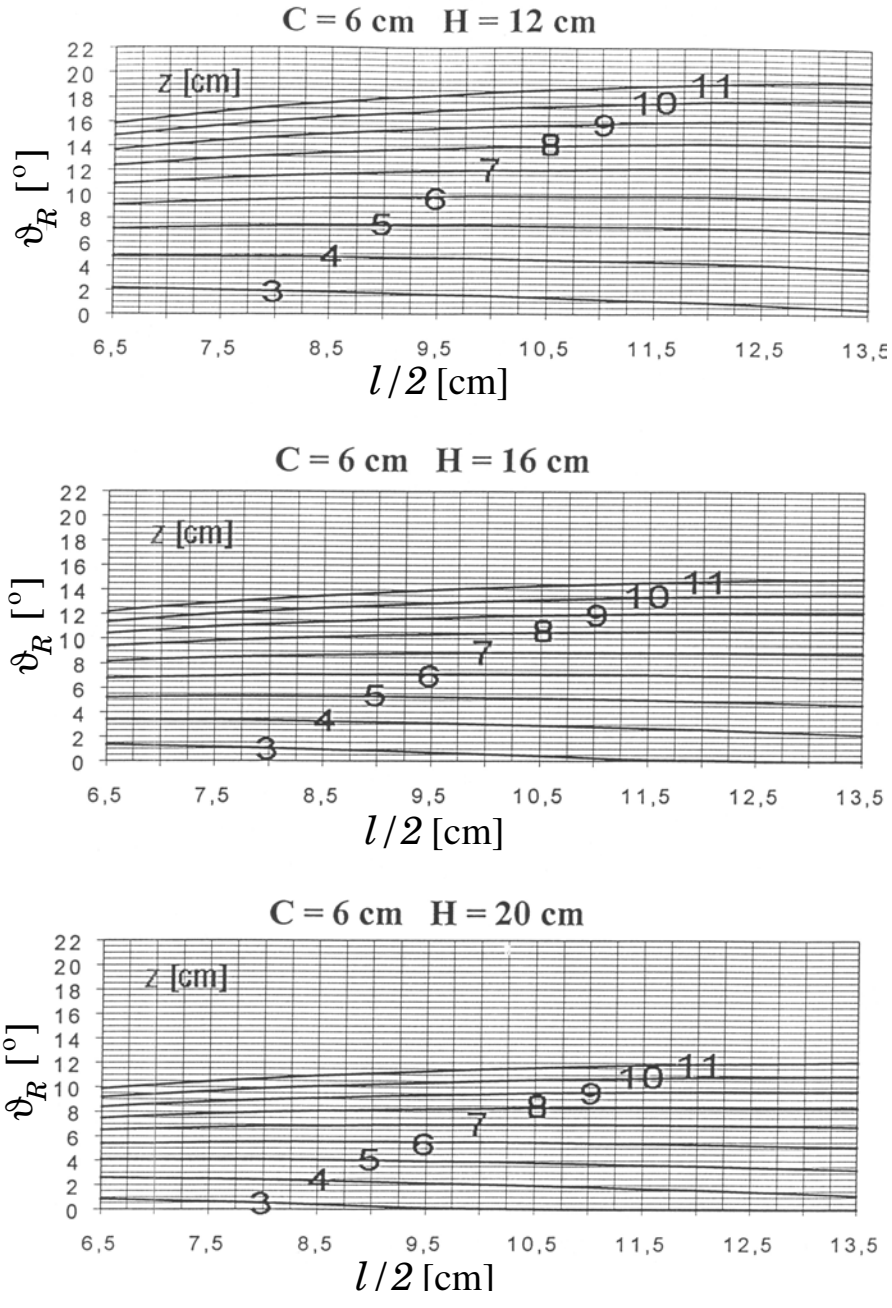

Figure J.5: The nomograms for determination of the inclination of the resultant hip force with respect to the vertical ϑ_R ($C = 6$ cm)

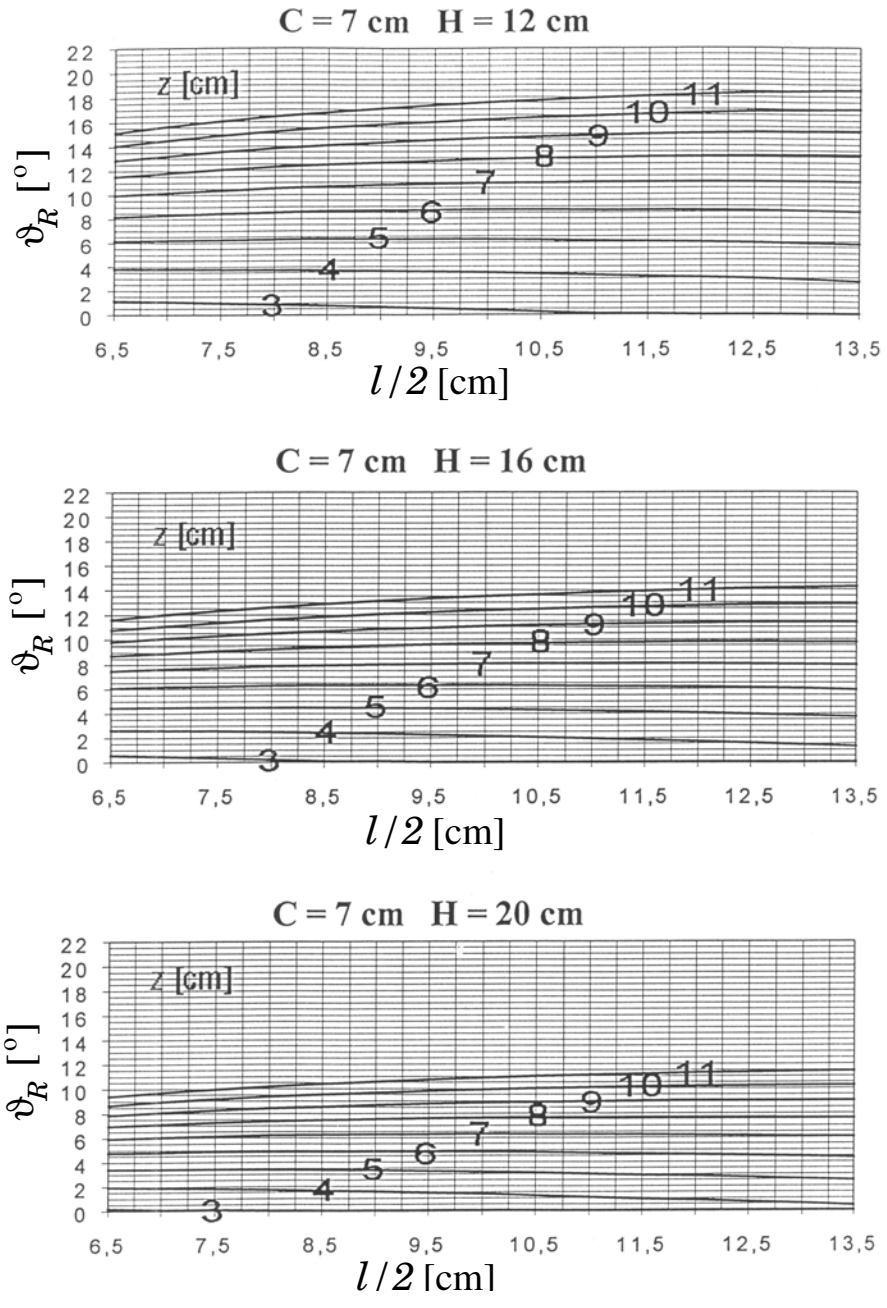

Figure J.6: The nomograms for determination of the inclination of the resultant hip force with respect to the vertical ϑ_R ($C = 7$ cm)

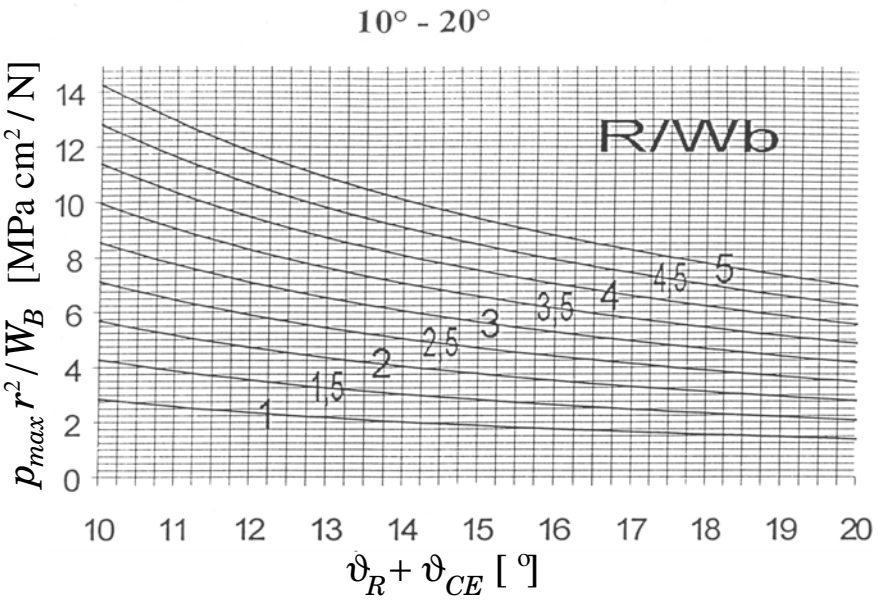

Figure J.7: The nomogram for determination of the maximal stress on the weight bearing area divided by the body weight and multiplied by the square of the femoral head radius $p_{max}\, r^2/W_B$ ($\vartheta_R + \vartheta_{CE}$ between 15 and 20 degrees).

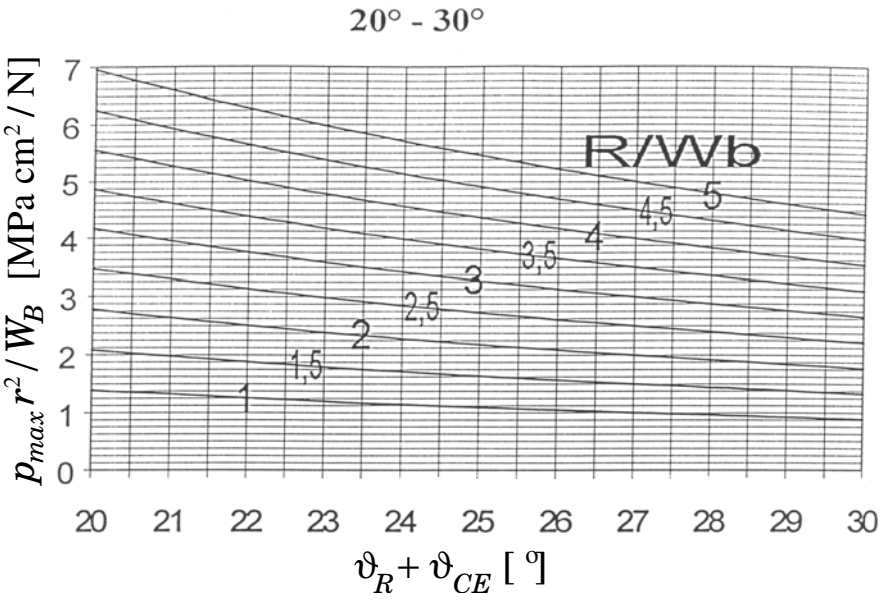

Figure J.8: The nomogram for determination of the maximal stress on the weight bearing area divided by the body weight and multiplied by the square of the femoral head radius $p_{max}\, r^2/W_B$ ($\vartheta_R + \vartheta_{CE}$ between 20 and 30 degrees).

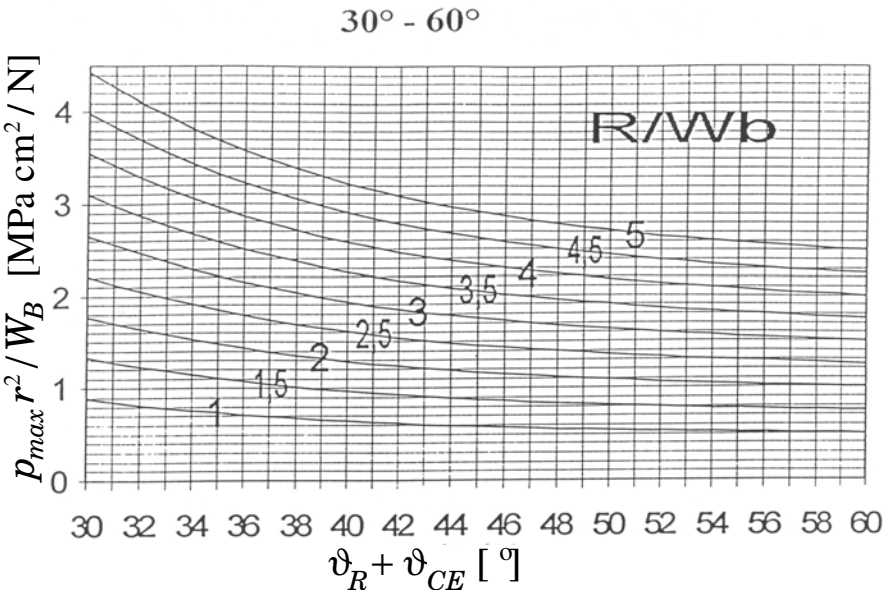

Figure J.9: The nomogram for determination of the maximal stress on the weight bearing area divided by the body weight and multiplied by the square of the femoral head radius $p_{max}\, r^2/W_B$ ($\vartheta_R + \vartheta_{CE}$ between 30 and 60 degrees).

Appendix K

AUXILIARY SCRIPTS

The following text contains auxiliary m-scripts for GNU Octave required to run scripts described in sections A, C, D, G, and H.

Software requirements	:	GNU Octave, version 2.1.50
List of files	:	`RotateX.m` - rotation of vector around the x-axis
		`RotateY.m` - rotation of vector around the y-axis
		`RotateZ.m` - rotation of vector around the z-axis
		`Cart2Sph.m` - vector transformation function from the Cartesian coordinate system to the spherical coordinate system
		`Sph2Cart.m` - vector transformation function from the spherical coordinate system to the Cartesian coordinate system
		`VekSize.m` - magnitude of the vector

RotateX.m

```
function [rotateX] = RotateX(X,fi)
  rotateX = 0;
  if (is_vector(X)) && (length(X)==3)
    MatRotX = [1,0,0; 0,cos(fi), -sin(fi);0,sin(fi),cos(fi)]
    rotateX = X * MatRotX
  else
    error ("RotateX: expecting vector argument");
  endif
endfunction
```

RotateY.m

```
function [rotateY] = RotateY(Y,fi)
  rotateY = 0;
  if (is_vector(Y)) && (length(Y)==3)
    MatRotY = [cos(fi), 0,-sin(fi);0, 1, 0; sin(fi), 0, cos(fi)];
    rotateY = Y * MatRotY;
  else
    error ("RotateY: expecting vector argument");
  endif
endfunction
```

RotateZ.m

```
function [rotateZ] = RotateZ(Z,fi)
  rotateZ = 0;
  if (is_vector(Z)) && (length(Z)==3)
    MatRotZ = [cos(fi), -sin(fi), 0; sin(fi),cos(fi),0;0,0,1];
    rotateZ = Z * MatRotZ;
  else
    error ("RotateZ: expecting vector argument");
  endif
endfunction
```

Cart2Sph.m

```
function [S] = Cart2Sph (X)
  if (is_vector(X)) && (length(X)==3)
    R = VekSize(X);
    Phi = atan2(X(2),X(1));
    Theta = atan2 (sqrt( X(1)^2+X(2)^2 ), X(3));
    S = [Theta, Phi, R];
  else
    error ("RotateX: expecting vector argument");
  endif
endfunction
```

Sph2Cart.m

```
function [V] = Sph2Cart (Theta, Phi, R)
  X = R * cos(Phi) * sin(Theta);
  Y = R * sin(Phi) * sin(Theta);
  Z = R * cos(Theta);
  V = [X, Y, Z];
endfunction
```

VekSize.m

```
function [VekSize] = VekSize(X)
  tmp = 0;
  if (is_vector(X))
    for i=1:length(X)
      tmp = tmp + X(i)^2;
    endfor
    VekSize = sqrt(tmp);
  else
    error ("VekSize: expecting vector argument");
  endif
endfunction
```

Appendix L

DATA CDROM